

IL-1R  
DRIVES ACUTE  
DISEASE TOLERANCE,  
LIVER AND SKELETAL  
MUSCLE FIBROSIS,  
AND SUSTAINED  
CACHEXIA DURING  
*T. GONDII* INFECTION

Stephanie Jean Melchor

Auburn, Alabama

Bachelor of Science in Microbiology,  
Brigham Young University, 2012

A Dissertation presented to the Graduate Faculty of  
the University of Virginia in Candidacy for the  
Degree of Doctor of Philosophy

Department of Pathology

University of Virginia

May, 2020

## Abstract

*Toxoplasma gondii* (*T. gondii*) is a protozoan parasite that chronically infects a wide range of warm-blooded hosts, including humans and mice. After an acute phase of infection, when the parasite is replicating quickly and inducing rampant inflammation and tissue damage throughout the body, *T. gondii* transitions to a chronic stage where it remains in a protective cyst for the rest of the host's life. It has been known in the *T. gondii* field for decades that infection in rodents leads to prolonged wasting; however, the mechanism of this wasting has not been probed in the modern molecular era. Here we characterize *T. gondii*-induced wasting as cachexia, a deadly muscle wasting disease associated with most chronic human illness. The discovery that *T. gondii* causes cachexia is a critical tool for the cachexia field, as it introduces a natural infection model that allows for mechanisms of wasting to be studied over the course of months rather than days to weeks (the span of most popular experimental models of cachexia today). *T. gondii*-induced cachexia occurs independently of intestinal inflammation and sustained dysbiosis, but does require signaling through the type I interleukin-1 receptor (IL-1R), as IL-1R<sup>-/-</sup> are protected from cachexia while maintaining a comparable parasite burden as wildtype mice. Importantly, while IL-1R signaling remains dispensable for control of the parasite during the acute period as well, it promotes pathways of tissue tolerance to infection and inflammation. IL-1R<sup>-/-</sup> have significantly worse tissue damage in the liver and adipose tissue than wildtype mice, despite having the same number of parasites. Together these observations suggest a paradigm that while pathways controlling disease tolerance pathways may be beneficial in the short-term (for example, protection from acute liver and adipose tissue damage), unchecked activation of them can lead to pathology, like cachexia. In addition to cachexia, IL-1R is also necessary for the perivascular fibrosis that arises in the skeletal muscle and liver of cachectic mice, a heretofore unobserved phenomenon in experimental cachexia models, despite being seen in clinical cachexia.

## Acknowledgments

### Pre-Graduate School Teachers

To all of my teachers who encouraged my interest in writing, especially **Jeff Gray**, **Rebecca Hardy**, and **Dr. Cory Callahan**: thank you. It's been literally decades since I took your classes, but your influence cannot be understated. To my sixth grade science teacher **Sarah Stone**, for encouraging my earliest efforts at science writing. I wrote a story about an anthropomorphized water droplet witnessing the destruction of Pompeii, and you asked me to read it in front of the class, calling it "phenomenal." I hope someday you'll know how important that encouragement was for me. To **Mary Dalrymple**, who taught me IB Biology in twelfth grade: you taught me the principles of biology that were foundational to everything I've done (and will do) since. You sparked my passion for the elegant messiness of biological systems, and were committed to helping me find ways to test unconventional hypotheses (I'll never forget your homemade CO<sub>2</sub> generator!), which has clearly left an impression. Reading *The Hot Zone* for your class was absolutely formative for my interest in infectious diseases, and showed me by example how powerful good science writing can be.

To **Dr. Sandra Hope**, for single-handedly making me fall in love with immunology. Your elegant whiteboard diagrams and energetic lectures blew my mind, and are still impressive to think about today. I am an immunologist today, nine years later, because of you. Thank you also for giving me the first opportunity to overcome my fear of working with mice. That has certainly come in handy. To **Dr. John Bell** at for teaching my first biology class at Brigham Young University, and for letting me do research with your lab for eighteen months, despite me having no prior lab experience. Your kindness and generosity of spirit to let me pursue a research project out of the area of the lab's expertise that didn't lead to much useful data for the Bell Lab, but showed me my passion and stubbornness that not only got me into graduate school, but got me through it. I know I wasn't as involved in lab as most of the other students in our group were, but I so appreciate the time you put in to help me write my ORCA grant, work on my project, and apply to graduate school. I am where I am now because of you. To **Dr. Rob McFarland**, first and foremost, for helping me realize what a fierce feminist I am. Who knew Peter Altenberg's poetry could be so life-changing? You saw a spark in me that has taken years for me to see in myself, and I can never thank you enough for encouraging me to aim higher, dream bigger, and write better (and faster!). Your encouragement and mentorship have made me who I am, and I can never stop thanking you. Vielen, vielen Dank. Also to your wife **Mary Ann McFarland**, for sitting down with me in your office that afternoon and encouraging me to not hold myself back professionally because I'm a woman: thank you.

### The Petri Lab

It would be wrong to not acknowledge how formative my first two years in graduate school as part of the Petri Lab were. To **Dr. Bill Petri**, for welcoming me into your lab, trusting me with the Reg1 project, and giving me opportunities to present my work from Philadelphia to Campeche, Mexico. I am so grateful for how I was treated like part of the team from the moment I joined the lab, even before I had qualified, and am grateful for the brilliant and beautiful people I met during my time here. Thank you for your continual gracious support of me. That you came to see *The Sound of Music* (on the coldest night of the run, no less!) meant the world to me, and speaks so much your character. To **Andrew Irving**, for the delightfully thoughtful conversations during one of my roughest times in graduate school. To **Dr. Chelsea Marie Braun**, for teaching me how to do my signature technique (qPCR) and for providing me with an endless supply of washi tape, adorable hand-me-down clothes, parking at your house, and for always coming to me in times of need. You are always and forever my fairy godmother, and I am so honored to know you. Perhaps most importantly, to **Dr. Shaun Steele**, for teaching me that good things come to those who *work*, for seeing a spark of potential in me when I couldn't, and for the hours you patiently spent watching me unsuccessfully trying to scruff mice. You taught me almost everything I know, and I still cannot believe how incredibly generous you were with your time to train a baby graduate student who felt very lost and very scared. I would not be graduating with a PhD if it hadn't been for you, and I can never thank you enough for your patience, good humor, tough love, and remarkably perceptive friendship (even after I spitefully covered all of your lab supplies with little pictures of sheep that one night).

### The Ewald Lab

To **Dr. Sarah Ewald**, for so, so much. For taking a chance on a student in search of a new lab, and guiding me through this truly beautiful biological story that follows in the 100+ pages after this behemoth of an acknowledgments section. I know there were many times where you felt like you had to drag me along, which was uncomfortable for both of us, but I never for a second felt like you were ready to give up on me. Thank you for helping me become a more sophisticated writer and presenter, for training me (mostly) to stop procrastinating, for insisting that I turn to the data before making any kind of arguments or conclusions, for helping me overcome my anxiety-induced executive dysfunction to actually be able to test the questions I was concerned about, for supporting my career transition into science writing, and, most importantly, for instilling in me a mortal fear of endotoxin contamination.

To **Jessica Hatter**. Girl, where do I even start? This dissertation belongs to you as much as it belongs to me, and I want that in writing for as long as this document exists. You taught me how to count cysts, how to do infections, how to do basically everything in 3706. Your dogged determination and dedication to the project and to our friendship is how we were able to get *so much* done during our almost two years together. There aren't a lot of things I'll miss about bench work, but mishearing lyrics to eighties rock songs with you while dissecting mice is something I miss every day. I cannot wait to see you continue to grow in your training. Also to your amazing partner **William Koenig** for convincing me to watch *Avatar: The Last Airbender*, because...obviously that was life-changing. To **Xiaoyu (Harry) Zhao**, for your

quick wit, gentle humor, liquid nitrogen expertise, help with the mouse experiments, ability to answer all of my questions (sometimes I think you should be the senior graduate student, although I guess you are now!), taking care of Blue Fish during quarantine, and for coining the best one-liner the world has ever known (“You can cry, but it won’t change.”). You are amazing, and I’m so lucky to know you. To **Dr. Bocheng Yin**, for the unbelievably juicy stories, the sass, and for helping me so much with the LSM 880. I don’t think our projects could be any more different, but I am so grateful to call you my colleague and my friend. To **Samy Lempke**, for being my baby graduate student. Thank you for letting me mentor you, and for your determination to pull me out of the Bat Cave (both physically and metaphorically) and back into the light. You are one of the biggest reasons the last year of grad school has been so happy. I’m so proud of everything you’ve accomplished so far, and can’t wait to see what you do next. Last but not least, to my incredible undergrads over the years. To **Kari Byrnes** for being the first person I ever mentored, and for being so patient during this process! To **Haider Ghumman** for overcoming your fear of mice in order to help with the weighing. To **Claire Saunders** for counting *so* many cysts, for figuring out ImageJ when I was still scared of it, and for the hours you put into the slide scans and the PCRs. I know the work was drudgery, but it was so important. Thank you for being the chill foil to my manic, and for always being willing to help out. To **Imani Sanders** for being the last one standing! For helping with the mice, even though it wasn’t your primary (or secondary) project, and for your patience, great attitude, and for introducing me to your mom’s Etsy shop. To **Érika LaTorre**, our honorary lab member and summer student: I am in awe at how much you were able to accomplish during your time in the lab. I honor your persistence and your dedication to your project, and am so grateful for your gorgeous a-SMA blots. It would’ve taken me much longer than a summer to get my blots looking as good as yours!

### Thesis Committee

To my thesis committee: **Dr. Heather Ferris**, **Dr. Thurl Harris**, **Dr. Tajie Harris**, **Dr. Kenneth Tung**, **Dr. Tom Braciale**, and **Dr. Janet Cross**, thank you for your thoughtful feedback on such a big (and quickly evolving) project. This was a new project for our lab in many ways, and its success absolutely relied on the collective expertise of each of my committee members. Special thanks to **Dr. Janet Cross** for reading and commenting on my entire dissertation (!!!), and for becoming such a valuable confidante and ally during all of my time in graduate school. I so appreciate her commitment to helping students not just survive, but thrive, in this program, and am grateful to have benefited immensely from her mentorship and guidance.

### UVa Labs

Working on a new project in a brand-new lab brought out a scrappiness and a dependency on the generosity of others that I hadn’t needed to rely on before. I am so grateful for how so many labs at UVa have donated their time and reagents to help us develop the many arms of this project. To **Samantha Batista**, my project would look very different if it hadn’t been for your careful and exciting observation of the IL-1R<sup>-/-</sup> rescue from cachexia. Thank you for your openness, your patience, and your willingness to share and help me troubleshoot protocols. I’m honored to consider you a friend (and fellow Slytherin), and can’t wait to see where you

go next. To **Marissa Gonzalez**, for being my favorite Disney princess and for teaching me everything I know about flow cytometry. Thank you for bailing me out with reagents and flow wisdom so many times when I was panicking, and for being such a beautiful human being. To **Trip Gill**, for your infallible sunshine, friendship, and ability to fix anything and everything. Thank you for helping me step outside myself when things were hard, and for reminding me that, “Everything does suck, but not everyone hates [me].” You have been an incredible friend, and I’m going to miss you. To the **Barker Lab** for being so generous with your reagents and time as I trained to become an expert in fibrosis. To **Dr. Claire Rosean** and the rest of the Rutkowski lab for their help with developing our flow cytometry protocols as well and honestly, to everyone who has loaned me reagents. Thank you.

### Cores and Companies

I would be lost without some of UVA’s core services. To **Sheri VanHoose** and **Lisa Vohwinkel** of the Research Histology Core, for processing *so many* of my samples, teaching me how to improve my sample prep, and for being so very lovely and kind. To **Alice Kenney** and her crew in the MR6 vivarium, especially **Macon Lamb**, for taking such astonishingly good care of my mice. To **Stefan Hargett** for helping both Jessica and me so extensively with the metabolic cages, from set-up to analysis. Your willingness to help was really wonderful, and I so appreciate it. To **Peggy Morris** and **Shawn Wood** of the CIC administrative staff, thank you for all of the times you scheduled rooms, tracked down information for us, helped us with lost keys, and, especially, for always coming to my rescue whenever I needed it. You two are amazing, and the CIC truly couldn’t run without you. This isn’t a UVA core, but to **ThermoFisher Technical Support**: I can’t count the number of times I breathlessly called you (the only number on speed dial besides my husband), exclaiming, “I’m a frazzled graduate student and just messed up x, y, z.” Every single time, your technical support team validated my distress and then offered useful solutions. You were like the postdoc I always needed and I’m so grateful for all the scrapes you helped me out of.

### Outside of Grad School

**Christina Fleming**, I can’t write this without crying. In 2018, I desperately sent a message to you, telling you I wanted to sing more seriously and didn’t want to self-sabotage my way into quitting. You were (and are) so gentle and so patient, and encouraged me to compete in NATS the day I was going to tell you I needed to take a break for a few months. You have shown me what practice and passion can do, and have shown me what I can achieve when I trust myself. You really have been better than therapy, and I cannot thank you enough for what I’ve learned about myself and for what I have been able to accomplish because of you. In a similar vein, to **Nicolas Pallesen**, who I met under the most auspicious circumstances, for teaching me that I had nothing to prove and everything to share. You have no idea how many times I’ve whispered that to myself in the year since I met you, and how desperately I’ve needed to hear it every time.

To **Brian Clowdus**, the entire cast and crew of *The Sound of Music* (especially my fourteen perfect little Von Trappings), and those mountains at Wintergreen: Performing with all of you was life-changing. You all helped me climb higher and harder mountains last year than I ever thought I’d have to climb, and I can’t thank you enough for

trusting me with your hearts, for the hugs, and your patience with my imperfections. Brian, thank you so much for casting me, and for trusting me to understudy Maria. Being able to learn her role on top of mine within in a week (in addition to working full-time in the lab) is one of the most empowering things I have ever done. Thank you for having confidence in me. “I go to the hills when my heart is lonely/I know I will hear what I’ve heard before. My heart will be blessed with the sound of music, and I’ll sing once more.” Thank you for singing with me, my darlings.

To members of the science writing community who have welcomed me with open arms, especially **Josh Barney**, **Seth Mnookin**, and especially **Erika Check Hayden**: your collective confidence in me and assurance that you were waiting on the other side helped me get through the last year of graduate school. I truly cannot wait to work with you more.

To all the other people, things, and ideas that literally helped me survive graduate school: to all the dry shampoo and PopTarts: truly, I’d be lost without you. To **Lin Manuel-Miranda** and the **Original Broadway Cast of *Hamilton*** for helping me find my hustle, and for helping me realize that to get what I want, I need to write like I’m running out of time. To the **creators and cast of *Hadestown*** for going with me to hell and back again, and for reminding me that there *are* songs so beautiful that they’ll make spring come again. To **Richard Holmes**, author of *The Age of Wonder*, I have never read a book so inspiring, or one that tugged at my heartstrings in such a specific way as your book. You were my Virgil as I wrestled with the turmoil of choosing between a life devoted to science or one devoted to art, and in the end, you showed me a way that I can do both. Thank you. To **Mary Wollstonecraft Shelley** (yes, *that* Mary Shelley), *Frankenstein* singlehandedly kept me in graduate school in way that no living person could have. Your words struck me in the heart right when I needed them, and have changed my life forever.

To my **2018 SEP students**, the smartest kids I will ever meet, thank you for reminding me how much I love immunology, and how much I love trying to make other people love immunology too. I can’t wait to see where you all end up. To all my **Reviewers 1, 2, and 3**: So far, your comments have only ever been thoughtful, thorough, and very helpful. All of my manuscripts are so much better because of the time you put in, and I’m so very grateful.

### **Friends**

To **Ruth Duersch Ray**, for being one of my oldest friends, for asking the best questions and for helping me want to be the person you tell me I am. Thank you for taking me on my first international trip and helping me realize how brave I can be when I have a friend (and a sister) by my side. **Nathan Warenski**, you gave me the courage to even get on the plane to go to my UVa interview weekend. You’ve been there since I was still deciding where to go to grad school, since I did worse on the GRE than I wanted to, and you’ve been here through every single year of graduate school, until the very end. Thank you for being the lion in my pocket, my star brother, and for believing in me the way I believe in you. **Katie Kirk**, I can barely remember a time when I *didn’t* know you. I’m so glad that in the crazy ways we’ve both grown up since *The Secret Garden*, we’ve found ways to stay together. Yale won’t know what hit it this fall when you make your mark. So proud to know you, and can’t wait to see where you go

next. To **Ammon Loveless** for making the summer at Blickenstaff's before graduate school unbelievably magical, for always believing in me, and for still being my friend, after all this time. I love you so much, but not like that. To **Riley Hannan**, for reminding me to be grateful and happy, even when I don't want to be, and for helping me get the help I needed when happy thoughts weren't enough. For the hours spent hiding in your microscope cave when life and lab got too hard, *allllll* the advice and reagents as I was learning about fibrosis, and for literally feeding me when even eating was too hard. You're a champ. To **Dr. Jaimys Arnott**, for virtually keeping me company during the final sleepless nights of dissertation-formatting, when everyone else in my hemisphere was asleep. Thank you for your friendship and good humor, for watching my defense in the middle of the night, and mostly for being my personal source of amazing Australian animal trivia. I *will* see a cassowary one day, and I hope you get to be there too (mostly because it'll likely be terrifying, and, by default, you're the closest thing to Steve Irwin I've got). To (almost!) **Dr. Michael Pilosov**, I think it's pretty obvious we've actually known each other since the beginning of time, but thank you for materializing out of the fabric of the universe exactly when I needed you. You're going to rock the world (in the best possible way), and I am so profoundly fortunate to know you.

### **Family**

To my **Melchor family**: thank you for welcoming me into your family and for being so supportive of my dreams and ambitions, even though they meant we've been living so far away. Thank you for understanding when I had to work over the holidays, for your interest in my work, and, of course, for giving me David. Thank you to my darling nieces and nephews who literally prayed that I'd be able to finish my JI paper, and for being such a good excuse to *not* work over the holidays. Los amo muchisimo!

To my **Brown family**: To each of my siblings, who make me want to be as beautiful and as brilliant as they are: Allison, Matt (who designed the gorgeous title page!), Jeff, Becca, Rachel, and Stewart. To my parents, **Steve** and **Melanie Brown**, for accepting this very dense book that no one will read as a substitute for a grandchild, for always encouraging my passions (no matter how obscure they were), for being the reason I fell in love with UVa in the first place, and for being so very, very loving and supportive throughout all of this.

To my sweet dogs **Raven** and **Persephone**, for being so forgiving of all the time I spent with my mice instead of you, for giving me excuses to get outside, and for filling me with a love so inexplicably whole that it's completely counterbalanced the gut-wrenching misery of grad school. Raven, thank you for being my first baby, for the world's sloppiest kisses, and for your patience as I learned how to love in a completely new way. I miss you, pretty girl. Persephone, like your name implies, you brought the spring after a long, bleak winter, and I am so grateful for you bringing so much light back into our home. To my husband, best friend, and partner-in-crime **David Melchor**: I am the most verbose person I know, and I do have not enough words to thank you for everything you've done for me: You are mi media naranja, the grounding earth to my volatile fire, and the *only* person I want by my side forever. Here's to another 10 years of *not* being in graduate school and chasing our dreams together. I can't wait to see where we go next, mi amor.

## Table of Contents

Abstract.....	i
Acknowledgments.....	ii
List of Tables and Figures.....	3
List of Abbreviations.....	5
Chapter 1: Introduction.....	6
Introduction: disease tolerance vs. resistance.....	6
Reinterpreting the immune response to <i>Toxoplasma</i> in the framework of disease tolerance.....	7
Immune cell-mediated mechanisms of tolerance during <i>T. gondii</i> infection.....	9
Host metabolic dysregulation in <i>Toxoplasma</i> infection.....	10
Current Knowledge Gaps.....	13
Summary of Dissertation.....	13
Figures.....	15
Chapter 2: Materials and Methods.....	19
Chapter 3: <i>Toxoplasma gondii</i> infection triggers chronic cachexia and sustained commensal dysbiosis in mice.....	27
Acknowledgments.....	27
Background.....	27
Results.....	29
Discussion.....	33
Figures.....	35
Chapter 4: IL-1R regulates disease tolerance and cachexia in <i>T. gondii</i> infection.....	41
Acknowledgments.....	41
Background.....	41
Results.....	42
Discussion.....	45
Figures.....	49
Chapter 5: <i>T. gondii</i> infection induces IL-1R dependent chronic cachexia and perivascular fibrosis in the liver and skeletal muscle.....	59
Acknowledgments.....	59
Background.....	59
Results.....	60
Discussion.....	65
Figures.....	67
Chapter 6: Implications, Outstanding Questions, and Future Directions	85
Is chronic infection with <i>T. gondii</i> necessary for sustained cachexia?..	85
Is induction of cachexia in an adaptation of <i>T. gondii</i> to promote transmission to felines?.....	85

How does chronic <i>T. gondii</i> -induced cachexia cause disruptions in lipid metabolism?.....	86
Is IL-1 $\alpha$ or IL-1 $\beta$ primarily responsible for acute disease tolerance?....	89
When and where is IL-1R signaling required to cause cachexia?.....	91
How does IL-1R cause cachexia?.....	92
Concluding Remarks.....	94
Figures.....	95
<b>References.....</b>	<b>104</b>

## List of Tables and Figures

<b>Figure</b>	<b>Title</b>	<b>Page</b>
<b>Figure 1.1</b>	Summary of restriction versus tolerance mechanisms.	15
<b>Figure 1.2</b>	<i>Toxoplasma gondii</i> induces host tolerance and resistance mechanisms in successful infections.	16
<b>Figure 1.3</b>	Summary of <i>T. gondii</i> life cycle.	17
<b>Table 1.1</b>	Summary of literature describing immunoregulatory pathways during <i>Toxoplasma gondii</i> infection.	18
<b>Figure 3.1</b>	C57BL/6 mice orally infected with <i>T. gondii</i> develop chronic cachexia.	35
<b>Figure 3.2</b>	C57BL6/J and CBA/J mice are susceptible to cachexia following <i>Toxoplasma</i> infection, but BALB/c mice are not.	37
<b>Figure 3.3</b>	Mice recover from severe acute inflammation and parasite growth in the small intestine.	38
<b>Figure 3.4</b>	Changes in the commensal community are amplified in chronic infection.	40
<b>Figure 4.1</b>	IL-1R <sup>-/-</sup> mice survive chronic <i>T. gondii</i> infection better than wildtype mice independent of parasite burden.	49
<b>Figure 4.2</b>	Wildtype and IL-1R <sup>-/-</sup> mice have inflammation in the brain during chronic infection.	50
<b>Figure 4.3</b>	IL-1R signaling limits cell death in the adipose tissue during acute <i>T. gondii</i> infection.	51
<b>Figure 4.4</b>	IL-1R signaling limits caspase-3 activation in the liver during acute <i>T. gondii</i> infection.	52
<b>Figure 4.5</b>	IL-1R ligands are elevated in the liver and vWAT at 2 weeks post-infection.	53
<b>Figure 4.6</b>	TUNEL staining and ASC speck formation can be detected at similar levels between WT and IL-1R <sup>-/-</sup> mice at 2 wpi.	54
<b>Figure 4.7</b>	IL-1R signaling does not control immune infiltrate in vWAT and liver at 2 weeks post-infection.	55
<b>Figure 4.8</b>	Acute weight loss is IL-1-independent, but IL-1R <sup>-/-</sup> mice are protected from chronic <i>Toxoplasma</i> -induced cachexia.	56
<b>Figure 4.9</b>	IL-1 $\alpha$ remains chronically elevated in the circulation, liver, and brain of cachectic mice.	57
<b>Figure 4.10</b>	IL-1 $\alpha$ <sup>-/-</sup> and IL-1 $\beta$ <sup>-/-</sup> mice are partially protected from chronic cachexia.	58
<b>Figure 5.1</b>	Chronic <i>Toxoplasma</i> infection causes sustained cachexia in mice.	67
<b>Figure 5.2</b>	Skeletal muscle is wasted in mice chronically infected with <i>T. gondii</i> .	69
<b>Figure 5.3</b>	<i>T. gondii</i> -induced chronic cachexia occurs independently of non-shivering thermogenesis and insulin resistance.	70
<b>Figure 5.4</b>	<i>Toxoplasma</i> -induced cachexia does not induce the transcriptional signature associated with adipose tissue beigeing at 17 weeks post-infection.	71

<b>Figure 5.5</b>	Cachectic mice have reduced activity and RER compared to uninfected mice.	72
<b>Figure 5.6</b>	Lipolysis is not a main driver of <i>Toxoplasma</i> -induced cachexia.	74
<b>Figure 5.7</b>	<i>T. gondii</i> -induced cachexia is associated with perivascular fibrosis in metabolic organs.	75
<b>Figure 5.8</b>	Cells expressing IL-1 $\alpha$ and IL-1R are observed in the fibrotic liver environment.	77
<b>Figure 5.9</b>	Inflammatory cytokines are not chronically elevated in the muscle or vWAT.	78
<b>Figure 5.10</b>	IL-1 induces contractility and alpha smooth muscle actin expression in murine embryonic fibroblasts and primary hepatic stellate cells.	79
<b>Figure 5.11</b>	IL-1 does not promote survival or proliferation in mouse endothelial fibroblasts.	81
<b>Figure 5.12</b>	IL-1R <sup>-/-</sup> mice are protected from <i>T. gondii</i> -induced cachexia and cachexia-associated liver atrophy.	82
<b>Figure 5.13</b>	Cachectic mice develop IL-1R-dependent liver and skeletal muscle fibrosis.	83
<b>Figure 5.14</b>	IL-1R signaling does not control immune infiltrate in liver and vWAT at 9 weeks post-infection.	84
<b>Figure 6.1</b>	Acute aglistatin administration inhibits <i>T. gondii</i> growth in vivo.	95
<b>Figure 6.2</b>	Cachectic mice sustain dysregulation in circulating lipid species.	96
<b>Figure 6.3</b>	Mice with chronic <i>T. gondii</i> infection do not gain weight on a high fat diet.	97
<b>Figure 6.4</b>	Infected IL-1R <sup>-/-</sup> mice on a high fat diet have improvements in fat storage compared to wildtype mice.	98
<b>Table 6.1</b>	Significantly changed metabolites in the serum of cachectic mice compared to uninfected mice.	99
<b>Figure 6.5</b>	Administration of soluble IL-1Ra (anakinra) at acute or chronic infection is insufficient to protect mice from <i>T. gondii</i> -induced cachexia.	100
<b>Figure 6.6</b>	<i>IL-1R</i> transcript can be detected in multiple tissues at both acute and chronic infection	101
<b>Figure 6.7</b>	Inhibition of retrograde signaling through the vagus nerve does not protect mice from chronic <i>T. gondii</i> -induced cachexia.	102
<b>Figure 6.8</b>	Final Model	103

## List of Abbreviations

<b><math>\alpha</math>-SMA</b>	alpha smooth muscle actin	<b>LPS</b>	lipopolysaccharide
<b>ACC</b>	acetyl-CoA carboxylase	<b>Me49gLuc</b>	Me49 stably expressing GFP and luciferase
<b>AKT</b>	protein kinase B	<b>MLKL</b>	mixed lineage kinase domain-like
<b>ALT</b>	alanine aminotransferase	<b>MyD88</b>	myeloid differentiation factor 88
<b>ASC</b>	apoptosis-associated speck-like protein containing a CARD	<b>NK</b>	natural killer
<b>AST</b>	aspartate aminotransferase	<b>NLRP</b>	nucleotide-binding oligomerization domain, leucine rich repeat and pyrin domain containing
<b>ATGL</b>	adipose triglyceride lipase	<b>OTU</b>	operational taxonomic unit
<b>BAT</b>	brown adipose tissue	<b>p.o.</b>	per oral
<b>BFD1</b>	Bradyzoite-Formation Deficient 1	<b>Pgc1<math>\alpha</math></b>	peroxisome proliferator-activated receptor gamma coactivator 1-alpha
<b>BLI</b>	bioluminescent imaging	<b>PP</b>	Peyer's patch
<b>C/ebp1</b>	CCAAT/enhancer binding protein 1	<b>PPAR-<math>\gamma</math></b>	peroxisome proliferator-activated receptor gamma
<b>Cidea</b>	Cell Death Inducing DFFA Like Effector A	<b>Prdm16</b>	PR domain containing 16
<b>CLAMS</b>	Comprehensive laboratory animal monitoring system	<b>QUAD</b>	quadriceps
<b>Dpi</b>	days post-infection	<b>RER</b>	respiratory exchange ratio
<b>EDL</b>	extensor digitorum longus	<b>RLU</b>	relative light unit
<b>GA</b>	gastrocnemius	<b>ROP</b>	rhoptry
<b>H&amp;E</b>	hematoxylin and eosin	<b>scWAT</b>	subcutaneous white adipose tissue
<b>HFD</b>	high fat diet (45% kcal)	<b><i>T. gondii</i></b>	<i>Toxoplasma gondii</i>
<b>HSC</b>	hepatic stellate cell	<b>TA</b>	tibialis anterior
<b>HSL</b>	hormone sensitive lipase	<b>TGF-<math>\beta</math></b>	transforming growth factor beta
<b>i.p.</b>	intraperitoneal	<b>TLR</b>	Toll-like receptor
<b>IFN</b>	interferon	<b>TNF-<math>\alpha</math></b>	tumor necrosis factor alpha
<b>IL</b>	interleukin	<b>TUNEL</b>	terminal deoxynucleotidyl transferase dUTP nick end labeling
<b>IL-1Ra</b>	IL-1 receptor antagonist	<b>UCP-1</b>	uncoupling protein 1
<b>IRG</b>	immunity related GTPase	<b>VLDL</b>	very low-density lipoprotein
<b>kPa</b>	kilo-pascal	<b>vWAT</b>	visceral white adipose tissue
<b>LDH</b>	lactose dehydrogenase	<b>wpi</b>	weeks post-infection

## Chapter 1: Introduction

**The text and figures included in this chapter have been adapted from the following publication:** Melchor, S. J., and S. E. Ewald. 2019. Disease tolerance in *Toxoplasma* infection. *Front. Cell. Infect. Microbiol.* 9: 185.

### Introduction: disease tolerance vs. resistance

A successful immune response requires two distinct, but complementary components: “resistance mechanisms” and “tolerance mechanisms.” Resistance (or restriction) mechanisms directly target pathogens to limit microbial replication or dissemination. Examples of resistance mechanisms include antimicrobial peptides, complement, and degranulation by neutrophils or cytotoxic T cells. Disease tolerance mechanisms target host cell biology to improve tissue integrity and function in the setting of damage caused by a pathogen or the inflammatory response. Examples include extracellular matrix remodeling, the DNA damage response, antioxidant production, and shifts in cell metabolism (1–4) (**Fig. 1.1**). Although tolerance mechanisms are often induced by and intimately related to an immune response, many disease tolerance programs are carried out by non-immune (non-hematopoietic) cell types. In fact, disease tolerance mechanisms were first described in plants, which lack a distinct cellular immune system, where they have been associated with tissue integrity, growth, and reproductive capacity (5).

Historically, immunologists have used the word ‘tolerance’ to describe two processes that limit lymphocyte autoreactivity. In central tolerance, B or T lymphocytes with an affinity for self-antigens are deleted in the bone marrow or thymus before entering circulation. In peripheral tolerance, auto-reactive lymphocytes that arise later in development are deleted or rendered unresponsive to antigen (anergic) in peripheral tissues or in lymph nodes. Regulatory T cells (Tregs) play an important role in peripheral tolerance. Central and peripheral lymphocyte tolerance are included under the broader umbrella of so-called “disease tolerance” strategies because they are mechanisms of limiting inflammation and preventing auto-immunity but do not directly influence pathogen burden. In this thesis, we refer to the broader definition of “disease tolerance” as mechanisms that support host fitness and survival during infection, not by directly targeting pathogen biology, but by shifting homeostasis to maintain tissue function during infection and inflammation (6).

It is important to note that tolerance mechanisms, like resistance mechanisms, represent a shift from normal homeostasis. The costs of overactive resistance mechanisms are well established. Examples include bystander damage from reactive oxygen species, delayed wound healing, and recognition of autoantigens like DNA- or RNA-binding proteins. The negative effects of excessive tolerance programs are comparatively under-appreciated, but include mutations due to imperfect DNA repair, fibrotic wound healing and, potentially, metabolic disorders like Type II diabetes. We can assume that long-term reliance on tolerance mechanisms must be maladaptive, otherwise they would be selected for homeostatic function.

This is an important consideration, as tolerance programs are receiving attention as therapeutic targets to interrupt the maladaptive consequences of acute inflammation (for example sepsis or influenza infection) without increasing susceptibility to pathogens. As discussed in the following sections, it is also important to consider how promoting tolerance biology may benefit the life cycle of pathogens, particularly those that have evolved a strategy for long-term persistence within a host (**Fig. 1.2**).

## Reinterpreting the immune response to *Toxoplasma* in the framework of disease tolerance

*Toxoplasma gondii* (*T. gondii*) is an obligate intracellular protozoan parasite that establishes life-long infection in a wide range of warm-blooded intermediate hosts, including rodents and humans. Three major strains dominate Europe and North America: types I, II, and III, which differ in virulence by several logs. Feline definitive hosts support *T. gondii* sexual recombination and shed millions of environmentally stable, highly infectious oocysts in feces. This confers a tremendous benefit for the parasite in terms of genetic diversity and dissemination potential, which suggests that rodents may be an important intermediate host for *T. gondii*, given the predator-prey relationship between the two host organisms.

Intermediate hosts are infected by ingesting *T. gondii* oocysts or tissue cysts, the so-called bradyzoite form, from a previously infected intermediate host. *T. gondii* invades the small intestine, converting to the rapidly dividing tachyzoite form and inducing inflammation (**Fig. 1.3**) (7). This process activates an immune response that is critical to the parasite's life cycle in two major ways. First, *T. gondii* infects and replicates within infiltrating immune cells (8). The parasite uses immune cells to disseminate systemically, reaching tissue sites that support chronic infection, including the brain, muscle, and other tissues (9). Second, chronic infection is defined by parasites shifting to a bradyzoite transcriptional program and clearance of most tachyzoites. This involves synthesis of a saccharide-rich parasite cyst wall which is necessary for the parasite to survive transit through the gastrointestinal tract of the next host (9, 10). Thus, without a robust immune response, the parasite kills the host before this shift occurs and the opportunity for transmission is limited.

In the mouse, *T. gondii* is recognized by innate immune sensors including Toll-like receptors, the NLRP1 and NLRP3 inflammasomes, and IFN- $\gamma$ -regulated GTPases (IRGs). Mice deficient in Toll-like receptor 11 (TLR11) or its signaling adaptor MyD88 fail to control parasite replication after intraperitoneal (i.p.) infection (11). Similarly, mice lacking the inflammasome effector caspases-1 and -11 die of parasite overgrowth early in chronic infection (12, 13). Disabling the IRG system (GTPases which identify modified intracellular membranes and target them for degradation) leads to rapid parasite expansion and host death in inbred laboratory mice in a manner that depends on parasite genetics. Type II *T. gondii*, the most frequently isolated type in Europe and North America, expresses alleles of the effector proteins ROP5 and ROP18 which make it susceptible to IRG-mediated clearance. Hypervirulent type I and hypovirulent type III *T. gondii* express alleles of *rop5* and *rop18* that inactivate IRGs at the parasite vacuole improving intracellular replication in many inbred

strains of mice (14, 15). However, some wild-derived mouse strains are able to restrict growth of hypervirulent type I parasites in an IRG-dependent manner, suggesting that the IRG restriction pathway has imparted an important selective pressure on both host and parasite evolution (16).

Innate immune recognition of *T. gondii* promotes IL-12 release, NK cell-mediated IFN- $\gamma$  production, and a Th1-polarized adaptive immune response (17, 18). The cellular mechanisms of these responses and the importance of CD8<sup>+</sup> cytotoxic T cell response for host survival have been reviewed extensively elsewhere (19, 20). Importantly, many cytokines central to this response have been shown to be necessary for parasite resistance. Specifically, mice deficient in IL-12 (21), IFN- $\gamma$  (22, 23), IL-6 (24), TNF- $\alpha$  (25), iNOS (26) or their receptors die from parasite overgrowth in acute infection or early chronic infection. Host haplotype also plays a dominant role in parasite resistance. BALB/c mice are resistant to infection and express the H-2L<sup>d</sup> MHC haplotype, which presents an immunodominant peptide from the dense granule protein GRA6 (27). In contrast, C57BL/6 mice have the H2b haplotype which presents ROP5, a lower abundance rhoptry protein that elicits a weak CD8<sup>+</sup> T cell response, resulting in worse parasite restriction (28).

Immune pathways involved in *T. gondii* resistance have been well-characterized (as noted above); however, a number of pathways relevant to disease tolerance have also been identified. Many of these are immune cell driven pathways that mitigate Th1-mediated immunopathology during *T. gondii* infection (**Table 1.1**). At acute infection, mice deficient in the immunoregulatory cytokine IL-10 had a similar liver parasite burden as wildtype mice, but died from a cytokine storm of IL-12, TNF- $\alpha$ , and IFN- $\gamma$  (29, 30) This phenotype could be reversed by depleting CD4<sup>+</sup> T cells (29), or by depleting IFN- $\gamma$  (31), implicating CD4<sup>+</sup> T cells and IFN- $\gamma$  as mediators of lethal pathology. More recently, Jankovic *et al* showed that T-bet<sup>+</sup>Foxp3<sup>-</sup> Th1 cells were a major source of IL-10 during chronic i.p. infection with 20 ME49 cysts. These IL-10-producing cells were required to limit fatal immunopathology during both acute and chronic infection (32). In 2005, Wilson *et al.* found that chronically infected IL-10<sup>-/-</sup> mice develop lethal *T. gondii* encephalitis without developing higher parasite loads, implicating IL-10 as a tolerance effector in the central nervous system (CNS) during *T. gondii* infection (33). Similarly, mice lacking IL-4 were more susceptible to *T. gondii* infection despite having slightly reduced cyst burdens and microglial nodules in the brain at chronic infection (34). These data suggest that tolerance mechanisms induced during *T. gondii* infection are critical to the survival of host. Although the mechanistic basis for the protective effect of IL-4 during *T. gondii* infection is currently unclear, it has been well studied in other systems. One example is the rodent helminth *Nippostrongylus brasiliensis*. *N. brasiliensis* burrows through the skin then migrates to the lung where it is coughed up and swallowed to complete its life cycle in the gastrointestinal tract. *N. brasiliensis* chitin promotes IL-4, which drives alveolar macrophages to limit lung pathology by producing insulin-like growth factor 1, resistin-like molecule- $\alpha$ , and arginase-1 (35). These effectors dampen inflammation and promote a wound repair response (36). While these pathways don't directly impact the parasite, it is important to note that the parasite's egg-laying stage occurs in the gut, after trans-lung migration. There may be significant selective pressure for *N. brasiliensis* to activate tolerance programs to promote

wound healing in the lungs (and subsequently host survival) so that the parasite has sufficient time to complete its life cycle to ensure transmission.

### **Immune cell-mediated mechanisms of tolerance during *T. gondii* infection**

In addition to their widely accepted role in pathogen clearance and adaptive immune response activation, innate immune cells play a critical role in mitigating tissue pathology during *T. gondii* infection. A 2013 study from Yasmine Belkaid's laboratory found that lamina propria-infiltrating neutrophils generated "casts" containing cells and extracellular DNA over regions of small intestine damaged by per oral (p.o.) *T. gondii* infection. These casts appeared to limit bacterial translocation into host circulation. Depleting neutrophils with an  $\alpha$ -Gr-1 antibody increased mortality without increasing parasite burden, indicating that the immune-commensal axis also plays an important role in disease tolerance during *T. gondii* infection (37). During p.o. *T. gondii* infection, lamina propria-infiltrating Ly6C<sup>hi</sup> monocytes were also shown to release IL-10 and prostaglandin E<sub>2</sub> (PGE<sub>2</sub>) which limited neutrophil-induced pathology. Administration of a PGE<sub>2</sub> analog during infection was sufficient to reduce intestinal tissue pathology and immune infiltration in the absence of monocytes without affecting parasite burden (38).

5-lipoxygenase is the rate-limiting enzyme in the synthesis of lipoxin A<sub>4</sub>, an eicosanoid mediator of the resolution phase of an inflammatory response (39). The importance of this pathway in disease tolerance during *T. gondii* infection is underscored by the observation that 5-lipoxygenase deficient mice succumbed to i.p. infection with 20 ME49 cysts by 35 days post-infection, despite harboring significantly fewer brain cysts than wild type mice. Death was associated with encephalitis, increased T cell infiltration into the brain, and elevated circulating IL-12, IFN- $\gamma$ , and TNF- $\alpha$  (40). IL-27 is another important mediator of tolerance during *T. gondii* infection. IL-27 is part of the IL-12 family of JAK-STAT signaling cytokines. WSX-1 knockout mice (which lack the IL-27 receptor) i.p. infected with 20 ME49 cysts succumbed to infection within 13 days. No change in parasite burden was detected between knockout and wildtype mice in peritoneal lavage fluid at 7 days post-infection, but knockout mice had elevated circulating IL-12, IFN- $\gamma$ , increased inflammation and necrosis in the liver and lungs, and hyperactive and hyperproliferative CD4<sup>+</sup> T cells in the spleen. Survival was partially rescued when CD4<sup>+</sup> T cells were depleted (41). Subsequently, the same group found that IL-27 limited production of IL-2 by activated CD4<sup>+</sup> T cells, implicating IL-27 receptor as a negative regulator of T cell responses during *Toxoplasma* infection (42). This conclusion was also supported by a 2012 study from the Hunter Laboratory where mice were p.o. infected with 100 ME49 cysts or i.p. infected with 20 cysts. IL-27 promoted development of Tregs at primary sites of infection, the small intestine or peritoneal cavity, respectively. IL-27<sup>-/-</sup> mice succumbed to acute infection, which could be partially rescued by adoptive transfer of Treg cells (43). Although this result is consistent with a tolerance strategy, parasite burden was not directly measured.

IL-2 is also important for Treg biology in *Toxoplasma* infection. Using p.o. infection, several groups have shown a transient, but significant loss of Treg function in the small

intestine (44, 45). Addition of IL-2 promoted Treg survival and prevented liver pathology, consistent with a role in disease tolerance in the liver. However, IL-2 treatment also resulted in a higher brain cyst burden (44). Similarly, Benson *et al.* found that IL-2 treated mice had more Tregs and significantly higher brain cyst burdens causing lethality (45). Whether the inability to restrict cerebral *Toxoplasma* infection in these studies was due to Treg-mediated suppression of effector T cells or a direct effect of IL-2 on naïve or effector T cell activity is unclear. However, directly targeting effector T cell responses has been shown to reduce tissue damage in a mouse model of ocular toxoplasmosis. Specifically, in the retina both infiltrating antigen-presenting cells (MHCII-expressing) and tissue resident retinal cells expressed PD-L1, the ligand for the T cell inhibitory receptor PD-1. PD-L1 expressing retinal cells were able to suppress splenic T cell proliferation *ex vivo* using a co-culture system with *Toxoplasma*-antigen loaded dendritic cells (46). These results suggest that retinal cells may be able to moderate local immune responses and reduce tissue damage by directly suppressing T cell activation in the eye. Cumulatively, these studies underscore the importance of targeting the T cell response both restrict parasite growth and to limit tissue damage.

### Host metabolic dysregulation in *Toxoplasma* infection

There is a growing appreciation that immune responses are intimately linked with shifts in metabolic homeostasis. This is a critical arm of pathogen resistance. For example, T cell activation requires a glycolytic burst; anorexia during infection mobilizes glycogen and lipid stores to support gluconeogenesis for the immune system; metabolic shifts are also used to sequester trace metals or nutrients to limit pathogen growth, often referred to as nutritional immunity (47, 48). Shifts in nutrient utilization are also important mediators of disease tolerance. For example, diet restriction improves fruit fly survival during *S. typhimurium* infection without affecting bacterial load (1).

There is a growing body of literature showing metabolic shifts in the host during acute *T. gondii* infection. However, a role for these shifts in disease tolerance has not been addressed specifically. Using Swiss-Webster mice infected p.o. with 8 cysts of the human-derived Type II strain BGD-1, one group reported reduced circulating cholesterol and HDL at 14 days post infection (49). Untargeted proteomic analysis of sera isolated from BALB/c mice infected per orally with 10 Type II Pru cysts showed increased circulating amino acids and reduced choline levels in the first 21 days of infection (50). The same group observed an increase in choline-derived phosphatidylcholine and phosphatidylethanolamine in the brains of infected mice (51). Choline is an essential dietary nutrient as the precursor of phosphatidylcholine and the neurotransmitter acetylcholine. Phosphatidylcholine is a major component of cell membranes and is necessary for the packaging and export of very-low-density lipoproteins (VLDL) from the liver (52). Together, these studies suggest that *T. gondii* infected mice shift towards amino acid and fat metabolism and away from glycolytic metabolism during *T. gondii* infection. This is consistent with a well-described, although transient, period of anorexia during acute infection in *T. gondii* infected mice which would induce such programs (53–56). In mice infected with *L. monocytogenes*, anorexia-induced ketogenesis protected tissues from oxidative stress, whereas glucose supplementation increased mortality. Interestingly, the opposite effect was observed with influenza infection, suggesting that the effectiveness of disease tolerance programs, like restriction mechanisms, depend on the pathogen (57). Similar experiments to

look at the role of glycolytic and beta-oxidative host metabolism in *T. gondii* will be necessary to determine if anorexia represents a host disease tolerance strategy, or if the parasite capitalizes on altered host metabolism for infection.

It is well established that scavenging host lipids is necessary for *T. gondii* survival *in vivo* and *in vitro*. For example, most of the cholesterol in *T. gondii* is derived from scavenged host LDL (58). Metabolic labeling with <sup>14</sup>C-acetate showed that *T. gondii* must scavenge fatty acid precursors from its host to synthesize its full range of lipids (59). Recent studies indicate that *T. gondii* competes with the host cell for lipids at the level of lipid droplet recruitment, mitochondrial interaction, and vesicular transport for intracellular survival (60–62). Further studies are warranted to determine whether host metabolic shifts that mobilize lipid stores at a systemic (rather than a cellular) level benefit *T. gondii*.

By contrast, there is growing evidence that altered metabolism has a long-term negative impact on the host during *T. gondii* infection. A series of studies by Arsenijevic *et al.* demonstrated that mice orally infected with 10 Me49 cysts undergo anorexia-associated hypermetabolism during acute infection. Nearly half of the infected cohort could not regain weight as they progressed to chronic infection. These ‘non-gainers’ harbored a higher parasite load than mice that regained weight and sustained the hypermetabolic phenotype along with elevated circulating inflammatory cytokines (54, 63). A subsequent study showed that non-gainers challenged with LPS had a more severe inflammatory response, worse pathology, and a longer rebound period than infected mice that gained weight (64). More recently, the Wohlfert lab showed that oral infection with 5 Me49 cysts causes acute weight loss in mice and inability to regain weight as chronic infection progresses (56). Surprisingly, muscle inflammation and myositis were driven by Tregs, a population classically associated with tolerance, suggesting that sustained tolerance programs may negatively impact the host.

Loss of total gut commensal diversity and a shift towards “pathobiotic” Gram negative species is also a well-established phenotype in acute *T. gondii* infection (37, 53, 65, 66). Although the precise composition of outgrowth species is animal colony-dependent, several groups have reported *E. coli* outgrowth (37, 66–68). It is highly plausible that shifts in commensals influence nutrient availability, in addition to playing a better-described role in influencing host immunity during *T. gondii* infection.

*T. gondii* interactions in metabolic organs may have important implications for host metabolism as well. The liver coordinates dietary nutrient uptake (bile acid recycling), availability and storage (fat and glycogen), and detoxifies the blood. Liver resident macrophages called Kupffer cells screen incoming blood for pathogens and intestinal microbes that leak from the gut during intestinal inflammation, including during *T. gondii* infection (37). *T. gondii* has been detected in the livers of mice at acute infection using bioluminescence, histology, and PCR in a number of studies using Type II strains (69–72). In the first week of infection, *T. gondii* has been observed replicating in hepatocytes near regions of inflammatory infiltrate and focal necrosis in both Swiss-Webster and BALB/c mice (73, 74). Interestingly, Atmaca *et al.* also reported an expansion of hepatic stellate cells during *T. gondii* infection (74). During inflammation, hepatic stellate cells differentiate into myofibroblasts and produce extracellular matrix which is consistent with the induction of a

tissue remodeling tolerance program during *Toxoplasma* infection. However, an important caveat with these studies is that they were performed with lethal doses of the hypervirulent Type I strain RH, raising the question of relevance to hepatic infection with strains that are more commonly found in mice or humans. Using clinically isolated Type II strains, *T. gondii* cysts were found in the livers of infected Swiss-Webster mice as late as 33 weeks post-infection, indicating that the liver may be a reservoir for chronic infection (75). This is consistent with clinical reports of *T. gondii*-negative transplant recipients who have developed toxoplasmosis after receiving livers from sera positive donors (76, 77). While there are no studies directly implicating *T. gondii* infection in the development of liver disease, approximately 30% of patients with chronic liver disease test sera-positive for *T. gondii* compared to 6% in control populations (78). These *T. gondii*-infected patients had significantly elevated circulating ALT and AST, which are clinical markers of liver damage, compared to uninfected patients with liver disease. Although these data do not imply causality, they are consistent with the interpretation that chronic *T. gondii* infection may negatively impact host fitness in diseases of co-occurrence.

*T. gondii* infection may also change the metabolic landscape of the liver. In a recent liver proteomics study, BALB/c mice intraperitoneally infected with 200 type II PYS tachyzoites had reduced signatures of fatty-acid oxidation proteins and an upregulation of cell death, inflammatory, and stress response pathways at 6 days post-infection (70). A parallel liver transcriptomics study reported down-regulation of gene families involved in lipid metabolism, cholesterol and bile synthesis, and amino acid metabolism, with an increase in inflammatory transcripts (79). Together, these studies provide evidence that *T. gondii* occupies a liver niche in acute and chronic infection and may directly contribute to shifts in liver metabolic homeostasis.

Adipose tissue depots are another important site of calorie storage and immune regulation. Fat tissues have long been described as an anti-inflammatory environment that can become inflamed, such as during obesity and diabetes. As better tools have become available to survey low pathogen loads in tissue, researchers have begun to appreciate the frequency of microbial translocation to and persistence in this nutrient-rich environment. *M. tuberculosis*, *T. brucei*, and facultative pathogen strains of *E. coli* have been detected in this niche, indicating that it serves as a reservoir of infection for many pathogens (80–82). More recently, *T. gondii* has been reported in the visceral fat following intraperitoneal infection and oral infection by bioluminescence assay and PCR (69). Interestingly, using a stage-specific reporter system, di Cristina *et al.* detected parasites in visceral fat based on their expression of SSR9, a gene product enriched during bradyzoite differentiation, suggesting that *T. gondii* was able to encyst within the adipose tissue (69). Future studies will be necessary to determine if fat is a long-term reservoir for *T. gondii*, and whether colonization of the fat is related to host metabolic shifts.

*T. gondii* has evolved sophisticated mechanisms to evade sterilizing immunity, yet activating a robust immune response is necessary to ensure host survival long enough for *T. gondii* encystation and transmission. (83, 84). Disease tolerance programs are adaptations to cell biology and metabolism that allow tissues to function in the harsh environment of an inflammatory response (85). However, tolerance adaptations must come at a cost to the host,

otherwise they would be selected for homeostatic use. The literature reviewed here are consistent with a model where tolerance programs initiated in acute *T. gondii* infection, including immune-microbiota interactions, T cell-mediated responses and metabolic shifts, fail to return to homeostasis in chronic infection. Emerging studies suggest that these shifts in homeostasis have sustained negative consequences for the host, including muscle wasting, and impaired responses to secondary immune stimuli (53, 54, 86, 87).

## Current Knowledge Gaps

When I joined the Ewald Lab in November 2016, there were several unanswered questions that converged to drive the work in this thesis. The most notable questions, and the ones we aimed to answer in this dissertation, are listed below.

1. Why do mice chronically infected with *T. gondii* maintain weight loss? Is sustained weight loss due to long-term anorexia, or due to hypermetabolism/defects in nutrient storage? Does this wasting benefit the *T. gondii* growth in some way?
2. What is the role of interleukin-1 receptor (IL-1R) signaling during *T. gondii* infection? Is IL-1R signaling necessary to control parasite growth the way other innate cytokines like IL-12, TNF- $\alpha$ , IFN- $\gamma$ , and IL-6 are?
3. What is the role of chronic innate inflammation in driving cachexia?
4. Are disease tolerance programs activated during *T. gondii* infection? If so, what is the nature of these tolerance pathways during acute and chronic infection?
5. What novel observations can be made from using an experimental model of chronic cachexia versus acute cachexia? Are these observations relevant to clinical cachexia?

## Summary of Dissertation

We aim to use chronic inflammation as the common thread connecting several disparate immunological paradigms into one story. By mechanistically probing an observation that has existed in the *T. gondii* field for decades, we emerged with a novel model for studying cachexia. We present a story showing that, although not required for restriction of the parasite, IL-1R is an active player during *T. gondii* infection, controlling host homeostasis during both acute and chronic stages of infection through modulation of cell death, cachexia, and fibrosis pathways.

**Chapter 3** introduces the observation that has been noted in several studies with *T. gondii* – that chronically infected mice lose a significant percentage of their weight during acute infection, and then maintain that weight loss indefinitely. Here, we characterize this muscle wasting as cachexia, a clinically-defined disease characterized by transient anorexia, chronic muscle and adipose tissue wasting, and elevated circulating cytokines. While acute oral *T. gondii* infection causes severe intestinal inflammation, this inflammation resolves during chronic cachexia, indicating that sustained intestinal inflammation is likely not the cause of sustained

wasting. Importantly, while oral *T. gondii* infection does induce sustained dysbiosis in the gut (namely an expansion of Clostridia), this dysbiosis is also insufficient to fully explain the sustained wasting observed. The work in this chapter establishes chronic *T. gondii* as a robust and viable experimental model for cachexia that will be drawn upon in the following two chapters.

**Chapter 4** addresses the role of the interleukin-1 (IL-1) signaling axis during *T. gondii* infection. As a lab with extensive experience in innate inflammatory signaling and inflammasome biology, we were particularly interested in revisiting the role of IL-1 receptor (IL-1R) signaling in the context of *T. gondii* infection, which has not been clearly defined in the literature. In this chapter, we make two important discoveries. The first is that while IL-1R signaling is dispensable for parasite control during both acute and chronic infection, it is important for promoting disease tolerance in the adipose tissue and liver during acute *T. gondii* infection, as IL-1R<sup>-/-</sup> mice experience exacerbated acute pathology compared to wildtype mice, despite having comparable parasite burden. We found that in the long run, IL-1R signaling leads to pathology in the form of cachexia. 1) We learned valuable basic information about the role of IL-1R biology in its ability to promote disease tolerance, 2) we discovered that *T. gondii*-induced cachexia is IL-1R dependent, and 3) made the observation that pathways that trigger disease tolerance pathways can become pathogenic if activated for too long.

In **Chapter 5**, we revisit the cachexia model introduced in **Chapter 3** and **Chapter 4**. We perform a thorough metabolic analysis to try to place *T. gondii*-induced cachexia within the context of other well-accepted (but shorter term) experimental cachexia models. Although many pathways that are central to acute cachexia models, such as lipolysis and insulin resistance, are not the main drivers of chronic *T. gondii*-induced cachexia, our long-term model provided us with a unique discovery. Chronic cachexia is associated with perivascular fibrosis in metabolic tissues like the liver, skeletal muscle, and adipose tissue. Liver and skeletal muscle fibrosis are dependent upon IL-1R signaling, and this discovery may provide a key to understanding how IL-1R is driving cachexia (**Chapter 4**) and may illuminate future strategies for targeting cachexia.

## Figures

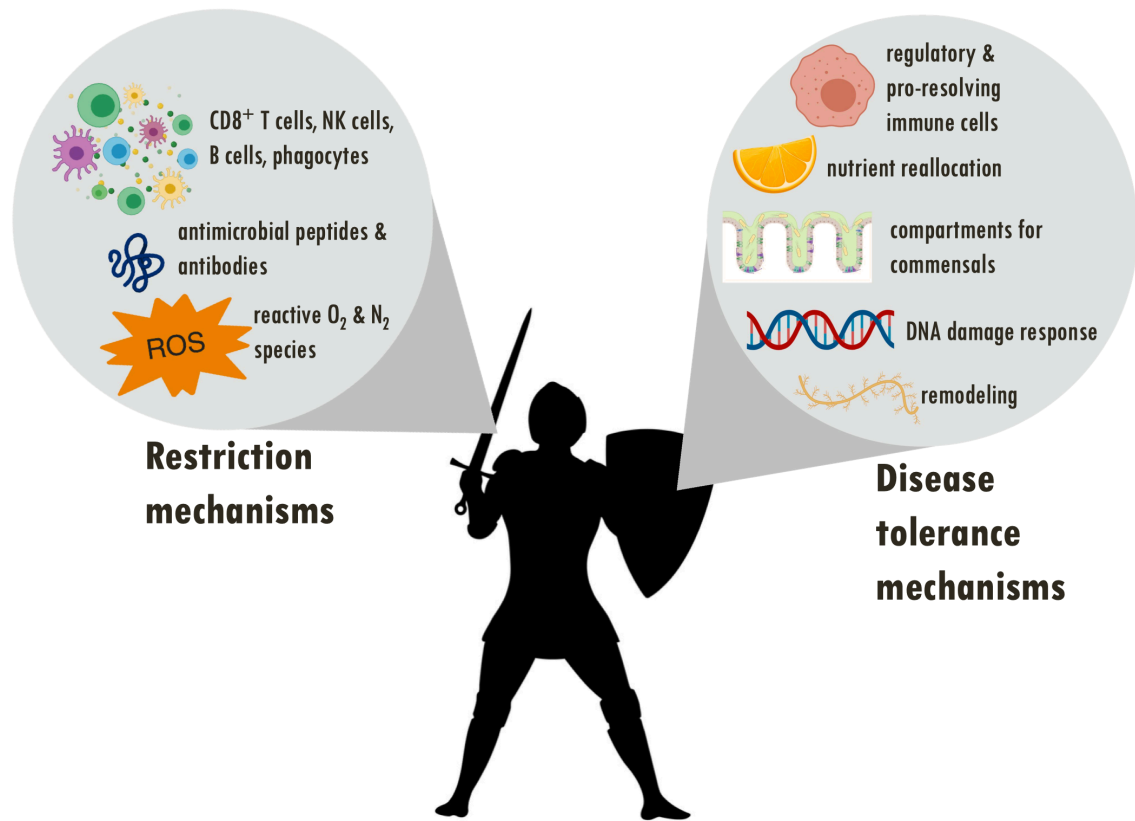


**Figure 1.1 Summary of restriction versus tolerance mechanisms.** While the immune system controls critical offensive tactics called restriction (or resistance) mechanisms that directly target the growth, spread, and/or virulence of invading micro-organisms, there is a growing appreciation for the evolution of disease tolerance mechanisms, that “shield” tissues and cells from damage that occurs during infection. Many of these pathways are parenchymal or stromal cell intrinsic, but are nonetheless essential for increased tolerance, recovery from, and survival of infectious insults.

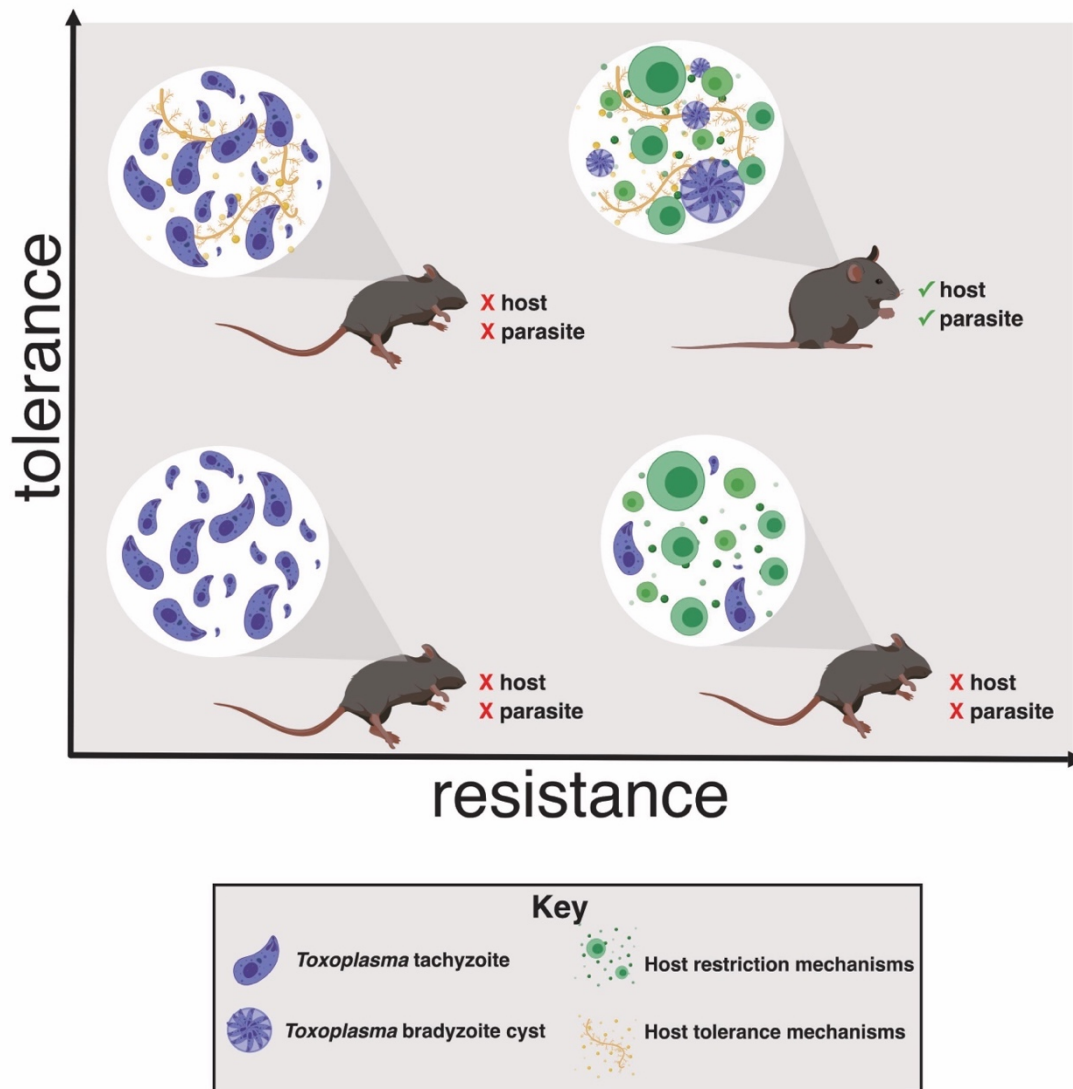


**Figure 1.2 *Toxoplasma gondii* induces host tolerance and resistance mechanisms in successful infections.** In the absence of a strong restrictive immune response the host succumbs to *Toxoplasma* overgrowth early in infection (left quadrants). Without tolerance mechanisms the host is susceptible to inflammation-induced pathology, even if parasite replication effectively restricted (lower right quadrant). Both resistance and tolerance mechanisms are necessary for host survival (upper right quadrant). This balance also benefits *Toxoplasma* by ensuring that the host survives long enough to enable bradyzoite cyst differentiation, a requirement for transmission to another host

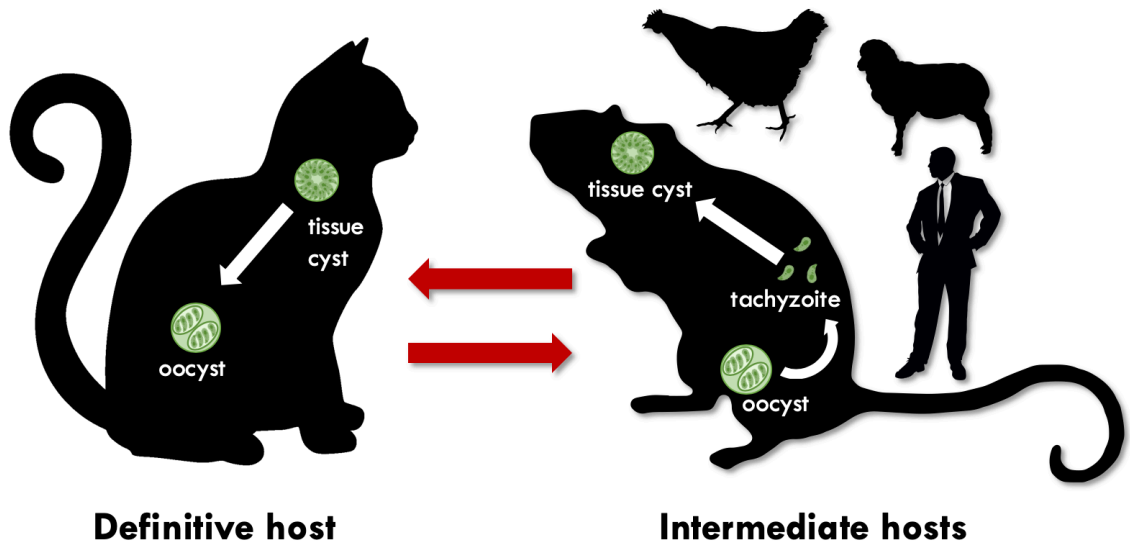


**Figure 1.3 Summary of *T. gondii* life cycle.** Infection of an intermediate host with *T. gondii* occurs when this host ingests parasite oocysts shed by a cat or tissue cysts found in another infected host. During acute infection, the parasite transitions to its fast-growing tachyzoite phase, where it spreads throughout the body and induces a robust immune response. The host immune system clears the majority of the parasites, although some will linger and transition to their slow-growing bradyzoite phase, where they are encased within a protective tissue cyst. From here, the parasite can cycle between intermediate hosts, or can be ingested by a feline, its definitive host, where it can undergo sexual recombination.

**Table 1.1 Summary of literature describing immunoregulatory pathways during *Toxoplasma gondii* infection.**

Observation	Ref.
IL-10 <sup>-/-</sup> mice die of acute encephalitis during <i>Toxoplasma</i> infection, associated with elevated cytokine levels, but not with enhanced parasite proliferation	Gazzinelli, 1996
IL-4 <sup>-/-</sup> mice succumb during acute <i>Toxoplasma</i> infection despite having fewer circulating parasites, but chronic IL-4 suppresses the restriction response, leading to increased pathogen burden and pathology	Roberts, 1996
Mice deficient in 5-lipoxygenase (the enzyme responsible for generating lipoxin A <sub>4</sub> ) succumb to otherwise sublethal doses of <i>Toxoplasma</i> , have elevated circulating IL-12, IFN-γ, and TNF-α, and have increased T cell infiltration, despite harboring lower cyst burdens than WT mice	Aliberti, 2002
Mice lacking the IL-27 receptor have enhanced mortality and CD4 <sup>+</sup> mediated tissue damage, independently of parasite burden during oral <i>Toxoplasma</i> infection	Villarino, 2003
Chronic IL-10 is required to limit fatal immunopathology mediated by CD4 <sup>+</sup> T cells in the brain during <i>Toxoplasma</i> infection	Wilson, 2005
IL-10 is required to limit fatal immunopathology at acute and chronic <i>Toxoplasma</i> infection. In this context, it is primarily produced by T-bet <sup>+</sup> Foxp3 <sup>-</sup> Th1 cells.	Jankovic, 2007
IL-27 signaling promotes a subset of Tregs that limit intestinal pathology and improve host survival during oral <i>Toxoplasma</i> infection	Hall, 2012
Lamina propria-infiltrating Ly6C <sup>hi</sup> monocytes release IL-10 and PGE <sub>2</sub> that limit neutrophil-induced tissue pathology in oral <i>Toxoplasma</i> infection	Grainger, 2013
Gut infiltrating neutrophils create multicellular casts to prevent bacterial translocation, improving host survival independently of parasite burden	Molloy, 2013

## Chapter 2: Materials and Methods

### Mouse strains/husbandry

CBA/J, BALB/cJ, C57BL/6, IL-1R<sup>-/-</sup> (B6.129S7-*Il1r1<sup>tm1Imx</sup>*), mice were purchased from Jackson Laboratories and IL-1 $\alpha$ <sup>-/-</sup> (88) and IL-1 $\beta$ <sup>-/-</sup> (89) mice were a gift from John Lukens at the University of Virginia. Mice receiving hepatic vagotomy (VAGOX) or sham surgery were purchased from Charles River. Mice were bred and housed and treated in accordance with the University of Virginia Institutional Animal Care and Use Committee AAALAC and IACUC protocol #4107-12-18.

### Infections

To generate cysts, 8-10 week female CBA/J mice were infected with 3-10 Me49 or Me49 stably expressing green fluorescent protein and luciferase (Me49-GFP-luciferase) bradyzoite cysts by intraperitoneal injection. 4–8 weeks following infection, mice were euthanized with CO<sub>2</sub> and brains were harvested, homogenized through a 70  $\mu$ m filter, washed 3 times in PBS, stained with dolichos biflorus agglutinin conjugated to either FITC or rhodamine (Vector labs) and the number of cysts were determined by counting FITC-positive cysts at 20x magnification using an EVOS FL imaging system (Thermo Fisher). Cysts were diluted to 50 cysts/mL in sterile PBS. 10-14 week male mice (unless otherwise noted) were infected with 10 Me49 or Me49-GFP-luciferase bradyzoite cysts by intraperitoneal infection (10 cysts/200 $\mu$ L dose, injected with a 1 mL tuberculin syringe, 25G x 5/8", Monoject by Covidien). Prior to infection, mice were cross-housed on dirty bedding for two weeks to normalize commensal microbiota. At the end of the experiment, mice were fasted for 4 hours and then euthanized by CO<sub>2</sub> (mice were not fasted for any experiments that only looked at inflammation and not at any metabolic parameters).

Chronic parasite burden was determined by dolichos staining, counting at 10X magnification (cyst diameter measured in Fiji) (53); or by qPCR of *T. gondii* 529bp Repeat Element (RE) compared to mouse beta actin as described (90) and analyzed using the  $\Delta$ Ct method. Brain DNA was extracted with TRIzol Reagent (Invitrogen) and used at 30 ng DNA per qPCR reaction (**Chapter 4**) or was isolated as described (91), and used at 100 ng DNA per qPCR reaction (**Chapter 5**). Adipose DNA was isolated by NucleoSpin DNA Lipid Tissue kit (Machery-Nagel), and used at 10-30 ng DNA per qPCR reaction. Liver DNA was isolated as described (91), and used at 500 ng DNA per qPCR reaction. qPCR on the Peyer's patches was performed by homogenizing flash frozen tissue and isolating RNA using Trizol. RNA. For each sample 10 $\mu$ g of RNA was digested and converted to cDNA using the qMax cDNA Synthesis Kit (Accuris). 7.2 $\mu$ L of cDNA was used in each 20 $\mu$ L qPCR reaction. reverse transcribing The following Taqman primer/probes were used: 529bp Repeat Element (RE) *forward*: 5'-CACAGAAGGGACAGAAGTTCGAA-3'; *reverse*: 5'-CAGTCCTGATATCTCTCCTCCAAGA-3'; *probe*: 5'-CTACAGACGCGATGCC-3' (IDT, (90)); mouse beta actin: Mm02619580\_g (ThermoFisher Scientific). qPCR was performed on a QuantStudio6 instrument (Applied Biosystems).

**High Fat Diet:** At four weeks post-infection, mice were shifted a high fat diet (D12451 (Research Diets, Inc.), 20% kcal protein, 35% kcal carbohydrates, and 45% kcal fat) or

remained on standard mouse chow (Teklad) and were fed ad libitum for the duration of the experiment (indicated on figure legends).

**Anakinra:** Mice were injected i.p. with 50 mg/kg/day anakinra (Kineret, Swedish Orphan Biovitrum) using insulin syringes. Anakinra was diluted fresh every day in sterile PBS to 1 mg/mL. Mice were either injected once per day or twice (every 12 hours), as noted in the figure legends.

**Atglistatin:** Atglistatin (Cayman Chemical Company) was resuspended at 2.5 mg/mL in 100% ethanol and was stored at -30°C as stock. Stock was diluted fresh into a working stock of 200 µg/mL (diluted in sterile PBS), and was injected daily at 1mg/kg/day with an insulin syringe.

### **Assessment of food intake**

To measure food intake, mice were housed on chip bedding and food was weighed daily. When animals began showing signs of sickness (1 week post infection) several pieces of food were placed in dishes on the floor of the cage which encouraged animals to eat without having to reach for the hopper. After 24 hours the food was removed from the hopper, the bedding was sifted to find intact pieces of food, and all remaining food was weighed. The 24-hour difference in food weight was normalized to the total body weight of all mice in the cage to determine the amount of food eaten. Of note, interventions including addition of moistened food, high caloric supplements or intra peritoneal injection of fluids were not implemented in this study. Extra nesting supplies were maintained in cages for the duration of the study.

### **Clinical scoring**

Mice were monitored daily for 1) ruffled fur, 2) hunching, 3) >20% weight loss, 4) squinting/eye discharge, 5) failure to move on an open hand. Mice that scored 5/5 based on these parameters were immediately euthanized. In chronic cachexia, most animals retain a sickness score of 1–2 due to weight loss and/or fur ruffling. Roughly 1/100 mice would be found dead in a cage, however, as this often occurred after the resolution of peak sickness, it is likely that these deaths were due to invasion of the parasite in a critical region of the brain leading to rapid lethality unrelated to other aspects of disease.

### **Body temperature measurements**

Mice were anesthetized with isoflurane at 10 days post-infection, and subcutaneously injected with temperature micro-transponders (Bio Medic Data Systems, Seaford, DE). Temperature was monitored daily (at the same time of day) using a telemetric reader.

### **Bioluminescence imaging and quantification**

For bioluminescence imaging (BLI), mice were injected in the intraperitoneal cavity with 200 µL of a 15 mg/mL stock solution of luciferin (Xenogen), anesthetized with isoflurane and imaged for 4 minutes on an IVIS system. To image organs, mice were injected 5 minutes prior to euthanasia, after which the organs were harvested and imaged for 4 minutes. Images were analyzed with LivingImage software and ImageJ.

### **Tissue weights and body mass composition**

Body mass composition was determined by using the EchoMRI™-100H Body Composition Analyzer. At the experimental end points, mice were euthanized with CO<sub>2</sub>. Blood was isolated by cardiac exsanguination. Abdominal subcutaneous white adipose depots, epididymal visceral white adipose depots, supraclavicular brown adipose depots, quadriceps, tibialis anterior, EDL and gastrocnemius muscles were isolated and placed in pre-weighed 2mL tubes for weighing and flash freezing. For small intestine, a Peyer's Patch containing regions of the distal jejunum or ileum were identified by eye. A 2cm section surrounding the Peyer's patch (or patches) was excised. Sections immediately adjacent to but excluding a Peyer's patch were harvested as well.

### **Bomb calorimetry and fecal lipid assessment**

Mice were individually housed for 24 hours at 10 weeks post-infection. Fecal pellets were collected every 2 hours during the daytime and flash-frozen. Pellets were lyophilized and then sent to University of Texas Southwestern Metabolic Phenotyping Core for bomb calorimetric analysis. For fecal lipid analysis, mice were singly-housed on isopads for 3 days. Stool was collected daily and stored at 4°C until time of analysis. Lipid extraction and measurement was according to previously published protocols (92).

### **Sera metabolomics and lipidomics**

At 7 weeks post-infection, isoflurane-anesthetized mice were retro-orbitally bled and sera was flash frozen and sent to the West Coast Metabolomics Center (UC Davis) for untargeted mass spectrometry analysis using the primary metabolism assay (GC/TOF MS) or the complex lipids (CSH-QTOF MS) assay.

### **CLAMS metabolic monitoring**

At 5 weeks post-infection, mice were individually housed in Oxymax cages for 5 days (CLAMS, Columbus Instruments, Columbus, OH) at the University of Virginia. Mice were maintained at 25°C with 12 hour light/dark cycles and had free access to food and water in all conditions. The first 24 hours of data was considered an acclimation period and excluded from analysis. 16-point rolling averages across the remaining data were used to visualize data across the recorded time periods.

### **Cytokine measurements**

Sera cytokines were measured by Luminex (courtesy of University of Virginia Flow Cytometry Core or the Stanford Human Immune Monitoring Core) or ELISA (Invitrogen unless noted). Tissue homogenate cytokines were measured by ELISA: IFN- $\gamma$  (88-7314); TNF- $\alpha$  (88-7324); IL-1 $\alpha$  (88-5019-88); IL-6 (eBioscience 50-112-8863); IL-1 $\beta$  (88-7013-88); IL-10 (88-7105-86); IL-1Ra (R&D DY480); TGF- $\beta$  (88-8350-22), and are normalized to total protein per well.

### **16S ribosomal sequencing and diversity analysis**

Fresh fecal pellets were collected from mice at the time points indicated and flash frozen. DNA was isolated using the MoBio PowerSoil Kit and barcoded primers were used to amplify the V4 region of the 16S rRNA gene. MoBio UltraClean-htp 96 Well PCR Clean-Up Kit was used to purify PCR products which were then quantified using Quant-iT ds DNA Assay Kit. 184 samples were pooled at equimolar ratios. 16S ribosomal sequencing was performed by the Mayo Clinic using a single lane of the Illumina HiSeq. Community composition and beta

diversity were determined using QIIME and beta diversity was visualized using EMPeror (93, 94) T-tests were performed using GraphPad Prism and corrected for multiple hypothesis using the FDR approach.

### **Sorting and culturing of primary hepatic stellate cells**

Primary murine hepatic stellate cells were isolated as previously described.<sup>42</sup> Following sorting on a BD Influx Cell Sorter in the University of Virginia Flow Cytometry Core, cells were seeded onto fibronectin coated 4 kPa polyacrylamide hydrogels (Matrigen) and stimulated with 10 ng/mL recombinant mouse IL-1 $\alpha$  (R&D), 10 ng/mL recombinant mouse TGF- $\beta$  (R&D), or media alone for 48 hours, after which hydrogels were fixed with 4% paraformaldehyde and stained with phalloidin-488 (Invitrogen) and anti  $\alpha$ -SMA antibody (Invitrogen, clone IA4). Cells were mounted with ProLong Diamond Anti-Fade mountant (Thermo Fisher Scientific), and imaged at room temperature on a Nikon Eclipse Ti microscope with an UltraView VoX imaging system (PerkinElmer) using a Nikon N Apo LWD 40X water objective (numerical aperture: 1.15) and cell area and  $\alpha$ -SMA intensity were determined using Volocity software.

### **Stimulation and staining of mouse embryonic fibroblasts**

Transformed mouse embryonic fibroblasts were cultured in (DMEM, 10% FBS, 1% L-glutamine, 1% penicillin/streptomycin, 1% HEPES, 1% sodium pyruvate) and used between passage 3-10.  $1 \times 10^4$  cells were seeded overnight onto poly-D-lysine coated glass coverslips in 24-well plates and then stimulated with 10 ng/mL recombinant mouse IL-1 $\alpha$  (R&D), 10 ng/mL recombinant mouse TGF- $\beta$  (R&D), or media alone for 48 hours. Coverslips were fixed in 4% paraformaldehyde for 10 minutes, permeabilized with 0.1% Triton X-100 for 15 minutes, blocked in 1% BSA for 30 minutes, and then stained overnight at 4°C with anti  $\alpha$ -SMA antibody (Invitrogen, clone IA4). The next day, coverslips were stained for 1 hour at room temperature with phalloidin-eFluor660 (eBioscience) or donkey anti-mouse-AF594 (Jackson ImmunoResearch), and mounted onto slides with Vectashield Mounting Medium containing DAPI (Vector Laboratories). Coverslips were imaged on a Zeiss Imager M2 microscope (Carl Zeiss) with an AxioCam Mrm camera (Carl Zeiss) using a 20X objective (numerical aperture: 0.80) and ZenBlue software (Carl Zeiss). Cell area was determined by manually tracing cells in Fiji software. For serum starvation experiments, 2,500 MEFs/well were seeded into a 96 well plate overnight and then treated for 48 hours with cytokine in media containing either 10% or 1% serum. At the end of the 48-hour period, cell proliferation and viability were determined using CellTiter-Glo reagent (Promega).

### **Western blots**

Flash-frozen tissues were homogenized by bead-beating in lysis buffer (25 mM Tris-HCl, 15 mM NaCl, 1 mM MgCl<sub>2</sub>, 2.7 mM KCl, 1 mM EDTA, 1 mM EGTA, 1 mM DTT, 1% Triton-X, and protease and phosphatase inhibitors (Roche EDTA-free protease inhibitor mini and Pierce™ Phosphatase Inhibitor Mini Tablets), and centrifuged. Protein concentration was measured using via BCA concentration (Pierce BCA Protein Assay Kit, Cat# 23225). Protein concentrations were equalized by diluting with 2X Laemmli buffer and lysate was then boiled at 95°C for 3 minutes. All protein samples were separated on 10% bis-Tris gels by SDS-PAGE and then transferred to PVDF membranes membranes using Trans-Blot Turbo Transfer System (Biorad). The membranes were blocked in 2% ECL Prime Blocking Reagent (GE Amersham RPN418) in TBS-T for 30 min, incubated in primary antibody for 1 hour at

room temperature, washed 3X in TBS-T, incubated in secondary antibody for 30 min at room temperature, washed 3X in TBS-T and then imaged on either the Bio-Rad ChemiDoc Imager (for HRP secondary antibodies) or the Leica Typhoon (for fluorescently-conjugated secondary antibodies). The following primary antibodies were used to probe protein levels by immunoblotting: anti-GAPDH (Cell Signaling Technology, clone D16H11), anti- $\beta$ -Actin (Santa Cruz Biotechnology, clone 1), anti- $\alpha$ -SMA (Santa Cruz Biotechnology, clone CGA7), anti-pACC $\alpha$  (Santa Cruz Biotechnology, clone F-2), anti-ATGL (Santa Cruz Biotechnology, clone F-7), anti-HSL (Cell Signaling Technology, #4107), anti-phospho-HSL (Ser660) (Cell Signaling Technology, #4126), anti-AKT (Cell Signaling Technology, clone C67E7), and anti-phospho-AKT (Cell Signaling Technology, clone D9E). The following secondary antibodies were used: goat anti-rabbit Cy5 (Jackson ImmunoResearch, 705-175-147), goat anti-mouse HRP (Thermo Scientific, PA1-28664). All primary antibodies were used at a 1:1000 dilution and secondary antibodies at a 1:10,000 dilution in 2% ECL Prime Blocking Reagent. The stripping protocol used was adapted from Yeung and Stanley, 2009. Briefly, blots were washed 2 times with TBS-T, incubated twice for 5 minutes each in GdnHCl stripping solution at room temperature (6 M GdnHCl, 0.2% NP-40, 0.1 M  $\beta$ -mercaptoethanol, 20 mM Tris-HCl), washed 4 times (3 minutes each) in wash buffer at room temperature (0.14 M NaCl, 10 mM Tris-HCl, 0.05% NP-40), and then blocked in 2% ECL Primer Blocking Reagent in TBS-T. Stripped blots were re-probed following the protocol described.

### **qPCR**

Flash frozen tissues were homogenized in TRIzol reagent (Invitrogen) by bead-beating and RNA was extracted following manufacturer's instructions. Following genomic DNA digestion and reverse transcription, RNA was run on a QuantStudio 6Flex (Applied Biosystems) using ABI Power SYBR Green PCR Master Mix (Applied Biosystems) using the primers listed in the table below. For *IL-1R* gene expression, the following PrimePCR probe sets were used with IQ Power-Mix (Bio-Rad): *IL-1R* (qMmuCIP0032372) and *ActB* (qMmuCEP0039589). Data were analyzed using the  $\Delta$ Ct method (relative to a housekeeping gene), and then normalized to the mean of the  $\Delta$ Ct of uninfected mice to get fold change. qPCR was performed on a QuantStudio6 instrument (Applied Biosystems) or a CFX-96 (Bio-Rad).

<b>SYBR Green Primer Sets</b>		
<b>Gene</b>	<b>Forward Primer (5'-3')</b>	<b>Reverse Primer (5'-3')</b>
<i>ActB</i>	GGCTGTATTCCTCCATCG	CCAGTTGGTAACAATGCCATGT
<i>Ucp-1</i>	ACTGCCACACCTCCAGTCATT	CTTTCCTCACTCAGGATTGG
<i>Prdm16</i>	GAAGTCACAGGAGGACACGG	CTCGCTCCTCAACACACCTC
<i>PGC1a</i>	ACAGCTTCTGGGTGGATTG	TGAGGACCGCTAGCAAGTTT
<i>Cidea</i>	TGCTCTTCTGTATCGCCAGT	GCCGTGTTAAGGAATCTGCTG
<i>C/ebp<math>\beta</math></i>	TGACGCAACACACGTGTAAGT	AACAACCCCGCAGGAACAT
<i>Pparg-2</i>	TCGCTGATGCACTGCCTATG	GAGAGGTCCACAGAGCTGATT

### **Flow Cytometry**

Liver and epididymal visceral white adipose tissues were prepared for flow cytometry after cardiac perfusion with 10 mL HBSS (5 mM HEPES, 0.5 mM EDTA), as described (95). Following mechanical disruption, tissue was Liberase (Roche)-digested for 30 minutes at 37°C

(shaking at 130 RPM) and filtered. Cells were separated on a 40% iodixanol density gradient by centrifugation at 1038 g for 25 minutes (no brake). Cells were blocked with anti-CD16/32, stained with Zombie Aqua (Biolegend) and antibodies (Biolegend): F4/80-FITC (BM8), Ly6C-PerCP/Cy5.5 (HK1.4), CD19-PE/Cy7 (6D5), CD11c-APC (N418), CD11b-AF700 (c1/70), I-A/I-E-APC/Cy7 (M5/114.15.2), CD45-PacBlue (30-F11), Ly6G-BV605 (1A8), CD3e-FITC (145-2C11), CD62L-PE-dazzle (MEL-14), CD8a-PerCP/Cy5.5 (53-6.7), PD-1-PE/Cy7 (29F.1A12), CD4-APC (GK1.5), CD44-BV605 (IM7). Beckman Coulter CytoFLEX and FlowJo were used to assess immune cell populations using the following gating strategy: Cells, singlets, live cells, CD4<sup>+</sup> T cells (CD45<sup>+</sup>CD3e<sup>+</sup>CD4<sup>+</sup>), CD8<sup>+</sup> T cells (CD45<sup>+</sup>CD3e<sup>+</sup>CD8<sup>+</sup>), B cells (CD45<sup>+</sup>CD19<sup>+</sup>), Kupffer cells (liver only, CD45<sup>+</sup>F480<sup>hi</sup>CD11b<sup>lo</sup>), macrophages (CD45<sup>+</sup>F480<sup>int</sup>CD11b<sup>hi</sup>Ly6c<sup>lo</sup>), inflammatory monocytes (CD45<sup>+</sup>F480<sup>int</sup>CD11b<sup>hi</sup>Ly6c<sup>hi</sup>), dendritic cells (CD45<sup>+</sup>F480<sup>int</sup>CD11c<sup>+</sup>MHCII<sup>+</sup>), and neutrophils (CD45<sup>+</sup>F480<sup>int</sup>CD11b<sup>+</sup>Ly6G<sup>+</sup>SSC<sup>hi</sup>).

### **Histology and Immunohistochemistry**

Tissues were fixed overnight in 4% paraformaldehyde at 4°C and paraffin-embedded and sectioned (by the University of Virginia Research Histology Core or the Stanford Department of Comparative Medicine Histology Core), and stained with hematoxylin and eosin, Von Kossa Stain Kit (American Mastertech Scientific), picosirius red, or anti-cleaved caspase-3 (Cell Signaling Technology, staining performed by the University of Virginia Biorespository and Tissue Research Facility).

**Jejunum pathological scoring:** Regions of the jejunum were selected based on the presence of a Peyer's patch. Adjacent regions of the Jejunum (not containing a Peyer's patch) were also harvested. Every other section was stained with H&E. A semi-quantitative scoring system of 1 to 5, (1 = no significant lesion, 2 = mild, 3 = moderate, 4 = marked, 5 = severe) was used to evaluate the severity of any lesions. Parameters included inflammatory cellular infiltrate, loss of Peyer's patch organization, villi destruction and villi shortening. For detailed scoring, each tissue section was blinded, divided into fields of view at 40X magnification, and an inflammation score was assigned to each field of view.

**vWAT pathological scoring:** H&E samples were scored for necrosis by a blinded pathologist using the following scale: 1 = 1%-25%, 2 = 26%-50%, 3 = 51%-75%, 4 = 76%-100% of the area affected. Inflammatory lesion diameter was measured with Fiji.

**Caspase-3 Quantification:** Caspase-3 staining was determined using the color deconvolution Fiji plug-in (96) and thresholded on negative controls.

**Picosirius red quantification:** Slides were imaged on an Olympus BX51 microscope with an Infinity 1 camera (Lumenera) for 5-10 blinded fields of view were acquired per mouse. To quantify percent area, images thresholded in the green channel on Fiji (97), and percentage of positive pixels per area was determined.

### **Immunofluorescence and microscopy**

Following euthanasia and harvest, tissues were fixed overnight in 4% paraformaldehyde at 4°C, after which they were submerged in 30% sucrose in PBS, embedded in Tissue-Tek®

O.C.T. Compound (VWR) and flash frozen on dry ice. Samples were submitted to the Research Histology Core at the University of Virginia for sectioning. When noted, paraffin-embedded sections were used. Slides were imaged on a Zeiss LSM 880 confocal microscope (Carl Zeiss) and images were processed in Fiji.

***T. gondii*:** Unstained sections were used to quantify *T. gondii* load. To deparaffinize, sections were passed twice through xylene, then through 100% ethanol, 80% ethanol and 50% ethanol and distilled water for 3 minutes each. Antigen retrieval was performed by incubating sections in sodium citrate buffer brought to a boil in the microwave and incubated for 15 minutes in a vegetable steamer (10mM Citric Acid, 0.05% Tween-20, pH6.0). Slides were cooled, washed once in PBS and outlined with a Pap pen to perform staining. Samples were blocked for 30 minutes in 5% goat sera in PBS. *T. gondii* was labeled with mouse anti-*Toxoplasma*-FITC (Thermo Scientific Clone J26A) at a concentration of 1  $\mu\text{g}/\mu\text{L}$  in 5% goat sera overnight. Samples were washed 3x in PBS, mounted in Vectashield with DAPI (Vector Laboratories) and imaged on an Olympus BX60 upright fluorescence microscope with a 4x, 10x, 40x or 100x objective. To quantify parasite load, each section was subdivided identically to the adjacent H&E section. The threshold of parasite signal at 488nm was determined by comparison to uninfected samples, each image was converted to binary and the dark pixels were counted using ImageJ.

**ASC/CD45 and TUNEL staining:** Following deparaffinization, slides were antigen-retrieved with boiling sodium citrate buffer (10 mM sodium citrate buffer + 0.05% Tween-20, pH 6.0), blocked and permeabilized for an hour (2% donkey serum, 2% goat serum, 0.1% Triton-X, 0.05% Tween-20), and stained overnight at 4°C with rabbit anti-mouse ASC (Santa Cruz, N-15), or rat anti-mouse CD45 (Biolegend, 30-F11) diluted 1:50 in blocking buffer. The next morning, following washing, samples were incubated for one hour at room temperature in secondary antibody diluted 1:200 in blocking buffer (donkey anti-rabbit AF594 (Jackson ImmunoResearch, 711-585-152) or goat anti-rat IgG AF647 (Life Technologies, A21247)). Following washing, samples were incubated for 5 minutes in 10  $\mu\text{g}/\text{mL}$  DAPI, washed 3 times in PBS, and mounted in Vectashield (Vector Laboratories). Click-iT™ Plus TUNEL Assay (Invitrogen) was used for TUNEL staining, following manufacturer's instructions. Slides were imaged on a Zeiss LSM 880 confocal microscope using the 40X or 63X objectives.

**IL-1 $\alpha$ :** Slides were blocked for 1 hour at room temperature in blocking buffer (2% donkey serum, 2% goat serum, 0.1% Triton-X, 0.05% Tween-20). Samples were incubated overnight at 4°C in primary antibody diluted in blocking buffer (R&D AF-400-NA goat anti-IL-1  $\alpha$ , 1:50; Novus Biologicals NB600-408 rabbit anti-collagen I, 1:50; Biolegend 103101 rat anti-CD45, 1:50). The next morning, samples were washed 3 times in PBS/0.1% Triton-X and were incubated in secondary antibody (donkey anti-goat Dylight 594, Novus NBP1-75607, 1:500; Invitrogen A21245 goat anti-rabbit AF647, 1:300; and donkey anti-rat AF488, 1:500), for 1 hour at room temperature, diluted in blocking buffer. Samples were stained with DAPI, mounted, and imaged as described above.

**IL-1R:** Antigen retrieval was performed as described above. Slides were blocked for 1 hour at room temperature in 2% donkey serum and CD16/CD32 (Biolegend, Clone 93, 1:200). Samples were incubated overnight at 4°C in primary antibody diluted in blocking buffer (R&D

AF771 goat anti-IL-1R, 1:50; Novus Biologicals NB600-408 rabbit anti-collagen 1, 1:50). The next morning, samples were washed 3 times in PBS/0.1% Triton-X and were incubated in secondary antibody (Novus NBP1-75607 donkey anti-goat Dylight 594, 1:250 and LifeTech A21206 donkey anti-rabbit AF488, 1:200), and the directly conjugated  $\alpha$ -SMA primary (Novus Biologicals NBP2-34760APC, 1:400) for 1 hour at room temperature, diluted in PBS/0.1% Triton-X. Samples were stained with DAPI, mounted, and imaged as described above.

**Collagen I/III:** Samples were antigen-retrieved as described above. They were blocked for 1 hour at room temperature in blocking buffer (2% donkey serum + 2% goat serum). Samples were incubated overnight at 4°C in primary antibody diluted in blocking buffer (Biolegend 103101 rat anti-CD45, 1:50; Novus Biologicals NB600-408 rabbit anti-collagen I, 1:50; Novus Biologicals NB600-594 rabbit anti-collagen III, 1:50). The next morning, samples were washed 3 times in PBS + 0.1% Triton-X and were incubated in secondary antibody (Invitrogen A-11007 goat-anti rat AF594, 1:500; LifeTech A21206 donkey anti-rabbit AF488, 1:200), and the directly conjugated  $\alpha$ -SMA primary (Novus Biologicals NBP2-34760APC, 1:400) diluted in PBS + 0.1% Triton-X for 1 hour at room temperature. Samples were stained with DAPI, mounted, and imaged as described above.

### **Statistical analysis**

Statistics were performed using GraphPad Prism 8. For comparison of two groups, two-tailed unpaired Student's t-tests were performed with a confidence level of 95%. The Holm-Sidak test was used to correct for multiple comparisons. If statistical outliers were removed using the ROUT method (Q=1%), it is indicated in the figure legend. Statistical significance threshold was set at  $P \leq 0.05$ . All data are presented as the mean  $\pm$  SEM.

## Chapter 3: *Toxoplasma gondii* infection triggers chronic cachexia and sustained commensal dysbiosis in mice

**The text and figures included in this chapter have been adapted from the following publication:** Hatter, J.A., Kouche, Y.M., Melchor, S.J., Ng, K., Bouley, D.M., Boothroyd, J.C., & S.E. Ewald. 2018. *Toxoplasma gondii* infection triggers chronic cachexia and sustained commensal dysbiosis in mice. PLoS ONE 13(10): e0204895.

### Acknowledgments

We would like to thank Peter Buckmaster and the Stanford Veterinary Student Summer Fellowship Program for student support and constructive criticism on this project. We would like thank Erica Sonnenburg for advice and reagents for 16S sequencing.

### Background

Chronic diseases account for over 85% of deaths in the first world and 70% of deaths globally (98). The cooccurrence of cachexia, or the progressive loss of lean body mass, is one of the best predictors of mortality across chronic disease. Cachexia is distinct from starvation or malabsorption and can be accompanied by anorexia, elevated inflammatory cytokines (IL-1, IL-6 and TNF- $\alpha$ ), loss of fat and insulin resistance (99). In human disease, therapeutic interventions that have proved effective in animal studies, including nutritional supplementation, appetite stimulants, steroid treatment, and TNF- $\alpha$  inhibitors have not proven widely successful to block or reverse cachexia (100). One reason for the potential disconnect in treatments that seem promising in animal studies failing in the clinic is that many current animal models of cachexia do not recapitulate the chronic nature of clinical disease. Specifically, low-dose endotoxin injection causes weight loss over a period of several days, but after repeated injections, mice develop tolerance and return to normal weights. Cancer cachexia models may take many weeks before the onset of symptoms; however, the period of weight loss is also limited to 1–2 weeks before animals succumb to the tumor. Renal and cardiac obstruction models have a similar 1–2 week time frame of disease before animals succumb to the surgery (101). Thus, there is a great need to develop animal models that recapitulate the long-term nature of clinical cachexia, both to understand the underlying mechanisms of disease and to test targets for disease intervention and potential reversal.

*Toxoplasma gondii* (*T. gondii*) is an obligate intracellular protozoan parasite that cycles between a broad range of mammalian intermediate hosts and definitive feline hosts. Intermediate hosts are infected for life and support haploid division/asexual expansion of parasite strains. Intermediate hosts are infected when they ingest either oocysts shed in cat in feces or tissue cysts, termed bradyzoites, in the muscle or brain of other intermediate hosts. Over the first three days post-ingestion, *T. gondii* migrates down the small intestine, converts to the rapidly dividing tachyzoite stage, and infects intestinal epithelial cells and immune cells (10, 37, 102). Acute infection is marked by severe, focal disruption of the villi, expansion of

secondary lymphoid structures and the appearance of “casts” formed from matrix and dead cells that form a physical barrier over damaged regions of the ileum (37). Several groups have reported a decrease in microbial diversity in the gut, marked by outgrowth of Gram-negative bacterial species, as well as commensal microbe translocation to the liver (37, 103, 104). However, whether these alterations to commensal homeostasis are maintained during chronic infection has not been addressed.

*T. gondii* benefits from local intestinal inflammation by infecting infiltrating monocytes and dendritic cells and using them to traffic throughout the host (9). Over the course of 3–4 weeks, a Th1-mediated adaptive immune response clears systemic parasitemia, except in select tissues (mainly the brain and skeletal muscle) which support stage conversion to bradyzoite tissue cysts. The bradyzoite form of *T. gondii* is characterized by altered transcriptional profiles, a shift to glycolytic metabolism, slow growth, and formation of a polysaccharide-rich wall that protects the parasites as they transit through the stomach of the subsequent host (105). Thus, parasite transmission requires a robust host immune response: ensuring that the host survives acute infection and enabling the parasite to access the tissues amenable for chronic infection. Once the parasite has converted to the bradyzoite form, transmission requires predation of the chronically infected host. Cats acquire *T. gondii* by eating intermediate hosts and play an important role in the parasite life cycle by: 1) facilitating sexual recombination of the parasite, thereby increasing genetic diversity, and 2) mediating range expansion of the parasite by shedding millions of highly stable and highly infectious oocysts (106, 107). The selective advantage conferred by infecting cats and the predator-prey relationship between cats and rodents suggest that mice and rats are critical intermediate hosts for *T. gondii*. The importance of this relationship is evident in the sophisticated mechanisms the parasite has evolved to intersect host signaling pathways (108), promoting intracellular survival, as well as the observation that *T. gondii* infected rodents lose their aversion to cat urine, a putative means to facilitate transmission (109, 110).

Here we show that in the first 10 days post-*T. gondii* infection, adult mice lose 20% of their body mass, which is associated with elevated circulating cytokines, anorexia and moribund behavior. The majority of *T. gondii* infected animals do not succumb to infection, yet the reduction of muscle mass and visceral white adipose depots is sustained, indicating that *T. gondii* infection is a robust and reproducible model of sustained cachexia. We show that *T. gondii* infects and replicates in distinct puncta along the distal jejunum and proximal ileum throughout the acute phase of infection. Peak inflammation correlates directly with parasite load but is resolved by 5 weeks post-infection (wpi). Using 16S sequencing, we identify an outgrowth of *Clostridia spp.* that is sustained during the chronic stages of disease. Importantly, co-housed uninfected animals exhibit a similar shift in commensal populations without exhibiting any signs of illness or weight loss, consistent with the conclusion that commensal alterations alone are not sufficient to explain the sustained cachexia disease. We propose that promoting muscle and fat wasting may be a means of enhancing the opportunity for rodent predation and transmission of this parasite to definitive feline hosts.

## Results

### C57BL/6 mice orally infected with *T. gondii* develop chronic cachexia

10–12 week male C57BL6 mice acquired from Jackson Labs were cross-housed on dirty bedding for two weeks. Mice were then infected per orally with 100–250 *T. gondii* cysts of the Me49 background engineered to express GFP and luciferase (Me49-GFP-luc). Body weight was monitored for the duration of infection. Mice lost a significant amount of weight during the acute phase of infection (7 to 14 days post infection (dpi)), but weight loss stabilized by 30 dpi, the onset of chronic infection (**Fig. 3.1A**). Although mice increased in weight over the chronic phase of infection (day 30–90) they remained 20% less massive than uninfected controls. Animals infected with 100 or 250 cysts had similar weight loss (**Fig. 3.1B**) and survival through 40 dpi (**Fig. 3.1C**). Although the precise reason for similar disease kinetics across this range of cyst doses is not known, these data suggest a bottleneck at the intestine that prevents parasites from disseminating systemically beyond a certain threshold. Parasites were sometimes visible by bioluminescence assay when imaged ventrally at day 7 dpi (**Fig. 3.1D**); however, by day 40 dpi, parasite signal was not detectable (**Fig. 3.1E**). Of note, we have determined that luminescence signal can be masked if the parasites invade a region of the intestine on the dorsal face of the abdominal cavity. Despite variability in ventral luciferase signal, infections were very similar across small intestines when imaged ex vivo (**Fig. 3.3**).

Because infected mice routinely lose over 20% of their initial body weight but recover other indicators of health, we determined that weight loss alone was not an accurate indicator of morbidity. We implemented a 5-point sickness score (ruffled fur, hunching, >20% weight loss, squinting or eye discharge, failure to move) to differentiate between animals that were almost certain to recover versus animals that required euthanasia (**Fig. 3.1F**). Most animals routinely exhibit 3/5 phenotypes or above for a few days. Any animals scoring 5/5 were immediately euthanized (**Fig. 3.1F**, red). During chronic infection most animals retained a score of 1–2 based on reduced body mass and fur ruffling. Although mice underwent a phase of anorexia during acute infection, they regained their appetites and consumed normal pre-infection food amounts by 15 dpi, indicating that sustained weight loss was not simply due to sustained anorexia (**Fig. 3.1G**). These results are consistent with a 1997 report from Arsenijevic et al. that showed that mice infected with *T. gondii* can be described in different response groups: death in acute infection, failure to regain body mass or partial recovery of body mass (54). Whether weight loss resulted from a loss of fat or lean mass, or both, was not determined in this study.

To identify the tissue types affected, abdominal subcutaneous fat depots (scWAT, a rapidly mobilized energy source), epididymal visceral white adipose depots (vWAT, a key metabolic regulatory tissue), and supraclavicular brown adipose depot (BAT, thermogenic fat) were harvested. At 10 dpi, there was already significant reduction in BAT and scWAT depots. vWAT depots were significantly reduced 5 weeks post-infection (wpi) (**Fig. 3.1H**). In contrast to fat depots, which were reduced early, tibialis anterior (TA), gastrocnemius (GA), and quadriceps (QUAD) muscles were significantly reduced at 5 wpi (**Fig. 3.1I**). Chronic muscle loss was consistent with a recent report describing T regulatory cell-dependent myositis during chronic *T. gondii* infection which leads to impaired animal strength (86).

At 7 dpi, the canonical cachexia cytokines IFN- $\gamma$ , IL-1 $\beta$ , TNF- $\alpha$ , and IL-6 were significantly upregulated in the sera (**Fig. 3.1J**, grey versus black). IFN- $\gamma$ , specifically, is well described to be necessary to control chronic parasite infection in mice (111–114). Consistent their potent inflammatory capacity, at chronic infection circulating IFN- $\gamma$  and TNF- $\alpha$  were substantially reduced compared to acute infection. However, levels of IFN- $\gamma$ , TNF- $\alpha$ , and IL-6 remained significant compared to uninfected mice (**Fig. 3.1J**, red versus black). Among the significantly upregulated cytokines in chronic infection were eotaxin, a CCR3 agonist (a receptor highly expressed on TH2 cells), and interferon-gamma-inducible protein 10 (IP-10), which has been reported to antagonize the same receptor, suggesting a complex layering of pro and anti-inflammatory signals in chronic infection (115). Elevated sera titers of eotaxin, IP-10 and MCP-1 (a chemoattractant for macrophage and T cells) have also been observed in long-term follow up on a cohort of patients with juvenile dermatomyositis, a disease characterized by inflammatory cells surrounding the blood vessels leading to destruction of muscle fibers and skin irritation (116). IP-10 upregulation is consistent with the sustained elevation in IFN- $\gamma$  (67, 111, 117). Cumulatively these data indicate that chronic infection with *T. gondii* meet a modern definition of cachexia put forth in 2008: the loss of 5% or more lean body mass accompanied by anorexia, fat loss and inflammation (IL-1, TNF, IL-6, acute phase proteins) and/or insulin resistance (99).

Previous studies have suggested that C57BL/6 mice are uniquely susceptible to infection with Me49 parasites (118). Importantly, the cachexia phenotype was not restricted to C57BL/6 mice as CBA/J mice also lost approximately 20% of their body mass (**Fig. 3.2**, black vs. blue solid lines); however, BALB/c mice were protected from all weight loss using our experimental conditions (**Fig. 3.2**, black vs orange solid lines). Whereas C57BL/6 and CBA/J mice express the H-2D<sup>b</sup> haplotype of MHC class I, BALB/c mice express the H-2L<sup>d</sup> haplotype of MHC class I (119). BALB/c H-2L<sup>d</sup> presents the *T. gondii* dense granule protein GRA6, leading to a more effective CD8-mediated immune response, limited acute parasitemia, decreased chronic cyst burden, decreased overall inflammation and minimal if any weight loss compared to C57BL/6 (27).

### **Mice recover from severe acute inflammation and parasite growth in the small intestine**

*T. gondii* is naturally acquired by ingestion of oocysts or tissue cysts leading to severe regional inflammation in the small intestine (37, 66, 104). We reasoned that cachexia could be the result of sustained gut inflammation, changes in intestinal architecture, and/or the gut commensal community. To address this question, we orally infected mice with 200 Me49-GFP-luc cysts. Three mice per day were euthanized to assess parasite load in the small intestine, mesenteric lymph node, and spleen by bioluminescence assay. Significant parasite signal was observed in the small intestine at 4 dpi and peaked 7–8 dpi (**Fig. 3.3A**, black bars). Parasites were observed in the mesenteric lymph nodes (**Fig. 3.3A**, green bars) and spleen (**Fig. 3.3A**, grey bars) as early as day 3. For as long as *T. gondii* was detected by BLI (**Fig. 3.3A**, 4-10dpi) the first luciferase signal was consistently found at 50% the length of the small intestine and the mean of all luciferase positive regions was identified at 2/3<sup>rd</sup> the length of the intestine (**Fig. 3.3B**) indicating that the parasites grow primarily in this niche for the majority of the time they are found in the small intestine.

These data are consistent with previous reports studying the first week of infection. Specifically, Gregg *et al.* have shown parasite infection along the mucosa of the small intestine in the duodenum, jejunum and ileum over the first 6 days of infection (10). Further, Molloy *et al.* demonstrated that 9 dpi, commensals were segregated from the epithelial layer in the ileum but not the jejunum by the presence of a ‘cast’-like pseudomembrane composed of dead host cells and invasive *E. coli*, suggesting that there is a distinct interplay between *T. gondii*, commensals, and the immune system in this tissue (37). While we did not observe parasite signal in the duodenum, this may be due the fact that we imaged intestines from the serosal side rather than the luminal aspect. In addition, the bioluminescence assay is not sensitive enough to detect small numbers of parasites that may be present elsewhere in the small intestine (10). Nonetheless, our data are consistent with the interpretation that the distal jejunum/proximal ileum is the major small intestinal niche for parasite replication throughout acute infection. This region of the small intestine is enriched in immune resident cells, specialized structures including M cells that allow for sampling of the lumen and can mediate pathogen transit into the host, as well as an expansion in microbial diversity. All elements could contribute to *Toxoplasma*'s predilection for residence in this niche (120).

Diet as well as reactive oxygen species derived from inflammatory infiltrate can produce auto-luminescent signal. To validate that the luciferase signal was derived from *T. gondii*, and to monitor the degree of inflammation, we harvested segments of the small intestine 7 dpi for histological analysis. Having observed that luciferase positive regions always occurred adjacent to at least one enlarged Peyer's patch, 2cm segments centered on a Peyer's patch (or Peyer's patches) were excised from the small intestine of infected and uninfected mice (**Fig. 3.3C-G**). This allowed us to assess parasite load and the degree of inflammation in matched regions of the intestine across time points without pre-existing knowledge about parasite location provided by BLI. These intestine segments were fixed and sectioned. One section was stained with H&E (**Fig. 3.3C-D, and 3.3G**) to assess inflammation. The adjacent section was deparaffinized and stained for *T. gondii* using an antibody specific to parasite lysate and for nuclei using DAPI (**Fig 2i-vi**). At 7 dpi, tachyzoites were observed throughout the villi and the lamina propria. Interestingly, in sections where a Peyer's patch was cross-sectioned, parasites were observed nearby but excluded from lymphoid follicle (**Fig.3.3Ci and 3.3Cii**). Necrosis was not observed in Peyer's patches at 7 dpi (**Fig. 3.3Ciii, 20x and 3.3G, 40x**). When H&E sections were examined at high magnification, vacuoles containing multiple tachyzoites were visible in intestinal epithelial cells, indicating that parasites were growing in this niche at 7dpi (**Fig.3.3Dv, 100x, asterisks**).

We noticed the fields of view closest to the Peyer's patch contained the most *T. gondii* (**Fig. 3.3D v versus iv and vi** fluorescence images 10x), whereas neighboring fields of view contained few parasites and were less morphologically disrupted (**Fig. 3.3Div-vi, 3.3H, & 3.3E**). To quantify this observation, 2cm segments of the intestine containing a Peyer's patch or 2cm segments immediately adjacent to but excluding Peyer's patches were isolated, sectioned, and stained for H&E or *T. gondii* as described above. Across each section, there was a significant positive correlation between inflammation score and parasite load (**Fig. 3.3E**, Pearson's correlation, Peyer's patch segments, red:  $r = 0.716$ ,  $n = 98$ ,  $p < 0.0001$ ; adjacent segments, grey:  $r = 0.602$ ,  $n = 81$ ,  $p < 0.0001$ ). Peyer's patch negative sections had a significantly lower overall inflammation score and parasite load (**Fig. 3.3E**, linear regression of

correlations, Peyer's patch segments:  $0.781 \pm 0.078$ ; Adjacent segments:  $0.296 \pm 0.044$ ,  $p < 0.0001$  and **Fig. 3.3F**). By 5 wpi there was not a significant difference in inflammation score between infected and uninfected intestinal segments (**Fig. 3.3F**). Also consistent with the conclusion that infection in the small intestine was resolved in chronic disease, Peyer's patch architecture, which had a highly disorganized germinal center 7 dpi, was indistinguishable from uninfected animals by H&E staining 5 wpi (**Fig. 3.3G**). Finally, *T. gondii* was no longer observed in the Peyer's patch-containing segments of the small intestine by 5 wpi by qPCR (**Fig. 3.3H**). Taken together, these results indicate that since acute inflammation in the small intestine is resolved by chronic infection, it is unlikely to drive the sustained cachexia in these animals.

### Changes in the commensal community are amplified in chronic infection

Several groups have observed that acute infection with *T. gondii* triggers a loss of microbial diversity, an enrichment in Gram negative bacteria associated with intestinal pathology, and, sometimes, lethal ileitis (37, 65, 121). However, it is not known if these changes in the commensal communities are transient or sustained in chronic infection. To address this, we collected fecal pellets from mice two days before infection (**Fig. 3.4**, pre-infection), or at 1 wpi, 2 wpi, and 5 wpi with *T. gondii* and analyzed microbial diversity by 16S ribosomal sequencing (**Fig. 3.4**). In each cage, 1–2 uninfected animals were co-housed with infected littermate controls.

Community composition analysis reflected significant expansion in *Clostridia spp.* Operational Taxonomic Units (OTUs) 5 wpi when compared to the pre-infection community (**Fig. 3.4A**, navy blue outset, 5 wpi  $0.599 \pm 0.142$  versus pre-infection  $0.147 \pm 0.015$  SEM,  $p = 0.0004$ ,  $q = 0.007$  student's T-test). This trend was also observed in uninfected animals, although it was not statistically significant (5 wpi  $0.373 \pm 0.181$  versus pre-infection  $0.100 \pm 0.005$  SEM,  $p = 0.319$ ,  $q = 0.569$ ). There was also a moderate, expansion in Verrucomicrobia at 1 week in both infected and uninfected animals that contracted by 5 weeks, although this change was not significant. The enrichment of *Clostridia spp.* in fecal pellets of infected mice was unexpected, based on previous observations that *T. gondii* infection can trigger an outgrowth of  $\gamma$ -proteobacteria in the lumen of the small intestine 7–9 dpi (37, 67, 103, 121). However, these mice were obtained from Jackson Lab (C57BL/6J), whereas previous reports describing  $\gamma$ -proteobacteria outgrowth were performed using C57BL/6N mice. In addition to harboring several important polymorphisms, C57BL/6N raised at the NIH are known to harbor an O21:H+ strains of *E. coli* associated with invasiveness (septicemia) and worse pathology in DSS colitis, AOFM-induced colon cancer, and a range of gastrointestinal bacterial infections (37, 67, 82, 122). In the context of these previous reports, our data are consistent with a model where the outgrowth species may reflect the facultative pathogens already present in the community (dependent on mouse genetic background and facility to facility variation) that capitalize on niche availability following an inflammatory insult. The outgrowth species, in turn is likely to have important implications on the immune response at both the site of the initial infection and systemically. These differences in the pre-existing members of the commensal community explain why our mice are more resistant to a high dose infection with Me49 cysts than others have reported in the past. As these pathological strains of *E. coli* have been associated with invasiveness, this may also explain why others have observed that Peyer's patches become necrotic in acute *T. gondii* infection where

we do not (**Fig. 3.3Ciii**, 20x and **3.3G** 1wpi 40x) (54, 104, 120). A second parameter that may explain why our mice are tolerant of high dose infection is that uninfected and infected animals were co-housed for the duration of our study. Coprophagia may have buffered the severity of the commensal shift in infected mice as well as altered the commensal population in uninfected animals, as discussed below.

When principal component analysis was used to assess beta diversity across fecal pellets, pre-infection animals (**Fig. 3.4B**, red) clustered distinctly from infected animals (**Fig. 3.4B**, small circles: yellow = 1 wpi, green = 2 wpi; magenta = 5 wpi). The shift in similarity away from pre-infected phenotype was most pronounced by 5 wpi (**Fig. 3.4B**, magenta, small circles = infected, large circles = uninfected). Interestingly, the co-housed uninfected animals had a shift in microbial diversity as well and represented an intermediate cluster between pre-infection and infected animals (**Fig. 3.4B**, 1 wpi yellow, large circles; 2 wpi green, large circles). As uninfected cohoused animals do not display symptoms of cachexia, we conclude that the observed changes to the microbial species are not sufficient to explain the cachexia phenotype alone. However, future studies will be needed to understand if the altered commensal community synergizes with immune or metabolic defects to promote cachexia maintenance.

## Discussion

Here we describe a sustained cachexia phenotype in adult C57BL/6 mice (age 10–12 weeks) following per oral *T. gondii* infection. *T. gondii* cachexia is characterized by a loss of 20% in body mass, including fat and muscle, transient anorexia, and an acute elevation in the hallmark cachexia cytokines IL-1, TNF, and IL-6. To our knowledge, *T. gondii* infection is the first model to study sustained cachexia in mice that meets the modern, standard definition of cachexia put forth in 2008 (99). This will be an important tool for future studies aimed at understanding the physiological and molecular mechanism of cachexia. It may even prove to be a model to test interventions that halt and potential reverse disease.

That *T. gondii* infection causes acute regional ileitis is well-established; however, a detailed analysis of how long intestinal inflammation is sustained or whether acute changes in commensal microbial communities are long-lived has not been addressed until now. Unexpectedly, we observed parasite signal in the same region of the distal jejunum throughout acute infection, suggesting that this is the major region of the small intestine supporting parasite replication. Perhaps more surprisingly, we found no evidence of sustained intestinal inflammation at 5 wpi. In addition, the changes in fecal commensal communities observed in acute infection became more polarized in chronic infection rather than recovering as the intestinal barrier appeared to do. Importantly, the commensal communities of co-housed infected and uninfected mice both shifted by 5 wpi. However, uninfected animals showed no signs of disease, suggesting that altered commensal microbiota alone is not sufficient to explain the sustained cachexia phenotype in infected animals.

Whether the cachexia program is beneficial to the host or the parasite remains to be determined. Anorexia and depletion of fat stores are classic signatures of infection that play an important role in restricting systemic bacterial pathogen replication, but can trigger a host-detrimental response during viral infection (57, 123). In tissue culture, the *T. gondii* vacuole accumulates host lipids and parasite growth can be inhibited by blocking host lipases,

suggesting that inducing lipolysis early in infection could benefit the parasite, although this has not been tested in vivo (60, 62). It is now well accepted that *T. gondii* infection triggers altered aversion behavior to feline urine (109, 110). This is hypothesized to be an adaptive strategy used by the parasite to facilitate transmission to the feline definitive host. Interestingly, the reduction in muscle mass during chronic *T. gondii* infection has been associated with reduced strength (86). Therefore, it is plausible that promoting cachexia during chronic infection represents a second adaptive strategy used by *T. gondii* to facilitate the likelihood of predation by the definitive feline host. By studying the pathways that *T. gondii* has evolved to manipulate to promote transmission, we may identify critical immune and metabolic interactions driving the progression of chronic cachexia that can be applied to other disease settings.

## Figures

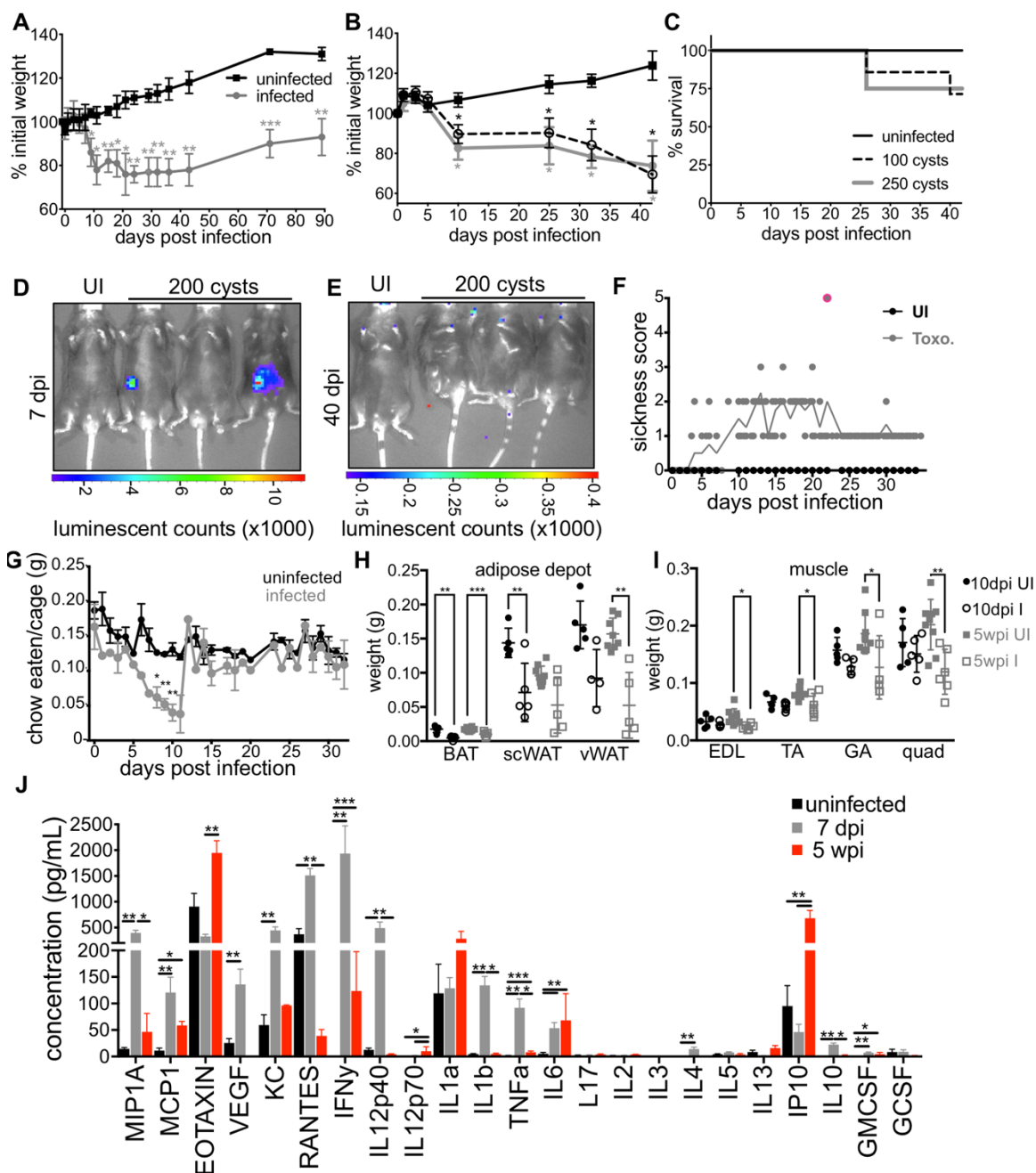


**Figure 3.1** C57BL/6 mice orally infected with *T. gondii* develop chronic cachexia. **A**, Following per oral infection with 120 Me49-GFP-luciferase cysts (grey) or mock infection (black) mice were monitored for weight loss. Data average of 8 experiments. **B**, Mice were infected as described in (A) with 100 cysts (dashed line), 250 cysts (grey) or mock infected (black) weight was monitored at the indicated time points. **C**, Survival curves for mice represented in (B). N = 4–7 mice per group, data representative at least 3 experiments. **D**, Mice were harvested at 7 days post infection (dpi) (E) or 40 dpi to assess parasite load by bioluminescence assay (legend continues on the next page).

**Figure 3.1 (continued from previous page) F**, Sickness scores for animals infected per orally with 100 Me49gfp-luc cysts (grey circles, toxo) or mock infected with PBS (black circles, UI). Animals were scored on a scale of 1–5: hunched posture, ruffled fur, failure to move when picked up, eyes closed or discharged, loss of over 20% weight. Mice were monitored twice daily at peak sickness and euthanized immediately if all 5 behaviors were observed (red outline). N = 5 mice per group. **G**, Every 24 hours food was weighed to determine the amount eaten and normalized to the weight of animals in the cage. Data are average of 2 experiments, N = 5 mice per group each experiment. Significance relative to uninfected at the same time point. **H**, Brown adipose tissue (BAT), sub cutaneous white adipose tissue (scWAT) or visceral white adipose tissue (vWAT) was harvest at 10 dpi (black) or 5 wpi (grey) and weighed. **I**, Extensor digitorum longus (EDL), tibialis anterior (TA), gastrocnemius (GA) and quadriceps (QUAD) muscles were weighed at 10 dpi (black) or 5 wpi (grey) post infection. Data is average of 2 experiments, N = 5–10 mice per time point. **J**, Luminex cytokine array was performed on sera from uninfected mice (black), 7 dpi (grey) or 5 wpi (red) mice. N = 3–10 mice per group. \*  $p \leq 0.01$ , \*\*  $p \leq 0.001$ , \*\*\*  $p \leq 0.001$ , SEM, student's T-test.

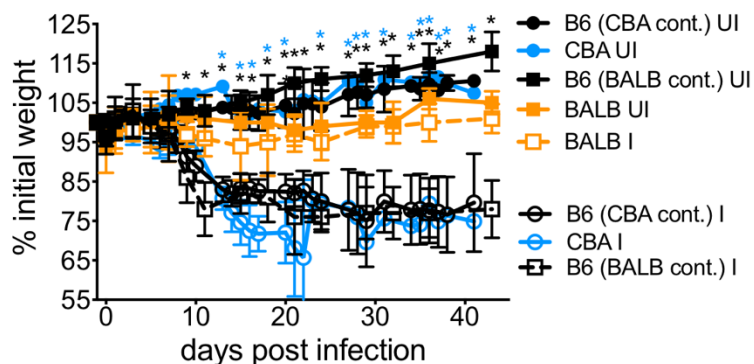


**Figure 3.2 C57BL6/J and CBA/J mice are susceptible to cachexia following *Toxoplasma* infection, but BALB/c mice are not.** BALB/c (orange square) or C57BL6/J mice (black square, B6 BALB cont.); CBA/J (blue circles) or C57BL6/J (black circles, CBA cont.) were infected with 120–200 cysts or mock infected. Weight was monitored at indicated time points. N = 4–8 mice per condition averaged across two independent experiments, significance is measured relative to uninfected at same time point.

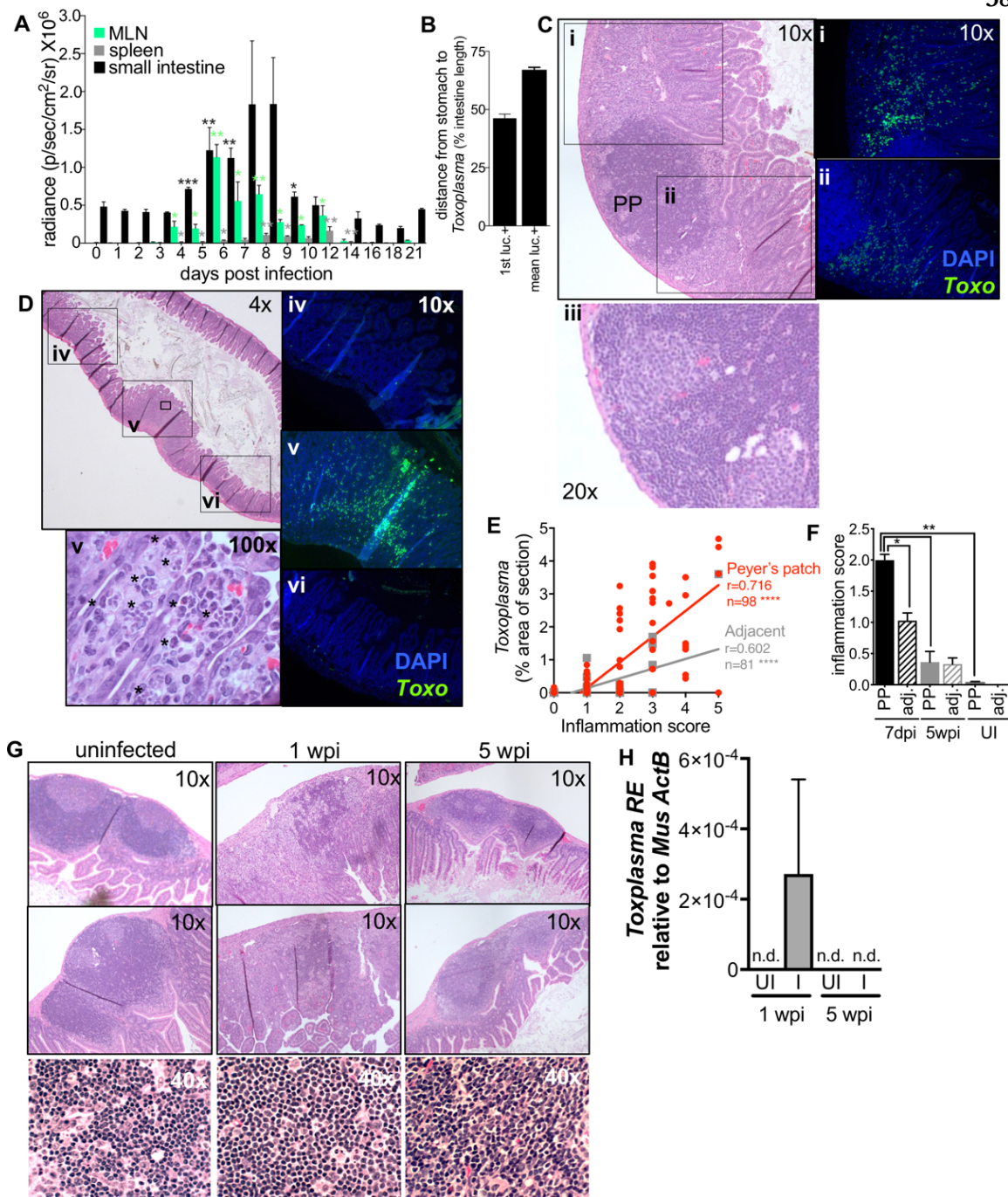


**Figure 3.3 Mice recover from severe acute inflammation and parasite growth in the small intestine.** **A-B**, Following per oral infection with 200 Me49-GFP-luc cysts, mice were euthanized and parasite load was determined by BLI in the small intestine (black), mesenteric lymph nodes (MLN, green) and spleen (grey). N = 3 animals per day, Significance is measured for each time point relative to day 3 post infection. Student's T-test \*  $p \leq 0.01$ , \*\*  $p \leq 0.001$ . **B**, For each intestine, the position of the luciferase signal was measured as distance from the stomach to the first luciferase positive region (1<sup>st</sup> luc+) or distance from the stomach to the mean of all luciferase positive regions (mean luc+). The position of luciferase signal was averaged from 4 to 10 dpi (**legend continues on the next page**).

**Figure 3.3 (continued from previous page) Mice recover from severe acute inflammation and parasite growth in the small intestine. C-H**, 2cm segments of the distal jejunum/ileum (the distal 50–90% of the small intestine) were excised for histology based on the presence of Peyer’s patches visible to the eye at 7dpi, 5wpi or from uninfected mice. **C-D**, Representative images of 7dpi sections stained with H&E to assess inflammation score at 10x or 20x (**iii**) magnification (scale of 1 = no detectable inflammation to 5 = complete disruption of lymphoid structure and/or villi). Parasites vacuoles were visible in the villi at 100x magnification (**v**, asterisks). In addition to staining a section for H&E, an adjacent section of each intestinal segment was stained with a *Toxoplasma*-specific antibody (green) and DAPI (blue) and imaged at 10x (**i-vi**) to assess parasite load. **E**, Correlation between parasite load and inflammation score in intestinal segments 7dpi. Segments containing a Peyer’s patch (red) or adjacent segments lacking a Peyer’s patch (grey), Pearson’s correlation \*\*\*\*  $p \leq 0.0001$ . Slopes were significantly different between the two groups: Peyer’s patch  $0.781 \pm 0.078$ , adjacent  $0.296 \pm 0.044$   $p < 0.0001$ , linear regression of correlations. **F**, Inflammation score for Peyer’s patch-containing segments (solid bars) and adjacent, Peyer’s patch negative segments (dashed bars) of the intestine from uninfected animals, 7 dpi (black) or 5wpi (grey). Student’s T-test \* $p \leq 0.05$ , \*\*  $p \leq 0.001$ , SEM, N = 4–6 segments from 3 mice per condition. **G**, Representative images of Peyer’s patch organization in uninfected, 1wpi and 5 wpi small intestines. **H**, Parasite load in the Peyer’s patch containing intestine segments 1wpi or 5wpi using quantitative PCR. *Toxoplasma* RE expression relative to host *actB*. N = 5.

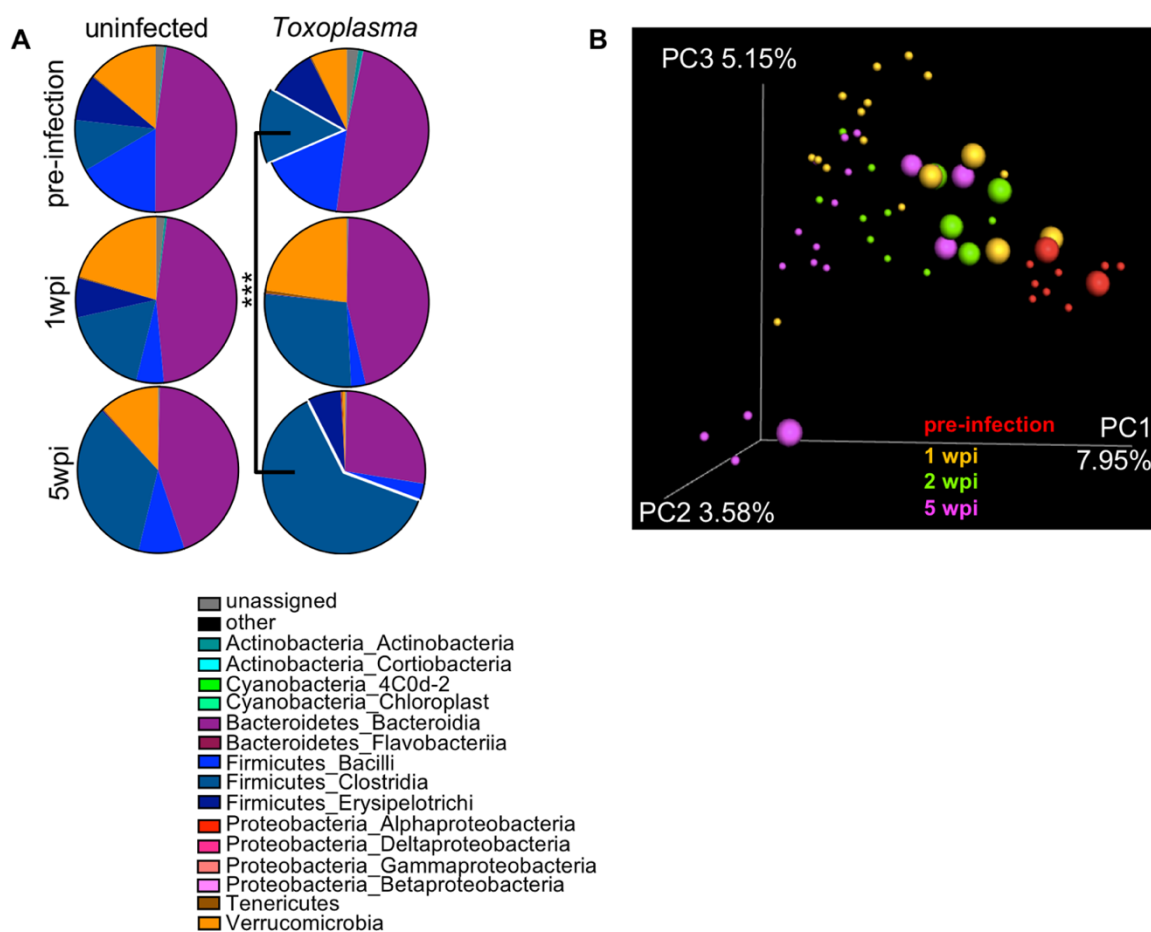


**Figure 3.4 Changes in the commensal community are amplified in chronic infection.** 16S profiling of commensal microbiota in fecal pellets gathered 2 days before infection (pre-infection), 1wpi or 5wpi with 120 *Toxoplasma* cysts. **A**, At chronic infection there is a significant outgrowth of *Firmicutes Clostridia* in comparison to pre-infection (navy blue, inset). *Toxoplasma* infected group: pre-infection mean  $0.147 \pm 0.015$  SEM, 5wpi mean  $0.599 \pm 0.142$  SEM, \*\*\* $p \leq 0.001$  student's T-test. Data represented as the mean of 3–8 mice per time point. **B**, Unweighted Unifrac principle component analysis of 16S ribosomal subunit diversity in the fecal pellets of mice 2 days before infection (pre-infection, red), 1 wpi (orange), 2 wpi (green) or 5 wpi (magenta). Small circles = infected, large circles = uninfected. Data representative of two experiments.

## Chapter 4: IL-1R regulates disease tolerance and cachexia in *T. gondii* infection

**The text and figures included in this chapter have been adapted from the following publication:** Melchor, S.J., Saunders, C.M., Sanders, I., Hatter, J.A., Byrnes, K.A., Coutermarsh-Ott, S., & S. E. Ewald. IL-1R Regulates Disease Tolerance and Cachexia in *Toxoplasma gondii* Infection. 2020. *The Journal of Immunology* 204 (10).

### Acknowledgements

We thank S. Batista and Dr. T. Harris for sharing the initial observation that IL-1R<sup>-/-</sup> mice regain weight after *T. gondii* infection and for critical feedback. We thank Dr. J. V. Cross for evaluation of the manuscript, Dr. K. Tung for histopathology advice, and M. Gonzalez for assistance with flow cytometry. The authors have no competing financial interest.

### Background

*Toxoplasma gondii* (*T. gondii*) is an obligate intracellular parasite that chronically infects a wide range of hosts. *T. gondii* is a natural rodent pathogen, but also infects humans. An estimated 30% of the global human population is infected (124). A host is infected by ingesting food contaminated with parasite cysts, which invade the small intestine. Over the first two weeks of infection, tachyzoites, the rapidly replicating form of the parasite, can be detected in almost every tissue (125). Infection elicits IL-12, IFN- $\gamma$ , and IL-6 to promote a TH1-polarized adaptive immune response that is necessary to restrict systemic infection. However, intermediate hosts remain infected for life, harboring low levels of bradyzoite tissue cysts in the brain, muscle, and other tissues. A sustained immune response is essential to suppress parasite growth during chronic infection: chronically infected mice and humans present with elevated sera titers of *T. gondii*-specific antibodies and IFN- $\gamma$ , and immune suppression triggers parasite recrudescence (126–128). However, the long-term consequences of sustained inflammation during *T. gondii* infection are not entirely clear.

Inflammasomes are cell-intrinsic innate immune signaling platforms linked to the release of IL-1 family cytokines and, often, inflammatory cell death. In *T. gondii* infection, mice deficient in the inflammasome sensors NLRP1 and NLRP3 and the effector caspases-1 and -11 have defects controlling parasite load (12, 13). These pathways release alarmins in the IL-1 family. However, there are conflicting reports regarding the role of IL-1 $\alpha$ , IL-1 $\beta$ , and their receptor IL-1R1 during *T. gondii* infection. Elevated IL-1 $\alpha$  and IL-1 $\beta$  have been observed in the sera (1 week post-*T. gondii* infection) and brain by 2-3 weeks post-infection (53, 129). Pretreating Swiss Webster mice with IL-1 $\alpha$  and IL-1 $\beta$  protected them from a lethal dose of *T. gondii* (130). One study reported increased mortality in IL-1R-deficient (IL-1R<sup>-/-</sup>) mice following intraperitoneal (i.p.) *T. gondii* infection (131), while another reported no deficiencies in parasite restriction (132). A third study reported that orally infected IL-1R<sup>-/-</sup> mice had

significantly improved survival, reduced intestinal pathology, and decreased parasite load compared to wildtype mice (133). Taken together, the role of the IL-1 axis on *T. gondii* burden and infection outcome is unclear.

We were interested in revisiting the requirement for IL-1R signaling in *T. gondii* infection based on an emerging role of the IL-1 axis in regulating disease tolerance during endotoxemia and bacterial infection (123, 134–136). Disease tolerance programs are defined as shifts in homeostasis that protect the host from bystander damage caused by infection and inflammation without directly affecting pathogen load (137). In contrast, resistance programs promote host fitness by directly mediating pathogen clearance. Tolerance mechanisms are as important for survival as restriction mechanisms, but are far less well understood, particularly in *T. gondii* infection. We found that IL-1R was not necessary to control parasite burden during acute or chronic i.p. *T. gondii* infection. Consistent with a role in disease tolerance, IL-1R<sup>-/-</sup> mice had increased cell death in the liver and adipose tissue compared to wildtype mice during acute infection. Unexpectedly, infected IL-1R<sup>-/-</sup> mice had better long-term survival than wildtype mice in chronic infection. IL-1R<sup>-/-</sup> mice recovered from acute weight loss, hepatomegaly and muscle atrophy. In contrast, wildtype mice exhibited sustained cachexia, an immune-metabolic wasting disease that led to a poor survival outcome in chronic infection (53, 56, 64, 99). These data indicate that IL-1R signaling controls cytoprotective disease tolerance programs that benefit the host during acute *T. gondii* infection. However, in the context of chronic disease, IL-1R can drive cachexia and ultimately impair host fitness.

## Results

### **IL-1R signaling impairs host survival during chronic *T. gondii* infection independent of parasite burden.**

Mice deficient in the IL-6 (24), TNF- $\alpha$  (138), and IFN- $\gamma$  (23) cytokine pathways succumb to acute or early chronic *T. gondii* infection due to a failure to restrict parasite growth. To test whether IL-1R signaling plays a similar role in parasite restriction, IL-1R-deficient (IL-1R<sup>-/-</sup>) or control C57BL/6 (WT) mice were intraperitoneally infected with 10 Me49 *T. gondii* cysts. Contrary to expectation, IL-1R<sup>-/-</sup> mice had significantly improved long-term survival compared to WT mice (**Fig. 4.1A**, 6-18 weeks post-infection). Improved survival was not due to better parasite clearance, as IL-1R<sup>-/-</sup> mice had a similar parasite load in the brain as WT mice at 9 weeks post-infection (**Fig. 4.1B-C**). *T. gondii* cyst morphology and inflammatory infiltrate in the brain were similar in infected IL-1R<sup>-/-</sup> and WT mice by H&E staining (**Fig. 4.2**).

### **IL-1R signaling limits cell death in the adipose tissue and liver during acute infection without affecting parasite load, consistent with a role in disease tolerance.**

Based on the observation that IL-1R<sup>-/-</sup> mice had better survival in chronic infection but similar parasite load, we reasoned that IL-1R signaling in acute infection could shape a fundamentally distinct immune environment with long-lasting effects on survival. Alternatively, sustained IL-1R signaling could prevent recovery in the chronic phase of infection. To assess the role of IL-1R signaling in acute infection, infected mice were euthanized at 2 weeks post-infection, when parasites are systemic and have infected most tissues in the mouse. We were surprised to observe numerous large lesions on the epigonadal

visceral white adipose tissue (vWAT) of IL-1R<sup>-/-</sup> mice (**Fig. 4.3A**, arrows). Although lesions were sometimes observed in the vWAT of infected WT mice, they were noticeably smaller and less frequent. These lesions were consistent with a histopathological definition of fat necrosis, which is acellular areas devoid of inflammation and occasional calcification (139, 140). Increased calcium deposition in IL-1R<sup>-/-</sup> vWAT was confirmed by Von Kossa stain (**Fig. 4.3B**, brown staining outlined, with pink nuclear counterstain). Necrotic lesions, defined as acellular regions surrounded by inflammatory infiltrate (**Fig. 4.3C**, outlined) were more frequent in IL-1R<sup>-/-</sup> vWAT than WT (**Fig. 2D**). By 9 weeks post-infection the lesions had largely resolved (**Fig. 4.3A, 4.3C-D**). *T. gondii* can directly induce tissue damage by lysing out of infected cells. *T. gondii* load was similar in WT and IL-1R<sup>-/-</sup> vWAT, indicating that the difference in necrosis was not due to parasite overgrowth in the IL-1R<sup>-/-</sup> mice (**Fig. 4.3E**).

Consistent with previous observations, hepatomegaly was also observed in WT and IL-1R<sup>-/-</sup> mice at 2 weeks post-infection (29, 141). The livers of WT and IL-1R<sup>-/-</sup> mice had focal, perivascular immune infiltrate of similar size and frequency (**Fig. 4.4A-B**). However, IL-1R<sup>-/-</sup> livers had significantly more enzymatically active caspase-3 staining by immunohistochemistry than WT livers (**Fig. 4.4C-D**), an early measure of apoptotic cell death. Immune infiltrate was also observed at 9 weeks post-infection (**Fig. 4.4A**), however, this was morphologically consistent with extramedullary hematopoiesis and active caspase-3 staining was not observed (**Fig. 4.4C**). Similar to the vWAT, WT and IL-1R<sup>-/-</sup> livers had similar *T. gondii* burden (**Fig. 4.4E**), indicating that the increased cell death in IL-1R<sup>-/-</sup> livers was not due to increased parasite load at 2 weeks post-infection. Taken together, these data are consistent with the conclusion that IL-1R signaling is cytoprotective in the liver and vWAT during acute infection, implicating a role in disease tolerance in acute *T. gondii* rather than the expected role in *T. gondii* resistance.

When IL-1 $\alpha$  and IL-1 $\beta$  protein levels were assessed in the tissue we found that IL-1 $\beta$  was elevated in the vWAT (**Fig. 4.5A**). IL-1 $\alpha$  and IL-1 $\beta$  were both significantly elevated in the liver of WT and IL-1R deficient mice. Other published disease tolerance models have reported significant differences in tissue pathology and function regulated independently of inflammatory cytokine levels or immune infiltrate (57, 123, 142). Consistent with these models, TNF- $\alpha$  and IL-6 were similar in the vWAT and liver of IL-1R<sup>-/-</sup> and WT mice at 2 weeks post-infection (**Fig. 4.5A-B**). IFN- $\gamma$  levels were not elevated in the vWAT, but were elevated in the liver, where IL-1R<sup>-/-</sup> livers had a slight but significantly elevated level compared to WT. Terminal deoxynucleotidyl transferase dUTP nick end labeling (TUNEL) is an indicator of late stage apoptosis as well as inflammatory, programmed cell death pathways that release IL-1 $\alpha$  and IL-1 $\beta$ , however, these processes can be difficult to detect in vivo due to immune clearance of damaged cells. A low but significant elevation of TUNEL positive cells were detected in the vWAT (**Fig. 4.6A**) and livers (**Fig. 4.6B**) of infected WT and IL-1R<sup>-/-</sup> vWAT. ASC ‘specks,’ which form downstream of some inflammasomes, were also observed in the vWAT of infected mice (**Fig. 4.6C**); and, very infrequently in liver sections (less than one per 10 fields of view at 40x, data not shown).

IL-10 is a regulatory cytokine necessary to control lethal immunopathology during *T. gondii* infection (29, 30, 33). Levels of IL-10 were not elevated in the vWAT of infected mice relative to uninfected controls, and were lower in infected WT and IL-1R<sup>-/-</sup> mice relative to

uninfected animals, suggesting that the cytoprotective effect of IL-1R in WT tissues was not mediated by IL-10. IL-1R antagonist (IL-1Ra) is a competitive inhibitor of IL-1R signaling that is transcriptionally regulated by IL-1R signaling among other NF- $\kappa$ B inducers (143). IL-1Ra was higher in the vWAT of infected mice relative to uninfected animals, although this was not significant. IL-1Ra was significantly higher in the liver (**Fig. 4.5B**) and sera (**Fig. 4.5C**) of infected WT and IL-1R<sup>-/-</sup> mice: however, there was significantly more IL-1Ra in the WT livers compared to IL-1R<sup>-/-</sup> mice, consistent with positive regulation of IL-1Ra by IL-1R signaling.

To determine if the increased pathology in IL-1R<sup>-/-</sup> was associated with a greater magnitude or altered distribution of immune infiltrating cells, mice were perfused with HBSS, and the liver and adipose tissues were dissociated for analysis by flow cytometry. Infected WT and IL-1R<sup>-/-</sup> mice had a similar overall number of infiltrating CD45<sup>+</sup> immune cells (**Fig. 4.7A**) and a similar distribution of infiltrating immune cell types in the adipose tissue and liver (**Fig. 4.7B-C**). Minimal contamination from blood-derived cells was confirmed by i.v. injecting anti-CD45-PacBlue five minutes prior to perfusion and staining with CD45-BV711 (data not shown) (144). While it is possible that more subtle difference in immune cell populations exist, these data indicate that the enhanced cell death in the IL-1R<sup>-/-</sup> mice was not simply due to a greater magnitude of inflammatory infiltrate, innate cytokine production, or altered parasite burden. These data also refute our initial hypothesis that chronic survival of IL-1R<sup>-/-</sup> is established during the acute phase of *T. gondii* infection.

#### **IL-1R signaling during *T. gondii* infection drives chronic cachexia.**

Based on our observation that IL-1R is cytoprotective during acute infection but negatively impacts long-term survival, we turned our attention to the role of IL-1R signaling during the chronic phase of disease. We, and others, have shown that infection with *T. gondii* can trigger sustained weight loss, inflammation, and muscle atrophy, consistent with the clinical definition of cachexia (53, 64, 145). Cachexia is an immune-metabolic disease of muscle wasting that predicts and directly contributes to mortality in a wide range of chronic diseases (99). IL-1, TNF- $\alpha$ , TNF, IL-6, and IFN- $\gamma$  comprise a cytokine signature conserved across etiologies of cachexia. We hypothesized that sustained IL-1 signaling during chronic *T. gondii* infection could promote cachexia, explaining the poor long-term survival of wildtype mice compared to IL-1R knockouts. To examine cachexia, we first measured body mass. Infected IL-1R<sup>-/-</sup> and WT mice both lost approximately 10% of their body mass by 1-4 weeks post infection (**Fig. 4.8A**), including fat and lean mass (**Fig. 4.8B**). However, IL-1R<sup>-/-</sup> mice regained weight between 5 and 11 weeks post-infection (**Fig. 4.8A-B**) whereas WT mice remained wasted. Infected IL-1R<sup>-/-</sup> and WT mice were anorexic at 1-2 weeks post-infection; however, both groups recovered eating during chronic infection (**Fig. 4.8C**). Infected IL-1R<sup>-/-</sup> mice lost significantly more muscle mass than WT mice by 2 weeks post-infection, but significantly regained muscle mass by 9 weeks post-infection. In contrast, WT mice continued to lose muscle mass from 2 to 9 weeks post-infection (**Fig. 4.8D**, Quad). Consistent with liver damage observed at acute infection, both WT and IL-1R<sup>-/-</sup> mice had hepatomegaly 2 weeks post-infection, although compared to uninfected mice, WT livers atrophied by 9 weeks post-infection whereas IL-1R<sup>-/-</sup> livers returned to normal weight (**Fig. 4.8D**, liver). Consistent with clinical observations that adipose tissue levels do not always correlate with cachexia severity,

WT and IL-1R<sup>-/-</sup> mice regained subcutaneous adipose tissue, but the vWAT remained significantly wasted in both genotypes at 9 weeks post-infection (**Fig. 4.8D**).

We next assessed levels of cachexia-associated cytokines in WT and IL-1R<sup>-/-</sup> mice at 9 weeks post-infection (99, 146). TNF- $\alpha$ , IL-6, and IFN- $\gamma$  were significantly elevated in WT and IL-1R<sup>-/-</sup> serum relative to uninfected controls (Fig. 6A). Although this was expected based on the essential role these cytokines play in restricting parasite growth (22, 24, 147), these data also suggest that elevated serum TNF- $\alpha$  (previously named cachectin), IL-6, and IFN- $\gamma$  are not sufficient to sustain cachexia during *T. gondii* infection in the absence of IL-1R signaling. IL-1 $\alpha$  and IL-1RA were also significantly elevated in sera of chronically infected, cachectic WT mice (**Fig. 4.9A**). When cytokine levels were assessed in wildtype tissues, IL-1 $\alpha$  was sustained in the liver of infected WT mice and brain lysates had increased IL-1 $\alpha$ , IL-1 $\beta$ , and IL-1RA protein levels relative to uninfected mice (**Fig. 4.9B**). Although IL-1 expression is not a direct measure of release, these data suggest that the liver and brain may be sites of sustained IL-1R signaling in chronic infection. Although IL-1 $\alpha$  and IL-1 $\beta$  were not elevated in muscle lysate, IL-1Ra was significantly increased, suggesting that skeletal muscle may be sensitive to IL-1R signaling due to circulating IL-1 $\alpha$  and/or IL-1 $\alpha$  or IL-1 $\beta$  levels in muscle microenvironments that are below the threshold of detection in whole tissue lysate.

To determine if IL-1 $\alpha$ , IL-1 $\beta$ , or both cytokines were necessary for chronic *T. gondii*-induced cachexia, IL-1 $\alpha$ <sup>-/-</sup> or IL-1 $\beta$ <sup>-/-</sup> mice were infected and weights were monitored for up to 16 wpi. Mice deficient in either IL-1 $\alpha$ <sup>-/-</sup> or IL-1 $\beta$ <sup>-/-</sup> had improved survival compared to wildtype animals (**Fig. 4.10A**). Both IL-1 $\alpha$ <sup>-/-</sup> and IL-1 $\beta$ <sup>-/-</sup> animals were partially protected from weight loss by 12 weeks post-infection (**Fig. 4.10B**). (Note that death of the most severely cachectic infected wildtype mice from 12-16 weeks post infection increased the mean body mass of this group and a loss of the statistically significant difference between infected IL-1 $\alpha$ <sup>-/-</sup> and IL-1 $\beta$ <sup>-/-</sup> groups). However, neither the IL-1 $\alpha$ <sup>-/-</sup> or IL-1 $\beta$ <sup>-/-</sup> groups fully regained body mass relative to uninfected animals by 16 weeks post infection. Similar to infected wildtype mice, the muscle and liver of infected IL-1 $\beta$ <sup>-/-</sup> mice were significantly wasted relative to uninfected controls (**Fig. 4.10C-D**). IL-1 $\alpha$ <sup>-/-</sup> mice had larger quadriceps muscles than IL-1 $\beta$ <sup>-/-</sup> mice, and the muscle and liver mass trended larger in IL-1 $\alpha$ <sup>-/-</sup> mice relative to WT, however, this was not significant (**Fig. 4.10C-D**). These data, in conjunction sustained tissue cytokine levels (**Figure 4.9**), suggest that IL-1 $\alpha$  and IL-1 $\beta$  both likely contribute to chronic cachexia during *T. gondii* infection. Together, our data demonstrate that the IL-1R axis plays a dual role in disease progression during *T. gondii* infection: IL-1R signaling limits tissue damage during acute infection; however, cachexia is a long-term cost of IL-1R signaling during the chronic phase of infection.

## Discussion

Our data indicate that IL-1R plays a distinct role in the innate inflammatory response during *T. gondii* infection. In contrast to better-studied effectors IL-6, TNF- $\alpha$ , and IFN- $\gamma$ , which are necessary for *T. gondii* resistance (22, 24, 147), IL-1R signaling protects mice from acute liver and adipose tissue pathology without affecting parasite load. This result is consistent with the definition of a disease tolerance mechanism, which is a tissue-intrinsic pathway that

enables tissue function during immunological stress without directly affecting pathogen burden (148). However, in the long-run, an intact IL-1R signaling axis negatively impacts host survival during chronic infection by driving cachexia.

Our studies suggest that IL-1 $\alpha$  and IL-1 $\beta$  may both contribute to acute weight loss and cachexia during *T. gondii* infection. Release of functional IL-1 $\beta$  requires cleavage by the effector caspase-1 downstream of inflammasome activation (149), whereas bioactive IL-1 $\alpha$  can be released downstream of a broader range of cell death and damage events. Unlike IL-1R<sup>-/-</sup> mice, mice deficient in the inflammasome adaptor ASC, sensors NLRP1 and NLRP3, or effector caspases-1 and/or caspase-11 cannot control *T. gondii* replication and have decreased survival in acute or early chronic infection (12, 13, 150, 151). Interpreting these data in the context of our results suggest that inflammasome activation restricts *T. gondii* growth through an IL-1R independent mechanism. Interestingly, pyroptotic cell death has not been observed in *T. gondii* infected mouse macrophage or human monocytes (12, 131, 152, 153). However, it is possible that other cell types undergo pyroptosis in response to *T. gondii* infection, or that there is crosstalk between the inflammasome and other pathways that restrict the parasite in vivo, like iNOS (154) and/or interferon-regulated GTPase pathways (155, 156). Alternatively, the inflammasome also mediates IL-18 release, which has been shown to be critical for parasite restriction (13).

Our study is not the first to investigate the role of IL-1R signaling in *T. gondii* infection; however, results, at least at the outset, seem to conflict. A 1998 study showed that IL-1 $\alpha$  or IL-1 $\beta$  administration one day before infection protected Swiss Webster mice from an LD100 dose of type III *T. gondii* (130). Although parasite load was not measured, all experimental groups had comparable *T. gondii* specific IgG and evidence of brain infection. In 2007 La Rosa and colleagues reported that IL-1R antagonist treatment did not affect parasite burden and stated that IL-1R<sup>-/-</sup> mice are no more susceptible to *T. gondii* infection than wildtype controls (132). By contrast, Gorfu *et al* found that mice deficient in IL-1R or the IL-18 axis were more susceptible than WT mice to i.p. infection with 10,000 type II 76K *T. gondii* tachyzoites, and susceptibility correlated with increased parasite load by luciferase assay (131). These data do not necessarily conflict with our results, in fact we might expect that a failure in tolerance biology would result in increased host death at an LD50, as used here, compared to our milder infection conditions. It is also important to note that although tolerance biology does not directly target pathogen growth, parasite load can be indirectly impacted over time.

In a study by Villeret *et al.* IL-1R-deficient mice orally infected with type II *T. gondii* (76K) had more severe acute gut pathology, increased neutrophil and myeloid cell recruitment, and elevated pro-inflammatory cytokines compared to wildtype mice (133). Several important differences between this model and our study may explain the pathological effects of IL-1R in the gut and the protective effect of IL-1R signaling we observed in the liver and fat. First, during oral infection, the small intestine barrier is compromised, leading to TLR recognition of commensal microbiota, so it is unclear whether changes in immune infiltration are due to a lack of IL-1R signaling directly or an indirect effect of increased interaction with commensals (37, 66, 157). A not mutually exclusive alternative is that the small intestine has a different tolerance threshold for inflammation, distinct IL-1R-responsive cell types, or overall levels IL-

1 $\alpha$  and/or IL-1 $\beta$  released than the fat and liver. Importantly, our conclusion agrees with the Villeret study in IL-1R signaling was not necessary to restrict *T. gondii* and, overall, the loss of IL-1 promoted host survival during *T. gondii* infection.

Future experiments will be necessary to determine if the cytoprotective effect IL-1R observed in the liver and adipose tissue is cell-intrinsic or indirect. IL-1 $\beta$  pretreatment has been shown to protect primary murine hepatocytes from Fas-ligand mediated death (158), and prevent hepatocyte death in vivo after treatment with a Fas activating antibody (159) or TNF- $\alpha$  (160). Ishibe *et al.* found that IL-1RA deficient mice (which have increased IL-1R signaling) are protected from acetaminophen-induced liver injury, and pretreatment with IL-1 $\alpha$  was sufficient to significantly attenuate liver pathology (161). Together, these studies indicate that IL-1R signaling can directly promote survival in liver parenchymal cells, however, less is known in adipose tissue.

From a clinical perspective, promoting tolerance biology has become a topic of therapeutic interest as a strategy to mitigate the negative aspects of inflammation without increasing the risk of infection. While this may be a beneficial treatment strategy to treat resolving infections or acute inflammatory events, an extension of the tolerance/resistance paradigm is that disease tolerance programs must come at a cost to the organism, otherwise they would be selected for homeostatic use. Consistent with this theoretical framework, our data indicate that IL-1R signaling is cytoprotective during acute infection, but ultimately promotes cachexia. Precisely how IL-1R signaling promotes cachexia remains to be determined; however, there is evidence to suggest central nervous system dependent and independent mechanisms could be at play.

IL-1R signaling in the central nervous system has been shown to be important for controlling appetite and eating behavior (162). However, in our model, anorexia is not IL-1R dependent or sustained. Both i.p. administration of IL-1 $\alpha$  and intracerebroventricular infusion of IL-1 $\beta$  in rats has been demonstrated to induce anorexia-independent muscle loss (163, 164). Mice that received tumor xenografts engineered to express IL-1 $\alpha$  had more severe wasting than mice that received control tumor xenografts (independent of food intake), and blockade of local IL-1R signaling by intra-tumoral administration of IL-1Ra significantly less fat and muscle wasting in the C-26 murine model of colon cancer (165, 166). The IL-1R axis has also been shown to regulate glucose and lipid metabolism (167, 168) Similar to metabolic shifts associated with cachexia, mice deficient in IL-1Ra are smaller, have impaired fat storage, abnormal lipid metabolism, and elevated resting baseline energy expenditure (168–170). Of note, the majority of these studies were performed before a modern clinical definition of cachexia was established, indicating that it may be time to revisit a role for IL-1 in current models of cachexia.

*T. gondii* infection has several unique advantages as a tool to study the inflammatory mediators in cachexia. First, the kinetics of *T. gondii* cachexia more closely resemble clinical disease than current surgical or tumor cachexia models, which are lethal after only several days of weight loss (171, 172). To our knowledge, this study is the first example of a genetic rescue of cachexia after peak weight loss has occurred. This result is significant because it indicates

that the inflammatory networks responsible for maintaining cachexia are distinct from those that initiate disease. Second, the parameter of pathogen burden can be used to distinguish between immune effectors primarily designed to promote inflammation (resistance biology) versus those targeting tissue homeostasis (tolerance biology). Targeting resistance effectors should reduce damage-to-self, but may not correct the tolerance-induced homeostatic shifts that occur in response to the inflammatory environment. Consistent with this model, blocking the cachexia-associated cytokine TNF- $\alpha$  (a pathogen resistance signaling molecule) has repeatedly failed to treat clinical cachexia (31). Recently, however, a first-in-class monoclonal antibody targeting IL-1 $\alpha$  (MABp1) was shown to improve body mass in a phase 1 dose escalation trial for metastatic cancers (173). While further studies in disease-matched cachectic and weight stable patients are necessary, these findings suggest that dual therapies targeting both tolerance and resistance pathways may be a more efficacious way to restore homeostasis during chronic diseases like cachexia. Given the conserved role IL-1 plays across etiologies of clinical cachexia, we anticipate that mechanisms uncovered in *T. gondii* cachexia may have important implications for cachexia in general.

## Figures

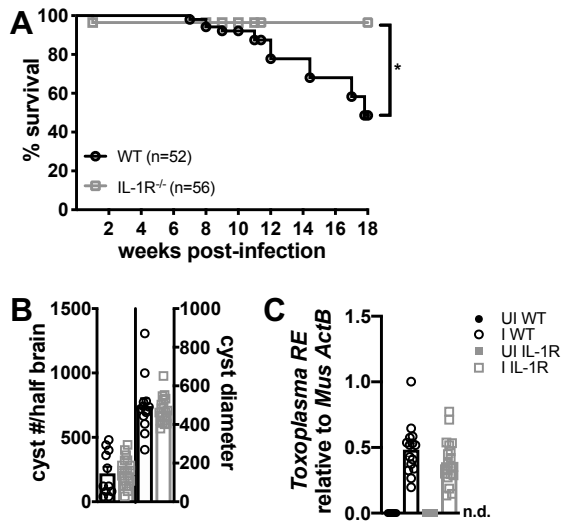


**Figure 4.1 IL-1R<sup>-/-</sup> mice survive chronic *T. gondii* infection better than wildtype mice independent of parasite burden.** 10-14 week old male C57Bl/6 (WT) or IL-1R<sup>-/-</sup> mice were intraperitoneally infected with 10 Me49 *Toxoplasma* cysts. **A**, Survival curves of infected C57BL/6 (WT) or IL-1R<sup>-/-</sup> mice ( $n = 52-55$  mice per group, data pooled from twelve experiments). p-value is 0.0210 by Log-rank test. **B**, Brain cyst burden and diameter at 9 weeks post-infection (wpi) ( $n = 12-21$  mice per group, data pooled from three experiments). **C**, qPCR quantification of *T. gondii* 529-bp repeat element (*T. gondii* RE) gDNA relative to mouse  $\beta$ -actin in the brain at 9 wpi ( $n = 7-20$  mice per group, data pooled from five experiments). n.d., not detectable. Data are shown as the mean  $\pm$  SEM. \*P < 0.05; \*\*P < 0.01; \*\*\*P < 0.001, \*\*\*\*P < 0.0001 by unpaired Student's T test with Holm-Sidak method to correct for multiple comparisons.

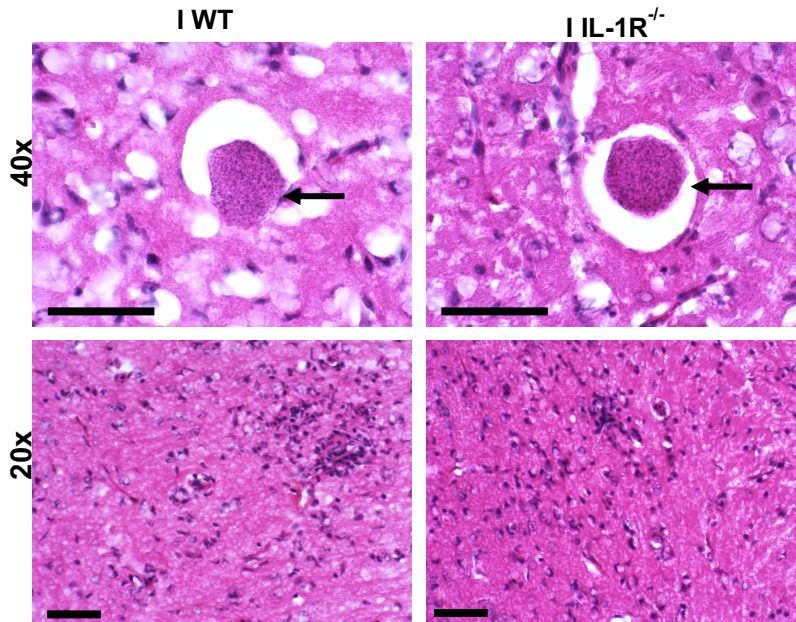


**Figure 4.2 Wildtype and IL-1R<sup>-/-</sup> mice have inflammation in the brain during chronic infection.** Brains were harvested at 5 weeks post-infection, fixed in 4% PFA, and frozen until they were cryosectioned, stained with H&E, and imaged. Scale bars = 50 μm. Arrows are pointing to *T. gondii* cysts.

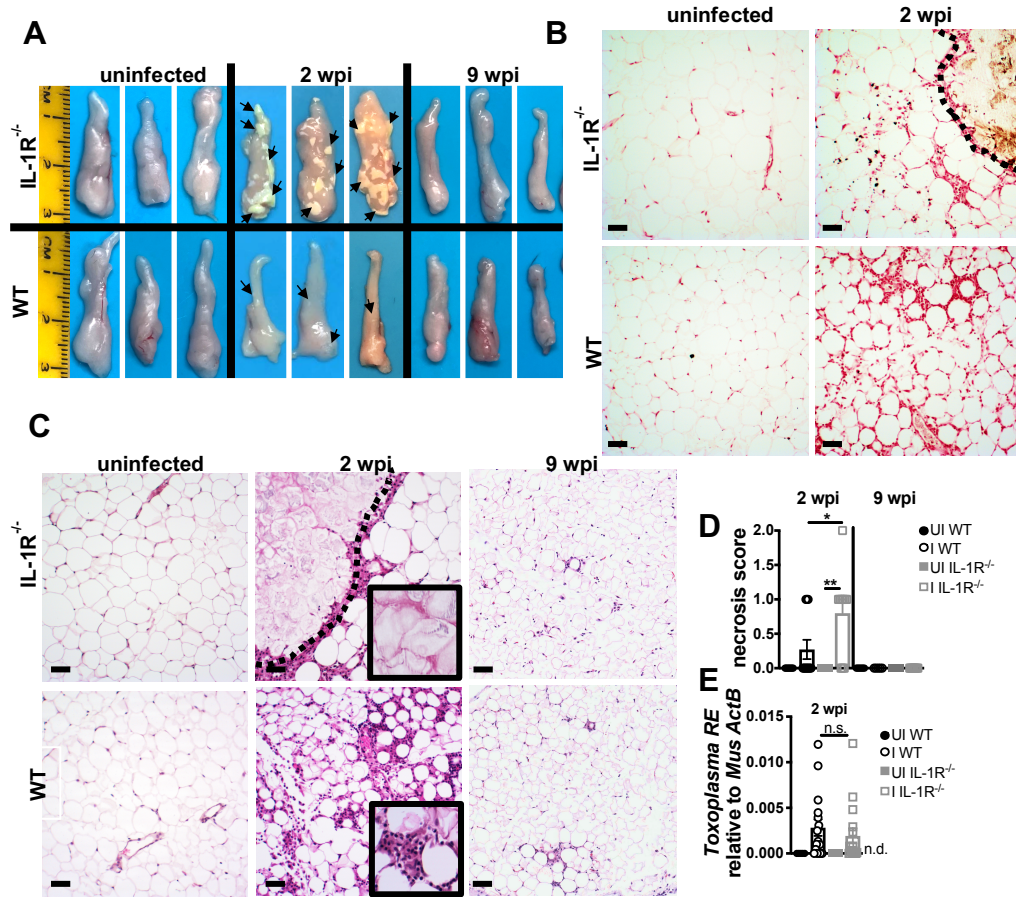


**Figure 4.3 IL-1R signaling limits cell death in the adipose tissue during acute *T. gondii* infection.** **A**, Epididymal visceral white adipose tissue (vWAT) was harvested at 2 wpi (representative of five experiments). vWAT was stained with Von Kossa stain (brown staining (outlined) denotes calcification) (**B**) or hematoxylin/eosin (H&E, necrotic lesion outlined) (**C**). **D**, Degree of vWAT necrosis in H&E scored by a blinded pathologist ( $n = 6-8$  mice, pooled from two experiments). **E**, qPCR quantification of *T. gondii* RE gDNA in the vWAT at 2 wpi, relative to mouse  $\beta$ -actin ( $n = 5-15$  mice per group, pooled from four experiments). Scale bars = 50  $\mu$ m. n.d., not detectable. Data are shown as the mean  $\pm$  SEM. \*,  $P < 0.05$ ; \*\*,  $P < 0.01$ ; \*\*\*,  $P < 0.001$ , n.s., not significant by unpaired Student's T test.

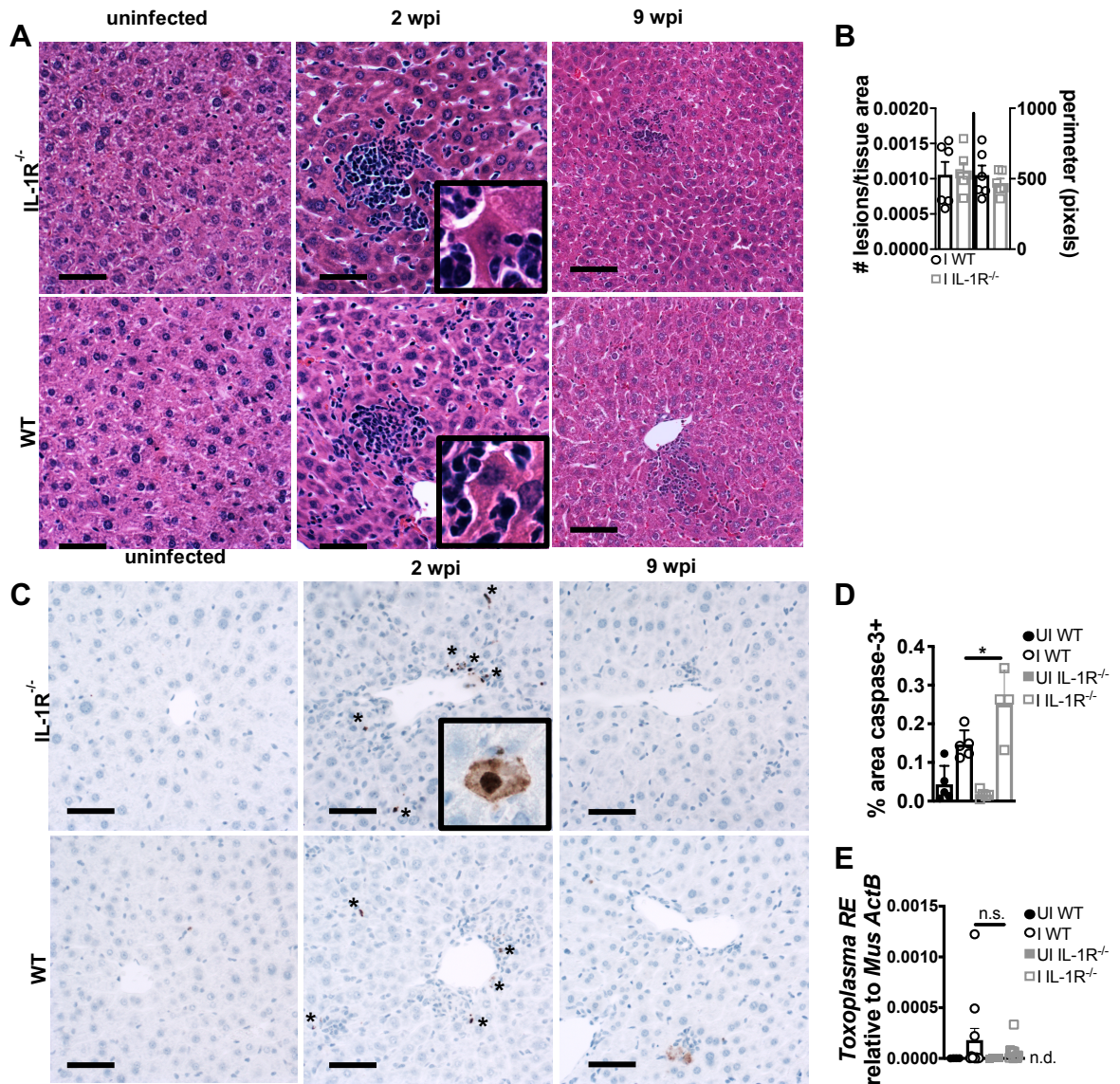


**Figure 4.4 IL-1R signaling limits caspase-3 activation in the liver during acute *T. gondii* infection.** At 2 wpi liver was harvested and sectioned for H&E staining (**A**). **B**, Focal immune lesions were counted across slide scans of whole liver sections and lesion perimeter was measured ( $n = 6$  mice per group, pooled from two experiments). **C**, Immunohistochemistry for cleaved caspase-3 (brown stain, asterisks) quantified in (**D**) ( $n = 4-5$  mice per group, representative of two experiments). **E**, qPCR quantification of *T. gondii* RE gDNA in the liver at 2 wpi, relative to mouse  $\beta$ -actin ( $n = 4-11$  mice per group, pooled from three experiments). Scale bars = 50  $\mu$ m. n.d., not detectable. Data are shown as the mean  $\pm$  SEM (except **D**, where they are SD). \*,  $P < 0.05$ ; \*\*,  $P < 0.01$ ; \*\*\*,  $P < 0.001$ , n.s., not significant by unpaired Student's T test.

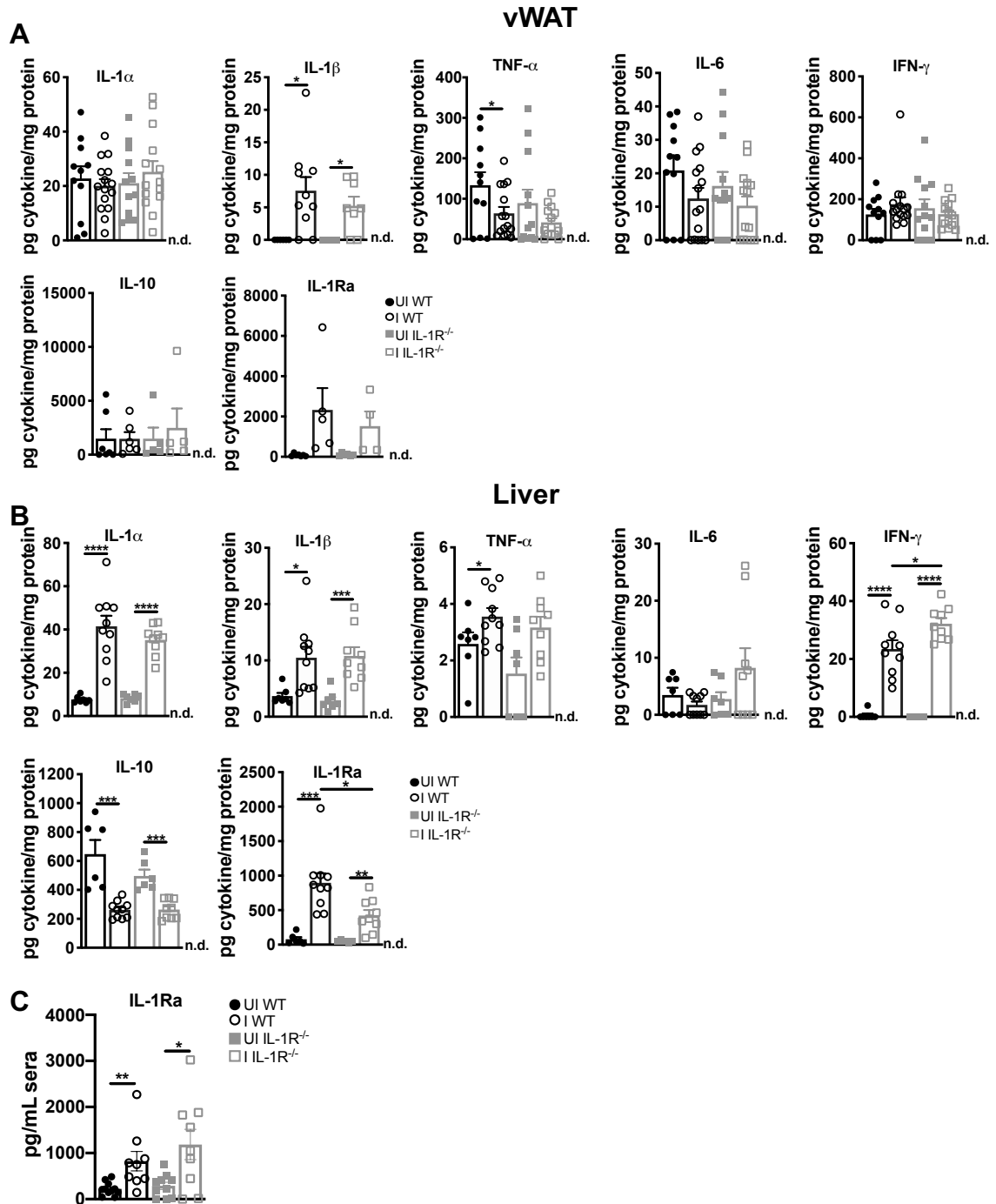


**Figure 4.5 IL-1R ligands are elevated in the liver and vWAT at 2 weeks post-infection.** Cytokine concentration in tissue lysate were measured by ELISA in **A**, vWAT ( $n = 5-15$  mice per group, pooled from three experiments). IL-1 $\beta$ , IL-10, and IL-1Ra are from two experiments) or **(B)** liver ( $n = 7-10$  mice per group, pooled from two experiments). n.d., not detectable. Data are shown as the mean  $\pm$  SEM. \* $P < 0.05$ ; \*\* $P < 0.01$ ; \*\*\* $P < 0.001$ , \*\*\*\* $P < 0.0001$ , n.s., not significant by unpaired Student's T test.

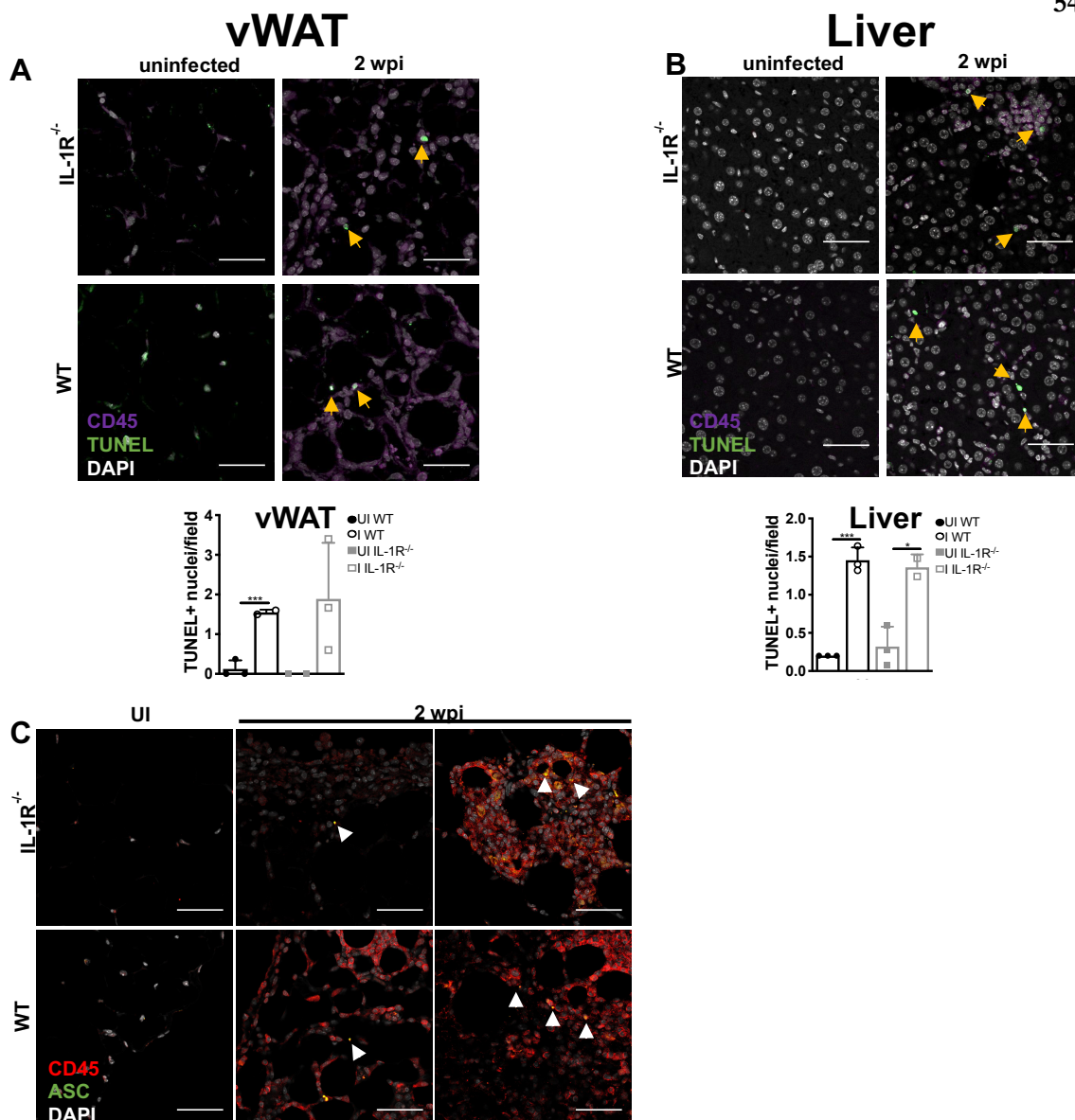


**Figure 4.6 TUNEL staining and ASC speck formation can be detected at similar levels between WT and IL-1R<sup>-/-</sup> mice at 2 wpi.** A-B, Tissues were harvested at 2 wpi and stained for CD45 and double-stranded DNA breaks using a TUNEL assay kit in (A) vWAT or (B) liver. (C) Alternatively, slides were stained for CD45 and ASC. ASC specks (indicated by white arrowheads) form upon inflammasome activation. Scale bars = 50  $\mu$ m. Data are shown as the mean  $\pm$  SD. \*P < 0.05; \*\*P < 0.01; \*\*\*P < 0.001, \*\*\*\*P < 0.0001, by unpaired Student's T test.

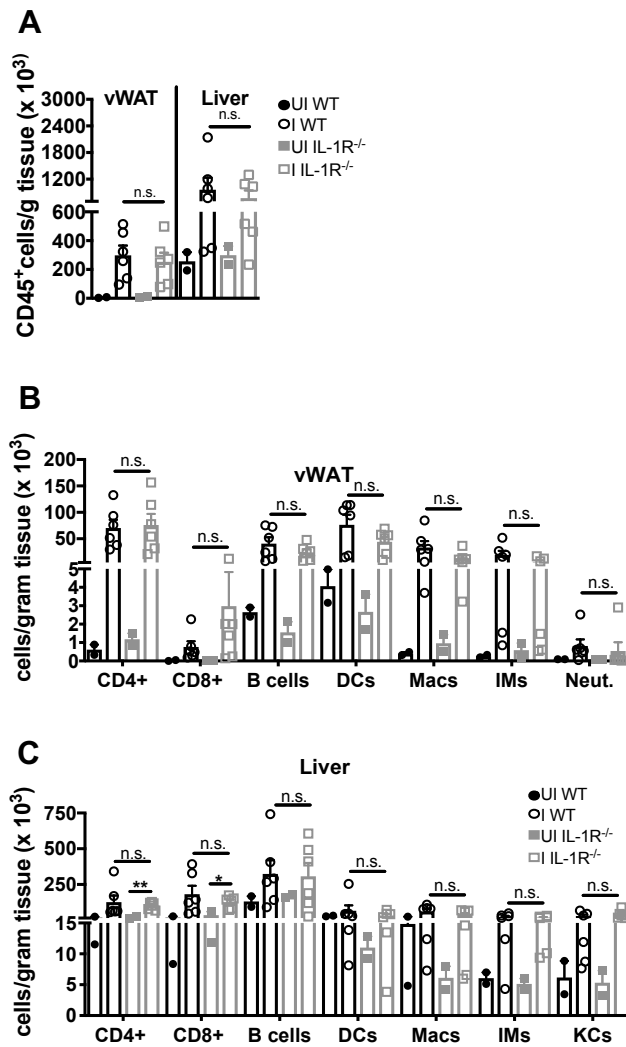


**Figure 4.7 IL-1R signaling does not control immune infiltrate in vWAT and liver at 2 weeks post-infection.** A-C, Following cardiac perfusion with HBSS, vWAT and liver were excised, dissociated, and numbers of infiltrating immune cells were determined by flow cytometry. **A**, Total number of infiltrating CD45<sup>+</sup> cells per gram of vWAT or liver at 2 wpi. CD4<sup>+</sup> T cells, CD8<sup>+</sup> T cells, B cells, dendritic cells (DCs), macrophages (Macs), inflammatory monocyte (IMs), Kupffer cells (KCs, liver only), and neutrophils (Neut., vWAT only) in the vWAT (**B**) or liver (**C**) at 2 wpi by flow cytometry ( $n = 2-6$  mice per group, pooled from two experiments). Data are shown as the mean  $\pm$  SEM. \* $P < 0.05$ ; \*\* $P < 0.01$ ; \*\*\* $P < 0.001$ , \*\*\*\* $P < 0.0001$ , n.s., not significant by unpaired Student's T test with Holm-Sidak method to correct for multiple comparisons.

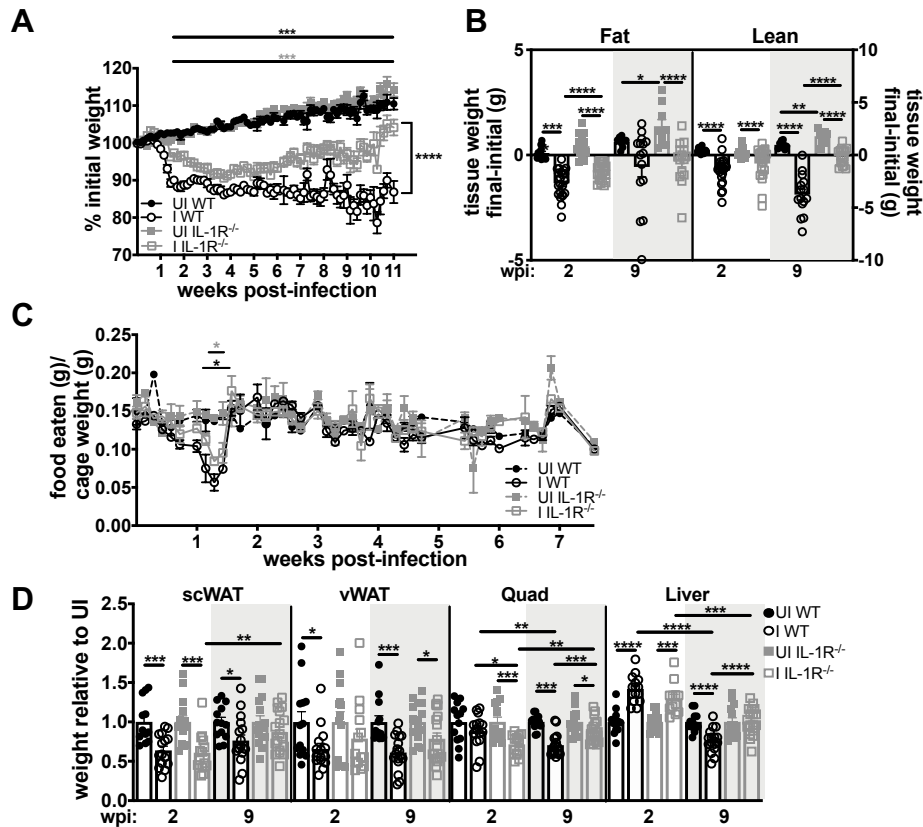


**Figure 4.8 Acute weight loss is IL-1-independent, but IL-1R<sup>-/-</sup> mice are protected from chronic *Toxoplasma*-induced cachexia.** **A**, Weight curves showing percent of initial weight from 0-11 wpi ( $n = 34-48$  mice, pooled from seven experiments). **B**, Echo MRI quantification of fat (left) and lean (right) mass at 2 or 9 wpi ( $n = 9-22$  mice, pooled from two to four experiments). **C**, Mouse chow was weighed daily, and food intake per cage normalized to total body weight was determined ( $n = 2-4$  cages per group, pooled from two experiments). Asterisks indicate significant differences between UI and I WT (black) or UI and I IL-1R<sup>-/-</sup> (gray). **D**, Inguinal subcutaneous white adipose tissue (scWAT), vWAT, quadriceps (Quad), and liver at 2 wpi or 9 wpi ( $n = 12-18$  mice per group, pooled from three experiments). Data are shown as the mean  $\pm$  SEM. \* $P < 0.05$ ; \*\* $P < 0.01$ ; \*\*\* $P < 0.001$ , \*\*\*\* $P < 0.0001$ , n.s., not significant by unpaired Student's T test with Holm-Sidak method to correct for multiple comparisons.

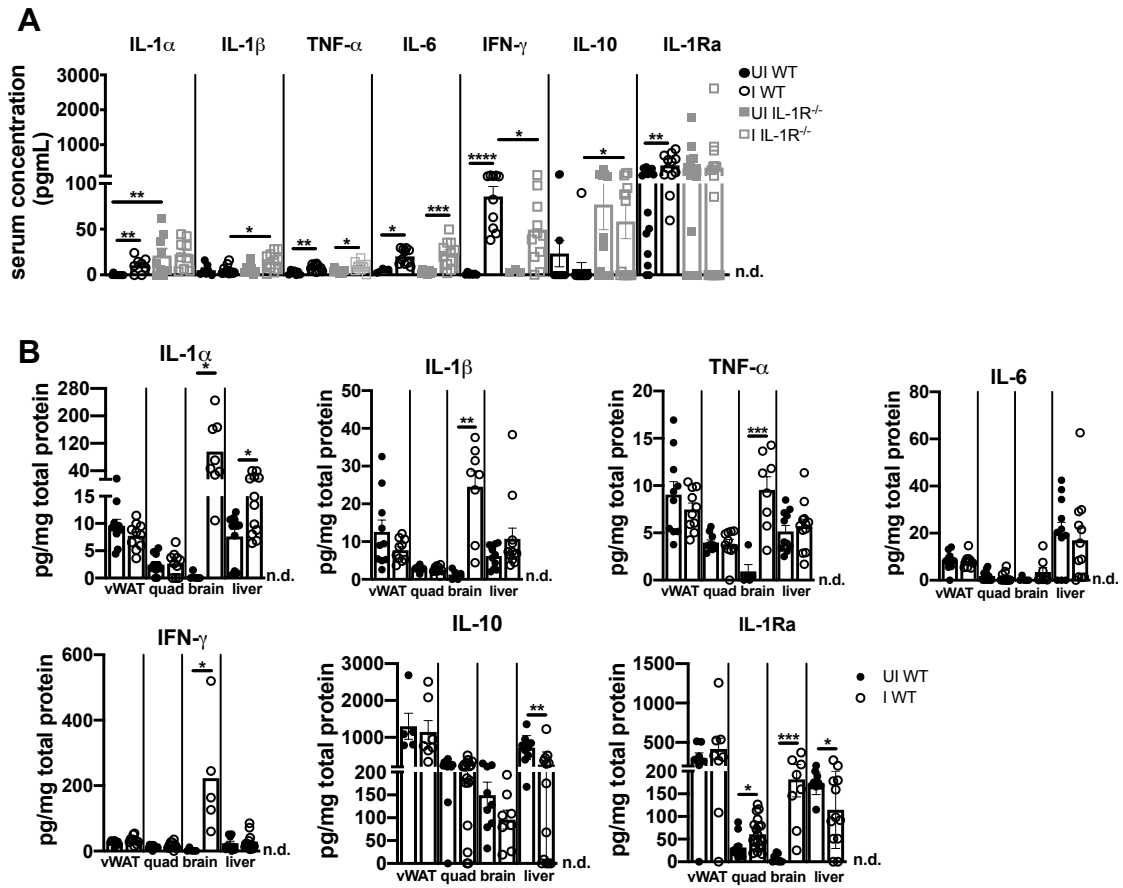


**Figure 4.9 IL-1 $\alpha$  remains chronically elevated in the circulation, liver, and brain of cachectic mice.** **A**, Serum cytokines at 9 wpi measured by Luminex ( $n = 3-10$  mice per group, pooled from two experiments) or ELISA (IL-1 $\alpha$ , IL-10, and IL-1Ra  $n = 9-17$  mice per group, pooled from two to three experiments). **B**, Cytokines in tissue lysates were determined by ELISA ( $n = 5-19$  mice per group, pooled from three experiments). Brain data pooled from two experiments). n.d., not detectable. Data are shown as the mean  $\pm$  SEM. \* $P < 0.05$ ; \*\* $P < 0.01$ ; \*\*\* $P < 0.001$ , \*\*\*\* $P < 0.0001$ , by unpaired Student's T test with Holm-Sidak method to correct for multiple comparisons.

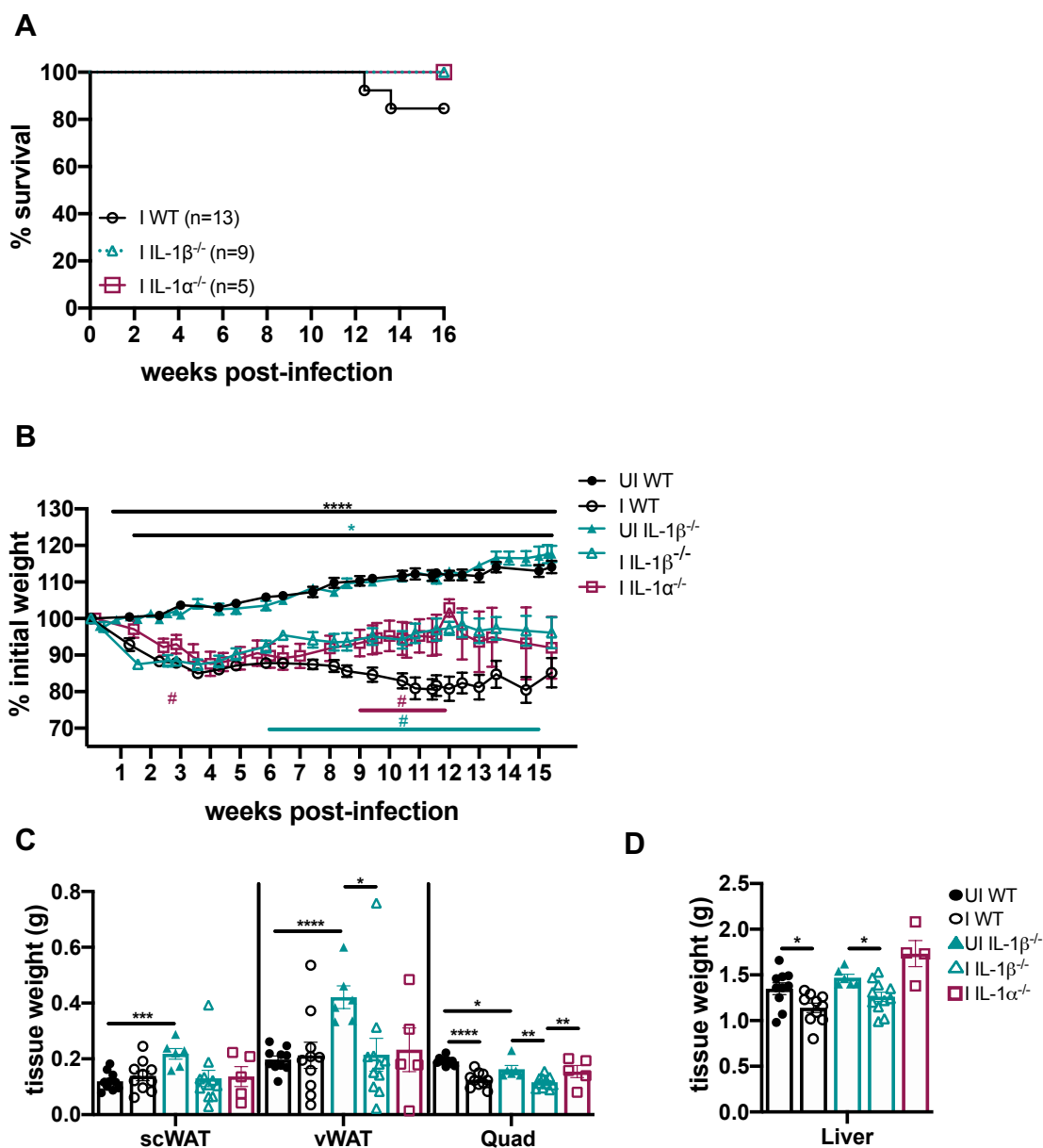


**Figure 4.10 IL-1 $\alpha^{-/-}$  and IL-1 $\beta^{-/-}$  mice are partially protected from chronic cachexia.** 10-15 week old C57BL/6J, IL-1 $\alpha^{-/-}$ , and IL-1 $\beta^{-/-}$  mice were intraperitoneally infected with 10 *Toxoplasma* cysts of the Me49 strain and monitored daily. **A**, Survival curves of infected C57BL/6 (WT), IL-1 $\alpha^{-/-}$ , or IL-1 $\beta^{-/-}$  ( $n = 5-13$  mice per group, data pooled from two to three experiments).  $p$ -value is 0.3259 by Log-rank test. **B**, Weight curves showing percent of initial weight. **C**, Inguinal subcutaneous white adipose tissue (scWAT), epididymal visceral white adipose tissue (vWAT), and quadriceps (Quad) were harvested at 16 wpi and weighed. **D**, Liver weights at 16 wpi ( $n = 6-13$  mice per group, data pooled from two to three experiments). Data are shown as the mean  $\pm$  SEM. \* $P < 0.05$ ; \*\* $P < 0.01$ ; \*\*\* $P < 0.001$ , \*\*\*\* $P < 0.0001$ , by unpaired Student's T test with Holm-Sidak method to correct for multiple comparisons.

## Chapter 5: *T. gondii* infection induces IL-1R dependent chronic cachexia and perivascular fibrosis in the liver and skeletal muscle

**The text and figures included in this chapter have been adapted from the following publication:** Melchor, S.J., Hatter, J.A., LaTorre Castillo, E.A., Saunders, C.M., Byrnes, K.A., Sanders, I., Abebayehu, D., Barker, T., & S. E. Ewald. *T. gondii* infection induces IL-1R dependent chronic cachexia and perivascular fibrosis in the liver and skeletal muscle. *Journal of Cachexia, Sarcopenia and Wasting* (under review at time of dissertation submission)

### Acknowledgements

We thank Dr. Ping Hu for assistance preparing hydrogels and Riley T. Hannan for extensive discussions of fibroblast biology. We thank Dr. Ken Tung for histopathology advice. We thank Stefan Hargett for assistance with the CLAMS metabolic monitoring and Thurl Harris for assistance assessing lipolytic machinery and fat metabolism.

### Background

Cachexia is defined as the loss of 5% of lean body mass in less than six months, accompanied by at least three of the following symptoms: weakness, fatigue, adipose tissue loss, abnormal blood biochemistry, and/or anorexia (99). Cachexia occurs in conjunction with a primary chronic disease, and prevalence can range from 5-15% in chronic heart failure and chronic pulmonary disease to over 80% in advanced cancer patients (174, 175). Beyond impairing quality of life, cachexia limits the effectiveness and duration of therapeutic interventions and can directly cause death in chronically ill patients (176–178). Currently, there are no broadly efficacious therapeutics for cachexia. Dietary supplementation and anabolic steroids have largely failed to reverse clinical cachexia (100). Circulating IL-1, IL-6, TNF- $\alpha$ , and IFN- $\gamma$  are a conserved inflammatory signature across etiologies of cachexia; however, TNF- $\alpha$  blockade has failed to halt or reverse cachexia in the clinic (179). More recently a first-in-class monoclonal antibody against IL-1 $\alpha$  has been shown to increase lean body mass and quality of life in patients with metastatic cancers (173). While these data suggest that there may be therapeutic value in targeting the IL-1 pathway for cachexia, a disease-matched study of cachectic and weight stable patients has not yet been performed.

Current animal models of cachexia recapitulate acute cachectic weight loss, but fail to model many aspects of long-term cachexia progression. Surgical interventions including cardiac, gastric, and renal obstructive surgeries are lethal after a rapid period of weight loss. Tumor models take longer to develop but have a similar 1-2 week window of weight loss before tumor growth is lethal. Interventions like low level endotoxin injection are transient, and in a new LCMV model of cachexia, mice recover weight once infection is cleared (171, 180). Although these studies have uncovered important aspects of acute cachexia biology, longer-term models may reveal novel pathways of homeostatic dysfunction and potential

therapeutic targets. Cachexia or cachexia-like disease is extraordinarily common in parasitic infection; however, animal models of parasite-induced cachexia have received comparatively little attention in the modern molecular era (181). We have recently shown that oral infection with the protozoan parasite *Toxoplasma gondii* (*T. gondii*) leads to a sustained loss of muscle mass that meets the current clinical definition of cachexia (53). *T. gondii* is a protozoan parasite that naturally infects humans and mice. During acute infection (the first 3 weeks of infection) the parasite can be found in most tissues in the body. Immune competent hosts largely clear systemic infection, but low levels of *T. gondii* tissue cysts persist for the life of the host in the brain and skeletal muscle, among other tissues (7). Controlling chronic infection depends on a sustained, low grade inflammatory response and TH1 immunity, characterized by IL-12, IFN- $\gamma$ , and CD4<sup>+</sup> and CD8<sup>+</sup> T cells.

We hypothesized that the robust and reproducible nature of *T. gondii* infection-induced cachexia would yield novel insight into the pathophysiology of chronic cachexia. Here we report that intraperitoneal injection of *T. gondii*, which limits the effect of commensal microbiota-induced inflammation, was sufficient to induce chronic cachexia characterized by long-term muscle and fat wasting, fatigue, and elevated circulating cytokines. The longevity of our model revealed that cachectic mice develop perivascular fibrosis in major metabolic tissues, including the visceral white adipose tissue, the muscle, and the liver. Chronic cachexia and cachexia-associated liver and skeletal muscle fibrosis was IL-1R dependent. This increase in fibrosis was not due to parasite overgrowth, as infection levels were similar between IL-1R<sup>-/-</sup> and wildtype mice. IL-1 $\alpha$  levels were elevated in sera and liver lysates of cachectic mice; in vitro, IL-1 $\alpha$  or IL-1 $\beta$  were sufficient to promote fibroblast contractility and expression of smooth muscle actin. These findings are consistent with a novel role for the IL-1R signaling axis as a driver of chronic cachexia and the development of cachexia-associated fibrosis during *T. gondii* infection.

## Results

### ***T. gondii* infection leads to sustained cachexia in mice**

Oral infection with *T. gondii* causes severe intestinal inflammation, leaky gut, and commensal-induced inflammation during the first two weeks of infection (65, 182, 183). We previously demonstrated that mice orally infected with *T. gondii* develop chronic cachexia that was sustained even after intestinal inflammation resolved (53). To determine if *T. gondii* infection induced cachexia when the gastrointestinal tract was bypassed entirely, 10-14 week old male C57BL/6J mice were intraperitoneally injected with 10 Type II *T. gondii* (Me49 strain) bradyzoite tissue cysts. *T. gondii*-infected mice lost 15-20% of their initial body mass during the first three weeks of infection (**Fig. 5.1A-B**), and remained significantly wasted compared to uninfected controls for up to twenty-one weeks (**Fig. 5.1B**). Chronic infection was confirmed by counting cysts in brain homogenate at nine weeks post-infection (**Fig. 5.1C**). Although infected mice went through a period of acute anorexia 8-10 days post-infection, they regained eating relative to uninfected controls, indicating that sustained weight loss was not due to prolonged anorexia (**Fig. 5.1D**). In fact, infected mice trended towards eating more chow per 24-hour period than uninfected mice, although this was not significant (**Fig. 5.1D, Fig. 5.1E**, left). Bomb calorimetry on fecal pellets confirmed that infected mice were absorbing a similar number of calories as uninfected mice (**Fig. 5.1E**, right).

Loss of lean muscle mass is the primary diagnostic marker of cachexia. By two weeks post-infection, infected mice had a significant reduction in both fat (**Fig. 5.1F**, left) and lean (**Fig. 5.1F**, right) body mass by EchoMRI Whole Body Composition Analysis. Importantly, while fat mass partially recovered by six weeks post-infection, lean body mass wasting progressed from two to six weeks post-infection (**Fig. 1F**). When individual tissues were dissected and weighed, we found that inguinal subcutaneous white adipose tissue (scWAT), epigonadal visceral white adipose tissue (vWAT), and quadriceps muscle mass (Quad) were significantly reduced at two weeks post-infection. Acute hepatomegaly was also observed, consistent with published reports of acute *T. gondii* infection in the liver (**Fig. 5.1G**) (141). By nine weeks post-infection, scWAT had recovered in mass but vWAT, quad, and liver were significantly reduced in size relative to uninfected littermate controls (**Fig. 5.1G**). Gastrocnemius (GA), tibialis anterior (TA), and extensor digitorus longum (EDL) muscles were also weighed. The TA and EDL were significantly smaller in infected mice relative to uninfected; the GA from infected mice trended smaller, although this was not significant due to variability in GA mass (**Fig. 5.2**). Elevated circulating inflammatory cytokines are a hallmark of cachexia that contribute to disease pathology (184). At one week post-infection, when *T. gondii* infection is systemic, mice had elevated circulating IFN- $\gamma$ , IL-1 $\beta$ , IL-6, and TNF- $\alpha$  compared to uninfected controls (**Fig. 5.1H**, grey background). Although TNF- $\alpha$ , IL-6, and IFN- $\gamma$  were reduced by five weeks post-infection, they were still significantly elevated relative to uninfected controls (**Fig. 5.1H**, white background). Based on these data, intraperitoneal *T. gondii* infection causes loss of adipose tissue, progressive muscle loss, transient anorexia, and elevated innate circulating cytokines, consistent with the current clinical definition of cachexia (99).

### ***T. gondii*-induced chronic cachexia is independent of non-shivering thermogenesis, insulin resistance, and elevated lipolysis**

Non-shivering thermogenesis and fat browning have been implicated as important mediators of wasting in animal models of acute cancer cachexia. (185–187) However, no sustained differences in body temperature (**Fig. 5.3A**) or expansion of brown adipose tissue (BAT) depots (**Fig. 5.3B**) were observed between uninfected and infected mice with *T. gondii*-induced cachexia (188). Although transcript levels of the mitochondrial uncoupling protein *Ucp-1* were increased in the scWAT and vWAT of cachectic mice, the regulator of brown fat differentiation *Prdm16* was lower in scWAT, and other fat browning-associated transcripts, including *Pgc1a*, *Cidea*, and *C/ebp1* were not significantly elevated in WAT or BAT of cachectic mice (**Fig. 5.4A-C**). (186) Additionally, we did not observe the morphological changes in vWAT histology associated with fat browning (**Fig. 5.4D**) (189). These data indicate that non-shivering thermogenesis or fat browning are likely not the central drivers of sustained cachexia in *T. gondii* infection.

Consistent with other cachexia models, *T. gondii*-infected mice had small but significant reductions in fasting and non-fasting blood glucose levels (**Fig. 5.3C-D**). (190, 191) However, no significant differences in serum insulin levels were observed (**Fig. 5.3E**), and glucose clearance in response to a bolus of insulin was similar in cachectic mice and uninfected mice (**Fig 5.3F**), suggesting that insulin resistance is not the primary driver of metabolic dysfunction during *T. gondii*-induced chronic cachexia.

To assess systemic metabolic function during *T. gondii*-induced cachexia, mice were individually housed in CLAMS metabolic monitoring cages. Cachectic mice had significantly reduced nighttime activity compared to uninfected mice (**Fig. 5.5A**), as well as decreased calculated heat production (**Fig. 5.5B**), consistent with cachexia-associated fatigue. However, the reduced activity confounds our ability to conclude that the reduced respiratory exchange ratio (RER) observed in cachectic mice was due to a shift towards beta-oxidative rather than glycolytic metabolism (**Fig. 5.5C-E**). To better address this question, we next measured levels of key lipolytic and metabolic signaling enzymes in vWAT, liver, and muscle by western blot. Although there was some animal-to-animal variability, no consistent differences were observed between uninfected and cachectic mice in the levels of hormone sensitive lipase (HSL), phospho-HSL (Ser660), AKT, phospho-Akt (Ser473), phospho-ACC, adipose triglyceride lipase (ATGL), phospho-ATGL, and perilipin in the WAT (**Fig. 5.6A**), muscle, or liver (**Fig. 5.6B**). Atglistatin, a pharmacological inhibitor of ATGL, has been shown to block muscle wasting in acute murine cancer cachexia; (192) however, it inhibits *T. gondii* growth (62) and could not be used to confirm the conclusion that increased lipolysis was not the major driver of chronic *T. gondii*-induced cachexia. That lipolysis pathways are not chronically activated during *T. gondii*-induced cachexia is consistent with our observation that adipose tissue does not continue to waste during chronic cachexia (scWAT weight rebounds and vWAT weight stabilizes (**Fig. 5.1F-G**)), as well as clinical observations that cachexia can co-occur with obesity, and that not all cachectic patients present with adipose tissue loss (99).

#### ***T. gondii*-induced cachexia is associated perivascular fibrosis in metabolic organs**

In the course of probing protein expression by western blot, we noticed that the  $\beta$ -actin loading control was significantly upregulated in infected mice relative to uninfected controls in all the tissues assessed (**Fig. 5.6A-B**).  $\beta$ -actin has over 90% sequence homology with alpha smooth muscle actin ( $\alpha$ -SMA), and most commercially available antibodies raised against  $\beta$ -actin cross-react with  $\alpha$ -SMA (193).  $\alpha$ -SMA is a marker of myofibroblast activation, which occurs when myofibroblast precursors (usually stromal cells with distinct homeostatic roles during quiescence) encounter local inflammation or mechanical stress. Upon activation, myofibroblasts upregulate  $\alpha$ -SMA and deposit extracellular matrix. While this is an important aspect of wound healing, a dysregulated myofibroblast response can lead to fibrosis and impaired tissue function. (194–196) To determine if  $\alpha$ -SMA was chronically elevated in cachectic metabolic tissues, tissue lysates were probed with an  $\alpha$ -SMA-specific antibody by western blot.  $\alpha$ -SMA was elevated in liver (**Fig. 5.7A**), muscle (**Fig. 5.7B**), and vWAT (**Fig. 5.7C**) of infected, cachectic mice relative to the uninfected mice at nine weeks post-infection. To determine if tissues with elevated  $\alpha$ -SMA were fibrotic, tissue sections were stained with Picrosirius Red, an anionic dye that labels elongated collagen fibers. Significantly more perivascular collagen was observed in the liver (**Fig. 5.7D**), muscle (**Fig. 5.7E**), and vWAT of cachectic mice relative to uninfected controls (**Fig. 5.7F**). Increased levels of collagen I and collagen III in the liver in proximity to  $\alpha$ -SMA-expressing cells was confirmed by immunofluorescence staining (**Fig. 5.7G**). These data indicate that perivascular fibrosis in major metabolic tissues occurs during *T. gondii* infection-induced chronic cachexia.

### IL-1 $\alpha$ and IL-1R are expressed in the fibrotic liver microenvironment

Transforming growth factor beta (TGF- $\beta$ ) is a canonical inducer of tissue remodeling and fibrosis, so we hypothesized that TGF- $\beta$  would be elevated in fibrotic tissues. Unexpectedly, TGF- $\beta$  was not significantly increased in liver, muscle or vWAT lysates (**Fig. 5.8A, Fig. 5.9A-B**). Based on these data, we also evaluated expression of IL-6, TNF- $\alpha$ , IFN- $\gamma$ , IL-1 $\alpha$ , and IL-1 $\beta$  because these inflammatory cytokine are frequently observed in cachexia as well as fibrotic diseases. (197) We found that IL-1 $\alpha$  was significantly higher in liver lysates (Fig. 5.8A) and the serum (**Fig. 5.8B**) of cachectic mice at 9 weeks post-infection relative to uninfected controls. Of note, IL-6, TNF- $\alpha$ , and IFN- $\gamma$ , which are also elevated in sera during chronic *T. gondii* infection, (**Fig. 5.1H**) play a well-established and essential role in controlling chronic *T. gondii* burden. The role of IL-1 $\alpha$ /IL-1R axis in *T. gondii* infection is comparatively understudied. IL-1 has been implicated in the development of liver fibrosis; (198–200) and altered liver biology, which is central to systemic metabolism, has been observed in a number of experimental and clinical cachexia models (201–204). To determine if IL-1 $\alpha$  was localized to areas of fibrosis, liver sections were stained with an IL-1 $\alpha$ -specific antibody for immunofluorescence assays. Cells expressing IL-1 $\alpha$  were observed within collagen I-rich perivascular fibrotic lesions, but did not co-stain with immune cell marker CD45, suggesting that these were likely liver-resident cells (**Fig. 5.8C**). IL-1 $\alpha$  signals through the type I IL-1 receptor (IL-1R). IL-1R staining was also observed within perivascular fibrotic lesions on a subset of  $\alpha$ -SMA positive cells with fibroblast morphology (**Fig. 5.8D**), suggesting that  $\alpha$ -SMA positive cells could directly respond to locally-released IL-1 $\alpha$  in the liver.

### IL-1 is sufficient to stimulate myofibroblast contractility in vitro

To determine if IL-1 $\alpha$  was sufficient to promote myofibroblast activation in vitro, murine embryonic fibroblasts (MEFs) were treated with media, IL-1 $\alpha$ , IL-1 $\beta$ , or TGF- $\beta$  (positive control) for 48 hours then stained for immunofluorescent imaging (**Fig. 5.10A**). Compared to media alone, IL-1 $\alpha$  treatment significantly induced  $\alpha$ -SMA expression and increased cell surface area (a measure of increased cell contractility) to a similar level as TGF- $\beta$  (**Fig. 5.10B-C**) (205). IL-1 $\beta$  treatment also increased cell spreading and  $\alpha$ -SMA expression, albeit to a lower level than IL-1 $\alpha$ . Neither IL-1 $\alpha$  or IL-1 $\beta$  promoted MEF proliferation or survival under serum starvation conditions (**Fig 5.11A**). To determine if IL-1 $\alpha$  was sufficient to induce myofibroblast differentiation in primary cells, we took advantage of a recent protocol to isolate primary hepatic stellate cells (HSCs), the major liver myofibroblast precursor cell type in the liver, based on the endogenous autofluorescence of vitamin A-containing granules (**Fig. 5.11B**) (206). Mechanosensing of rigid tissue culture plastic can spontaneously trigger HSC activation (207), potentially masking an activating effect of IL-1 $\alpha$ , so HSCs were plated on a 4kPa hydrogel to approximate normal liver rigidity. (208) IL-1 $\alpha$  or TGF- $\beta$  stimulation for 48 hours led to significantly increased cell area (**Fig. 5.10D, E**) and intracellular  $\alpha$ -SMA staining (**Fig. 5.10F**) relative to HSCs treated with media alone. HSCs stimulated with IL-1 $\beta$  for 24 hours also had significantly elevated cell area, and trended towards an increase in  $\alpha$ -SMA which was not significant over this shorter time frame (**Fig. 5.11C**). Taken together, these data indicate that IL-1 $\alpha$  is sufficient to promote myofibroblast activation in vitro.

### IL-1R is necessary for cachexia, as well as cachexia-associated liver and skeletal muscle atrophy and fibrosis during *T. gondii*-induced chronic cachexia

Both IL-1 $\alpha$  and IL-1 $\beta$  signal through the type I IL-1 receptor (IL-1R). To determine if the IL-1R pathway was necessary for development of fibrosis during *T. gondii* infection-induced chronic cachexia, wildtype or mice deficient in IL-1R (IL-1R<sup>-/-</sup>) were infected and fibrotic tissues were harvested at nine weeks post-infection. Importantly, IL-1R<sup>-/-</sup> mice were rescued from long-term weight loss (**Fig. 5.12A**). Protection was not due to better parasite clearance, as IL-1R<sup>-/-</sup> and wildtype mice had a comparable brain parasite load at chronic infection (**Fig. 5.12B**). This was surprising because mice deficient in IL-6 (24), TNF- $\alpha$  (147), and IFN- $\gamma$  (23) succumb to parasite overgrowth early in infection. When fibrotic tissues were weighed, infected IL-1R<sup>-/-</sup> mice had less pronounced muscle loss at nine weeks post-infection than infected wildtype mice, and by 18 weeks post-infection, IL-1R<sup>-/-</sup> muscle mass completely recovered while wildtype mass remained wasted compared to uninfected controls (**Fig. 5.12C**). Similarly, infected IL-1R<sup>-/-</sup> livers were significantly elevated in mass compared to infected wildtype livers at both nine and eighteen weeks post-infection (**Fig. 5.12D**). However, vWAT mass remained wasted in infected IL-1R<sup>-/-</sup> and wildtype mice (**Fig. 5.12E**).

In comparison to WT mice, which had fibrotic tissues at nine weeks post-infection, infected IL-1R<sup>-/-</sup> mice had levels of liver and muscle  $\alpha$ -SMA comparable to uninfected controls (**Fig. 5.13A-B**). Infected IL-1R<sup>-/-</sup> vWAT, which wasted in chronic infection (**Fig. 5.12E**), had more  $\alpha$ -SMA than uninfected controls, but  $\alpha$ -SMA levels were slightly lower than infected wildtype mice (**Fig. 5.13C**). When collagen was measured directly, infected IL-1R<sup>-/-</sup> mice had significantly less picrosirius red collagen staining in the liver (**Fig. 5.13D**) and skeletal muscle (**Fig. 5.13E**) compared to infected WT mice. Although IL-1 $\alpha$  and IL-1 $\beta$  were not significantly increased in skeletal muscle lysate by ELISA (**Fig. 5.9A**), the circulating IL-1 $\alpha$  (**Fig. 5.8B**) may be sufficient to promote perivascular fibrosis in the skeletal muscle. A not mutually exclusive possibility is that pockets of IL-1 $\alpha$  and/or IL-1 $\beta$  may exist in muscle fibrotic microenvironments which are below the level of detection in whole tissue lysate. In the vWAT, picrosirius red staining was similar between WT and IL-1R<sup>-/-</sup> mice at nine weeks post-infection (**Fig. 5.13F**) This was consistent with vWAT wasting and  $\alpha$ -SMA upregulation and suggest that IL-1R-independent pathways regulate collagen deposition and/or turnover in this tissue. Together, these data indicate that IL-1R drives chronic cachexia and the associated liver and skeletal muscle fibrosis during chronic *T. gondii* infection. Although there was significant immune infiltrate in infected livers and adipose tissue, immune infiltrate was not different between infected WT and infected IL-1R<sup>-/-</sup> mice in the liver (**Fig. 5.14A**) or vWAT (**Fig. 5.14B**), suggesting that changes in liver fibrosis were not mediated by different populations of immune cells.

## Discussion

Here we show that intraperitoneal *T. gondii* infection is a robust model for chronic cachexia that recapitulates critical aspects of clinical disease. This is supported by several previous reports describing chronic weight loss and muscle dysfunction during *T. gondii* infection (44, 53, 54, 63, 64). A major advantage of the *T. gondii* cachexia model is its longevity, which opens the door to studying mechanisms of disease reversal and testing therapeutic tools

(180, 209). Our data indicate that pathways critical to acute anorexia-cachexia progression (lipolysis and non-shivering thermogenesis) may not be central drivers of chronic cachexia. Moreover, the longevity of our model allowed us to observe fibrosis in the liver, adipose tissue, and skeletal muscle, a process that typically takes many weeks to develop. This finding complements recent studies from the Seelaender group, who has recently reported increased tumor and adipose tissue fibrosis in cachectic gastrointestinal cancer patients relative to age and disease-matched, weight stable cancer patients. (210, 211) Skeletal muscle fibrosis has also been reported in the quadriceps of cachectic patients with chronic heart failure,(212) as well as in the rectus abdominus of cachectic patients with pancreatic ductal adenocarcinoma (PDAC) compared to weight stable controls (213). In the latter study, skeletal muscle collagen levels directly correlated with weight loss and mortality.

While only a handful of studies have assessed fibrosis in cachectic patients, there is a strong association between cachexia and fibrotic diseases (174, 214). Emerging clinical data show a clear correlation between muscle wasting, disease progression, and mortality in liver cirrhosis, non-alcoholic fatty liver disease and hepatocellular carcinoma--the 4<sup>th</sup> leading worldwide cause of cancer related mortality (215–225). The liver is a central regulator of nutrient absorption, storage, and metabolism, and as such, liver fibrosis may influence aberrant metabolism in distal tissues. Additionally, fibrosis in the skeletal muscle physically restricts muscle regeneration (226) and fibrosis in other muscles like the heart and diaphragm could lead to dysfunction that is ultimately fatal. Historically, peripheral fibrosis during cachexia may have been overlooked because of the difficulty in obtaining biopsies from these tissues. However, muscle biopsy and assessment of adipose tissue removed during surgery are becoming increasingly common, which may enable a more thorough understanding of cachexia-associated fibrosis in the future.

Our experiments showed that IL-1R deficient mice are protected from developing cachexia, consistent with reports demonstrating that peripheral (163) and central (164) administration of IL-1 is sufficient to acutely recapitulate aspects of muscle wasting. In addition, mice deficient in MyD88, the signaling adaptor downstream of IL-1R and most Toll-like receptors, are protected from fat and lean muscle mass, fatigue, and increased mortality in a pancreatic cancer model of cachexia (227). IL-1R<sup>-/-</sup> mice are also protected from perivascular fibrosis in the liver and muscle during chronic cachexia. This finding is consistent with reports that SNPs in the IL-1R antagonist gene resulting in elevated IL-1 signaling are associated with an increased risk of developing both respiratory (228, 229) and liver fibrosis (230). Additionally, pharmacological or genetic blockade of IL-1R signaling in mice has been shown to attenuate fibrosis in the liver (145, 198, 231), heart (232, 233) and lungs (233, 234). We did not see elevated IL-1 $\alpha$  or IL-1 $\beta$  in the circulation during chronic cachexia; however, IL-1 $\alpha$ -expressing cell types were observed within perivascular fibrotic lesions in the liver. This observation, in conjunction with the observation that IL-1R is also expressed within fibrotic regions, suggests that local IL-1 $\alpha$  is sufficient to control tissue-wide development of fibrosis in the liver. As an alarmin, bioactive IL-1 $\alpha$  can be released via a broad range of cell damage or death inducers, and future work will be necessary to determine the source and mechanism of release of IL-1 $\alpha$ . Studies are also underway to identify precise myofibroblast cell or precursor populations that express IL-1R and test whether selectively eliminating or driving IL-1R

signaling on these cell types is sufficient to influence fibrosis and cachexia during *T. gondii* infection.

Like cachexia, fibrosis has been notoriously difficult to target and reverse in the clinic. Our data suggest that these conditions may be linked, which poses a potential explanation for why cachexia has been so difficult to reverse with nutritional supplementation and anabolic steroids. Additional experiments will be necessary to determine if fibrosis is causal for cachexia and/or limits recovery from acute cachectic weight loss, although a recent study found that experimental models of cirrhosis lead to muscle wasting (235). The relationship between IL-1R signaling, fibrosis and cachexia is an exciting new area for exploration in both animal models and clinical cachexia.

## Figures

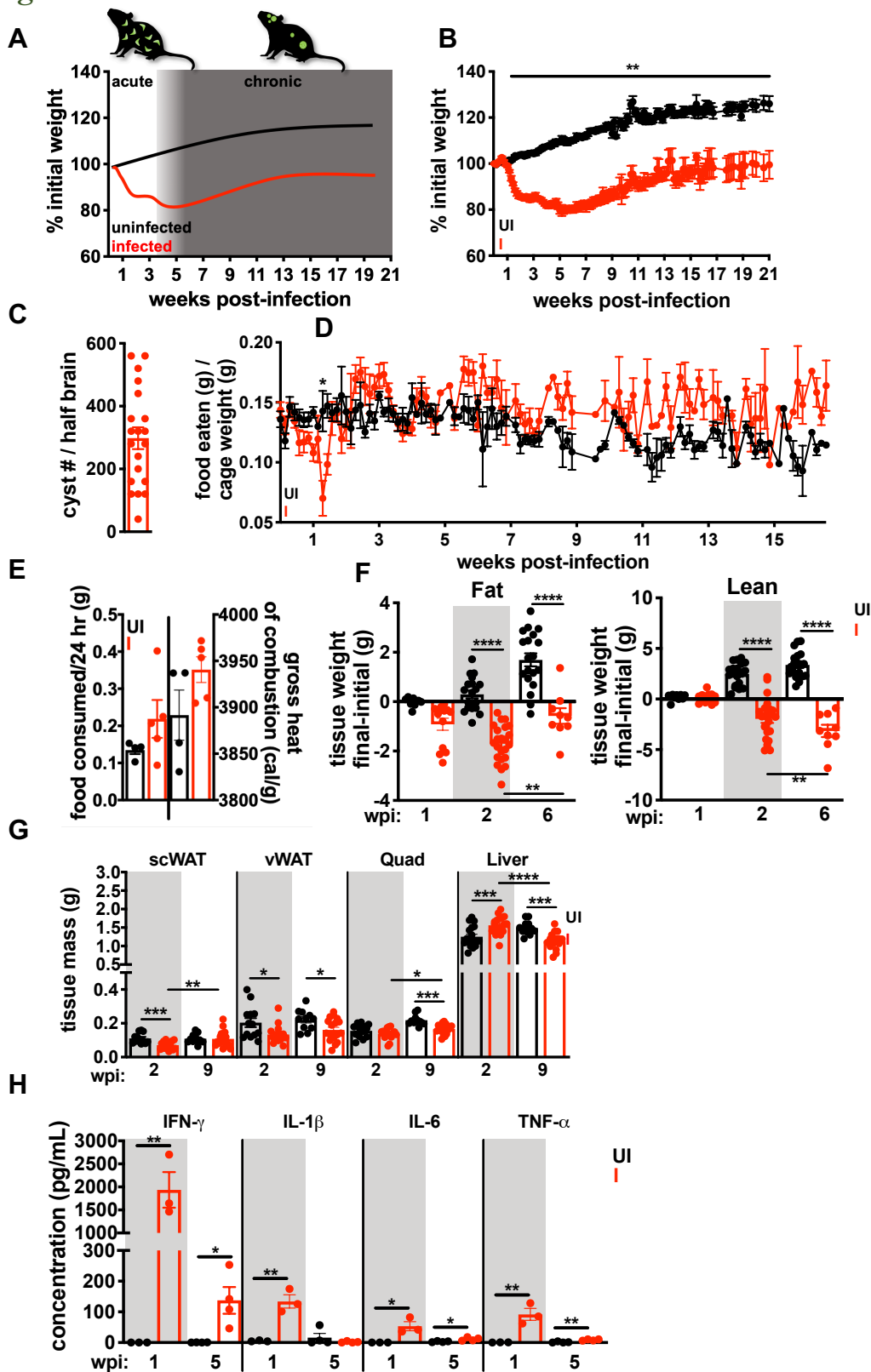
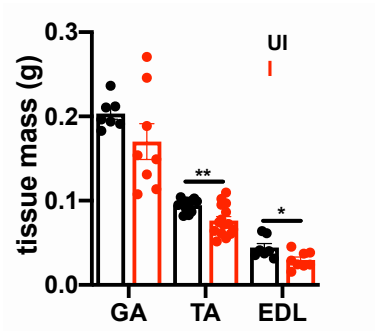
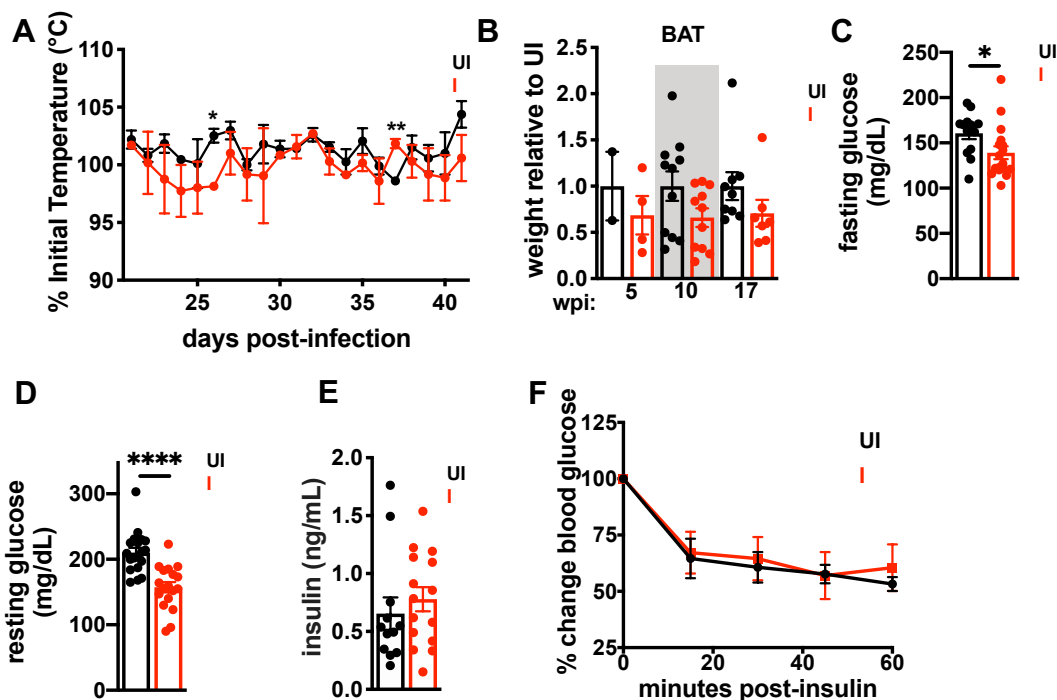


Figure 5.1 Chronic *Toxoplasma* infection causes sustained cachexia in mice (legend continue on the next page).

**Figure 5.1 Chronic Toxoplasma infection causes sustained cachexia in mice (legend continued from following page).** 10-14 week old C57BL/6J mice were intraperitoneally infected with 10 Toxoplasma cysts of the Me49-GFP-luciferase strain (I, red) or mock injected with PBS (UI, black). **A**, Schematic of weight loss relative to parasite distribution. The acute phase of infection (white) is dominated by Toxoplasma tachyzoites (green crescents) which spread systemically, infecting most tissues in the body. 4-6 weeks post-infection (wpi), systemic infection is largely cleared and parasites are driven to the chronic tissue cyst form (green circles). **B**, Mice lose up to 20% of their initial body mass in the first 4 wpi and fail to regain weight relative to uninfected controls. N=35-45 mice pooled from 3 independent experiments. **C**, Dolichos biflorous positive Toxoplasma cysts per half brain at 5-9 wpi. N=19 pooled from 6 independent experiments. **D**, Daily food intake per cage normalized to pooled weight of the mice in the cage measured every 24 hours. N=7-9 cages per group, pooled from 3 independent experiments. **E**, Mice were individually housed for 24 hours at 10 wpi and food intake over 24 hours was determined by weight (left) and caloric content of fecal pellets were determined by bomb calorimetry (right). **F**, Echo MRI quantification of fat (left) and lean (right) tissue mass at 2 or 6 wpi. N=28-45 mice per group, representative of 3 independent experiments. **G**, Inguinal subcutaneous white adipose tissue (scWAT), epididymal visceral white adipose tissue (vWAT), quadriceps (Quad) and liver weights at 2 wpi or 9wpi N=12-18 mice per group, pooled from 3 experiments. **H**, Serum cytokines measured by Luminex at 1 or 5 wpi. N=3-4 mice per group, representative of 2 experiments. Error bars are standard error of the mean. \*P < 0.05; \*\*P < 0.01; \*\*\*P < 0.001, \*\*\*\*P < 0.0001 by unpaired Student's T test with Holm-Sidak method to correct for multiple comparisons.



**Figure 5.2 Skeletal muscle is wasted in mice chronically infected with *T. gondii*.** Tissue weights of gastrocnemius (GA), tibialis anterior (TA) and extensor digitorum longus (EDL) at 10 wpi. N= 7-15 mice per group, pooled between 2-3 independent experiments.



**Figure 5.3** *T. gondii*-induced chronic cachexia occurs independently of non-shivering thermogenesis and insulin resistance. **A**, Male and female mice were subcutaneously injected with telemetric temperature probes at 11 days post-infection, and temperature was monitored daily. **B**, Supraclavicular brown adipose tissue (BAT) weights relative to the mean weight of uninfected tissue at 5, 10, or 17 wpi. N=2-11 mice per group. **C-D**, blood glucose was collected by tail snip and either measured after 4 hours of fasting at 9 wpi (**C**, N=13-17, pooled between 3 independent experiments) or after random feeding at 7-14 wpi (**D**, N=18-19 mice per group, pooled between 2 independent experiments) by glucometer. **E**, Serum insulin levels measured by ELISA at 7-10 wpi. N=12-15 mice per group, pooled between two independent experiments. **F**, Random-fed mice were intraperitoneally injected with 0.75 U insulin/kg body weight at 7-14 wpi, and blood glucose was measured every 15 minutes. N=7-9 mice per group, pooled between two independent experiments. \*P < 0.05; \*\*P < 0.01; \*\*\*P < 0.001, \*\*\*\*P < 0.0001 by unpaired Student's T test.

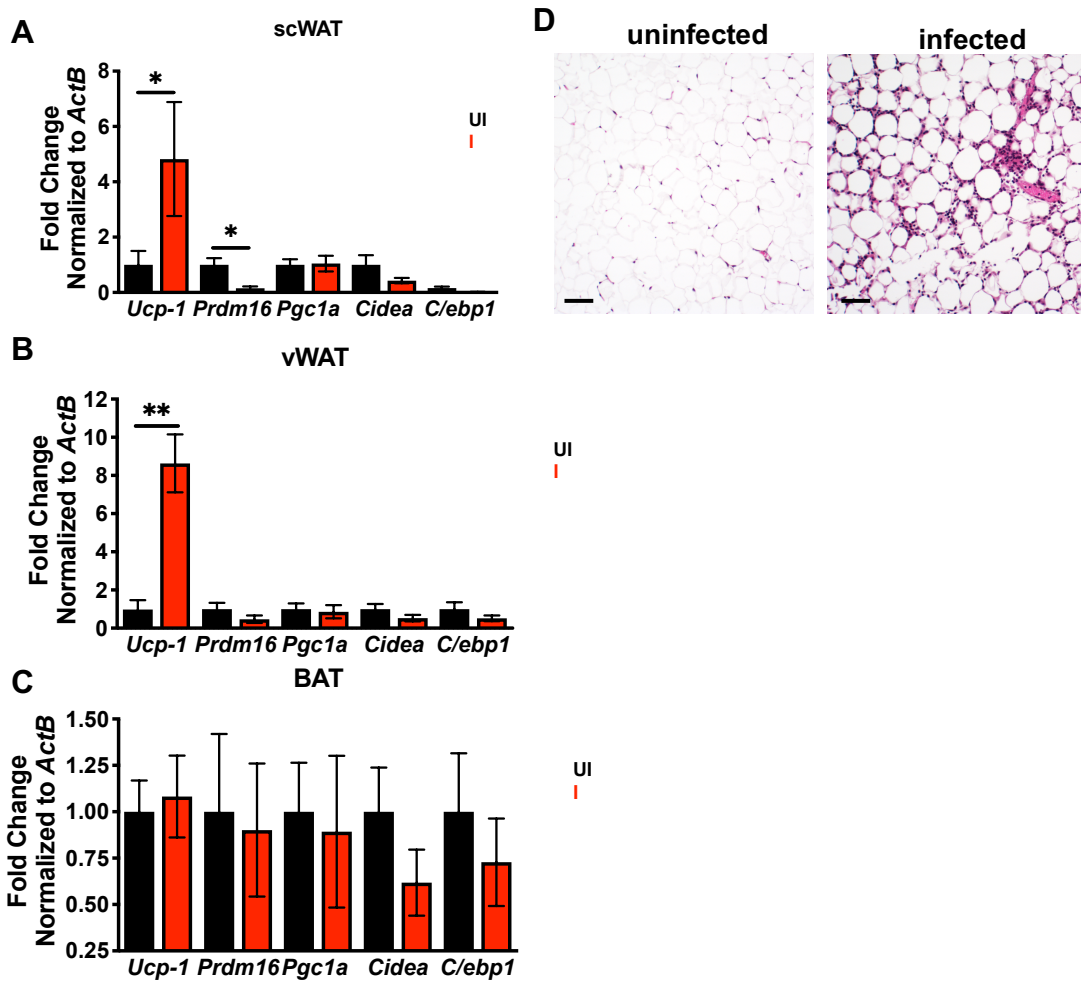


**Figure 5.4** *Toxoplasma*-induced cachexia does not induce the transcriptional signature associated with adipose tissue beiging at 17 weeks post-infection. 10-14 week old C57BL/6J mice (uninfected, UI and infected, I) were intraperitoneally infected with 10 Me49-GFP-luciferase *Toxoplasma* cysts. **A-C**, qPCR for markers of fat browning and thermogenesis in inguinal subcutaneous adipose tissue (scWAT) (**A**) epigonadal visceral white adipose tissue (vWAT) (**B**) or supraclavicular brown adipose tissue (BAT) (**C**) at 17 wpi. Error bars are standard error of the mean. N= 7-9 mice per group. \*P < 0.05; \*\*P < 0.01; \*\*\*P < 0.001 by unpaired Student's T test with Holm-Sidak method to correct for multiple comparisons. **D**, H&E staining of vWAT at 9 wpi.

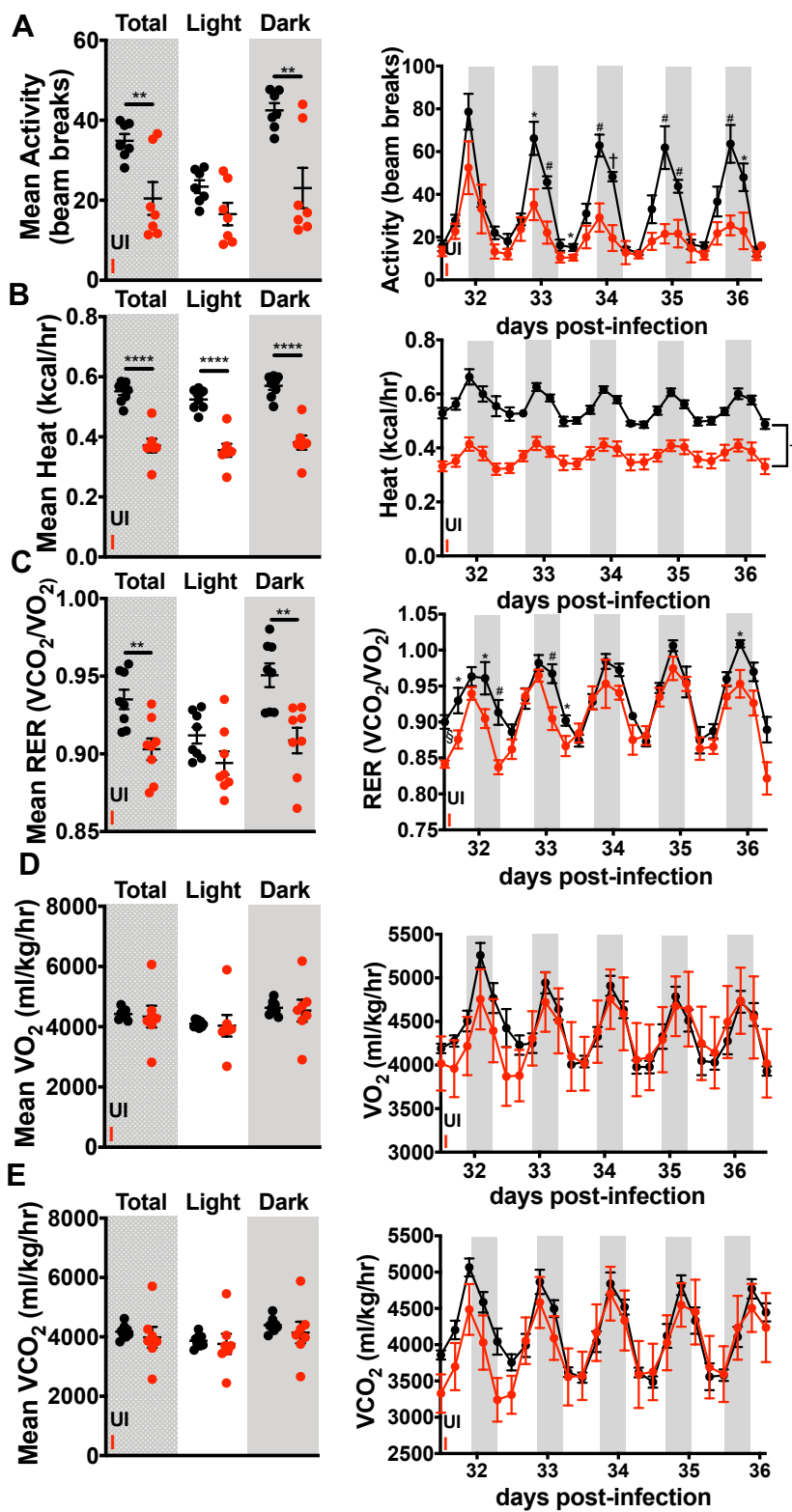
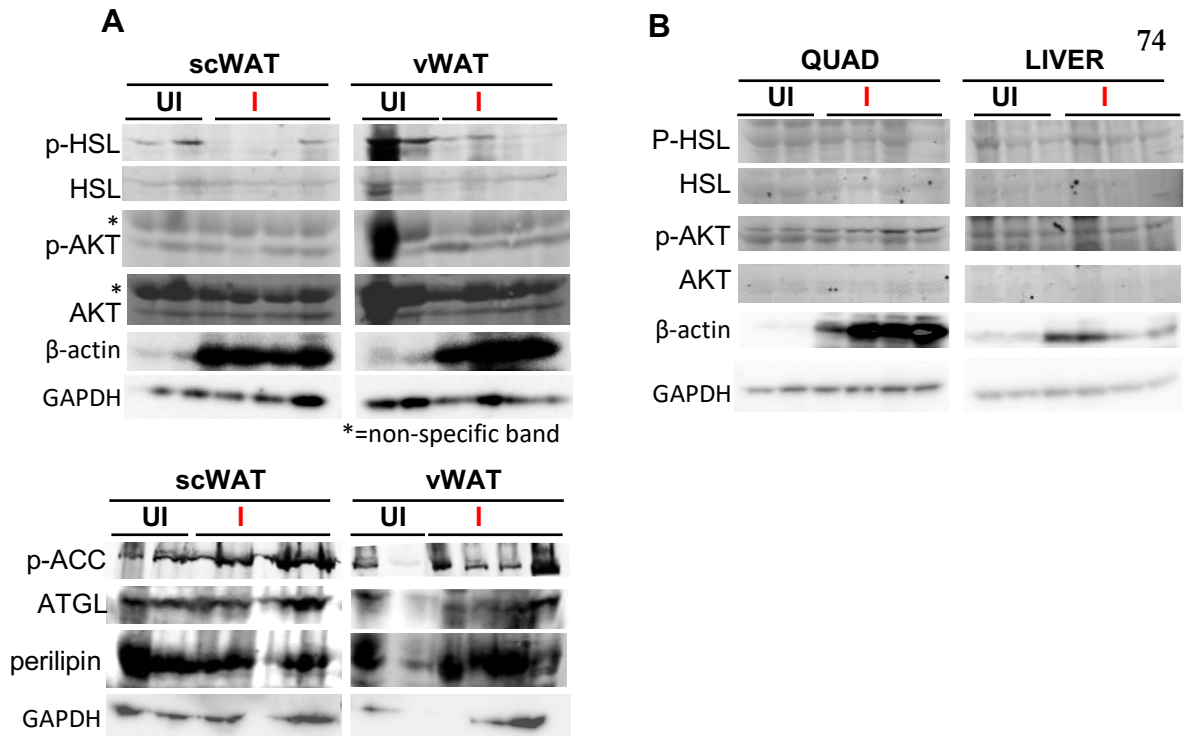
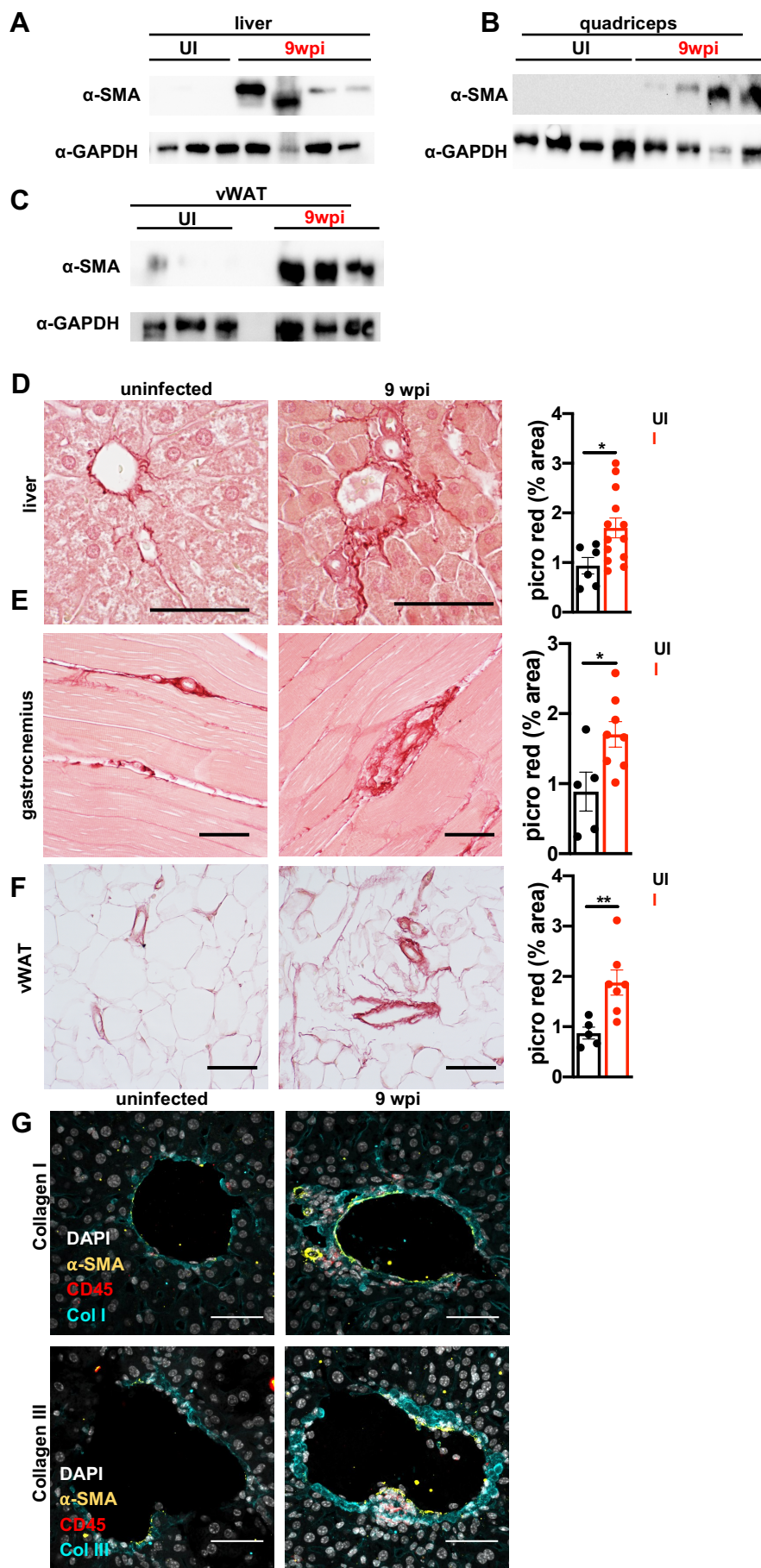


Figure 5.5 Cachectic mice have reduced activity and RER compared to uninfected mice. Mice were housed in OxyMax CLAMS metabolic cages during the time points indicated. Data from the first 24 hours in the cage were excluded (**legend continues on the next page**).

**Figure 5.5 Cachectic mice have reduced activity and RER compared to uninfected mice (legend continued from previous page).** Data on the left show mean of all the values from light (white bars) or dark cycles (shaded bars), or all time points combined (stippled bars). Data on the right show the 16 point rolling average of measurements with shaded bars representing the dark cycle over a 6 day span. **A**, Activity. **B**, Heat. **C**, Respiratory exchange ratio (RER). **D**,  $VO_2$  (normalized to lean body mass). **E**,  $VCO_2$  (normalized to lean body mass). N=7-8 animals per group, pooled between 2 independent experiments. Error bars are standard error of the mean \*,  $P < 0.05$ ; \*\*,  $P < 0.01$ ; \*\*\*,  $P < 0.001$ , by unpaired Student's T test with Holm-Sidak method to correct for multiple comparisons (mean data), and \*,  $P < 0.05$ ; #,  $P < 0.01$ ; †,  $P < 0.001$ , §,  $P < 0.0001$  (traces).



**Figure 5.6 Lipolysis is not a main driver of *Toxoplasma*-induced cachexia.** 10-14 week old C57BL/6J mice (uninfected, UI and infected, I) were intraperitoneally infected with 10 Me49-GFP-luciferase *Toxoplasma* cysts. **A-B**, Tissues were harvested at 5 wpi. Tissue lysates were made for subcutaneous white adipose tissue (scWAT) and epigonadal visceral white adipose tissue (vWAT) (**A**) or quadriceps muscle (QUAD) and liver (**B**), and blotted for lipolysis machinery: phosphorylated and non-phosphorylated hormone sensitive lipase (p-HSL, HSL), phosphorylated and non-phosphorylated AKT, phosphorylated (p-ACC), perilipin. Beta-actin and GAPDH were loading controls. Each lane is lysate from an individual mouse. Representative of 2 independent experiments.



**Figure 5.7 *T. gondii*-induced cachexia is associated with perivascular fibrosis in metabolic organs.** **A-C** Western blot for alpha smooth muscle actin ( $\alpha$ -SMA) or GAPDH on liver (**A**), quadriceps (**B**), and vWAT (**C**) lysate at 9 wpi. Representative of at least 3 independent experiments. Each lane represents an individual mouse. **D-F**, Picrosirius red staining on formalin-fixed paraffin-embedded liver (**D**), gastrocnemius (**E**), or vWAT (**F**) at 9 weeks post-infection. Representative images shown at left. Picrosirius red staining was quantified in ImageJ (right) and pixel density represented as % of each field of view. Each point represents 5 blinded fields of view averaged per mouse. **D**, N=6-13 mice per group, pooled between two independent experiments. **E-F**, N=5-8 mice per group, pooled between two independent experiments. Scale bars represent 50  $\mu$ m. Error bars are standard error of the mean. \*P < 0.05; \*\*P < 0.01; \*\*\*P < 0.001 by unpaired Student's T test. **G**, Livers were harvested at 9 wpi, formalin-fixed, and then cryosectioned and stained for markers of inflammation and liver fibrosis. Maximum intensity projections of 12-17  $\mu$ m thick liver sections with immunofluorescently labeled nuclei (DAPI white)  $\alpha$ -smooth muscle actin (yellow), CD45 (red) and Collagen1 $\alpha$  (top) or Collagen III (bottom) (blue) in the liver of uninfected or 9 wpi WT mice. Scale bars represent 50  $\mu$ m.

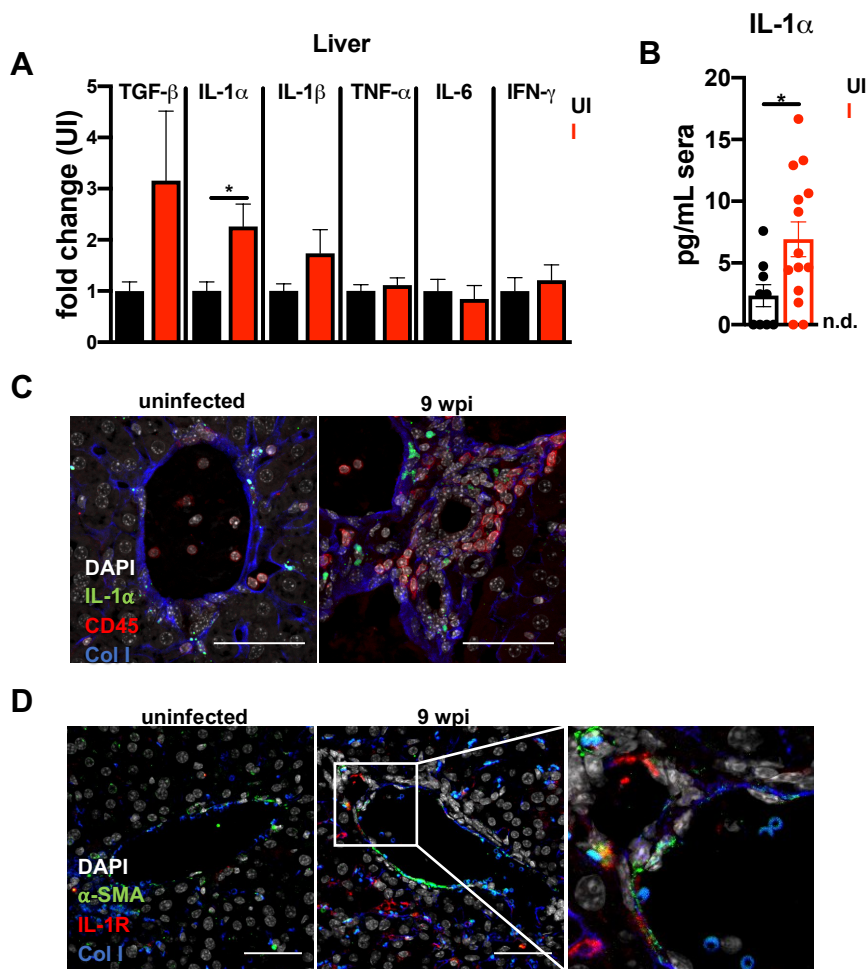


**Figure 5.8 Cells expressing IL-1 $\alpha$  and IL-1R are observed in the fibrotic liver environment.** **A**, Cytokines in tissue lysates from mice 9 wpi were measured by ELISA in liver. Data are presented as fold change relative to the mean of uninfected levels. N=11-12 mice per group, pooled from three independent experiments. N=4 mice for TGF- $\beta$ , which is representative of three experiments. **B**, IL-1 $\alpha$  levels in the sera at 9 wpi measured by ELISA. N=9-14 mice per group, pooled from four independent experiments. **C-D**, Immunofluorescence labeling of nuclei (DAPI white) IL-1 $\alpha$  (green), CD45 (red) and collagen1 $\alpha$ 1 (blue) (**C**) or nuclei (DAPI white),  $\alpha$ -smooth muscle actin (green), IL-1R (red), and collagen1 $\alpha$  (blue) in the liver of uninfected or 9 wpi WT or IL-1R<sup>-/-</sup> mice (**D**) Inset, arrow head represents  $\alpha$ -smooth muscle actin, IL-1R co-staining cells (arrow heads). (**C-D**) represent maximum intensity projections of 9-13  $\mu$ m thick z-stacks. Scale bar represents 50  $\mu$ m. Error bars are standard error of the mean. \*P < 0.05; \*\*P < 0.01; \*\*\*P < 0.001 by unpaired Student's T test with Holm-Sidak method to correct for multiple comparisons.

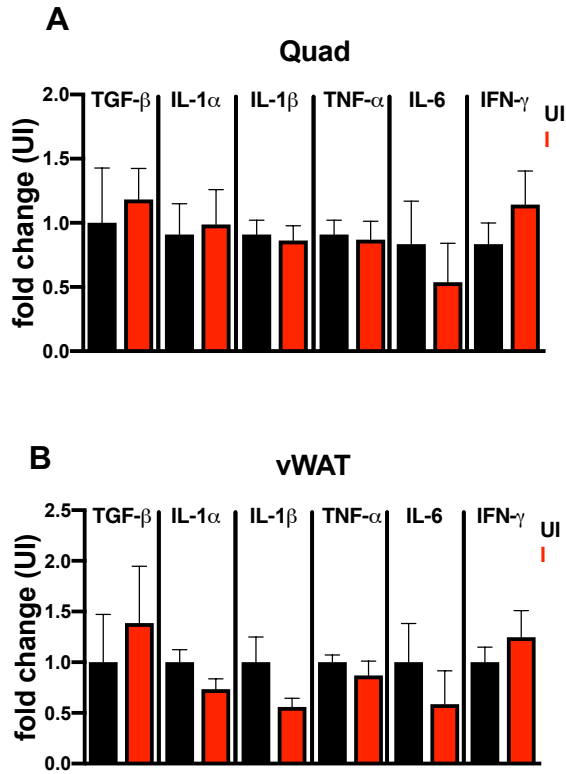


**Figure 5.9 Inflammatory cytokines are not chronically elevated in the muscle or vWAT.** **A-B**, Cytokines in tissue lysates from mice 9 wpi were measured by ELISA in quad (**A**) quad and vWAT (**B**). Data are presented as fold change relative to the mean of uninfected levels. N=11-12 mice per group, pooled from three independent experiments. N=4 mice for TGF- $\beta$ , which is representative of three experiments.

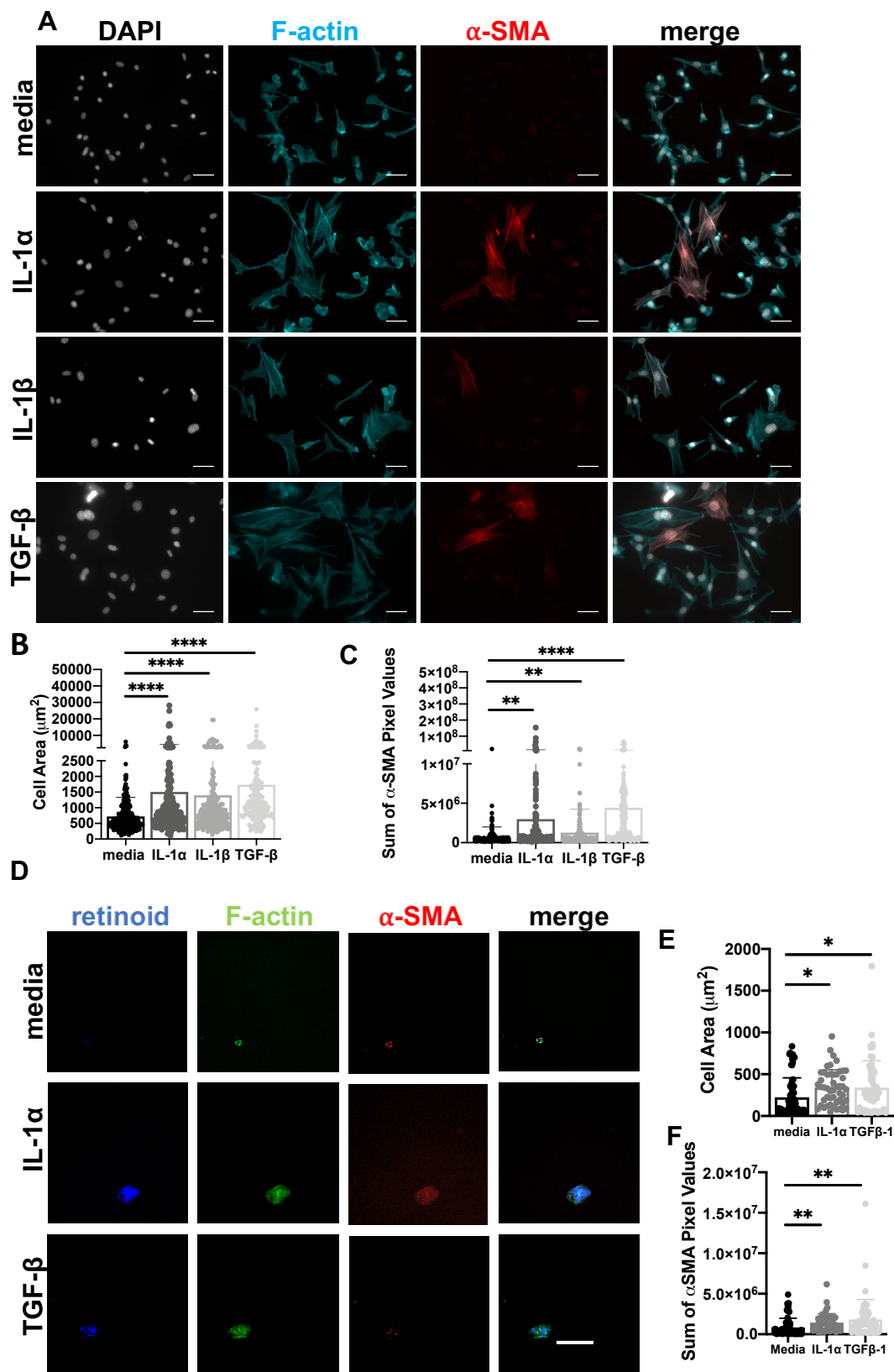
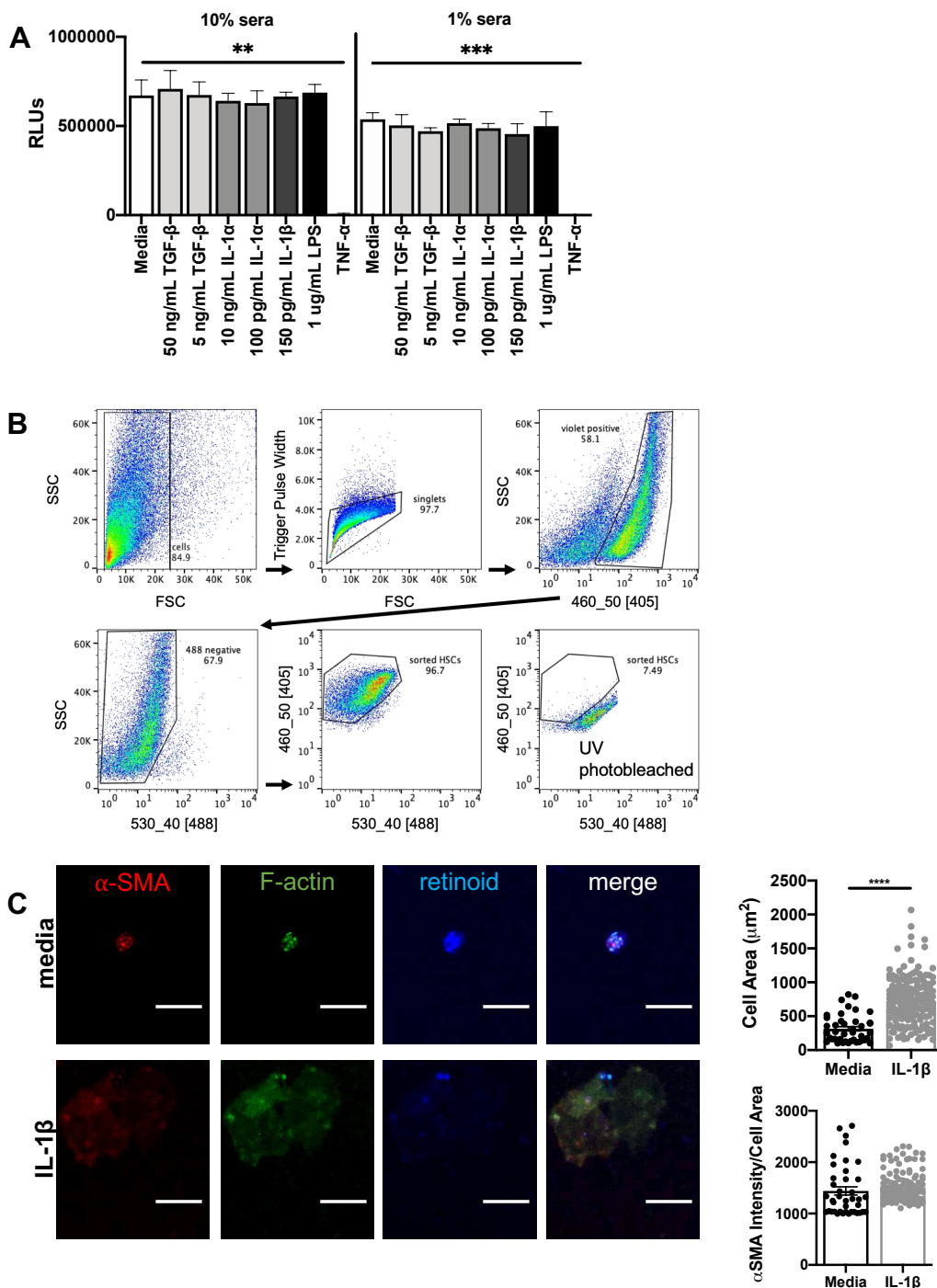
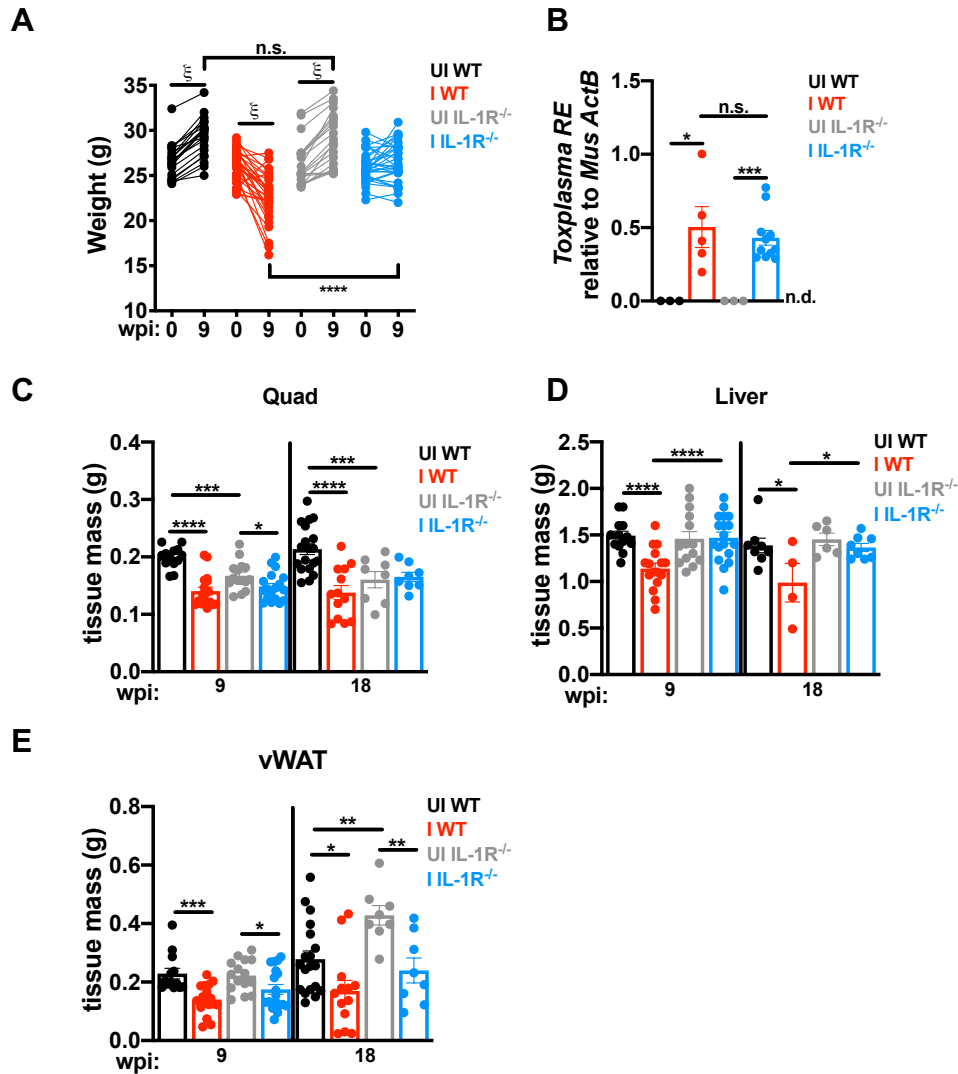


Figure 5.10 IL-1 induces contractility and alpha smooth muscle actin expression in murine embryonic fibroblasts and primary hepatic stellate cells (legend continues on the next page).

**Figure 5.10 IL-1 induces contractility and alpha smooth muscle actin expression in murine embryonic fibroblasts and primary hepatic stellate cells (legend continued from previous page).** **A-C**, MEFs were incubated with media, 10ng/mL IL-1 $\alpha$ , 150 pg/mL IL-1 $\beta$  or 10 ng/mL TGF $\beta$ -1 for 48 hours. After fixation, MEFs were stained for F-actin, and alpha-smooth muscle actin ( $\alpha$ -SMA), and cell spreading was quantified in **(B)**, and levels of  $\alpha$ -SMA expression were quantified in terms of pixels/cell **(C)**. Error bars are standard deviation, representative of 3 independent experiments. **D-F**, Primary hepatic stellate cells (HSCs) were isolated from uninfected mouse livers, and FACS-sorted based on endogenous retinoid fluorescence **(D)**. **E-F**, HSCs were seeded onto 4kPa hydrogels coated with 10ug/mL of fibronectin and cultured with 10ng/mL IL-1 $\alpha$ , 10 ng/mL TGF- $\beta$ , or media alone for 48 hours and then fixed and stained for F-actin and  $\alpha$ -SMA and imaged by confocal microscopy. Scale bar represents 50  $\mu$ m. Total cell area quantified in **(E)** and levels of  $\alpha$ -SMA expression were quantified in terms of pixels/cell in **(F)**. Error bars are standard deviation. \*P < 0.05; \*\*P < 0.01; \*\*\*P < 0.001, \*\*\*\*P < 0.0001 by unpaired Student's T test.



**Figure 5.11 IL-1 does not promote survival or proliferation in mouse endothelial fibroblasts.** **A**, MEF cells were plated on 96 well plates in 10% normal sera or 1% normal sera and incubated with media, IL-1 $\alpha$ , IL-1 $\beta$  or TGF $\beta$ -1 for 48 hours. Cell number was determined relative to a standard curve using CellTiter-Glo reagent. Data pooled between 3 experiments. \* $P < 0.05$ ; \*\* $P < 0.01$ ; \*\*\* $P < 0.001$  by unpaired Student's T test. **B-C**, Primary hepatic stellate cells (HSCs) were isolated from uninfected mouse livers, and FACS sorted based on endogenous retinoid fluorescence. HSCs were seeded onto 4kPa hydrogels coated with 10 $\mu$ g/mL of fibronectin and cultured with 10ng/mL of IL-1 $\beta$  or media alone for 24hrs and then fixed and stained for F-actin and  $\alpha$ -SMA and imaged by confocal microscopy. Error bars are standard error of the mean. \*\*\*\* $P < 0.0001$  by unpaired Student's T test. Statistical outliers were removed using the ROUT method ( $Q=1\%$ ). **D**, Representative images, scale bar represents 10  $\mu$ m.



**Figure 5.12** IL-1R<sup>-/-</sup> mice are protected from *T. gondii*-induced cachexia and cachexia-associated liver atrophy. Total body weight of mice pre-infection and 9 wpi. N=20-33 mice per group, pooled between 7 independent experiments.  $\xi$  P<0.0001 by paired Student's T test. \*\*\*\*P < 0.0001 by unpaired Student's T test. **B**, Quantity of *T. gondii* DNA relative to host beta-actin in the brain at 9 wpi. N=3-11 mice per group, representative of 3 independent experiments. **C-E**, tissue weights of quad (**C**), liver (**D**), and vWAT (**E**) at 9 or 18 wpi. P < 0.05; \*\*P < 0.01; \*\*\*P < 0.001, \*\*\*\*P < 0.0001 by unpaired Student's T test.

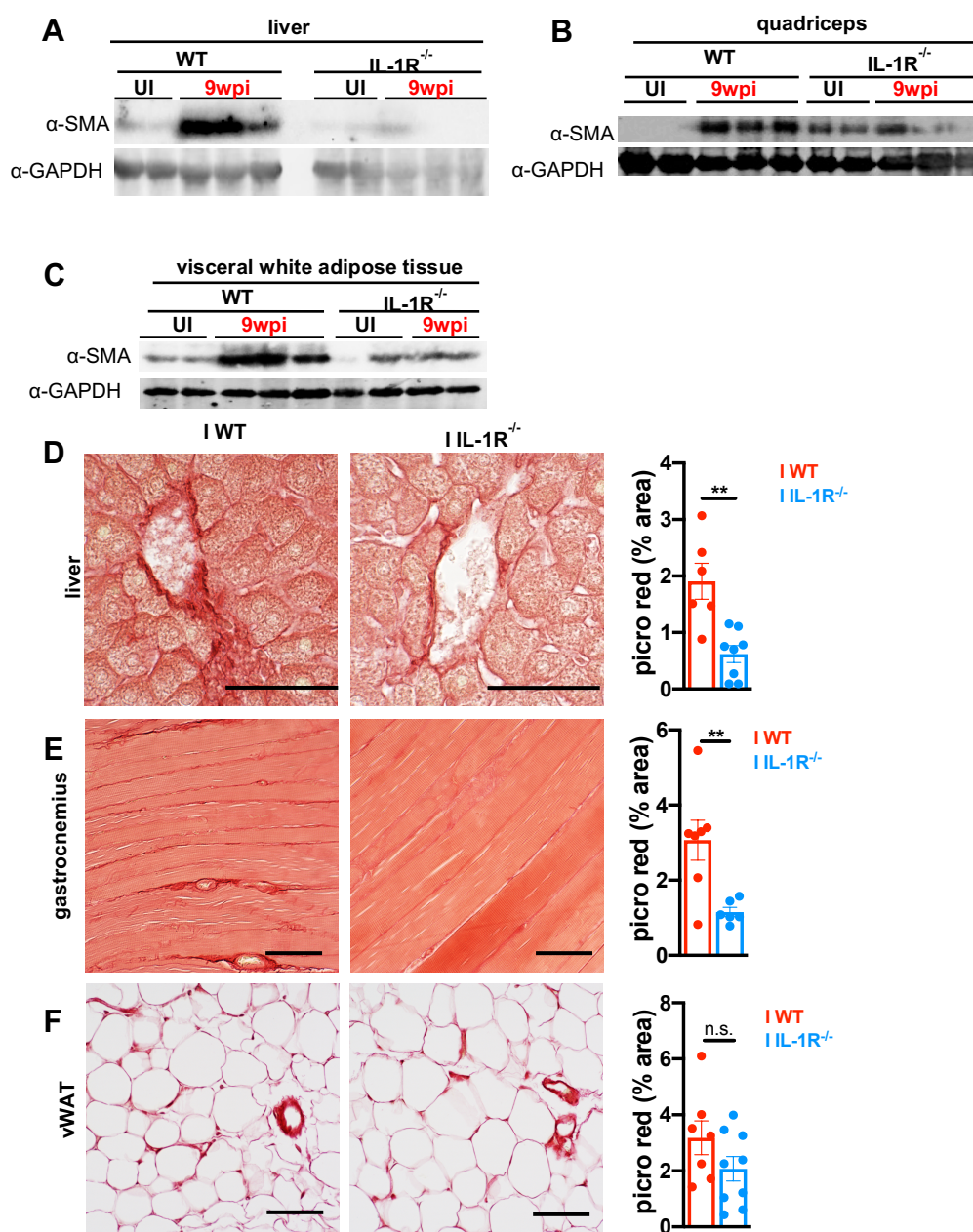


**Figure 5.13 Cachectic mice develop IL-1R-dependent liver and skeletal muscle fibrosis.** **A-C** Western blot for alpha smooth muscle actin ( $\alpha$ -SMA) or GAPDH on liver (**A**), gastrocnemius, (**B**), and vWAT (**C**) tissue lysate at 9 wpi. Representative of at least 2 independent experiments. Each lane represents an individual mouse. **D-F** Picrosirius red staining on formalin-fixed tissue at 9 weeks post-infection. Picrosirius red staining was quantified in ImageJ (below) and pixel density represented as % of each field of view (each point is 5 fields of view averaged per mouse) in the (**D**) liver, N=6-8 mice per group, pooled between 2 experiments, (**E**) gastrocnemius, N=6-7 mice per group, pooled between 2 experiments, and (**F**) vWAT, N=6-9 mice per group, pooled between 3 experiments. Error bars are standard error of the mean.  $P < 0.05$ ;  $**P < 0.01$ ;  $***P < 0.001$ ,  $****P < 0.0001$  by unpaired Student's T test.

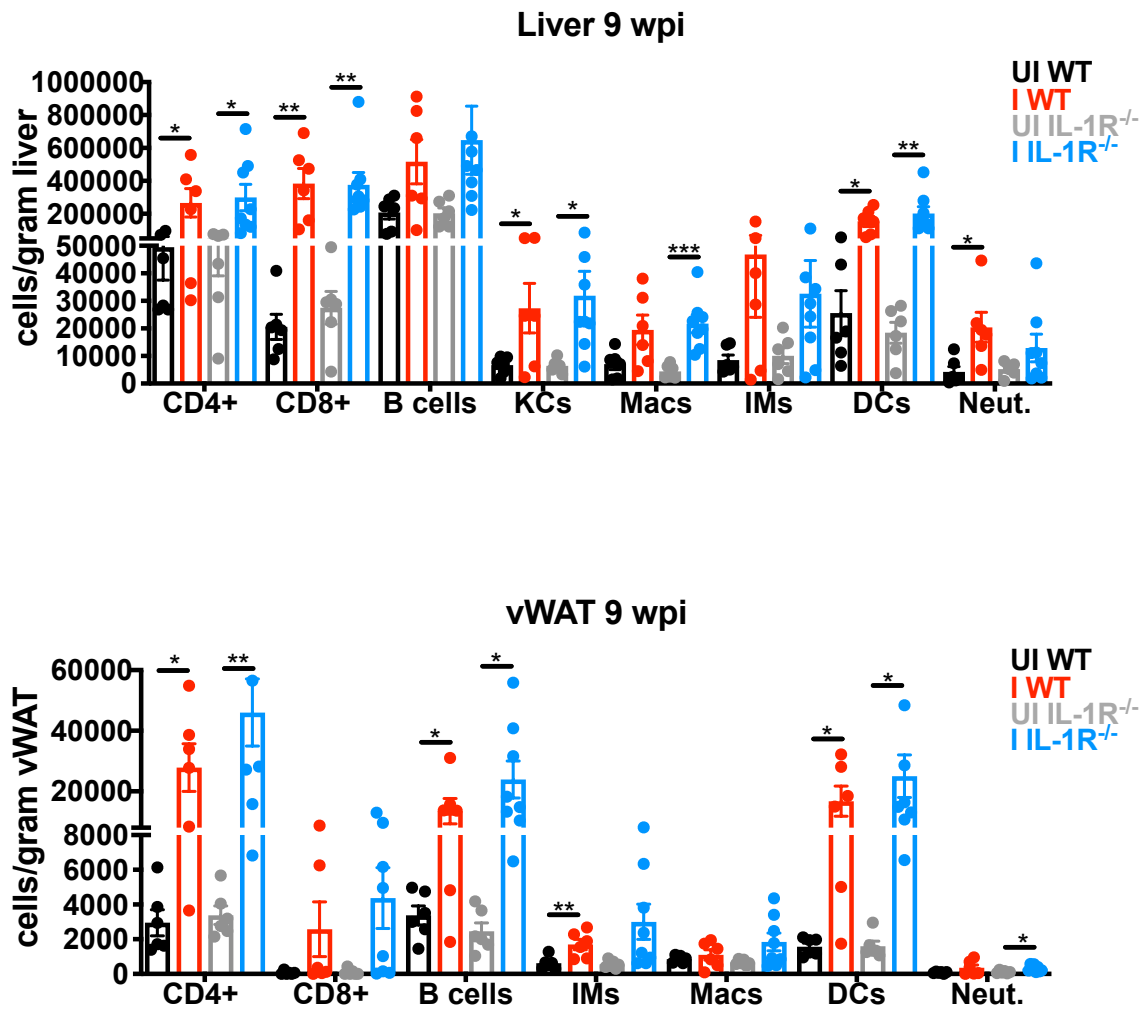


**Figure 5.14 IL-1R signaling does not control immune infiltrate in liver and vWAT nine weeks post-infection. A-C,** Following cardiac perfusion with HBSS, vWAT and liver were excised, dissociated, and numbers of infiltrating immune cells were determined by flow cytometry. **A-B,** CD4<sup>+</sup> T cells, CD8<sup>+</sup> T cells, B cells, Kupffer cells (KCs, liver only), macrophages (Macs), inflammatory monocyte (IMs), dendritic cells (DCs), and neutrophils (Neut.) in the liver (**A**) or vWAT (**B**) at 9 wpi by flow cytometry ( $n = 6-8$  mice per group, pooled from two experiments). Data are shown as the mean  $\pm$  SEM. \* $P < 0.05$ ; \*\* $P < 0.01$ ; \*\*\* $P < 0.001$ , \*\*\*\* $P < 0.0001$ , n.s., not significant by unpaired Student's T test with Holm-Sidak method to correct for multiple comparisons

## Chapter 6: Implications, Outstanding Questions, and Future Directions

### Is chronic infection with *T. gondii* necessary for sustained cachexia?

Because *T. gondii* induces chronic infection that persists for the life of the host, we have not been able to separate whether cachexia results from the long-term effects of acute infection, or from the sustained inflammation that results from chronic infection. There are currently no known strategies to pharmacologically target and kill *T. gondii* cysts (thus fully clearing infection) (236), and until recently, there were few parasite genetic tools that limited infection to the acute phase. Some of these tools include attenuated strains of *T. gondii* that lack critical virulence factors. For example, ROP5 is a *T. gondii* pseudokinase that controls parasite resistance to host immunity-related GTPases (IRGs). Infection with  $\Delta$ rop5 parasites (on a type II Prugniaud (Pru) background) in mice lead to a 99.5% reduction in brain cyst burden compared to the parent strain by three weeks post-infection (237). While this approach approximates a fully cleared infection, parasites weren't fully eliminated from the brain, and there was no assessment of unencysted parasites that could have perpetuating low levels of neuroinflammation, giving this approach limited utility for addressing the question at hand.

Bradyzoite-Formation Deficient 1 (BFD1) is a Myb-like transcription factor that controls *T. gondii* differentiation from the tachyzoite stage to the bradyzoite stage both in vitro and in vivo. With the recent discovery that ME49 parasites deficient in BFD1 ( $\Delta$ BFD1) cannot drive the tachyzoite to bradyzoite switch in response to alkaline stress in vitro or form detectable cysts in vivo (238), we have an alternative tool to address whether cachexia resolves or remains after parasite infection is fully cleared. Although more work is necessary to determine if the parasite is fully cleared in this model, monitoring cachexia in mice infected with  $\Delta$ BFD1 parasites could be an exciting opportunity to better understand and resolve the kinetics of the pathways that initiate cachexia versus those that sustain it. If chronic infection is necessary for sustained *T. gondii*-induced cachexia, a  $\Delta$ BFD1 infection model may be instructive for understanding the kinetics of recovery from acute fat and muscle wasting (particularly in the context of the IL-1R-driven pathways that prevent recovery during the chronic phase). Alternatively, if wasting persists in the absence of chronic parasite infection, this would suggest that acute insult is sufficient to cause long-term metabolic rewiring, resulting in cachexia. Additionally, this would provide much more flexibility in targeting the metabolic and/or inflammatory pathways sustaining cachexia without the confounding factor of targeting parasite growth.

### Is induction of cachexia in an adaptation of *T. gondii* to promote transmission to felines?

Induction of cachexia is not exclusive to *T. gondii* infection. Other infectious organisms like LCMV can also induce cachexia in mice (180). Parasites like *Trypanosoma cruzi* (239–241) and *Schistosoma mansoni* (242, 243) also induce cachexia in mice, and Leishmania infection

causes cachexia in Syrian hamsters (244). Many of these parasites also induce cachexia in human patients. However, *T. gondii* relies on rodents as critical intermediate hosts, as they are natural prey of its definitive felid host (245). *T. gondii* has a well-known association with dampened fear responses to feline urine in laboratory rodents, postulated to be a strategy of the parasite to return to a cat (110, 246, 247). It begs the question of whether or not activation of well-conserved cachexia induction pathways during *T. gondii* infection is another evolutionary adaptation of *T. gondii* to enhance transmission to a felid host. Mice with *T. gondii*-induced cachexia are smaller, less active (**Fig. 5.5A**) and weaker (56) than uninfected counterparts, all of which could render them less able to escape predation by a cat.

There are a number of ways to experimentally address this hypothesis. One way to test if *T. gondii*-induced cachexia enhances the loss of aversion behavior in mice would be to perform behavioral assays testing general fear responses (such as the open field test), as well as specific fear responses to the smell of cat urine using IL-1R<sup>-/-</sup> mice versus wildtype mice. This approach would uncouple which aspects of the reduced aversion phenotype are due to infection, and which (if any) are due to cachexia, with the expected outcome being that cachectic mice would spend more time near cat urine and/or in the open field when compared to non-cachectic mice with the same parasite burden.

For the studies presented in this thesis, the infectious dose of *T. gondii* cysts was titrated to produce a robust wasting phenotype in our inbred mice while minimizing mortality. It is currently unknown how widespread *T. gondii*-induced cachexia is within strains of inbred laboratory mice, although Swiss Webster mice (54) and CBA/J mice also develop cachexia in response to *T. gondii* infection, while BALB/c mice do not (53). BALB/c mice express a protective H-2D<sup>b</sup> haplotype that presents an immunodominant *T. gondii* antigen (GRA6), leading to stronger T cell responses and more effective parasite clearance compared to CBA/J and C57BL/6 mice (27), so whether protection from cachexia is due to innate differences in pathways related to cachexia initiation or differences in parasite restriction is unclear. It is also unknown whether wild mice develop cachexia in response to the level of dosing (and the strain of parasite) they'd be likely to encounter in nature. As *T. gondii* studies in wild-derived mice are becoming more common (16), monitoring cachexia in these mice infected with *T. gondii* would be a compelling way to understand the parasite's long evolutionary history with a significant intermediate host like mice.

## **How does chronic *T. gondii*-induced cachexia cause disruptions in lipid metabolism?**

Although cachexia is primarily a disease of muscle wasting, adipose tissue homeostasis is becoming a subject of interest in cachexia research. Fat wasting typically precedes muscle loss in both clinical and experimental cachexia (192, 248), and both decreased fat mass and low circulating phospholipids predict mortality in advanced cancer patients (249). While cachexia-associated anorexia is partially responsible for loss of adipose tissue, the prevailing hypothesis is that lipolysis, or the breakdown of lipids into fatty acids and glycerol, is the primary driver of adipose tissue loss in cachectic subjects (250). In vivo lipolysis (measured by normalizing circulating concentrations of fatty acids and glycerol to total amount of body fat)

was significantly increased in cachectic patients with gastrointestinal cancer compared to disease-matched weight stable controls. Additionally, mature primary adipocytes from cachectic patients had significantly higher rates of lipolysis when stimulated *ex vivo* with noradrenaline or natriuretic peptide compared to adipocytes from non-cachectic controls, suggesting that lipolysis may be hyperactivated during cachexia (251).

Adipose tissue is an important energy reservoir and a major regulator of glucose utilization and secretion of adipokines like leptin and adiponectin. When circulating glucose is low, adipocytes release fatty acids into the circulation as fuel for skeletal muscle and other organs (252). Thus, the rapid loss of adipose tissue should lead to widespread defects in lipid and glucose homeostasis. In addition, lipolysis could be directly promoting muscle wasting. Genetic ablation of adipose triglyceride lipase (ATGL), the enzyme that catalyzes the first step in lipolysis, has been shown to rescue muscle wasting in Lewis lung carcinoma and B16 melanoma cachexia models (192), suggesting that excessive lipolysis during acute cachexia promotes muscle wasting. Although the precise mechanisms are unclear, one hypothesis is that adipose tissue wasting liberates fatty acids as substrate for the muscle to perform beta-oxidation. Reactive oxygen species generated by beta-oxidation can activate the p38 MAPK pathway, which regulates catabolic signaling in skeletal muscle (253). Notably, blockade of beta-oxidation prevents muscle wasting *in vitro* and *in vivo*, suggesting a direct means by which lipolysis could lead to muscle wasting (254).

Based on the sustained visceral white adipose tissue wasting observed during *T. gondii*-induced cachexia, as well as *T. gondii*'s well-characterized reliance on host lipid scavenging, we hypothesized that lipolysis was a major component of *T. gondii*-induced cachexia. To test whether blocking lipolysis could prevent muscle wasting in our model, mice were treated with atglistatin (a pharmacological inhibitor of ATGL) during either acute or chronic infection. Mice treated with atglistatin during acute infection were protected from acute weight loss and maintained weight comparable to uninfected mice for the duration of the experiment (**Fig. 6.1A**); however, assessment of parasite burden at chronic infection revealed that the early atglistatin treatment had largely cleared the parasite (**Fig. 6.1B**). Shortly after this experiment was performed, the observation that atglistatin inhibits *T. gondii* growth *in vitro* was published by another group (62). Based on these observations, it was considered unlikely that we'd be able to experimentally block cachexia-related lipolysis without the intervention having off-target effects on parasite growth.

To test whether there was systemic dysregulation in lipid metabolism, sera was collected from infected and uninfected mice at seven weeks post-infection and was sent for untargeted lipidomic analysis by CSH-QTOF MS/MS that screened for 550 identified lipid species. Infected mice had substantial dysregulation in a number of lipid species. Notably, fatty acyls were significantly decreased in cachectic mice relative to healthy mice (**Fig. 6.2A-B**). An increase in lipolysis should lead to elevated, not decreased, circulating fatty acyls. Of the few lipid species that were significantly elevated in the circulation of *T. gondii*-infected mice, most of these were sphingolipids, which are important lipid mediators of inflammation. These data, in conjunction with the western blots in **Fig. 5.6** showing that levels of lipolysis-related enzymes are not chronically elevated in adipose tissue, muscle, or the liver of cachectic mice, suggest that the sustained dysregulation of lipid metabolism in cachectic mice is likely not due to increased lipolysis.

Nevertheless, the circulating lipidomics data and sustained vWAT wasting still indicate that there is altered lipid metabolism in mice with *T. gondii*-induced cachexia. In addition to fatty acyls being decreased, there was also a substantial decrease in many glycerophospholipid species, particularly glycerophosphocholines, consistent with other published metabolomics data during *T. gondii* infection (50). Glycerophospholipids are the main component of cell membranes (255) and glycerophosphocholines are precursors to phosphatidylcholine. Liver phosphatidylcholine is essential for exporting triglycerides into the circulation (in the form of VLDL), as well as for bile secretion (52). Given the liver fibrosis described in **Chapter 5** and the sustained metabolic dysregulation that could result from liver dysfunction, it is possible that low circulating glycerophosphocholines are poised upstream of a number of the metabolic phenotypes we have observed. Ob/ob mice fed a choline-deficient diet had significantly less fat and decreased plasma glucose than ob/ob mice fed standard chow (256), suggesting that dietary cholines are necessary for fat storage and regulation of glucose homeostasis. One way to test whether choline deficiency is similarly upstream of these phenomena in our cachectic mice (who have significantly less fat and lower blood glucose) is to supplement with extra dietary choline and measure changes in fat accumulation and blood glucose levels.

To determine more broadly if supplementation of excess fat in the diet was sufficient to rescue fat and/or muscle wasting, mice were infected with *T. gondii* and then shifted to a high fat diet (HFD, 45% kcal fat) at four weeks post-infection. While uninfected mice were able to quickly gain fat after five weeks on the HFD, cachectic mice did not (**Fig. 6.3A-B**). Cachectic mice were still unable to gain weight, even the experiment was extended to fourteen weeks post-infection. (**Fig. 6.3 C-D**). To determine if the defect in weight gain was due to an inability to absorb fats, total lipids in the stool were measured. Cachectic mice on normal chow shed significantly more lipids than diet-matched uninfected mice, and this increased shedding was exacerbated in HFD-fed cachectic mice, confirming a defect in lipid absorption at the level of the gut (**Fig. 6.3F**).

Additionally, HFD-fed cachectic mice developed greasy fur within one day of the diet shift, suggesting impairments in lipid localization and/or utilization during cachexia (**Fig. 6.3E**). Future experiments will be necessary to determine 1) where defects in fat storage and localization are occurring, and 2) whether targeting it will improve overall cachexia outcomes. A possible explanation for the fat storage defect could be that mRNA levels of the transcription factor *PPAR- $\gamma$*  were significantly downregulated in the vWAT and scWAT of cachectic mice at 17 weeks post-infection (**Fig. 6.3G**). PPAR- $\gamma$  is a master regulator of adipogenesis and lipid storage, and PPAR- $\gamma^{-/-}$  mice cannot store fat while on a high fat diet (257). PPAR- $\gamma$  agonism may be a compelling target in the future for rescuing lipid dysregulation in mice with *T. gondii*-induced cachexia

To test whether IL-1R signaling during chronic cachexia was contributing to the inability of cachectic mice to absorb and/or store fat, wildtype or IL-1R $^{-/-}$  mice were i.p. infected with 10 Me49 cysts and monitored for nine weeks. At four weeks post-infection, half of the mice from each genotype were shifted to a HFD, while half remained on control chow. By nine weeks post-infection, infected IL-1R $^{-/-}$  mice on the high-fat diet had gained significantly more fat than IL-1R $^{-/-}$  mice on the regular chow diet, while wildtype mice on the HFD remained the same weight as their normal chow counterparts, as observed previously

(**Fig. 6.4A**). Mice of both genotypes on the HFD had significantly greater vWAT mass than normal chow mice, although only IL-1R<sup>-/-</sup> mice had significantly greater scWAT mass with the HFD. Neither genotype had significant changes in muscle mass on the HFD (**Fig. 6.4B**). Levels of fecal lipids were comparable between wildtype and IL-1R<sup>-/-</sup> mice on the high fat diet, suggesting that IL-1 driven component of the fat storage defect was not occurring at the level of intestinal absorption (**Fig. 6.4C**). Additionally, this finding suggests that defects in fat absorption are insufficient to fully explain the inability to wildtype mice to store fat, as both wildtype and IL-1R<sup>-/-</sup> mice shed comparable levels of lipids, but the only the IL-1R<sup>-/-</sup> mice were able to gain significant fat stores in both fat depots. When chronic parasite burden in the brain was measured, there were significantly fewer *T. gondii* cysts in the brains of HFD-fed IL-1R<sup>-/-</sup> mice compared to HFD-fed wildtype mice (**Fig. 6.4D**), confounding our interpretations of the data. It is not clear from this experiment if the IL-1R<sup>-/-</sup> mice were able to gain more fat because they are protected from IL-1R driven signaling cascades preventing fat storage, or because they were benefitting from having a lower parasite burden (eg, lower systemic inflammation). Additional experiments will be necessary to determine the contribution of IL-1R signaling to lipid metabolism during *T. gondii*-induced cachexia, as well as to test if excessive lipid availability leads to parasite toxicity. Integrating data of other significantly changed metabolites from the sera of mice at seven weeks post-infection may lead to a more thorough understanding of how defects in fat metabolism may be affecting nutrient utilization on a broader scale (**Table 6.1**).

### Is IL-1 $\alpha$ or IL-1 $\beta$ primarily responsible for acute disease tolerance?

Because IL-1 $\alpha$  and IL-1 $\beta$  both signal through IL-1R, an important question is whether the acute IL-1R-mediated disease tolerance observed in the liver and vWAT is primarily mediated by IL-1 $\alpha$ , IL-1 $\beta$ , or both. Although both IL-1 isoforms are able to initiate the same signaling cascade downstream of IL-1R ligation, there could be differences in binding affinity or recruitment of unknown accessory proteins. Additionally, because IL-1 $\alpha$  is canonically released downstream of cell damage and death and IL-1 $\beta$  is released downstream of inflammasome activation, each cytokine may be accompanied by a different milieu of cofactors that would stimulate a different response (inflammation versus tolerance, for example). A more thorough understanding of the kind of cell death occurring in both the vWAT and the liver will help reveal whether IL-1 $\alpha$  or IL-1 $\beta$  (or both) are predominantly released during acute *T. gondii* infection. A major caveat to measuring IL-1 $\alpha$  or IL-1 $\beta$  in whole cell lysate by ELISA is that this technique does not distinguish between released cytokine and cytokine that was still inside cells at the time of lysis, nor does it distinguish between cleaved and uncleaved forms. Western blot for IL-1 $\beta$  distinguishes between cleaved and uncleaved forms of the cytokine (only the cleaved form is bioactive and cleavage is thought to be required for release). While IL-1 $\alpha$  can be cleaved, it is also released and capable of binding to IL-1R in its uncleaved form (258), so western blotting may be less informative.

Since IL-1 $\beta$  is released downstream of inflammasome activation, ASC speck formation in the liver and vWAT was assessed in **Chapter 4** as a marker for inflammasome activation and (potentially) precursor of pyroptosis. ASC specks were apparent in the vWAT but not in the liver at two weeks post-infection, suggesting inflammasome activation may be

a major driver of IL-1 release in vWAT but not the liver at this time point. (It is possible that looking in the liver two weeks post-infection is missing an earlier window of inflammasome activation. This could be addressed by looking at ASC speck formation at one week post-infection). A more sensitive tool to confirm ASC visualization is using ASC-citrine mice, which express ASC fused to citrine so that speck formation can be visualized directly (without antibody staining) (259). Western blots showing cleavage of caspase-1 and gasdermin D would strengthen the hypothesis that IL-1 $\beta$  is released downstream of pyroptosis in the vWAT at two weeks post-infection. Distinguishing what kind of cell death could be leading to IL-1 $\alpha$  release is more complicated, although tissues were histologically/pathologically scored for necrosis, and IHC of cleaved caspase-3 was used as a proxy for caspase-3 mediated cell death in **Chapter 4**. Annexin V staining and western blot of cleaved caspase-3 are additional ways to characterize whether there is likely to be significant amounts of apoptosis, and blotting or staining for MLKL is likely to reveal whether there is necroptosis, which is thought to be an important source of IL-1 $\alpha$  release (260, 261).

In addition to determining what kind of cell death is leading to the release of IL-1 $\alpha$  and/or IL-1 $\beta$  in peripheral tissues during acute *T. gondii* infection, it is also important to understand what cell death pathways IL-1R signaling is targeting to effect its role in disease tolerance. One way to test this on a gross level would be to culture primary adipocytes or hepatocytes, infect the cells with *T. gondii*, treat with IL-1 $\alpha$  and/or IL-1 $\beta$  or media alone, and then measure changes in cell viability using LDH release or ATP levels as a readout. If IL-1 treatment significantly improves viability, western blotting for proteins that moderate critical junctions of cell death pathways would be one way to understand where IL-1R is acting. There are a few caveats to this approach. One is that it assumes that the tissue damage in acute vWAT and liver is caused directly by the parasite, instead of it resulting from bystander damage downstream of immune infiltration or being secondary to damage in other tissues. For example, the necrotic lesions seen in the fat are characteristic of what has been observed during acute pancreatitis, when pancreatic lipases are released into the circulation and begin digesting fat tissue (262). A different approach could be to stimulate various cell death pathways with known ligands and test whether addition of IL-1 $\alpha$  or IL-1 $\beta$  inhibits cell death. It is currently unclear if IL-1R is mediating disease tolerance through cell-intrinsic or cell-extrinsic mechanisms, so another caveat with this reductionist approach is that it does not account for cross-talk between parenchymal cells and stromal cells within the liver and vWAT. For example, dying parenchymal cells may release IL-1 $\alpha$  that acts on IL-1R on stromal cells, leading to release of pro-survival factors and/or tissue remodeling that limits cell death. A co-culture model of parenchymal cells and fibroblasts may mitigate this issue.

A way to test the respective roles of the IL-1 isoforms in disease tolerance during acute *T. gondii* infection in vivo is to infect IL-1 $\alpha$ <sup>-/-</sup> or IL-1 $\beta$ <sup>-/-</sup> mice, harvest tissues during acute infection, and quantify the degree of adipose tissue necrosis, and caspase-3 cleavage in the liver (using IL-1R<sup>-/-</sup> mice as positive controls of exacerbated pathology). Weight loss curves shown in **Chapter 4** indicate that IL-1 $\alpha$ <sup>-/-</sup> mice lose significantly less weight than wildtype mice by three weeks post-infection, whereas IL-1 $\beta$ <sup>-/-</sup> lose comparable amounts of weight to wildtype mice, suggesting that IL-1 $\alpha$ <sup>-/-</sup> may be regulating the initial drop in weight during acute infection. A preliminary experiment with acutely infected IL-1 $\beta$ <sup>-/-</sup> mice revealed that these mice did not have necrotic lesions in the adipose tissue (suggesting that IL-1 $\alpha$  may be the primary

driver of disease tolerance in the vWAT); however, additional experiments with the proper controls are necessary to conclude this for certain. Because there may be different forms of cell death occurring in the liver and adipose tissue, it is possible that each isoform will have a dominant effect in only one of the tissues assessed. Additionally, IL-1Ra, which is also elevated in acute vWAT and liver, has been recently shown to directly bind to and significantly reduce the activity of caspase 8 and caspase 9, thus preventing certain forms of cell death (263). This finding raises the question of whether IL-1 $\alpha$  or IL-1 $\beta$  could be having effects independently of IL-1R signaling, and these questions should be considered when using IL-1 $\alpha$ <sup>-/-</sup> and IL-1 $\beta$ <sup>-/-</sup> mice.

### When and where is IL-1R signaling required to cause cachexia?

Upon noticing the robust protection from chronic cachexia in IL-1R<sup>-/-</sup> mice, two of our biggest questions were when and where IL-1R signaling was occurring to promote cachexia. One hypothesis is that IL-1R signaling during acute infection is sufficient to trigger long-term inflammatory/metabolic rewiring that drives chronic cachexia. Another (not mutually exclusive) hypothesis is that chronic IL-1R signaling is necessary for cachexia. To test both of these hypotheses, *T. gondii*-infected mice were treated daily with 50 mg/kg recombinant IL-1Ra (anakinra) i.p. during multiple timepoints during either acute or chronic infection. None of these interventions improved the cachexia phenotype (**Fig. 6.5A-C**), although the failure of injected anakinra to phenocopy the IL-1R<sup>-/-</sup> could have been due to anakinra's short half-life or because the concentration in circulation was insufficient to block high local concentrations of IL-1 $\alpha$ /IL-1 $\beta$  in tissues. A more refined way to test the temporal requirement for IL-1R signaling would be to cross an IL-1R<sup>fl/fl</sup> mouse with a mouse having an inducible Cre recombinase so IL-1R could be genetically deleted during either acute or chronic infection and test effects on cachexia could be monitored. A major caveat to using a tamoxifen-inducible Cre mouse is that tamoxifen has been shown to be hepatotoxic in mice (264), and this hepatotoxicity could confound effects of liver damage caused by the parasite/the immune system. Nevertheless, understanding the kinetics of when IL-1R signaling is necessary for causing cachexia is important for clinical considerations of intervention. For example, if acute IL-1R signaling is sufficient to cause permanent metabolic rewiring, pharmacologically blocking IL-1R signaling during advanced cachexia is unlikely to be effective.

Another key question is where IL-1R is signaling occurring to promote cachexia and fibrosis. While delivering drugs to inhibit IL-1R signaling in a specific cell type may be unlikely at this point, understanding the downstream effects of IL-1R signaling may lead to identification of other potential therapeutic targets. IL-1 $\alpha$  and IL-1 $\beta$  are elevated in the circulation (**Fig. 5.1H**), in the liver (**Fig. 4.5B**) and the vWAT (IL-1 $\beta$  only, **Fig. 4.5A**) of acutely infected mice, indicating multiple biological compartments within which acute IL-1R signaling could be occurring to induce long-lasting effects. Additionally, IL-1 $\alpha$  is chronically elevated in the brain (**Fig. 4.9B**), liver (**Fig. 4.9B**), and the circulation (**Fig. 4.9A** & **Fig. 5.8B**). IL-1R was difficult to detect by immunofluorescence, although it has been shown to be expressed on brain endothelial cells (265). Transcript levels of *IL-1R* are detectable in the spleen, vWAT, quad, and brain during both acute and chronic infection (**Fig. 6.6A-B**), although additional characterization is necessary to define which cell types within these tissues

are the dominant IL-1R expressers. One way to test where IL-1R signaling is occurring to drive cachexia is by making tissue-specific IL-1R knockout mice by crossing an IL-1R<sup>fl/fl</sup> mouse with a mouse driving Cre on a variety of tissue-specific promoters, including E-cadherin (endothelial cells), albumin (hepatocytes), adiponectin (adipocytes), L-retinol acetyltransferase (LRAT, hepatic stellate cells), etc. This approach may help determine which aspects of IL-1R-dependent cachexia are dependent on certain cell types (IL-1R on fibroblasts may be driving fibrosis, but IL-1R on adipocytes may be changing fat metabolism, etc.). Failure to see one of the cell-specific IL-1R knockouts phenocopy the whole-body knockout would likely be indicative that IL-1R-driven cachexia requires integration from IL-1R signaling on multiple different cell types.

To address whether IL-1R induced fibrosis is upstream of muscle wasting, one approach would be to cross an IL-1R<sup>fl/fl</sup> mouse with a mouse driving Cre recombinase on the  $\alpha$ -SMA promoter, thus allowing deletion of IL-1R in any cells expressing  $\alpha$ -SMA (presumably all activated myofibroblasts and smooth muscle cells). If these mice were infected and taken out to chronic infection, degree of cachexia (by muscle wasting, fat wasting, circulating inflammation), as well as degree of fibrosis (by picrosirius red) could be assessed. If IL-1R-driven fibrosis causes cachexia, the mice with both the IL-1R<sup>fl/fl</sup> and the  $\alpha$ -SMA Cre would have reduced fibrosis and would be at least partially protected from cachexia. The caveat with this experimental setup is that IL-1R would only be deleted after  $\alpha$ -SMA was expressed (after myofibroblast activation), meaning that we would be potentially missing the chance to block IL-1R in during the initiation of the fibrotic response. A more refined (and tissue specific) approach would be to drive the Cre on a promoter for tissue specific myofibroblast precursors. Although  $\alpha$ -SMA expression is a nearly ubiquitous marker of activated myofibroblasts, myofibroblast precursors are an extraordinarily heterogenous population (266). Almost every tissue has its own precursor cell type (these are often stromal cells that play homeostatic roles during quiescence). Driving the Cre on a protein expressed during quiescence and activation would allow us to target the IL-1R-driven myofibroblast response to a particular tissue and would not need to rely on activation of the myofibroblast to precede the IL-1R deletion. This experimental approach would enable us to target IL-1R driven fibrosis in multiple tissues and discern how fibrosis in each of those tissues was affecting systemic metabolism and muscle wasting.

## How does IL-1R cause cachexia?

IL-1 $\alpha$  and IL-1 $\beta$  are pleiotropic cytokines that influence inflammation, lipid metabolism, glucose metabolism, eating behavior, nutrient regulation, and fibrosis, among other pathways. Because *T. gondii*-induced cachexia is controlled by a signaling axis that has a such a broad range of effects, it would not be surprising if IL-1R signaling were acting through many of these pathways to promote metabolic dysregulation; however, isolating which (if any) of these pathways are having dominant effects on the cachexia phenotype is important to understanding the utility of IL-1R blockade as a potential therapeutic strategy in the clinic.

Gut-derived IL-1 $\beta$  signals through the afferent vagus nerve during *Salmonella* infection, causing anorexia and reduced ability to tolerate infection (123), and peripheral IL-1 $\beta$  has long been known to signal through the afferent vagus to affect such processes as fever induction

(267) and anorexia (123). Additionally, efferent vagal signaling can control satiety and secretion of pancreatic enzymes and bile acids (268), suggesting multiple ways vagal signaling could be promoting cachexia. The afferent vagus nerve connects the microbiota-gut-brain axis, and is able to sense nutrients, bacterial metabolite flux, and PAMPs in the gut, sending messages to the brain that can then signal through the efferent vagus to regulate gut motility, cholinergic signaling, and the inflammatory reflex (269, 270). To determine if retrograde IL-1R signaling through the vagus nerve was a responsible for cachexia, we hypothesized that surgically vagotomized mice would be protected from cachexia, either through modulation of eating behavior or through controlling metabolism. Although chronically cachectic mice do not remain anorexic (**Fig. 5.1D**), we wondered if preventing the initial drop in weight during acute infection due to anorexia would improve chronic recovery and/or that peripheral IL-1 could be signaling through the vagus nerve to control other nutrient-utilization pathways, independently of eating behavior. Mice who had received a surgical hepatic vagotomy or mice who had received sham surgery were i.p. infected with 10 Me49gLuc cysts and monitored daily for changes in weight and food consumption. There was considerable mortality in the sham-operated group during the acute infection (**Fig. 6.7A**), which makes it hard to draw conclusions from these data, although it does raise the interesting question of whether afferent vagal signaling is affecting survival by playing some sort of detrimental role in parasite restriction (by modulating inflammatory tone) or inhibiting disease tolerance. Additional experiments with greater numbers of mice will be necessary to determine whether vagotomy significantly improves survival during acute *T. gondii* infection. Importantly, there was no difference in eating behavior in acute or chronic infection between the groups (**Fig. 6.7B**). However, since infected IL-1R<sup>-/-</sup> mice consume the same amount of chow per gram as infected wildtype mice (**Chapter 4**) and are protected from cachexia, sustained anorexia is likely not the way IL-1R is mediating cachexia. To determine if vagal signaling was controlling nutrient usage and/or metabolism such that it could be promoting loss of muscle or fat, total change in body weight and body composition was measured. However, vagotomized mice were not protected from overall weight loss, or from fat or muscle wasting, (**Fig. 6.7C-D**) suggesting that signaling through the afferent vagus nerve is not a major mechanism of *T. gondii*-induced cachexia. Although there may not have been much IL-1R signaling in the gut during i.p. infection, it is important to note that a hepatic vagotomy denervates several other critical organs, including the pancreas, distal stomach, and the liver, where high chronic IL-1 has been observed (123).

Because the vagus can sense changes in bacterial metabolites, it would be interesting to return to the oral model of *T. gondii* infection to test whether the afferent vagus responds to the sustained microbial dysbiosis that results from oral *T. gondii* infection to affect cachexia in any way. Overall, though, these data lead us to conclude that peripheral IL-1R signaling through the afferent vagus nerve was likely not the major pathway driving *T. gondii*-induced cachexia.

## Concluding Remarks

The initial goal of this project was to understand the nature of the chronic wasting in mice infected with *T. gondii*. Through careful characterization, we have defined this wasting as cachexia, a devastating and deadly clinical disease characterized by significant muscle and

adipose tissue wasting and elevated circulating inflammatory cytokines. In the course of developing this model, we realized that the role of IL-1R signaling during acute and chronic *T. gondii* infection has not been clearly established in the literature. Unlike other innate cytokines like IL-6, IL-12, TNF- $\alpha$ , and IFN- $\gamma$ , we found that IL-1R signaling is not required to restrict parasite burden during either acute or chronic infection. Interestingly, we found that IL-1R promotes disease tolerance during acute *T. gondii* infection, mitigating cell death in the adipose tissue and liver during acute infection without affecting parasite burden. Importantly, in the long term, IL-1R<sup>-/-</sup> mice are protected from *T. gondii*-induced cachexia, suggesting that while acute IL-1R signaling is protective, chronic IL-1R signaling becomes pathogenic (**Figure 6.8**). Most mechanisms of disease tolerance have been identified in the context of acute, self-resolving infections, and have not been studied during longer-term insults. Our observations bear the important implication that although disease tolerance mechanisms may be beneficial during acute infection, chronic activation of these pathways leads to pathology. As there is increasing discussion of developing therapies targeting disease tolerance pathways instead of pathogen restriction pathways in the clinic, our findings caution against excessive activation of disease tolerance mechanisms, especially in the setting of chronic disease.

The longevity of our *T. gondii* model revealed that *T. gondii*-induced cachexia is associated with perivascular fibrosis in metabolic organs such as the vWAT, liver, and skeletal muscle. Although fibrosis has been observed in these tissues of patients with cachexia, to our knowledge, this is the first time it has been observed in a mouse model of cachexia. Liver and skeletal muscle fibrosis are dependent on intact IL-1R signaling, and may be the key to the observation that IL-1R<sup>-/-</sup> mice recover from acute cachexia while wildtype mice do not. Our observations imply that dual therapies targeting both pro-inflammatory and pro-fibrotic pathways may be more effective at reversing clinical cachexia than therapies targeting inflammation alone.

While this project has answered many questions, our studies raise many more. How does IL-1R signaling promote disease tolerance, and are these mechanisms exclusive to *T. gondii* infection? Is IL-1R-induced liver and skeletal muscle fibrosis the main driver behind sustained muscle wasting and metabolic dysregulation during *T. gondii*-fibrosis? Is it conserved in other experimental and clinical instances of cachexia? Future work addressing these questions will provide valuable insight into the basic biology of IL-1R signaling as well as potential therapeutic strategies for cachexia.

## Figures

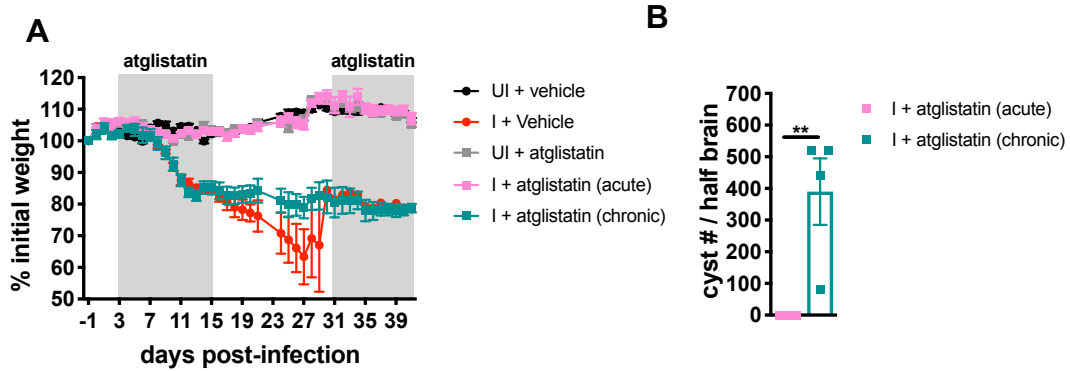


**Figure 6.1 Acute atglistatin administration inhibits *T. gondii* growth in vivo.** 10-14 week C57Bl6/J mice were infected with 10 Me49gLuc cysts i.p. and treated with 1 mg/kg/day atglistatin at the time points indicated. **A**, Weight curves showing percent of initial weight from 0-11 wpi ( $n = 5-2$  mice per group). **B**, Brain cyst burden 7 weeks post-infection (wpi) ( $n = 4$  mice per group). Data are shown as the mean  $\pm$  SEM. \*,  $P < 0.05$ ; \*\*,  $P < 0.01$ ; \*\*\*,  $P < 0.001$ , n.s., by unpaired Student's T test.



**Figure 6.2 Cachectic mice sustain dysregulation in circulating lipid species.** 10-14 week old C57BL/6J mice were intraperitoneally infected with 10 Me49gLuc *T. gondii* cysts of the strain or mock infected with PBS. At 7 wpi, mice were retro-orbitally bled and sera was flash-frozen sent off for untargeted analysis of complex lipids by CSH-QTOF MS/MS. Plots represent fold change (either positive or negative) of infected mice to uninfected mice in **A**, broad families of complex lipids or **B**, more specialized sub-classes. Volcano plots were generated in R.  $n = 7$  mice per group.

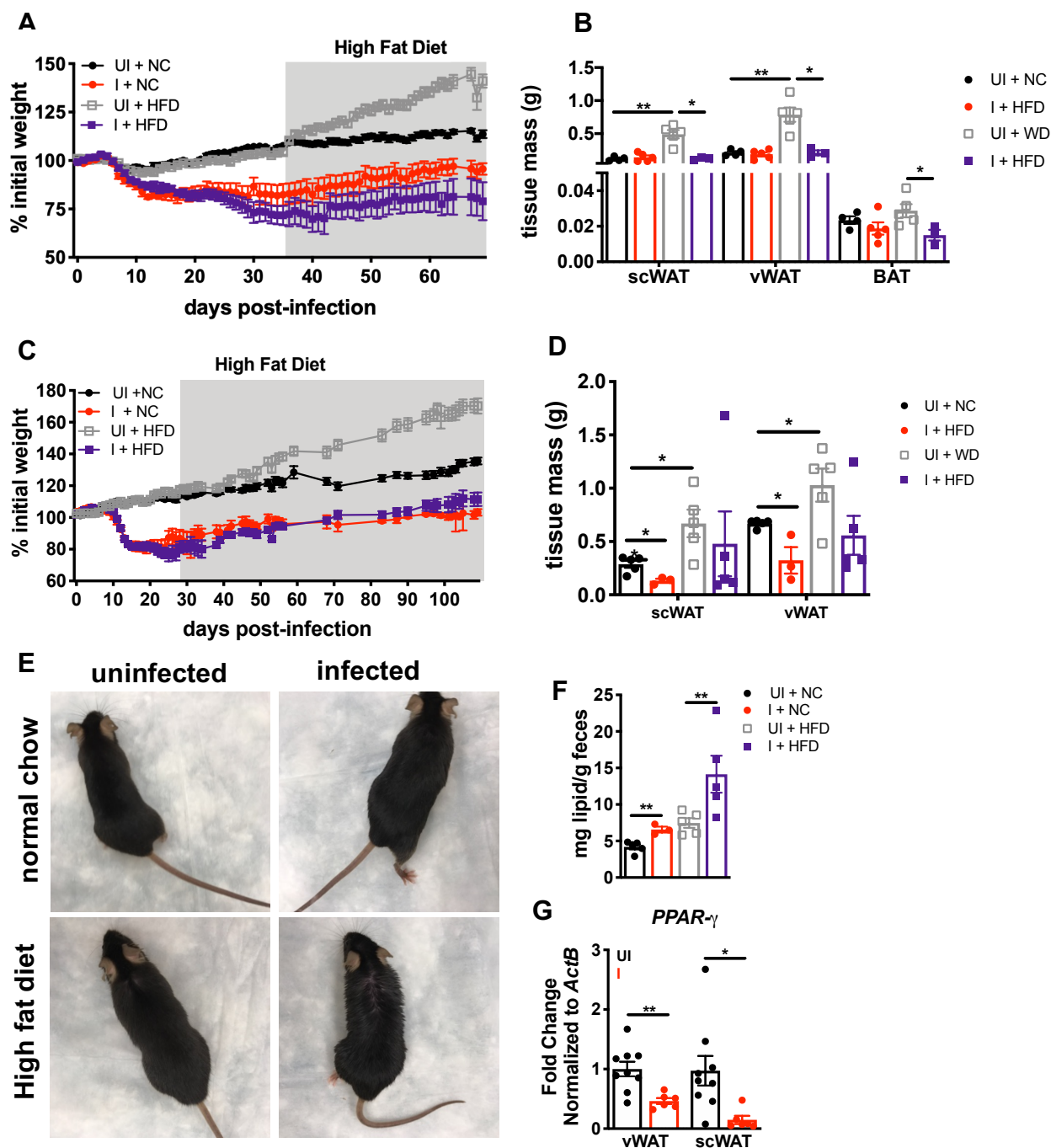


**Figure 6.3** Mice with chronic *T. gondii* infection do not gain weight on a high fat diet. 10-14 week C57Bl6/J mice were infected with 10 Me49gLuc (**A-B, G**) or Me49 (**C-F**) cysts i.p. At 5 wpi, mice in the indicated groups were switched to a high fat diet (45% kcal fat) or remained on standard chow *ad libitum* for the time points indicated ( $n = 3-5$  mice per group). Fat depots were weighed at 9 wpi (**B**) or 14 wpi (**D**). **E**, Experimental mice at 9 wpi, after being on the diet for 5 weeks. **F**, fecal lipids from stool collected at 8 wpi (3 weeks of being on the diet). **G**, qPCR for transcript levels of *PPAR- $\gamma$*  in adipose tissue at 17 wpi normalized to *Actb* and presented as fold change relative to uninfected ( $n = 6-9$  mice per group). \* $P < 0.05$ ; \*\*,  $P < 0.01$ ; \*\*\*,  $P < 0.001$ , n.s., by unpaired Student's T test.

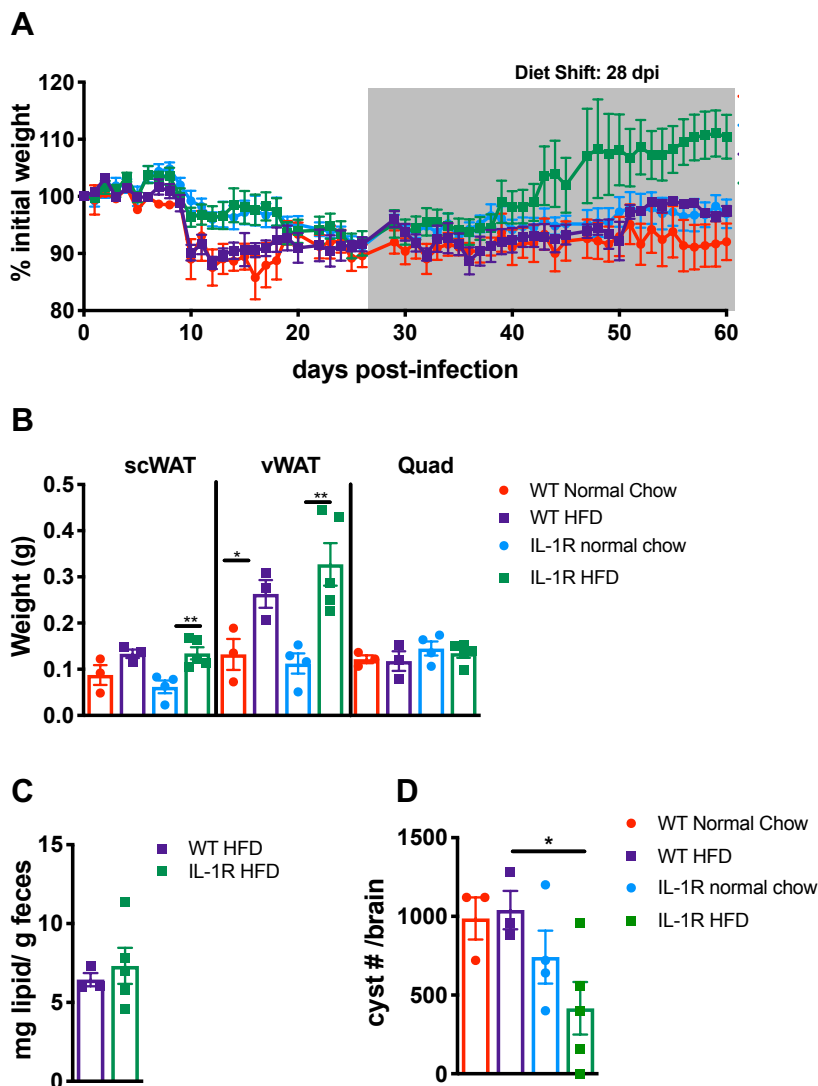


**Figure 6.4** Infected  $IL-1R^{-/-}$  mice on a high fat diet have improvements in fat storage compared to wildtype mice. 10-14 week C57Bl6/J or  $IL-1R^{-/-}$  mice were infected with 10 Me49 cysts i.p. At 4 wpi, mice in the indicated groups were switched to a high fat diet (45% kCal fat) or remained on standard chow *ad libitum* for the time points indicated ( $n = 3-5$  mice per group). **B**, Tissue weights of adipose tissue and skeletal muscle depots were weighed at 9 wpi. **C**, fecal lipids from stool collected at 9 wpi (4 weeks of being on the diet). **D**, Brain cyst burden at 9 wpi \* $P < 0.05$ ; \*\*,  $P < 0.01$ ; \*\*\*,  $P < 0.001$ , n.s., by unpaired Student's T test.

Name	p-value	Fold Change
pinitol	0.0344	3.4
2-deoxytetronic acid	0.0004	2.0
methylphosphate	0.0048	1.8
trehalose	0.0310	1.7
ribonic acid	0.0248	1.6
fructose	0.0004	1.4
ribitol	0.0362	1.3
phenylalanine	0.0047	1.3
oxoproline	0.0059	1.3
hydroxycarbamate NIST	0.0035	1.3
threonine	0.0119	1.2
hexuronic acid	0.0333	0.8
glycerol	0.0219	0.8
palmitoleic acid	0.0339	0.7
glycerol-3-galactoside	0.0195	0.7
glucose	0.0171	0.7
succinic acid	<0.0000	0.5
2-hydroxybutanoic acid	0.0177	0.5
creatinine	0.0064	0.5
2-ketoisocaproic acid	0.0004	0.4
2-hydroxyglutaric acid	<0.0000	0.4
sorbitol	<0.0010	0.4
alpha-ketoglutarate	<0.0000	0.3
malic acid	<0.0000	0.3
fumaric acid	<0.0000	0.3

**Table 6.1 Significantly changed metabolites in the serum of cachectic mice compared to uninfected mice.** 10-14 week C57Bl6/J mice were infected with 10 Me49 gLuc cysts i.p. or were mock infected with PBS. At 7 wpi, mice were bled and sera was sent for untargeted mass spectrometry (GCTOF MS). The results shown here are fold change in either direction that was significantly ( $P < 0.05$ ) different in infected mice versus uninfected.  $n = 7$  mice per group

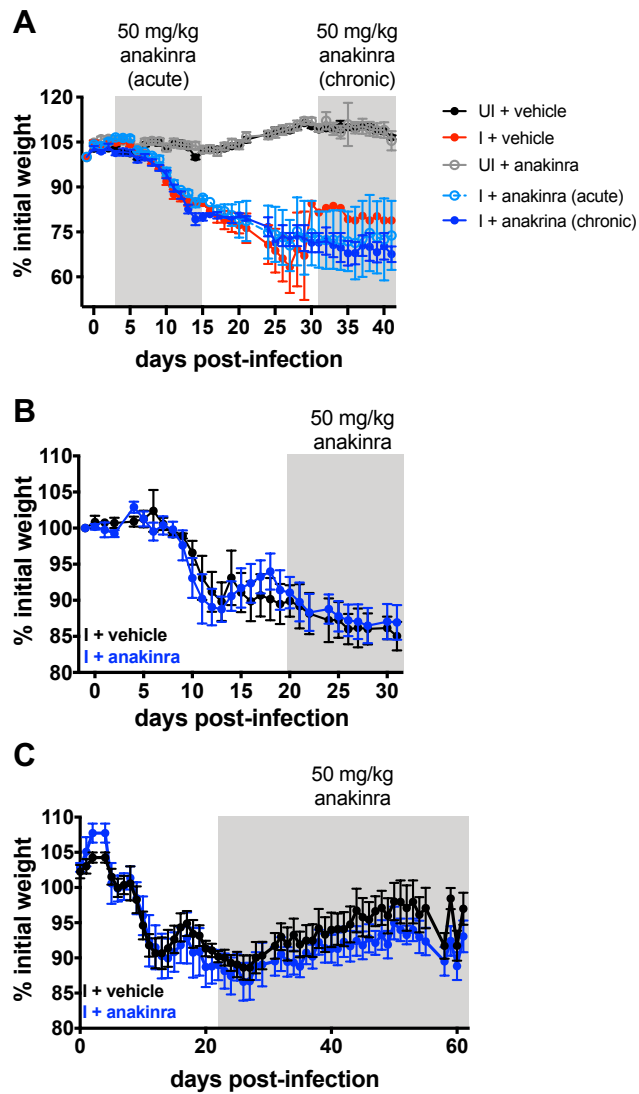


**Fig. 6.5 Administration of soluble IL-1Ra (anakinra) at acute or chronic infection is insufficient to protect mice from *T. gondii*-induced cachexia.** 10-14 week C57Bl6/J mice were infected with 10 Me49 cysts i.p. At the time intervals indicated by the gray bar, mice received i.p. injections of 50mg/kg anakinra either twice a day (**A**) or once a day (**B-C**).  $n = 3-5$  mice per group.

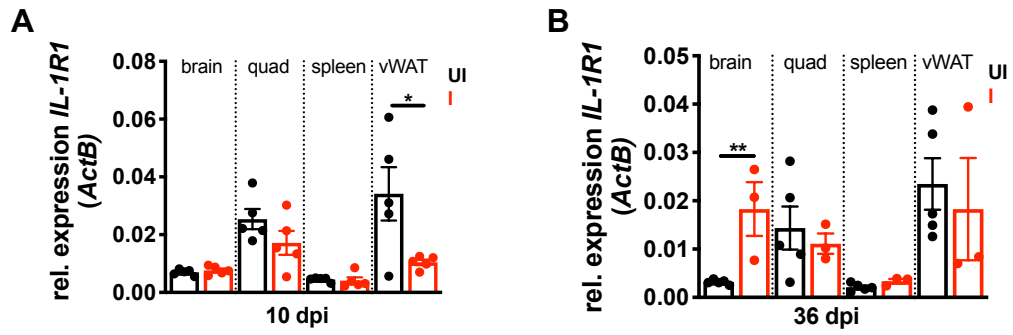


**Fig. 6.6** *IL-1R* transcript can be detected in multiple tissues at both acute and chronic infection. qPCR for *IL-1R* transcript in the brain, quadriceps, spleen, and vWAT at 10 dpi (A) or 36 dpi (B).  $n = 3-5$  mice per group. \* $P < 0.05$  by unpaired Student's T test.

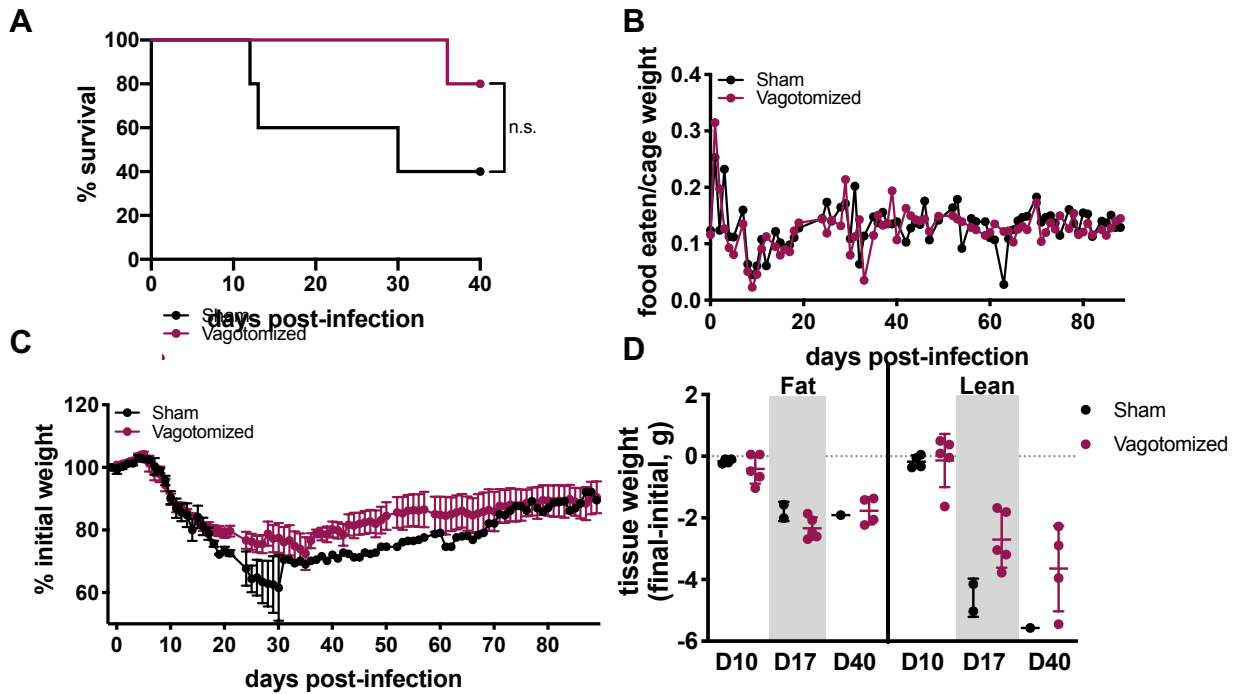


**Fig. 6.7** Inhibition of retrograde signaling through the vagus nerve does not protect mice from chronic *T. gondii*-induced cachexia. Sham-operated or mice that had received a hepatic vagotomy were infected with 10 Me49gLuc cysts IP. **A**, survival curve showing mortality infected mice. **B**, Daily food intake per cage normalized to pooled weight of the mice in the cage measured every 24 hours. **C**, percent initial weight during the course of infection. **D**, EchoMRI of fat and lean body mass composition. There were originally 5 mice in each group, but the end of the experiment, there was only one sham-operated mouse left.

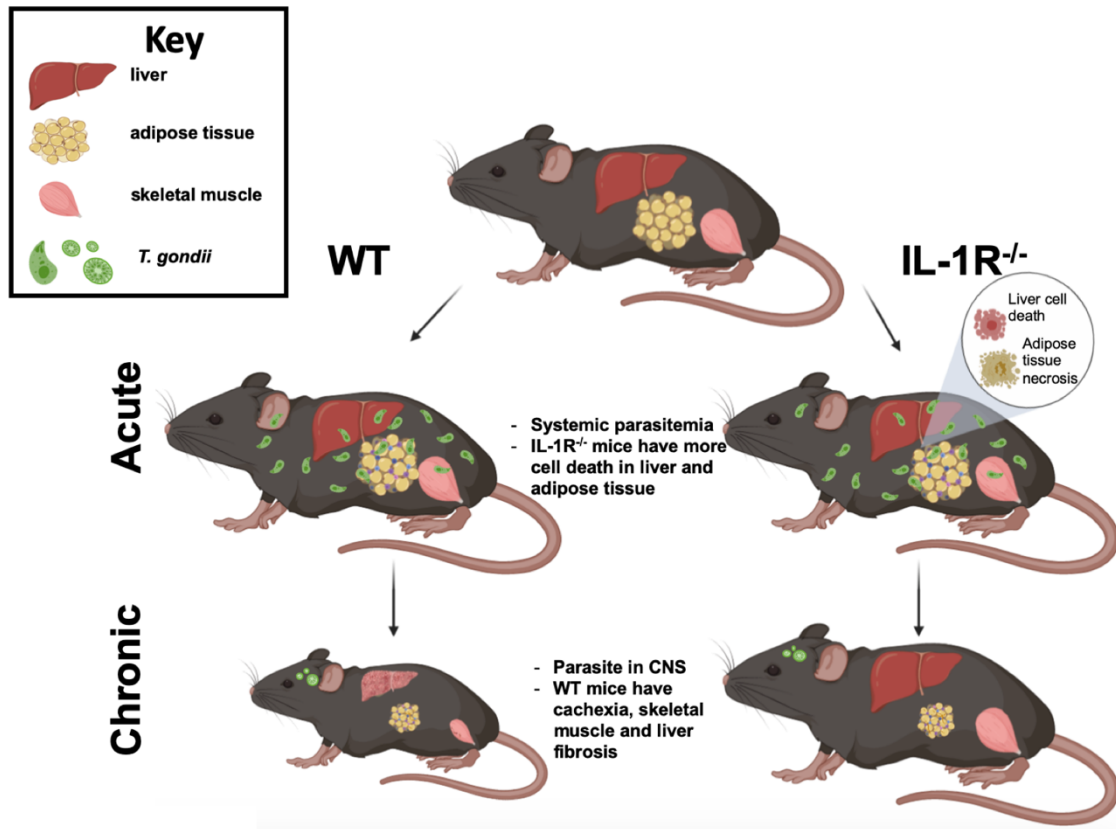


**Fig. 6.8 Final model.** During acute *T. gondii* infection, both IL-1R<sup>-/-</sup> and wildtype (WT) mice harbor comparable parasite burdens; however, IL-1R<sup>-/-</sup> mice have increased evidence of cell death in the liver and adipose tissue, suggesting a role for IL-1R signal in controlling a disease tolerance mechanism(s) during acute *T. gondii* infection. During chronic infection, IL-1R<sup>-/-</sup> mice recover from acute weight loss, but have chronic adipose tissue fibrosis and wasting. WT mice become cachectic, develop liver, adipose tissue, and skeletal muscle fibrosis, and have increased mortality, despite maintaining comparable parasite burdens to IL-1R<sup>-/-</sup> mice.

## References

1. Ayres, J. S., and D. S. Schneider. 2009. The Role of Anorexia in Resistance and Tolerance to Infections in *Drosophila*. *PLoS Biol.* 7: e1000150.
2. Ayres, J. S., and D. S. Schneider. 2012. Tolerance of Infections. *Annu. Rev. Immunol.* 30: 271–294.
3. Medzhitov, R., D. S. Schneider, and M. P. Soares. 2012. *Disease tolerance as a defense strategy*. NIH Public Access ; :936–941.
4. Soares, M. P., R. Gozzelino, and S. Weis. 2014. Tissue damage control in disease tolerance. *Trends Immunol.* 35: 483–494.
5. Caldwell, R. M., J. F. Schafer, L. E. Compton, and F. L. Patterson. 1958. Tolerance to cereal leaf rusts. *Science (80- )*. 128: 714–715.
6. Martins, R., A. R. Carlos, F. Braza, J. A. Thompson, P. Amador-Bastos, S. Ramos, and M. P. Soares. 2019. Disease Tolerance as an Inherent Component of Immunity. *Annu. Rev. Immunol.* 13: 405–37.
7. Dubey, J. P., D. S. Lindsay, and C. A. Speer. 1998. Structures of *Toxoplasma gondii* tachyzoites, bradyzoites, and sporozoites and biology and development of tissue cysts. *Clin. Microbiol. Rev.* 11: 267–99.
8. Courret, N., S. Darce, P. Sonigo, G. Milon, D. Buzoni-Gâtel, and I. Tardieux. 2006. CD11c- and CD11b-expressing mouse leukocytes transport single *Toxoplasma gondii* tachyzoites to the brain. *Blood* 107: 309–16.
9. Bierly, A. L., W. J. Shufesky, W. Sukhumavasi, A. E. Morelli, and E. Y. Denkers. 2008. Dendritic Cells Expressing Plasmacytoid Marker PDCA-1 Are Trojan Horses during *Toxoplasma gondii* Infection. *J. Immunol.* 181.
10. Gregg, B., B. C. Taylor, B. John, E. D. Tait-Wojno, N. M. Girgis, N. Miller, S. Wagage, D. S. Roos, and C. A. Hunter. 2013. Replication and distribution of *Toxoplasma gondii* in the small intestine after oral infection with tissue cysts. *Infect. Immun.* 81: 1635–43.
11. Yarovsky, F., S. Hieny, and A. Sher. 2008. Recognition of *Toxoplasma gondii* by TLR11 prevents parasite-induced immunopathology. *J. Immunol.* 181: 8478–84.
12. Ewald, S. E., J. Chavarria-Smith, and J. C. Boothroyd. 2014. NLRP1 is an inflammasome sensor for *Toxoplasma gondii*. *Infect. Immun.* 82: 460–8.
13. Gorfou, G., K. M. Cirelli, M. B. Melo, K. Mayer-Barber, D. Crown, B. H. Koller, S. Masters, A. Sher, S. H. Leppla, M. Moayeri, J. P. J. Saeij, and M. E. Grigg. 2014. Dual role for inflammasome sensors NLRP1 and NLRP3 in murine resistance to *Toxoplasma gondii*. *MBio* 5: 1–12.
14. Etheridge, R. D., A. Alaganan, K. Tang, H. J. Lou, B. E. Turk, and L. D. Sibley. 2014. The *Toxoplasma* pseudokinase ROP5 forms complexes with ROP18 and ROP17 kinases that synergize to control acute virulence in mice. *Cell Host Microbe* 15: 537–550.
15. Reese, M. L., G. M. Zeiner, J. P. J. Saeij, J. C. Boothroyd, and J. P. Boyle. 2011. Polymorphic family of injected pseudokinases is paramount in *Toxoplasma* virulence. *Proc. Natl. Acad. Sci. U. S. A.* 108: 9625–9630.
16. Lilue, J., U. B. Müller, T. Steinfeldt, and J. C. Howard. 2013. Reciprocal virulence and resistance polymorphism in the relationship between *Toxoplasma gondii* and the house

mouse. *Elife* 2: e01298.

17. Sher, A., I. P. Oswald, S. Hieny, and R. T. Gazzinelli. 1993. *Toxoplasma gondii* induces a T-independent IFN-gamma response in natural killer cells that requires both adherent accessory cells and tumor necrosis factor-alpha.
18. Hunter, C. A., C. S. Subauste, V. H. V. A. N. Cleave, and J. S. Remington. 1994. *Production of Gamma Interferon by Natural Killer Cells from Toxoplasma gondii-Infected SCID Mice : Regulation by Necrosis Factor Alpha*.
19. Sasai, M., A. Pradipta, and M. Yamamoto. 2018. Host immune responses to *Toxoplasma gondii*. *Int. Immunol.* 30: 113–119.
20. Dupont, C. D., D. A. Christian, and C. A. Hunter. 2012. Immune response and immunopathology during toxoplasmosis. *Semin. Immunopathol.* 34: 793–813.
21. Yap, G., M. Pesin, and A. Sher. 2000. Cutting edge: IL-12 is required for the maintenance of IFN-gamma production in T cells mediating chronic resistance to the intracellular pathogen, *Toxoplasma gondii*. *J. Immunol.* 165: 628–31.
22. Suzuki, Y., M. A. Orellana, R. D. Schreiber, and J. S. Remington. 1988. Interferon-gamma: the major mediator of resistance against *Toxoplasma gondii*. *Science* 240: 516–8.
23. Deckert-Schlüter, M., A. Rang, D. Weiner, S. Huang, O. D. Wiestler, H. Hof, and D. Schlüter. 1996. Interferon-gamma receptor-deficiency renders mice highly susceptible to toxoplasmosis by decreased macrophage activation. *Lab. Invest.* 75: 827–41.
24. Jebbari, H., C. W. Roberts, D. J. Ferguson, H. Bluethmann, and J. Alexander. 1998. A protective role for IL-6 during early infection with *Toxoplasma gondii*. *Parasite Immunol.* 20: 231–9.
25. Schlüter, D., L.-Y. Kwok, S. Lütjen, S. Soltek, S. Hoffmann, H. Körner, and M. Deckert. 2003. Both lymphotoxin-alpha and TNF are crucial for control of *Toxoplasma gondii* in the central nervous system. *J. Immunol.* 170: 6172–82.
26. Scharon-Kersten, T. M., G. Yap, J. Magram, and A. Sher. 1997. Inducible Nitric Oxide Is Essential for Host Control of Persistent but Not Acute Infection with the Intracellular Pathogen *Toxoplasma gondii*. *J. Exp. Med* 185: 1261–1273.
27. Blanchard, N., F. Gonzalez, M. Schaeffer, N. T. Joncker, T. Cheng, A. J. Shastri, E. A. Robey, and N. Shastri. 2008. Immunodominant, protective response to the parasite *Toxoplasma gondii* requires antigen processing in the endoplasmic reticulum. *Nat. Immunol.* 9: 937–944.
28. Grover, H. S., H. H. Chu, F. D. Kelly, S. J. Yang, M. L. Reese, N. Blanchard, F. Gonzalez, S. W. Chan, J. C. Boothroyd, N. Shastri, and E. A. Robey. 2014. Article Impact of Regulated Secretion on Antiparasitic CD8 T Cell Responses. *CellReports* 7: 1716–1728.
29. Gazzinelli, R. T., M. Wysocka, S. Hieny, T. Scharon-Kersten, A. Cheever, R. Kühn, W. Müller, G. Trinchieri, and A. Sher. 1996. In the absence of endogenous IL-10, mice acutely infected with *Toxoplasma gondii* succumb to a lethal immune response dependent on CD4+ T cells and accompanied by overproduction of IL-12, IFN-gamma and TNF-alpha. *J. Immunol.* 157: 798–805.
30. Neyer, L. E., G. Grunig, M. Fort, J. S. Remington, D. Rennick, and C. A. Hunter. 1997. Role of interleukin-10 in regulation of T-cell-dependent and T-cell-independent mechanisms of resistance to *Toxoplasma gondii*. *Infect. Immun.* 65: 1675–82.
31. Suzuki, Y., A. Sher, G. Yap, D. Park, E. Neyer, O. Liesenfeld, M. Fort, H. Kang, and E. Gufwoli. 2000. IL-10 Is Required for Prevention of Necrosis in the Small Intestine and Mortality in Both Genetically Resistant BALB/c and Susceptible C57BL/6 Mice Following

- Peroral Infection with *Toxoplasma gondii*. *J. Immunol.* 164.
32. Jankovic, D., M. C. Kullberg, C. G. Feng, R. S. Goldszmid, C. M. Collazo, M. Wilson, T. A. Wynn, M. Kamanaka, R. A. Flavell, and A. Sher. 2007. Conventional T-bet+Foxp3<sup>-</sup> Th1 cells are the major source of host-protective regulatory IL-10 during intracellular protozoan infection. *J. Exp. Med.* 204: 273–283.
  33. Wilson, E. H., U. Wille-Reece, F. Dzierzinski, and C. A. Hunter. 2005. A critical role for IL-10 in limiting inflammation during toxoplasmic encephalitis. *J. Neuroimmunol.* 165: 63–74.
  34. Roberts, C. W., D. J. P. Ferguson, H. Jebbari, A. Satoskar, H. Bluethmann, J. Alexander, and A. J. Alexander. 1996. *Different Roles for Interleukin-4 during the Course of Toxoplasma gondii Infection.* ; :897–904.
  35. Chen, F., Z. Liu, W. Wu, C. Roza, S. Bowdridge, A. Millman, N. Van Rooijen, J. F. U. Jr, T. A. Wynn, and W. C. Gause. 2012. An essential role for T H 2-type responses in limiting acute tissue damage during experimental helminth infection. *Nat. Med.* 18: 262–268.
  36. Knipper, J. A., S. Willenborg, M. Hammerschmidt, J. E. Allen, S. A. Eming, J. A. Knipper, and S. Willenborg. 2015. Interleukin-4 Receptor a Signaling in Myeloid Cells Controls Collagen Fibril Assembly in Skin Repair Article Interleukin-4 Receptor a Signaling in Myeloid Cells Controls Collagen Fibril Assembly in Skin Repair. 803–816.
  37. Molloy, M. J., J. R. Grainger, N. Bouladoux, T. W. Hand, L. Y. Koo, S. Naik, M. Quinones, A. K. Dzutsev, J.-L. Gao, G. Trinchieri, P. M. Murphy, and Y. Belkaid. 2013. Intraluminal containment of commensal outgrowth in the gut during infection-induced dysbiosis. *Cell Host Microbe* 14: 318–28.
  38. Grainger, J. R., E. A. Wohlfert, I. J. Fuss, N. Bouladoux, M. H. Askenase, F. Legrand, L. Y. Koo, J. M. Brenchley, I. D. C. Fraser, and Y. Belkaid. 2013. Inflammatory monocytes regulate pathologic responses to commensals during acute gastrointestinal infection. *Nat. Med.* 19: 713–721.
  39. Colgan, S. P., C. N. Serhan, C. A. Parkos, C. Delp-Archer, and J. L. Madara. 1993. Lipoxin A4 modulates transmigration of human neutrophils across intestinal epithelial monolayers. *J. Clin. Invest.* 92: 75–82.
  40. Aliberti, J., C. Serhan, and A. Sher. 2002. Parasite-induced Lipoxin A 4 Is an Endogenous Regulator of IL-12 Production and Immunopathology in *Toxoplasma gondii* Infection. *J. Exp. Med.* • 196: 1253–1262.
  41. Villarino, A., L. Hibbert, L. Lieberman, E. Wilson, T. Mak, H. Yoshida, R. A. Kastelein, C. Saris, and C. A. Hunter. 2003. The IL-27R (WSX-1) Is Required to Suppress T Cell Hyperactivity during Infection. *Immunity* 19: 645–655.
  42. Villarino, A. V., J. S. Stumhofer, C. J. M. Saris, R. A. Kastelein, F. J. de Sauvage, and C. A. Hunter. 2006. IL-27 limits IL-2 production during Th1 differentiation. *J. Immunol.* 176: 237–47.
  43. Hall, A. O., D. P. Beiting, C. Tato, B. John, G. Oldenhove, C. G. Lombana, G. H. Pritchard, J. S. Silver, N. Bouladoux, J. S. Stumhofer, T. H. Harris, J. Grainger, E. D. T. Wojno, S. Wagage, D. S. Roos, P. Scott, L. A. Turka, S. Cherry, S. L. Reiner, D. Cua, Y. Belkaid, M. M. Elloso, and C. A. Hunter. 2012. The cytokines interleukin 27 and interferon- $\gamma$  promote distinct Treg cell populations required to limit infection-induced pathology. *Immunity* 37: 511–23.
  44. Oldenhove, G., N. Bouladoux, E. A. Wohlfert, J. A. Hall, D. Chou, L. Dos santos, S. O'Brien, R. Blank, E. Lamb, S. Natarajan, R. Kastenmayer, C. Hunter, M. E. Grigg, and Y. Belkaid. 2009. Decrease of Foxp3<sup>+</sup> Treg Cell Number and Acquisition of Effector Cell Phenotype during Lethal Infection. *Immunity* 31: 772–786.

45. Benson, A., S. Murray, P. Divakar, N. Burnaevskiy, R. Pifer, J. Forman, and F. Yarovinsky. 2012. Microbial Infection-Induced Expansion of Effector T Cells Overcomes the Suppressive Effects of Regulatory T Cells via an IL-2 Deprivation Mechanism. *J. Immunol.* 188: 800–810.
46. Charles, E., S. Joshi, J. D. Ash, B. A. Fox, A. D. Farris, D. J. Bzik, M. L. Lang, and I. J. Blader. 2010. CD4 T-cell suppression by cells from *Toxoplasma gondii*-infected retinas is mediated by surface protein PD-L1. *Infect. Immun.* 78: 3484–92.
47. Núñez, G., K. Sakamoto, and M. P. Soares. 2018. Innate Nutritional Immunity. *J. Immunol.* 201: 11–18.
48. Hood, M. I., and E. P. Skaar. 2012. Nutritional immunity: transition metals at the pathogen-host interface. *Nat. Rev. Microbiol.* 10: 525–37.
49. Milovanović, I., M. Busarčević, A. Trbovich, V. Ivočić, A. Uzelac, and O. Djurković-Djaković. 2017. Evidence for host genetic regulation of altered lipid metabolism in experimental toxoplasmosis supported with gene data mining results. *PLoS One* 12: 1–15.
50. Zhou, C.-X., D.-H. Zhou, H. M. Elsheikha, Y. Zhao, X. Suo, and X.-Q. Zhu. 2016. Metabolomic Profiling of Mice Serum during Toxoplasmosis Progression Using Liquid Chromatography-Mass Spectrometry. *Sci. Rep.* 6: 19557.
51. Zhou, C.-X., D.-H. Zhou, H. M. Elsheikha, G.-X. Liu, X. Suo, and X.-Q. Zhu. 2015. Global Metabolomic Profiling of Mice Brains following Experimental Infection with the Cyst-Forming *Toxoplasma gondii*. *PLoS One* 10: e0139635.
52. Corbin, K. D., and S. H. Zeisel. 2012. Choline metabolism provides novel insights into nonalcoholic fatty liver disease and its progression. *Curr. Opin. Gastroenterol.* 28: 159–65.
53. Hatter, J. A., Y. M. Kouche, S. J. Melchor, K. Ng, D. M. Bouley, J. C. Boothroyd, and S. E. Ewald. 2018. *Toxoplasma gondii* infection triggers chronic cachexia and sustained commensal dysbiosis in mice. *PLoS One* 13: e0204895.
54. Arsenijevic, D., L. Girardier, J. Seydoux, H. R. Chang, and A. G. Dulloo. 1997. Altered energy balance and cytokine gene expression in a murine model of chronic infection with *Toxoplasma gondii*. *Am. J. Physiol.* 272: E908-17.
55. Weiss, L. M., and J. P. Dubey. 2009. Toxoplasmosis: A history of clinical observations. *Int. J. Parasitol.* 39: 895–901.
56. Jin, R. M., S. J. Blair, J. Warunek, R. R. Heffner, I. J. Blader, E. A. Wohlfert, R. Reid, I. J. Blader, E. A. Wohlfert, R. M. Jin, S. J. Blair, J. Warunek, R. R. Heffner, I. J. Blader, and E. A. Wohlfert. 2017. Regulatory T Cells Promote Myositis and Muscle Damage in *Toxoplasma gondii* Infection. *J. Immunol.* 198: 352–362.
57. Wang, A., S. C. Huen, H. H. Luan, S. Yu, C. Zhang, J.-D. Gallezot, C. J. Booth, and R. Medzhitov. 2016. Opposing Effects of Fasting Metabolism on Tissue Tolerance in Bacterial and Viral Inflammation. *Cell* 166: 1512-1525.e12.
58. Bisanz, C., O. Bastien, D. Grando, J. Jouhet, E. Maréchal, and M.-F. Cesbron-Delauw. 2006. *Toxoplasma gondii* acyl-lipid metabolism: *de novo* synthesis from apicoplast-generated fatty acids versus scavenging of host cell precursors. *Biochem. J.* 394: 197–205.
59. Sehgal, A., S. Bettiol, M. Pypaert, M. R. Wenk, A. Kaasch, I. J. Blader, K. A. Joiner, and I. Coppens. 2005. Peculiarities of Host Cholesterol Transport to the Unique Intracellular Vacuole Containing *Toxoplasma*. 1125–1141.
60. Hu, X., D. Binns, and M. L. Reese. 2017. The coccidian parasites *Toxoplasma* and *Neospora* dysregulate mammalian lipid droplet biogenesis. *J. Biol. Chem.* 292: 11009–11020.
61. Pernas, L., C. Bean, J. C. Boothroyd, and L. Scorrano. 2018. Mitochondria Restrict Growth of the Intracellular Parasite *Toxoplasma gondii* by Limiting Its Uptake of Fatty Acids. *Cell Metab.* 27: 886-897.e4.

62. Nolan, S. J., J. D. Romano, I. Coppens, I. Mellman, F. Gartner, and M. Provenzano. 2017. Host lipid droplets: An important source of lipids salvaged by the intracellular parasite *Toxoplasma gondii*. *PLoS Pathog.* 13: e1006362.
63. Arsenijevic, D., F. D. Bilbao, P. Giannakopoulos, L. Girardier, S. Samec, and D. Richard. 2001. A role for interferon-gamma in the hypermetabolic response to murine toxoplasmosis. *Eur. Cytokine Netw.* 12: 518–527.
64. Arsenijevic, D., L. Girardier, J. Seydoux, J. C. Pechere, I. Garcia, R. Lucas, H. R. Chang, and A. G. Dulloo. 1998. Metabolic-cytokine responses to a second immunological challenge with LPS in mice with *T. gondii* infection. *Am. J. Physiol.* 274: E439–45.
65. Heimesaat, M. M., S. Bereswill, A. Fischer, D. Fuchs, D. Struck, J. Niebergall, H.-K. Jahn, I. R. Dunay, A. Moter, D. M. Gescher, R. R. Schumann, U. B. Göbel, and O. Liesenfeld. 2006. Gram-Negative Bacteria Aggravate Murine Small Intestinal Th1-Type Immunopathology following Oral Infection with *Toxoplasma gondii*. *J. Immunol.* 177.
66. Benson, A., R. Pifer, C. L. Behrendt, L. V Hooper, and F. Yarovinsky. 2009. Gut Commensal Bacteria Direct a Protective Immune Response against *Toxoplasma gondii*. *Cell Host Microbe* 6: 187–196.
67. Raetz, M., S. Hwang, C. L. Wilhelm, D. Kirkland, A. Benson, C. R. Sturge, J. Mirpuri, S. Vaishnava, B. Hou, A. L. DeFranco, C. J. Gilpin, L. V Hooper, and F. Yarovinsky. 2012. Parasite-induced TH1 cells and intestinal dysbiosis cooperate in IFN- $\gamma$ -dependent elimination of Paneth cells. *Nat. Immunol.* .
68. Fonseca, D. M. Da, T. W. Hand, S. J. Han, M. Y. Gerner, A. G. Zaretsky, A. L. Byrd, O. J. Harrison, A. M. Ortiz, M. Quinones, G. Trinchieri, J. M. Brenchley, I. E. Brodsky, R. N. Germain, G. J. Randolph, and Y. Belkaid. 2015. Microbiota-Dependent Sequelae of Acute Infection Compromise Tissue-Specific Immunity. *Cell* 163: 354–366.
69. Di Cristina, M., D. Marocco, R. Galizi, C. Proietti, R. Spaccapelo, and A. Crisanti. 2008. Temporal and spatial distribution of *Toxoplasma gondii* differentiation into Bradyzoites and tissue cyst formation in vivo. *Infect. Immun.* 76: 3491–501.
70. He, J. J., J. Ma, H. M. Elsheikha, H. Q. Song, D. H. Zhou, and X. Q. Zhu. 2016. Proteomic profiling of mouse liver following acute toxoplasma gondii infection. *PLoS One* 11: 1–15.
71. Zhou, C. X., D. H. Zhou, H. M. Elsheikha, G. X. Liu, X. Suo, and X. Q. Zhu. 2015. Global metabolomic profiling of mice brains following experimental infection with the cyst-forming *Toxoplasma gondii*. *PLoS One* 10: 1–22.
72. Silva, N. M., C. V Rodrigues, M. M. Santoro, L. F. L. Reis, J. I. Alvarez-leite, R. T. Gazzinelli, S. E. T. Al, and I. N. I. Mmun. 2002. Expression of Indoleamine 2, 3-Dioxygenase, Tryptophan Degradation, and Kynurenine Formation during In Vivo Infection with *Toxoplasma gondii*: Induction by Endogenous Gamma Interferon and Requirement of Interferon Regulatory Factor 1. 70: 859–868.
73. Bottari, N. B., A. A. Tonin, R. Figuera, M. M. Flores, R. T. França, G. Camillo, G. Toscan, F. S. F. Vogel, M. B. Sangoi, G. V Bochi, R. N. Moresco, S. T. A. Lopes, and A. S. Da. 2014. Experimental Parasitology *Neospora caninum* and *Toxoplasma gondii*: Relationship between hepatic lesions, cytological and biochemical analysis of the cavity liquid during the acute phase of the diseases in experimental models. *Exp. Parasitol.* 136: 68–73.
74. Atmaca, H. T. K., A. N. Gazya C, S. L. Canpolat, O. U. Kul, A. Gazyagcı, S. L. Canpolat, and O. U. Kul. 2013. Hepatic stellate cells increase in *Toxoplasma gondii* infection in mice. *Parasit. Vectors* 6: 135.
75. Autier, B., S. Dion, and F. Robert-gangneux. 2018. The liver as an organ at risk for

Toxoplasma transmission during transplantation : myth or reality? 763–766.

76. Assi, MA, Rosenblatt, JE, Marshall, W. 2007. Donor-transmitted toxoplasmosis in liver transplant recipients : a case report and literature review. *Transpl. Infect. Dis.* 9: 132–136.
77. Gutí, F. 2019. Does *Toxoplasma gondii* infection impact liver transplantation outcomes? A systematic review. 499–506.
78. El-Sayed, N. M., M. E. Ramadan, and M. E. Ramadan. 2016. *Toxoplasma gondii* Infection and Chronic Liver Diseases: Evidence of an Association. *Trop. Med. Infect. Dis.* 1: 1–8.
79. He, J. J., J. Ma, H. M. Elsheikha, H. Q. Song, S. Y. Huang, and X. Q. Zhu. 2016. Transcriptomic analysis of mouse liver reveals a potential hepato-enteric pathogenic mechanism in acute *Toxoplasma gondii* infection. *Parasites and Vectors* 9.
80. Neyrolles, O., R. Hernández-Pando, F. Pietri-Rouxel, P. Fornès, L. Tailleux, J. A. B. Payán, E. Pivert, Y. Bordat, D. Aguilar, M.-C. Prévost, C. Petit, and B. Gicquel. 2006. Is Adipose Tissue a Place for *Mycobacterium tuberculosis* Persistence? *PLoS One* 1: e43.
81. Trindade, S., F. Rijo-Ferreira, T. Carvalho, D. Pinto-Neves, F. Guegan, F. Aresta-Branco, F. Bento, S. A. Young, A. Pinto, J. Van Den Abbeele, R. M. Ribeiro, S. Dias, T. K. Smith, and L. M. Figueiredo. 2016. *Trypanosoma brucei* Parasites Occupy and Functionally Adapt to the Adipose Tissue in Mice. *Cell Host Microbe* 19: 837–48.
82. Schieber, A. M. P., Y. M. Lee, M. W. Chang, M. Leblanc, B. Collins, M. Downes, R. M. Evans, and J. S. Ayres. 2015. Disease tolerance mediated by microbiome *E. coli* involves inflammasome and IGF-1 signaling. *Science* 350: 558–63.
83. Bohne, W., J. Heesemann, and U. Gross. 1993. Induction of bradyzoite-specific *Toxoplasma gondii* antigens in gamma interferon-treated mouse macrophages. *Infect. Immun.* 61: 1141–5.
84. Bohne, W., J. Heesemann, and U. Gross. 1994. Reduced replication of *Toxoplasma gondii* is necessary for induction of bradyzoite-specific antigens: a possible role for nitric oxide in triggering stage conversion. *Infect. Immun.* 62: 1761–7.
85. Tzelepis, F., J. Blagih, N. Khan, J. Gillard, L. Mendonca, D. G. Roy, E. H. Ma, P. Joubert, R. G. Jones, and M. Divangahi. 2018. Mitochondrial cyclophilin D regulates T cell metabolic responses and disease tolerance to tuberculosis. *Sci. Immunol.* 3: eaar4135.
86. Jin, R. M., S. J. Blair, J. Warunek, R. R. Heffner, I. J. Blader, and E. A. Wohlfert. 2017. Regulatory T Cells Promote Myositis and Muscle Damage in *Toxoplasma gondii* Infection. *J. Immunol.* 198: 352–362.
87. Kugler, D. G., F. A. Flomerfelt, D. L. Costa, K. Laky, O. Kamenyeva, P. R. Mittelstadt, R. E. Gress, S. P. Rosshart, B. Rehermann, J. D. Ashwell, A. Sher, and D. Jankovic. 2016. Systemic toxoplasma infection triggers a long-term defect in the generation and function of naive T lymphocytes. 3041–3056.
88. Matsuki, T., S. Nakae, K. Sudo, R. Horai, and Y. Iwakura. 2006. Abnormal T cell activation caused by the imbalance of the IL-1/IL-1R antagonist system is responsible for the development of experimental autoimmune encephalomyelitis. *Int. Immunol.* 18: 399–407.
89. Shornick, L. P., P. De Togni, S. Mariathasan, J. Goellner, J. Strauss-Schoenberger, R. W. Karr, T. A. Ferguson, and D. D. Chaplin. 1996. Mice deficient in IL-1beta manifest impaired contact hypersensitivity to trinitrochlorobenzene. *J. Exp. Med.* 183: 1427–1436.
90. Kasper, D. C., K. Sadeghi, A.-R. Prusa, G. H. Reischer, K. Kratochwill, E. Förster-Waldl, N. Gerstl, M. Hayde, A. Pollak, and K. R. Herkner. 2009. Quantitative real-time polymerase chain reaction for the accurate detection of *Toxoplasma gondii* in amniotic fluid. *Diagn. Microbiol. Infect. Dis.* 63: 10–15.

91. Pearson, H., and D. Stirling. 2003. DNA Extraction from Tissue. In *PCR Protocols* Humana Press, New Jersey. 33–34.
92. Kraus, D., Q. Yang, and B. B. Kahn. 2015. Lipid Extraction from Mouse Feces. *Bio-protocol* 5.
93. Vázquez-Baeza, Y., M. Pirrung, A. Gonzalez, and R. Knight. 2013. EMPeror: a tool for visualizing high-throughput microbial community data. *Gigascience* 2: 16.
94. Caporaso, J. G., J. Kuczynski, J. Stombaugh, K. Bittinger, F. D. Bushman, E. K. Costello, N. Fierer, A. G. Peña, J. K. Goodrich, J. I. Gordon, G. A. Huttley, S. T. Kelley, D. Knights, J. E. Koenig, R. E. Ley, C. A. Lozupone, D. McDonald, B. D. Muegge, M. Pirrung, J. Reeder, J. R. Sevinsky, P. J. Turnbaugh, W. A. Walters, J. Widmann, T. Yatsunenko, J. Zaneveld, and R. Knight. 2010. QIIME allows analysis of high-throughput community sequencing data. *Nat. Methods* 7: 335–336.
95. Mohar, I., K. J. Brempelis, S. A. Murray, M. R. Ebrahimkhani, and I. N. Crispe. 2015. Isolation of Non-parenchymal Cells from the Mouse Liver. In Humana Press, New York, NY. 3–17.
96. Ruifrok, A. C., and D. A. Johnston. 2001. Quantification of histochemical staining by color deconvolution. *Anal. Quant. Cytol. Histol.* 23: 291–9.
97. Schindelin, J., I. Arganda-Carreras, E. Frise, V. Kaynig, M. Longair, T. Pietzsch, S. Preibisch, C. Rueden, S. Saalfeld, B. Schmid, J.-Y. Tinevez, D. J. White, V. Hartenstein, K. Eliceiri, P. Tomancak, and A. Cardona. 2012. Fiji: an open-source platform for biological-image analysis. *Nat. Methods* 9: 676–682.
98. Vaughn, A. R., T. A. Bell, E. Gibbons, C. Askew, H. Franchino, K. Hirsche, L. Kemsley, S. Melchor, E. Moulton, M. Schwab, J. Nelson, and J. D. Bell. 2015. Biochimica et Biophysica Acta Relationships between membrane water molecules and Patman equilibration kinetics at temperatures far above the phosphatidylcholine melting point. *BBA - Biomembr.* 1848: 942–950.
99. Evans, W. J., J. E. Morley, J. Argilés, C. Bales, V. Baracos, D. Guttridge, A. Jatoi, K. Kalantar-Zadeh, H. Lochs, G. Mantovani, D. Marks, W. E. Mitch, M. Muscaritoli, A. Najand, P. Ponikowski, F. Rossi Fanelli, M. Schambelan, A. Schols, M. Schuster, D. Thomas, R. Wolfe, and S. D. Anker. 2008. Cachexia: A new definition. *Clin. Nutr.* 27: 793–799.
100. Tisdale, M. J. 1997. Biology of Cachexia. *JNCI J. Natl. Cancer Inst.* 89: 1763–1773.
101. Deboer, M. D. 2009. Animal models of anorexia and cachexia. *Expert Opin. Drug Discov.* 4: 1145–1155.
102. Coombes, J. L., B. A. Charsar, S.-J. Han, J. Halkias, S. W. Chan, A. A. Koshy, B. Striepen, and E. A. Robey. 2013. Motile invaded neutrophils in the small intestine of *Toxoplasma gondii*-infected mice reveal a potential mechanism for parasite spread. *Proc. Natl. Acad. Sci. U. S. A.* 110: E1913-22.
103. von Klitzing, E., I. Ekmekciu, A. A. Kühl, S. Bereswill, M. M. Heimesaat, and J. Wal. 2017. Intestinal, extra-intestinal and systemic sequelae of *Toxoplasma gondii* induced acute ileitis in mice harboring a human gut microbiota. *PLoS One* 12: e0176144.
104. Heimesaat, M. M., S. Bereswill, A. Fischer, D. Fuchs, D. Struck, J. Niebergall, H.-K. Jahn, I. R. Dunay, A. Moter, D. M. Gescher, R. R. Schumann, U. B. Göbel, and O. Liesenfeld. 2006. Gram-Negative Bacteria Aggravate Murine Small Intestinal Th1-Type Immunopathology following Oral Infection with *Toxoplasma gondii*. *J. Immunol.* 177: 8785–8795.
105. Kim, K., and L. M. Weiss. 2004. *Toxoplasma gondii*: The model apicomplexan. *Int. J. Parasitol.* 34: 423–432.
106. Dubey, J. P. 2009. History of the discovery of the life cycle of *Toxoplasma gondii*. *Int. J.*

*Parasitol.* 39: 877–82.

107. Boothroyd, J. C. 2009. Expansion of host range as a driving force in the evolution of *Toxoplasma*. *Mem. Inst. Oswaldo Cruz* 104: 179–84.

108. Blader, I. J., and J. P. Saeij. 2009. *Communication between Toxoplasma gondii and its host: Impact on parasite growth, development, immune evasion, and virulence.* *APMIS* ; :458–476.

109. Vyas, A., S.-K. Kim, N. Giacomini, J. C. Boothroyd, and R. M. Sapolsky. 2007. Behavioral changes induced by *Toxoplasma* infection of rodents are highly specific to aversion of cat odors. *Proc. Natl. Acad. Sci.* 104: 6442–6447.

110. Berdoy, M., J. P. Webster, and D. W. Macdonald. 2000. Fatal attraction in rats infected with *Toxoplasma gondii*. *Proc. R. Soc. B Biol. Sci.* 267: 1591–1594.

111. Scharton-Kersten, T. M., T. A. Wynn, E. Y. Denkers, S. Bala, E. Grunvald, S. Hieny, R. T. Gazzinelli, and A. Sher. 1996. In the absence of endogenous IFN-gamma, mice develop unimpaired IL-12 responses to *Toxoplasma gondii* while failing to control acute infection. *J. Immunol.* 157: 4045–54.

112. Fleckenstein, M. C., M. L. Reese, S. Könen-Waisman, J. C. Boothroyd, J. C. Howard, and T. Steinfeldt. 2012. A *Toxoplasma gondii* pseudokinase inhibits host irg resistance proteins. *PLoS Biol.* 10: 14.

113. Beaman, M. H., C. A. Hunter, and J. S. Remington. 1994. Enhancement of intracellular replication of *Toxoplasma gondii* by IL-6. Interactions with IFN-gamma and TNF-alpha. *J. Immunol.* 153: 4583–7.

114. Yap, G. S., and A. Sher. 1999. Effector cells of both nonhemopoietic and hemopoietic origin are required for interferon (IFN)-gamma- and tumor necrosis factor (TNF)-alpha-dependent host resistance to the intracellular pathogen, *Toxoplasma gondii*. *J. Exp. Med.* 189: 1083–92.

115. Loetscher, P., A. Pellegrino, J. H. Gong, I. Mattioli, M. Loetscher, G. Bardi, M. Baggiolini, and I. Clark-Lewis. 2001. The Ligands of CXC Chemokine Receptor 3, I-TAC, Mig, and IP10, Are Natural Antagonists for CCR3. *J. Biol. Chem.* 276: 2986–2991.

116. Sanner, H., T. Schwartz, B. Flatø, M. Vistnes, G. Christensen, and I. Sjaastad. 2014. Increased levels of eotaxin and MCP-1 in juvenile dermatomyositis median 16.8 years after disease onset; associations with disease activity, duration and organ damage. *PLoS One* 9: e92171.

117. Schluter, D., L.-Y. Kwok, S. Lutjen, S. Soltek, S. Hoffmann, H. Korner, and M. Deckert. 2003. Both Lymphotoxin- and TNF Are Crucial for Control of *Toxoplasma gondii* in the Central Nervous System. *J. Immunol.* 170: 6172–6182.

118. Schreiner, M., and O. Liesenfeld. 2009. Small intestinal inflammation following oral infection with *Toxoplasma gondii* does not occur exclusively in C57BL/6 mice: Review of 70 reports from the literature. *Mem. Inst. Oswaldo Cruz* 104: 221–233.

119. Grover, H. S., H. H. Chu, F. D. Kelly, S. J. Yang, M. L. Reese, N. Blanchard, F. Gonzalez, S. W. Chan, J. C. Boothroyd, N. Shastri, and E. A. Robey. 2014. Impact of Regulated Secretion on Antiparasitic CD8 T Cell Responses. *Cell Rep.* 7: 1716–1728.

120. Mowat, A. M., and W. W. Agace. 2014. Regional specialization within the intestinal immune system. *Nat. Rev. Immunol.* 14: 667–685.

121. Heimesaat, M. M., A. Fischer, B. Siegmund, A. Kupz, J. Niebergall, D. Fuchs, H.-K. K. Jahn, M. Freudenberg, C. Loddenkemper, A. Batra, H.-A. A. Lehr, O. Liesenfeld, M. Blaut, U. B. Göbel, R. R. Schumann, and S. Bereswill. 2007. Shift towards pro-inflammatory intestinal bacteria aggravates acute murine colitis via toll-like receptors 2 and 4. *PLoS One* 2: e662.

122. Zhu, W., M. G. Winter, M. X. Byndloss, L. Spiga, B. A. Duerkop, E. R. Hughes, L. Büttner, E. De Lima Romão, C. L. Behrendt, C. A. Lopez, L. Sifuentes-Dominguez, K. Huff-Hardy, R. P. Wilson, C. C. Gillis, Ç. Tükel, A. Y. Koh, E. Burstein, L. V Hooper, A. J. Bäumlner, and S. E. Winter. 2018. Precision editing of the gut microbiota ameliorates colitis. *Nature* 553: 208–211.
123. Rao, S., A. M. P. Schieber, C. P. O'Connor, M. Leblanc, D. Michel, and J. S. Ayres. 2017. Pathogen-Mediated Inhibition of Anorexia Promotes Host Survival and Transmission. *Cell* 168: 503–516.e12.
124. Flegr, J., J. Prandota, M. Sovičková, and Z. H. Israili. 2014. Toxoplasmosis—a global threat. Correlation of latent toxoplasmosis with specific disease burden in a set of 88 countries. *PLoS One* 9: e90203.
125. Di Cristina, M., D. Marocco, R. Galizi, C. Proietti, R. Spaccapelo, and A. Crisanti. 2008. Temporal and spatial distribution of *Toxoplasma gondii* differentiation into Bradyzoites and tissue cyst formation in vivo. *Infect. Immun.* 76: 3491–501.
126. Pernas, L., R. Ramirez, T. H. Holmes, J. G. Montoya, and J. C. Boothroyd. 2014. Immune profiling of pregnant toxoplasma-infected US and Colombia patients reveals surprising impacts of infection on peripheral blood cytokines. *J. Infect. Dis.* 210: 923–931.
127. Luft, B. J., and J. S. Remington. 1992. Toxoplasmic Encephalitis in AIDS. *Clin. Infect. Dis.* 15: 211–222.
128. Khurana, S., and N. Batra. 2016. Toxoplasmosis in organ transplant recipients: Evaluation, implication, and prevention. *Trop. Parasitol.* 6: 123–128.
129. Hunter, C. A., J. S. Abrams, M. H. Beaman, and J. S. Remington. 1993. *Cytokine mRNA in the central nervous system of SCID mice infected with Toxoplasma gondii: Importance of T-cell-independent regulation of resistance to T. gondii.*
130. Chang, H. R., G. E. Grau, and J. C. Pechère. 1990. Role of TNF and IL-1 in infections with *Toxoplasma gondii*. *Immunology* 69: 33–7.
131. Gorfu, G., K. M. Cirelli, M. B. Melo, K. Mayer-Barber, D. Crown, B. H. Koller, S. Masters, A. Sher, S. H. Leppla, M. Moayeri, J. P. J. J. Sacij, and M. E. Grigg. 2014. Dual role for inflammasome sensors NLRP1 and NLRP3 in murine resistance to *Toxoplasma gondii*. *MBio* 5: 1–12.
132. LaRosa, D. F., J. S. Stumhofer, A. E. Gelman, A. H. Rahman, D. K. Taylor, C. A. Hunter, and L. A. Turka. 2008. T cell expression of MyD88 is required for resistance to *Toxoplasma gondii*. *Proc. Natl. Acad. Sci. U. S. A.* 105: 3855–60.
133. Villeret, B., L. Brault, A. Couturier-Maillard, P. Robinet, V. Vasseur, T. Secher, I. Dimier-Poisson, M. Jacobs, S.-G. Zheng, V. F. Quesniaux, and B. Ryffel. 2013. Blockade of IL-1R signaling diminishes Paneth cell depletion and *Toxoplasma gondii* induced ileitis in mice. *Am. J. Clin. Exp. Immunol.* 2: 107–16.
134. Bersudsky, M., L. Luski, D. Fishman, R. M. White, N. Ziv-Sokolovskaya, S. Dotan, P. Rider, I. Kaplanov, T. Aychek, C. A. Dinarello, R. N. Apte, and E. Voronov. 2014. Non-redundant properties of IL-1 $\alpha$  and IL-1 $\beta$  during acute colon inflammation in mice. *Gut* 63: 598–609.
135. Alves-Rosa, F., M. Vulcano, M. Beigier-Bompadre, G. Fernández, M. Palermo, and M. A. Isturiz. 2002. Interleukin-1beta induces in vivo tolerance to lipopolysaccharide in mice. *Clin. Exp. Immunol.* 128: 221–8.
136. Benjamin, J. T., D. J. Moore, C. Bennett, R. van der Meer, A. Royce, R. Loveland, and J. L. Wynn. 2018. Cutting Edge: IL-1 $\alpha$  and Not IL-1 $\beta$  Drives IL-1R1–Dependent Neonatal Murine Sepsis Lethality. *J. Immunol.* 201: 2873–2878.

137. Melchor, S. J., and S. E. Ewald. 2019. Disease tolerance in Toxoplasma infection. *Front. Cell. Infect. Microbiol.* 9: 185.
138. Schlüter, D., L.-Y. Kwok, S. Lütjen, S. Soltek, S. Hoffmann, H. Körner, and M. Deckert. 2003. Both lymphotoxin-alpha and TNF are crucial for control of Toxoplasma gondii in the central nervous system. *J. Immunol.* 170: 6172–82.
139. Kiryu, H., W. Rikihisa, and M. Furue. 2000. Encapsulated fat necrosis - A clinicopathological study of 8 cases and a literature review. *J. Cutan. Patbol.* 27: 19–23.
140. Misumi, I., J. Starmer, T. Uchimura, M. A. Beck, T. Magnuson, and J. K. Whitmire. 2019. Obesity Expands a Distinct Population of T Cells in Adipose Tissue and Increases Vulnerability to Infection. *Cell Rep.* 27: 514-524.e5.
141. Atmaca, H. T. K., A. N. Gazya C, S. L. Canpolat, and O. U. Kul. 2013. Hepatic stellate cells increase in Toxoplasma gondii infection in mice. *Parasit. Vectors* 6: 135.
142. Luan, H. H., A. Wang, B. K. Hilliard, F. Carvalho, C. E. Rosen, A. M. Ahasic, E. L. Herzog, I. Kang, M. A. Pisani, S. Yu, C. Zhang, A. M. Ring, L. H. Young, and R. Medzhitov. 2019. GDF15 Is an Inflammation-Induced Central Mediator of Tissue Tolerance. *Cell* 178: 1231-1244.e11.
143. La, E., and S. M. Fischer. 2001. Transcriptional regulation of intracellular IL-1 receptor antagonist gene by IL-1 alpha in primary mouse keratinocytes. *J. Immunol.* 166: 6149–55.
144. Gibbings, S. L., and C. V Jakubzick. 2018. Isolation and Characterization of Mononuclear Phagocytes in the Mouse Lung and Lymph Nodes. *Methods Mol. Biol.* 1809: 33–44.
145. Zhang, C., J. Feng, J. Du, Z. Zhuo, S. Yang, W. Zhang, W. Wang, S. Zhang, Y. Iwakura, G. Meng, Y. X. Fu, B. Hou, and H. Tang. 2018. Macrophage-derived IL-1 $\alpha$  promotes sterile inflammation in a mouse model of acetaminophen hepatotoxicity. *Cell. Mol. Immunol.* 15: 973–982.
146. Matthys, P., and A. Billiau. 1997. Cytokines and cachexia. *Nutrition* 13: 763–770.
147. Johnson, L. L. 1992. A protective role for endogenous tumor necrosis factor in Toxoplasma gondii infection. *Infect. Immun.* 60: 1979–83.
148. Medzhitov, R., D. S. Schneider, and M. P. Soares. 2012. Disease Tolerance as a Defense Strategy. *Science (80-. )*. 335: 936–941.
149. Martinon, F., K. Burns, and J. Tschopp. 2002. The inflammasome: a molecular platform triggering activation of inflammatory caspases and processing of proIL-beta. *Mol. Cell* 10: 417–26.
150. López-Yglesias, A. H., E. Camanzo, A. T. Martin, A. M. Araujo, and F. Yarovinsky. 2019. TLR11-independent inflammasome activation is critical for CD4+ T cell-derived IFN- $\gamma$  production and host resistance to Toxoplasma gondii. *PLOS Pathog.* 15: e1007872.
151. Coutermarsh-Ott, S. L., J. T. Doran, C. Campbell, T. M. Williams, D. S. Lindsay, and I. C. Allen. 2016. Caspase-11 Modulates Inflammation and Attenuates *Toxoplasma gondii* Pathogenesis. *Mediators Inflamm.* 2016: 1–14.
152. Fisch, D., H. Bando, B. Clough, V. Hornung, M. Yamamoto, A. R. Shenoy, and E. Frickel. 2019. Human GBP 1 is a microbe-specific gatekeeper of macrophage apoptosis and pyroptosis. *EMBO J.* 38.
153. Pandori, W. J., T. S. Lima, S. Mallya, T. H. Kao, L. Gov, and M. B. Lodoen. 2019. Toxoplasma gondii activates a Syk-CARD9-NF- $\kappa$ B signaling axis and gasdermin D-independent release of IL-1 $\beta$  during infection of primary human monocytes. *PLOS Pathog.* 15: e1007923.
154. Khan, I. A., J. D. Schwartzman, T. Matsuura, and L. H. Kasper. 1997. A dichotomous

- role for nitric oxide during acute *Toxoplasma gondii* infection in mice. *Proc. Natl. Acad. Sci.* 94: 13955–13960.
155. Halonen, S. K., G. A. Taylor, and L. M. Weiss. 2001. Gamma interferon-induced inhibition of *Toxoplasma gondii* in astrocytes is mediated by IGTP. *Infect. Immun.* 69: 5573–6.
156. Zhao, Y. O., A. Khaminets, J. P. Hunn, and J. C. Howard. 2009. Disruption of the *Toxoplasma gondii* parasitophorous vacuole by IFN $\gamma$ -inducible immunity-related GTPases (IRG proteins) triggers necrotic cell death. *PLoS Pathog.* 5: e1000288.
157. Liesenfeld, O. 2002. Oral Infection of C57BL/6 Mice with *Toxoplasma gondii*: A New Model of Inflammatory Bowel Disease? *J. Infect. Dis.* 185: S96–S101.
158. Lutz, A., J. Sanwald, M. Thomas, R. Feuer, O. Sawodny, M. Ederer, C. Borner, M. Humar, and I. Merfort. 2014. Interleukin-1 $\beta$  Enhances FasL-Induced Caspase-3/-7 Activity without Increasing Apoptosis in Primary Mouse Hepatocytes. *PLoS One* 9: e115603.
159. Takehara, T., N. Hayashi, T. Tatsumi, T. Kanto, E. Mita, Y. Sasaki, A. Kasahara, and M. Hori. 1999. Interleukin 1 $\beta$  protects mice from Fas-mediated hepatocyte apoptosis and death. *Gastroenterology* 117: 661–668.
160. Bohlinger, I., M. Leist, J. Barsig, T. Uhlig, G. Tiegs, and A. Wendel. 1995. Interleukin-1 and nitric oxide protect against tumor necrosis factor  $\alpha$ -induced liver injury through distinct pathways. *Hepatology* 22: 1829–1837.
161. Ishibe, T., A. Kimura, Y. Ishida, T. Takayasu, T. Hayashi, K. Tsuneyama, K. Matsushima, I. Sakata, N. Mukaida, and T. Kondo. 2009. Reduced acetaminophen-induced liver injury in mice by genetic disruption of IL-1 receptor antagonist. *Lab. Invest.* 89: 68–79.
162. Layé, S., G. Gheusi, S. Cremona, C. Combe, K. Kelley, R. Dantzer, and P. Parnet. 2000. Endogenous brain IL-1 mediates LPS-induced anorexia and hypothalamic cytokine expression. *Am. J. Physiol. Integr. Comp. Physiol.* 279: R93–R98.
163. Fong, Y., L. L. Moldawer, M. Marano, H. Wei, A. Barber, K. Manogue, K. J. Tracey, G. Kuo, D. A. Fischman, and A. Cerami. 1989. Cachectin/TNF or IL-1 alpha induces cachexia with redistribution of body proteins. *Am. J. Physiol.* 256: R659-65.
164. Braun, T. P., X. Zhu, M. Szumowski, G. D. Scott, A. J. Grossberg, P. R. Levasseur, K. Graham, S. Khan, S. Damaraju, W. F. Colmers, V. E. Baracos, and D. L. Marks. 2011. Central nervous system inflammation induces muscle atrophy via activation of the hypothalamic-pituitary-adrenal axis. *J. Exp. Med.* 208: 2449–2463.
165. Strassmann, G., Y. Masui, R. Chizzonite, and M. Fong. 1993. Mechanisms of experimental cancer cachexia. Local involvement of IL-1 in colon-26 tumor. *J. Immunol.* 150: 2341–5.
166. Kumar, S., H. Kishimoto, H. L. Chua, S. Badve, K. D. Miller, R. M. Bigsby, and H. Nakshatri. 2003. Interleukin-1 alpha promotes tumor growth and cachexia in MCF-7 xenograft model of breast cancer. *Am. J. Pathol.* 163: 2531–41.
167. Burke, S. J., H. M. Batdorf, D. H. Burk, T. M. Martin, T. Mendoza, K. Stadler, W. Alami, M. D. Karlstad, M. J. Robson, R. D. Blakely, R. L. Mynatt, and J. J. Collier. 2018. Pancreatic deletion of the interleukin-1 receptor disrupts whole body glucose homeostasis and promotes islet  $\beta$ -cell de-differentiation. *Mol. Metab.* 14: 95–107.
168. Matsuki, T., R. Horai, K. Sudo, and Y. Iwakura. 2003. IL-1 plays an important role in lipid metabolism by regulating insulin levels under physiological conditions. *J. Exp. Med.* 198: 877–88.
169. Somm, E., E. Henrichot, A. Pernin, C. E. Juge-Aubry, P. Muzzin, J.-M. Dayer, M. J. H. Nicklin, and C. A. Meier. 2005. Decreased fat mass in interleukin-1 receptor antagonist-deficient mice: impact on adipogenesis, food intake, and energy expenditure. *Diabetes* 54: 3503–

9.

170. Hirsch, E., V. M. Irikura, S. M. Paul, and D. Hirsh. 1996. Functions of interleukin 1 receptor antagonist in gene knockout and overproducing mice. *Proc. Natl. Acad. Sci. U. S. A.* 93: 11008–13.
171. Deboer, M. D. 2009. Animal models of anorexia and cachexia. *Expert Opin. Drug Discov.* 4: 1145–1155.
172. Ballarò, R., P. Costelli, and F. Penna. 2016. Animal models for cancer cachexia. *Curr. Opin. Support. Palliat. Care* 10: 281–287.
173. Hong, D. S., D. Hui, E. Bruera, F. Janku, A. Naing, G. S. Falchook, S. Piha-Paul, J. J. Wheler, S. Fu, A. M. Tsimberidou, M. Stecher, P. Mohanty, J. Simard, and R. Kurzrock. 2014. MABp1, a first-in-class true human antibody targeting interleukin-1 $\alpha$  in refractory cancers: an open-label, phase 1 dose-escalation and expansion study. *Lancet Oncol.* 15: 656–666.
174. von Haehling, S., and S. D. Anker. 2014. Prevalence, incidence and clinical impact of cachexia: facts and numbers—update 2014. *J. Cachexia. Sarcopenia Muscle* 5: 261–263.
175. Suzuki, H., A. Asakawa, H. Amitani, N. Nakamura, and A. Inui. 2013. Cancer cachexia - Pathophysiology and management. *J. Gastroenterol.* 48: 574–594.
176. Dewys, W. D., C. Begg, P. T. Lavin, P. R. Band, J. M. Bennett, J. R. Bertino, M. H. Cohen, H. O. Douglass, P. F. Engstrom, E. Z. Ezdinli, J. Horton, G. J. Johnson, C. G. Moertel, M. M. Oken, C. Perlia, C. Rosenbaum, M. N. Silverstein, R. T. Skeel, R. W. Sponzo, and D. C. Tormey. 1980. Prognostic effect of weight loss prior to chemotherapy in cancer patients. *Am. J. Med.* 69: 491–497.
177. Kalantar-Zadeh, K., C. Rhee, J. J. Sim, P. Stenvinkel, S. D. Anker, and C. P. Kovesdy. 2013. Why cachexia kills: examining the causality of poor outcomes in wasting conditions. *J. Cachexia. Sarcopenia Muscle* 4: 89–94.
178. Farkas, J., S. von Haehling, K. Kalantar-Zadeh, J. E. Morley, S. D. Anker, and M. Lainscak. 2013. Cachexia as a major public health problem: frequent, costly, and deadly. *J. Cachexia. Sarcopenia Muscle* 4: 173–8.
179. Cohen, S., J. A. Nathan, and A. L. Goldberg. 2015. Muscle wasting in disease: molecular mechanisms and promising therapies. *Nat. Rev. Drug Discov.* 14: 58–74.
180. Baazim, H., M. Schweiger, M. Moschinger, H. Xu, T. Scherer, A. Popa, S. Gallage, A. Ali, K. Khamina, L. Kosack, B. Vilagos, M. Smyth, A. Lercher, J. Friske, D. Merkler, A. Aderem, T. H. Helbich, M. Heikenwälder, P. A. Lang, R. Zechner, and A. Bergthaler. 2019. CD8+ T cells induce cachexia during chronic viral infection. *Nat. Immunol.* 20: 701–710.
181. Tracey, K. J., and A. Cerami. 1989. Studies of Cachexia in Parasitic Infection. *Ann. N. Y. Acad. Sci.* 569: 211–218.
182. McLeod, R., P. Eisenhauer, D. Mack, C. Brown, G. Filice, and G. Spitalny. 1989. Immune responses associated with early survival after peroral infection with *Toxoplasma gondii*. *J. Immunol.* 142: 3247–55.
183. López-Yglesias, A. H., E. Burger, A. Araujo, A. T. Martin, and F. Yarovinsky. 2018. T-bet-independent Th1 response induces intestinal immunopathology during *Toxoplasma gondii* infection. *Mucosal Immunol.* 11: 921–931.
184. Morley, J. E., D. R. Thomas, and M.-M. G. Wilson. 2006. Cachexia: pathophysiology and clinical relevance. *Am. J. Clin. Nutr.* 83: 735–743.
185. Tsoli, M., M. Moore, D. Burg, A. Painter, R. Taylor, S. H. Lockie, N. Turner, A. Warren, G. Cooney, B. Oldfield, S. Clarke, and G. Robertson. 2012. Activation of Thermogenesis in Brown Adipose Tissue and Dysregulated Lipid Metabolism Associated with Cancer Cachexia in Mice. *Cancer Res.* 72.

186. Petruzzelli, M., M. Schweiger, R. Schreiber, R. Campos-Olivas, M. Tsoli, J. Allen, M. Swarbrick, S. Rose-John, M. Rincon, G. Robertson, R. Zechner, and E. F. Wagner. 2014. A Switch from White to Brown Fat Increases Energy Expenditure in Cancer-Associated Cachexia. *Cell Metab.* 20: 433–447.
187. Kir, S., J. P. White, S. Kleiner, L. Kazak, P. Cohen, V. E. Baracos, and B. M. Spiegelman. 2014. Tumour-derived PTH-related protein triggers adipose tissue browning and cancer cachexia. *Nature* 513: 100–4.
188. van der Lans, A. A. J. J., J. Hoeks, B. Brans, G. H. E. J. Vijgen, M. G. W. Visser, M. J. Vosselman, J. Hansen, J. A. Jörgensen, J. Wu, F. M. Mottaghy, P. Schrauwen, and W. D. van Marken Lichtenbelt. 2013. Cold acclimation recruits human brown fat and increases nonshivering thermogenesis. *J. Clin. Invest.* 123: 3395–403.
189. Zhang, F., G. Hao, M. Shao, K. Nham, Y. An, Q. Wang, Y. Zhu, C. M. Kusminski, G. Hassan, R. K. Gupta, Q. Zhai, X. Sun, P. E. Scherer, and O. K. Oz. 2018. An Adipose Tissue Atlas: An Image-Guided Identification of Human-like BAT and Beige Depots in Rodents. *Cell Metab.* 27: 252-262.e3.
190. Johnen, H., S. Lin, T. Kuffner, D. A. Brown, V. W.-W. Tsai, A. R. Bauskin, L. Wu, G. Pankhurst, L. Jiang, S. Junankar, M. Hunter, W. D. Fairlie, N. J. Lee, R. F. Enriquez, P. A. Baldock, E. Corey, F. S. Apple, M. M. Murakami, E.-J. Lin, C. Wang, M. J. During, A. Sainsbury, H. Herzog, and S. N. Breit. 2007. Tumor-induced anorexia and weight loss are mediated by the TGF- $\beta$  superfamily cytokine MIC-1. *Nat. Med.* 13: 1333–1340.
191. Asp, M. L., M. Tian, A. A. Wendel, and M. A. Belury. 2010. Evidence for the contribution of insulin resistance to the development of cachexia in tumor-bearing mice. *Int. J. Cancer* 126: 756–763.
192. Das, S. K., S. Eder, S. Schauer, C. Diwoy, H. Temmel, B. Guertl, G. Gorkiewicz, K. P. Tamilarasan, P. Kumari, M. Trauner, R. Zimmermann, P. Vesely, G. Haemmerle, R. Zechner, and G. Hoefler. 2011. Adipose Triglyceride Lipase Contributes to Cancer-Associated Cachexia. *Science (80-. )*. 333: 233–238.
193. Perrin, B. J., and J. M. Ervasti. 2010. The actin gene family: function follows isoform. *Cytoskeleton (Hoboken)*. 67: 630–4.
194. Nouchi, T., Y. Tanaka, T. Tsukada, C. Sato, and F. Marumo. 1991. Appearance of alpha-smooth-muscle-actin-positive cells in hepatic fibrosis. *Liver* 11: 100–5.
195. Carpino, G., S. Morini, S. Ginanni Corradini, A. Franchitto, M. Merli, M. Siciliano, F. Gentili, A. Onetti Muda, P. Berloco, M. Rossi, A. . Attili, and E. Gaudio. 2005. Alpha-SMA expression in hepatic stellate cells and quantitative analysis of hepatic fibrosis in cirrhosis and in recurrent chronic hepatitis after liver transplantation. *Dig. Liver Dis.* 37: 349–356.
196. Moreira, R. K. 2007. *Hepatic Stellate Cells and Liver Fibrosis*.
197. Mack, M. 2018. Inflammation and fibrosis. *Matrix Biol.* 68–69: 106–121.
198. Gieling, R. G., K. Wallace, and Y.-P. Han. 2009. Interleukin-1 participates in the progression from liver injury to fibrosis. *Am. J. Physiol. Gastrointest. Liver Physiol.* 296: G1324–31.
199. Sgroi, A., C. Gonelle-Gispert, P. Morel, R. M. Baertschiger, N. Niclauss, G. Mentha, P. Majno, V. Serre-Beinier, and L. Buhler. 2011. Interleukin-1 Receptor Antagonist Modulates the Early Phase of Liver Regeneration after Partial Hepatectomy in Mice. *PLoS One* 6: e25442.
200. Miura, K., Y. Kodama, S. Inokuchi, B. Schnabl, T. Aoyama, H. Ohnishi, J. M. Olefsky, D. A. Brenner, and E. Seki. 2010. Toll-like receptor 9 promotes steatohepatitis by induction of interleukin-1beta in mice. *Gastroenterology* 139: 323–34.e7.
201. Narsale, A. A., R. T. Enos, M. J. Puppa, S. Chatterjee, E. A. Murphy, R. Fayad, M. O.

- Pena, J. L. Durstine, and J. A. Carson. 2015. Liver inflammation and metabolic signaling in ApcMin/+ mice: the role of cachexia progression. *PLoS One* 10: e0119888.
202. Plauth, M., and E.-T. Schütz. 2002. Cachexia in liver cirrhosis. *Int. J. Cardiol.* 85: 83–87.
203. Martignoni, M. E., C. Dimitriu, J. Bachmann, H. Krakowski-Rosen, K. Ketterer, R. Kinscherf, and H. Friess. 1994. Liver macrophages contribute to pancreatic cancer-related cachexia. *Oncol. Rep.* 21: 363–369.
204. Jones, A., K. Friedrich, M. Rohm, M. Schäfer, C. Algire, P. Kulozik, O. Seibert, K. Müller-Decker, T. Sijmonsma, D. Strzoda, C. Sticht, N. Gretz, G. M. Dallinga-Thie, B. Leuchs, M. Kögl, W. Stremmel, M. B. Diaz, and S. Herzig. 2013. TSC22D4 is a molecular output of hepatic wasting metabolism. *EMBO Mol. Med.* 5: 294–308.
205. Fiore, V. F., S. S. Wong, C. Tran, C. Tan, W. Xu, T. Sulchek, E. S. White, J. S. Hagood, and T. H. Barker. 2018.  $\alpha v \beta 3$  Integrin drives fibroblast contraction and strain stiffening of soft provisional matrix during progressive fibrosis. *JCI Insight* 3.
206. Mederacke, I., D. H. Dapito, S. Affò, H. Uchinami, and R. F. Schwabe. 2015. High-yield and high-purity isolation of hepatic stellate cells from normal and fibrotic mouse livers. *Nat. Protoc.* 10: 305–15.
207. Pelham, R. J., and Y. I Wang. 1997. Cell locomotion and focal adhesions are regulated by substrate flexibility. *Proc. Natl. Acad. Sci. U. S. A.* 94: 13661–5.
208. Yin, C., K. J. Evason, K. Asahina, and D. Y. R. Stainier. 2013. Hepatic stellate cells in liver development, regeneration, and cancer. *J. Clin. Invest.* 123: 1902–10.
209. Konishi, M., N. Ebner, S. von Haehling, S. D. Anker, and J. Springer. 2015. Developing models for cachexia and their implications in drug discovery. *Expert Opin. Drug Discov.* 10: 743–752.
210. Batista, M. L., F. S. Henriques, R. X. Neves, M. R. Olivian, E. M. Matos-Neto, P. S. M. Alcântara, L. F. Maximiano, J. P. Otoch, M. J. Alves, and M. Seelaender. 2016. Cachexia-associated adipose tissue morphological rearrangement in gastrointestinal cancer patients. *J. Cachexia. Sarcopenia Muscle* 7: 37–47.
211. Alves, M. J., R. G. Figuerêdo, F. F. Azevedo, D. A. Cavallaro, N. I. P. Neto, J. D. C. J. Lima, E. Matos-Neto, K. Radloff, D. M. Riccardi, R. G. Camargo, P. S. M. De Alcântara, J. P. Otoch, M. L. B. Junior, and M. Seelaender. 2017. Adipose tissue fibrosis in human cancer cachexia: the role of TGF  $\beta$  pathway. 1–12.
212. Filippatos, G. S., C. Kanatselos, D. D. Manolatos, B. Vougas, A. Sideris, D. Kardara, Stefan D. Anker, F. Kardaras, and B. Uhal. 2003. Studies on apoptosis and fibrosis in skeletal musculature: a comparison of heart failure patients with and without cardiac cachexia. *Int. J. Cardiol.* 90: 107–113.
213. Judge, S. M., R. L. Nosacka, D. Delitto, M. H. Gerber, M. E. Cameron, J. G. Trevino, and A. R. Judge. 2018. Skeletal Muscle Fibrosis in Pancreatic Cancer Patients with Respect to Survival. *JNCI Cancer Spectr.* 2.
214. von Haehling, S., and S. D. Anker. 2010. Cachexia as a major underestimated and unmet medical need: Facts and numbers. *J. Cachexia. Sarcopenia Muscle* 1: 1–5.
215. Dasarathy, S., and M. Merli. 2016. Sarcopenia from mechanism to diagnosis and treatment in liver disease. *J. Hepatol.* 65: 1232–1244.
216. van Vugt, J. L. A., S. Levolger, R. W. F. de Bruin, J. van Rosmalen, H. J. Metselaar, and J. N. M. IJzermans. 2016. Systematic Review and Meta-Analysis of the Impact of Computed Tomography-Assessed Skeletal Muscle Mass on Outcome in Patients Awaiting or Undergoing Liver Transplantation. *Am. J. Transplant.* 16: 2277–2292.

217. Ukwaja, K. N., R. Malekzadeh, S. Dey, A. Chitheer, T. Wakayo, G. A. Kumar, S. Abera, F. Pourmalek, T. Fürst, D. U. Ekwueme, F. Ogbo, R. Topór-Madry, N. Yonemoto, V. Vlassov, C. J. L. Murray, T. Vos, C. McAlinden, S. Sepanlou, T. Akinyemiju, A. Kasaeian, J. Sun, Y.-H. Khang, M. Satpathy, S. I. Hay, L. Zhu, L. Dandona, M. Moradi-Lakeh, C. Fitzmaurice, J. Sanabria, W. Mendoza, E. Weiderpass, M. Younis, A. Mokdad, Y. Khader, N. Alvis-Guzman, M. Sawhney, M. Ahmed, R. Dandona, B. Cowie, J.-Y. Choi, M. A. Alemayohu, R. Lunevicius, Z. Zaidi, G. Patton, D. T. Mengistu, S. H. Jee, Q. Nguyen, G. Nguyen, A. Lopez, J. Castillo-Rivas, G. Nagel, G. Roshandel, H. Phuc, M. Kutz, A. Berhane, M. Qorbani, A. Radfar, C. Allen, K. Shackelford, M. Naghavi, C. Yu, D. Dicker, F. Fischer, J. A. Salomon, J. Hancock, N. Alam, A. Barac, R. Al-Raddadi, B. Tran, M. E. S. Zaki, Y. Amoako, A. Artaman, P. Hotez, A. Werdecker, H. Larson, S. E. Vollset, D. M. Pereira, T. Meier, Z. Bhutta, B. Sartorius, I. Bensenor, H. Shore, and T. A. Ayele. 2017. The Burden of Primary Liver Cancer and Underlying Etiologies From 1990 to 2015 at the Global, Regional, and National Level. *JAMA Oncol.* 3: 1683.
218. Koo, B. K., D. Kim, S. K. Joo, J. H. Kim, M. S. Chang, B. G. Kim, K. L. Lee, and W. Kim. 2017. Sarcopenia is an independent risk factor for non-alcoholic steatohepatitis and significant fibrosis. *J. Hepatol.* 66: 123–131.
219. Han, E., Y. H. Lee, B. K. Kim, J. Y. Park, D. Y. Kim, S. H. Ahn, B. W. Lee, E. S. Kang, B. S. Cha, K. H. Han, and S. U. Kim. 2018. Sarcopenia is associated with the risk of significant liver fibrosis in metabolically unhealthy subjects with chronic hepatitis B. *Aliment. Pharmacol. Ther.* 48: 300–312.
220. Ishimoto, T., M. A. Lanasa, C. J. Rivard, C. A. Roncal-Jimenez, D. J. Orlicky, C. Cicerchi, R. H. McMahan, M. F. Abdelmalek, H. R. Rosen, M. R. Jackman, P. S. Maclean, C. P. Diggle, A. Asipu, S. Inaba, T. Kosugi, W. Sato, S. Maruyama, L. G. Sánchez-Lozada, Y. Y. Sautin, J. O. Hill, D. T. Bonthron, and R. J. Johnson. 2013. High-fat and high-sucrose (western) diet induces steatohepatitis that is dependent on fructokinase. *Hepatology* 58: 1632–1643.
221. Montano-Loza, A. J., J. Meza-Junco, C. M. M. Prado, J. R. Lieffers, V. E. Baracos, V. G. Bain, and M. B. Sawyer. 2012. Muscle Wasting Is Associated With Mortality in Patients With Cirrhosis. *Clin. Gastroenterol. Hepatol.* 10: 166-173.e1.
222. Hanai, T., M. Shiraki, K. Nishimura, S. Ohnishi, K. Imai, A. Suetsugu, K. Takai, M. Shimizu, and H. Moriwaki. 2015. Sarcopenia impairs prognosis of patients with liver cirrhosis. *Nutrition* 31: 193–199.
223. Hayashi, F., Y. Matsumoto, C. Momoki, M. Yuikawa, G. Okada, E. Hamakawa, E. Kawamura, A. Hagihara, M. Toyama, H. Fujii, S. Kobayashi, S. Iwai, H. Morikawa, M. Enomoto, A. Tamori, N. Kawada, and D. Habu. 2013. with compensated viral liver cirrhosis. 1264–1275.
224. Kalafateli, M., C. Konstantakis, K. Thomopoulos, C. Triantos, M. Kalafateli, and C. Konstantakis. 2015. Impact of muscle wasting on survival in patients with liver cirrhosis. 21: 7357–7361.
225. Watt, K. D., R. A. Bhanji, H. Malhi, A. M. Allen, and P. Narayanan. 2017. Sarcopenia in hiding: The risk and consequence of underestimating muscle dysfunction in nonalcoholic steatohepatitis. *Hepatology* 66: 2055–2065.
226. Mahdy, M. A. A. 2019. Skeletal muscle fibrosis: an overview. *Cell Tissue Res.* 375: 575–588.
227. Zhu, X., K. G. Burfeind, K. A. Michaelis, T. P. Braun, B. Olson, K. R. Pelz, T. K. Morgan, and D. L. Marks. 2019. MyD88 signalling is critical in the development of pancreatic cancer cachexia. *J. Cachexia. Sarcopenia Muscle* 10: 378.

228. Barlo, N. P., C. H. M. van Moorsel, N. M. Korthagen, M. Heron, G. T. Rijkers, H. J. T. Ruven, J. M. M. van den Bosch, and J. C. Grutters. 2011. Genetic variability in the IL1RN gene and the balance between interleukin (IL)-1 receptor agonist and IL-1 $\beta$  in idiopathic pulmonary fibrosis. *Clin. Exp. Immunol.* 166: 346–51.
229. Whyte, M., R. Hubbard, R. Meliconi, M. Whidborne, V. Eaton, C. Bingle, J. Timms, G. Duff, A. Facchini, A. Pacilli, M. Fabbri, I. Hall, J. Britton, I. Johnston, and F. Di Giovine. 2000. Increased risk of fibrosing alveolitis associated with interleukin-1 receptor antagonist and tumor necrosis factor- $\alpha$  gene polymorphisms. *Am. J. Respir. Crit. Care Med.* 162: 755–758.
230. Takamatsu, M., M. Yamauchi, Y. Maezawa, M. Ohata, S. Saitoh, and G. Toda. 1998. *Correlation of a Polymorphism in the Interleukin-1 Receptor Antagonist Gene with Hepatic Fibrosis in Japanese Alcoholics*. John Wiley & Sons, Ltd (10.1111) ; :141S-144S.
231. Kamari, Y., A. Shaish, E. Vax, S. Shemesh, M. Kandel-Kfir, Y. Arbel, S. Olteanu, I. Barshack, S. Dotan, E. Voronov, C. A. Dinarello, R. N. Apte, and D. Harats. 2011. Lack of interleukin-1 $\alpha$  or interleukin-1 $\beta$  inhibits transformation of steatosis to steatohepatitis and liver fibrosis in hypercholesterolemic mice. *J. Hepatol.* 55: 1086–1094.
232. Bageghni, S. A., M. J. Drinkhill, and N. A. Turner. 2019. Fibroblast-specific deletion of interleukin-1 receptor-1 reduces adverse cardiac remodeling following myocardial infarction Find the latest version : .
233. Bui, C. B., M. Kolodziej, E. Lamanna, K. Elgass, A. Sehgal, I. Rudloff, D. O. Schwenke, H. Tsuchimochi, M. A. G. M. Kroon, S. X. Cho, A. Maksimenko, M. Cholewa, P. J. Berger, M. J. Young, J. E. Bourke, J. T. Pearson, M. F. Nold, and C. A. Nold-Petry. 2019. Interleukin-1 Receptor Antagonist Protects Newborn Mice Against Pulmonary Hypertension. *Front. Immunol.* 10: 1–15.
234. Gasse, P., C. Mary, I. Guenon, N. Noulin, S. Charron, S. Schnyder-Candrian, B. Schnyder, S. Akira, V. F. J. Quesniaux, V. Lagente, B. Ryffel, and I. Couillin. 2007. IL-1R1/MyD88 signaling and the inflammasome are essential in pulmonary inflammation and fibrosis in mice. *J. Clin. Invest.* 117: 3786–3799.
235. Giusto, M., L. Barberi, F. Di Sario, E. Rizzuto, C. Nicoletti, F. Ascenzi, A. Renzi, N. Caporaso, G. D'Argenio, E. Gaudio, A. Musarò, and M. Merli. 2017. Skeletal muscle myopenia in mice model of bile duct ligation and carbon tetrachloride-induced liver cirrhosis. *Physiol. Rep.* 5: 1–13.
236. Sinai, A. P., E. A. Watts, A. Dhara, R. D. Murphy, M. S. Gentry, and A. Patwardhan. 2016. Reexamining Chronic *Toxoplasma gondii* Infection: Surprising Activity for a “Dormant” Parasite. *Curr. Clin. Microbiol. reports* 3: 175–185.
237. Fox, B. A., L. M. Rommereim, R. B. Guevara, A. Falla, M. A. Hortua Triana, Y. Sun, and D. J. Bzik. 2016. The *Toxoplasma gondii* Rhoptry Kinome Is Essential for Chronic Infection. *MBio* 7.
238. Waldman, B. S., D. Schwarz, M. H. Wadsworth, J. P. Saeij, A. K. Shalek, and S. Lourido. 2020. Identification of a Master Regulator of Differentiation in *Toxoplasma*. *Cell* 180: 359-372.e16.
239. Filtjens, J., N. Coltel, S. Cencig, S. Taveirne, E. Van Ammel, A. Van Acker, T. Kerre, P. Matthys, T. Taghon, B. Vandekerckhove, Y. Carlier, C. Truyens, and G. Leclercq. 2016. The Ly49E Receptor Inhibits the Immune Control of Acute *Trypanosoma cruzi* Infection. *Front. Immunol.* 7: 472.
240. Truyens, C., F. Torrico, R. Lucas, P. De Baetselier, W. A. Buurman, and Y. Carlier. 1999. The endogenous balance of soluble tumor necrosis factor receptors and tumor necrosis factor

- modulates cachexia and mortality in mice acutely infected with *Trypanosoma cruzi*. *Infect. Immun.* 67: 5579–86.
241. TRUYENS, C., F. TORRICO, A. ANGELO-BARRIOS, R. LUCAS, H. HEREMANS, P. DE BAETSELIER, and Y. CARLIER. 1995. The cachexia associated with *Trypanosoma cruzi* acute infection in mice is attenuated by anti-TNF- $\alpha$ , but not by anti-IL-6 or anti-IFN- $\gamma$  antibodies. *Parasite Immunol.* 17: 561–568.
242. Herbert, D. R., T. Orekov, A. Roloson, M. Ilies, C. Perkins, W. O'Brien, S. Cederbaum, D. W. Christianson, N. Zimmermann, M. E. Rothenberg, and F. D. Finkelman. 2010. Arginase I suppresses IL-12/IL-23p40-driven intestinal inflammation during acute schistosomiasis. *J. Immunol.* 184: 6438–46.
243. Herbert, D. R., T. Orekov, C. Perkins, and F. D. Finkelman. 2008. IL-10 and TGF- $\beta$  Redundantly Protect against Severe Liver Injury and Mortality during Acute Schistosomiasis. *J. Immunol.* 181: 7214.
244. De Alencar, J. E., J. Castracane, S. M. B. Jeronimo, T. Evans, R. D. Pearson, J. S. Drew, and G. Cox. 1992. Visceral Leishmaniasis: a Model for Infection-Induced Cachexia. *Am. J. Trop. Med. Hyg.* 47: 8–15.
245. Müller, U. B., and J. C. Howard. 2016. The impact of *Toxoplasma gondii* on the mammalian genome. *Curr. Opin. Microbiol.* 32: 19–25.
246. Ingram, W. M., L. M. Goodrich, E. A. Robey, and M. B. Eisen. 2013. Mice Infected with Low-Virulence Strains of *Toxoplasma gondii* Lose Their Innate Aversion to Cat Urine, Even after Extensive Parasite Clearance. *PLoS One* 8: e75246.
247. Vyas, A., S.-K. S.-K. Kim, N. Giacomini, J. C. Boothroyd, and R. M. Sapolsky. 2007. Behavioral changes induced by *Toxoplasma* infection of rodents are highly specific to aversion of cat odors. *Proc. Natl. Acad. Sci. U. S. A.* 104: 6442–7.
248. Bing, C. 2011. Lipid mobilization in cachexia. *Curr. Opin. Support. Palliat. Care* 5: 356–360.
249. Murphy, R. A., M. S. Wilke, M. Perrine, M. Pawlowicz, M. Mourtzakis, J. R. Lieffers, M. Maneshgar, E. Bruera, M. T. Clandinin, V. E. Baracos, and V. C. Mazurak. 2010. Loss of adipose tissue and plasma phospholipids: Relationship to survival in advanced cancer patients. *Clin. Nutr.* 29: 482–487.
250. Dalal, and Shalini. 2018. Lipid metabolism in cancer cachexia. *Ann. Palliat. Med.* 8: 13–23.
251. Agustsson, T., M. Rydén, J. Hoffstedt, V. van Harmelen, A. Dickert, J. Laurencikiene, B. Isaksson, J. Permert, and P. Arner. 2007. Mechanism of Increased Lipolysis in Cancer Cachexia. *Cancer Res.* 67: 5531–5537.
252. Rosen, E. D., and B. M. Spiegelman. 2006. Adipocytes as regulators of energy balance and glucose homeostasis. *Nature* 444: 847–53.
253. Kim, J., K.-J. Won, H. M. Lee, B.-Y. Hwang, Y.-M. Bae, W. S. Choi, H. Song, K. W. Lim, C.-K. Lee, and B. Kim. 2009. p38 MAPK Participates in Muscle-Specific RING Finger 1-Mediated Atrophy in Cast-Immobilized Rat Gastrocnemius Muscle. *Korean J. Physiol. Pharmacol.* 13: 491–6.
254. Fukawa, T., B. C. Yan-Jiang, J. C. Min-Wen, E. T. Jun-Hao, D. Huang, C.-N. Qian, P. Ong, Z. Li, S. Chen, S. Y. Mak, W. J. Lim, H. Kanayama, R. E. Mohan, R. R. Wang, J. H. Lai, C. Chua, H. S. Ong, K.-K. Tan, Y. S. Ho, I. B. Tan, B. T. Teh, and N. Shyh-Chang. 2016. Excessive fatty acid oxidation induces muscle atrophy in cancer cachexia. *Nat. Med.* 22: 666–671.
255. Triebel, A. 2016. Glycerophospholipids. In *Encyclopedia of Lipidomics* Springer Netherlands, Dordrecht. 1–4.

256. Wu, G., L. Zhang, T. Li, G. Lopaschuk, D. E. Vance, and R. L. Jacobs. 2012. Choline deficiency attenuates body weight gain and improves glucose tolerance in ob/ob mice. *J. Obes.* 2012: 1–7.
257. Jones, J. R., C. Barrick, K.-A. Kim, J. Lindner, B. Blondeau, Y. Fujimoto, M. Shiota, R. A. Kesterson, B. B. Kahn, and M. A. Magnuson. 2005. Deletion of PPAR $\gamma$  in adipose tissues of mice protects against high fat diet-induced obesity and insulin resistance. *Proc. Natl. Acad. Sci. U. S. A.* 102: 6207–12.
258. Groß, O., A. S. Yazdi, C. J. Thomas, M. Masin, L. X. Heinz, G. Guarda, M. Quadroni, S. K. Drexler, and J. Tschopp. 2012. Inflammasome Activators Induce Interleukin-1 $\alpha$  Secretion via Distinct Pathways with Differential Requirement for the Protease Function of Caspase-1. *Immunity* 36: 388–400.
259. Tzeng, T.-C., S. Schattgen, B. Monks, D. Wang, A. Cerny, E. Latz, K. Fitzgerald, and D. T. Golenbock. 2016. A Fluorescent Reporter Mouse for Inflammasome Assembly Demonstrates an Important Role for Cell-Bound and Free ASC Specks during In Vivo Infection. *Cell Rep.* 16: 571–582.
260. Yoon, S., A. Kovalenko, K. Bogdanov, and D. Wallach. 2017. MLKL, the Protein that Mediates Necroptosis, Also Regulates Endosomal Trafficking and Extracellular Vesicle Generation. *Immunity* 47: 51-65.e7.
261. England, H., H. R. Summersgill, M. E. Edye, N. J. Rothwell, and D. Brough. 2014. Release of interleukin-1 $\alpha$  or interleukin-1 $\beta$  depends on mechanism of cell death. *J. Biol. Chem.* 289: 15942–50.
262. Patel, K., R. N. Trivedi, C. Durgampudi, P. Noel, R. A. Cline, J. P. DeLany, S. Navina, and V. P. Singh. 2015. Lipolysis of Visceral Adipocyte Triglyceride by Pancreatic Lipases Converts Mild Acute Pancreatitis to Severe Pancreatitis Independent of Necrosis and Inflammation. *Am. J. Pathol.* 185: 808–819.
263. Spinello, A., E. Vecile, A. Abbate, A. Dobrina, and A. Magistrato. 2019. How Can Interleukin-1 Receptor Antagonist Modulate Distinct Cell Death Pathways? *J. Chem. Inf. Model.* 59: 351–359.
264. Gao, F. F., J. W. Lv, Y. Wang, R. Fan, Q. Li, Z. Zhang, and L. Wei. 2016. Tamoxifen induces hepatotoxicity and changes to hepatocyte morphology at the early stage of endocrinotherapy in mice. *Biomed. Reports* 4: 102–106.
265. Batista, S. J., K. M. Still, D. Johanson, J. A. Thompson, C. A. O'Brien, J. R. Lukens, and T. H. Harris. 2020. Gasdermin-D-dependent IL-1 $\alpha$  release from microglia promotes protective immunity during chronic *Toxoplasma gondii* infection. *bioRxiv* 2020.01.22.915652.
266. Hannan, R. T., S. M. Peirce, and T. H. Barker. 2018. Fibroblasts: Diverse Cells Critical to Biomaterials Integration. *ACS Biomater. Sci. Eng.* 4: 1223–1232.
267. Hansen, M. K., K. A. O'Connor, L. E. Goehler, L. R. Watkins, and S. F. Maier. 2001. The contribution of the vagus nerve in interleukin-1 $\beta$ -induced fever is dependent on dose. *Am. J. Physiol. Integr. Comp. Physiol.* 280: R929–R934.
268. de Lartigue, G. 2016. Role of the vagus nerve in the development and treatment of diet-induced obesity. *J. Physiol.* 594: 5791–5815.
269. Bonaz, B., T. Bazin, and S. Pellissier. 2018. The Vagus Nerve at the Interface of the Microbiota-Gut-Brain Axis. *Front. Neurosci.* 12.
270. Pavlov, V. A., and K. J. Tracey. 2012. The vagus nerve and the inflammatory reflex--linking immunity and metabolism. *Nat. Rev. Endocrinol.* 8: 743–54.